Bhairavi Doshi

TOWARDS A SUSTAINABLE VALORISATION OF SPILLED OIL BY ESTABLISHING A GREEN CHEMISTRY BETWEEN A SURFACE ACTIVE MOIETY OF CHITOSAN AND OILS

ACTA UNIVERSITATIS LAPPEENRANTAENSIS 861

Bhairavi Doshi

TOWARDS A SUSTAINABLE VALORISATION OF SPILLED OIL BY ESTABLISHING A GREEN CHEMISTRY BETWEEN A SURFACE ACTIVE MOIETY OF CHITOSAN AND OILS

Dissertation for the degree of Doctor of Science (Technology) to be presented with due permission for public examination and criticism in the Auditorium of Mikkeli University Consortium (MUC), Mikkeli, Finland on the 15th of August, 2019, at noon.

Acta Universitatis
Lappeenrantaensis 861

Supervisors Professor Mika Sillanpää
LUT School of Engineering Science
Lappeenranta-Lahti University of Technology LUT
Finland

Associate Professor Eveliina Repo
LUT School of Engineering Science
Lappeenranta-Lahti University of Technology LUT
Finland

Reviewers Professor Vijay T. John
Department of Chemical and Biomolecular Engineering
Tulane University
USA

Professor Srinivasa R. Raghavan
Department of Chemical and Biomolecular Engineering
University of Maryland
USA

Opponent Professor Monika Österberg
Department of Bioproducts and Biosystems
Aalto University
Finland

ISBN 978-952-335-392-3
ISBN 978-952-335-393-0 (PDF)
ISSN-L 1456-4491
ISSN 1456-4491

Lappeenranta-Lahti University of Technology LUT
LUT University Press 2019

Abstract

Bhairavi Doshi
Towards a sustainable valorisation of spilled oil by establishing a green chemistry between a surface active moiety of chitosan and oils
Lappeenranta 2019
82 pages
Acta Universitatis Lappeenrantaensis 861
Diss. Lappeenranta-Lahti University of Technology LUT
ISBN 978-952-335-392-3, ISBN 978-952-335-393-0 (PDF), ISSN-L 1456-4491 ISSN 1456-4491

This thesis presents fabrication of sustainable surfactants from bio-polymer and demonstrates their performance in dispersion of spilled oil with different quality of water and climatic conditions, to provide a sustainable environmental technology for the oil spill treatment.

One of the biggest threats to marine ecosystem is an oil spill, since the presence of an abundant amount of hydrocarbons alters the natural phenomenon of marine creatures. Moreover, for Arctic regions, the harsh climatic conditions and remoteness make the oil spill response more challenging. Various oil spill response techniques such as skimmers, booms, in-situ burning and dispersants were used. For large spill, mechanical methods are too slow to respond in the cold ice-affected waters and therefore, the most feasible response option is chemical surfactant. However, despite of their effectiveness, the use of synthetic dispersing agents such as Corexit 9527 and 9500 are proven to be more toxic than spilled oil. Therefore, an eco-friendly and sustainable approach towards the environment has introduced many non-toxic and biodegradable materials, such as cellulose and chitosan, for the removal and recovery of oil from water resources.

Chitin is the second most abundant natural polymer obtained from crustaceans of crabs, lobsters and shrimps. Chitosan, which has two surface-active functional groups, hydroxyl and amino groups, is obtained from the deacetylation of chitin. In this work, these groups were modified via carboxymethylation and acylation to enhance the water solubility and hydrophobicity of chitosan. These modification routes can provide potential surfactant properties on chitosan as the polar chitosan skeleton will likely orientate towards the water phase and non-polar alkyl-groups towards the oil phase in oil-water system enabling dispersion of oil droplets. The decrease in temperature enlarged the oil droplet size. The formation of emulsion by breaking the oil in seawater requires more amount of chitosan materials than deionized water, and this was overcome by the cross-combination of chitosan materials with orange peels. Therefore, such approach of using biowaste-based surfactant as one of the component in dispersant formulation would minimise the traces of hazardous chemicals in the marine ecosystem as well as enhance the oil bio-remediation.

Keywords
Chitosan, oil-in-water emulsion, carboxymethylation, acylation, hydrophobic modification, adsorption, stabilization of oil droplets, marine diesel, seawater, orange peels, electrosteric stabilization.

Acknowledgements

This work was carried out in the Department of Green Chemistry at Lappeenranta-Lahti University of Technology LUT, Mikkeli, Finland, during November 2015–August 2018. The research conducted in this study has received funding from the EAKR project 'Improvement of the oil spill prevention and response with the green chemicals (VIKE)' and the Academy of Finland (decision number 283200).

First of all, I express my sincere gratitude to my supervisor Prof. Mika Sillanpää for all the support he provided during this entire research. I also thank him for giving me an opportunity to enter the fascinating field of oil spill. I am grateful to Assoc. Prof. Eveliina Repo for introducing me to the booming field of bio-polymers through scientific discussions and valuable guidance. In addition, their encouragement and enthusiasm have been a source of inspiration which kept me going forward.

I am grateful to Prof. Vijay T. John and Prof. Srinivasa R. Raghavan for reviewing this thesis and giving valuable comments and suggestions, which improved the content of the thesis.

I would like to thank Dr. Simo Kalliola for fruitful discussions during my studies. My sincere thanks also go to Assoc. Prof. Henrikki Liimatainen, Dr. Ossi Laitinen, Dr. Juho Sirviö, Dr. Juha Heiskanen, Dr. Ali Ayati and Dr. Sami Hietala. Working with them was a rewarding experience of learning.

I also express my sincere thanks to friends and colleagues Deepika, Marina, Mirka, Varsha, Sidra, Indu, Zhao, Evgenia, Mahsa, Gao, Khum, Fangping, Feiping, Tam, Olga, Nikolai, and other members of the department for their support and making friendly working atmosphere. A very special thanks to Sanna Tomperi for all her help and administrative assistance, and also to Sari Damsten and Saara Merritt for their support and guidance in the dissertation process.

A special thanks to Ulla Vainikka and her family, and Laura Jouhkimo and her family for all special gatherings that had helped me to a great extent in bringing balance between work and leisure.

My heartfelt gratitude to my parents Bharat and Aruna Doshi, and my aunt Manorama, for their love and motivation during my entire journey. Thanks for the cherish moments to my lovely brother Nirav and his wife Devangi, and my nephew Shubh, for adding more. I also convey my appreciation to my husband's parents Mita and Pradip Shah, grandmother and brother for their kind support. My special gratitude I express to my beloved husband Srujal, for his unconditional love, firm faith and support. I thank my son Dharin, for bringing happiness during this journey of my life.

Bhairavi Doshi
June 2019
Mikkeli, Finland

Contents

List of publications

This thesis is based on the following papers. The rights have been granted by the publishers to include the papers in the dissertation.

I. Doshi, B., Repo, R., Heiskanen, J. P., Sirviö, J. A. and Sillanpää, M. (2017). Effectiveness of N,O-carboxymethyl chitosan on destabilization of Marine Diesel, Diesel and Marine-2T oil for oil spill treatment. *Carbohydrate Polymers*, 167, pp. 326-336.

II. Doshi, B., Repo, R., Heiskanen, J. P., Sirviö, J. A. and Sillanpää, M. (2018). Sodium salt of oleoyl carboxymethyl chitosan: A sustainable adsorbent in the oil spill treatment. *Journal of Cleaner Production*, 170, pp. 339-350.

III. Doshi, B., Ayati, A., Tanhaei, B., Repo, E. and Sillanpää, M. (2018). Partially carboxymethylated and partially cross-linked surface of chitosan versus the adsorptive removal of dyes and divalent metal ions. *Carbohydrate Polymers*, 197, pp. 586-597.

IV. Doshi, B., Hietala, S., Sirviö, J. A., Repo, E. and Sillanpää, M. (2019). A powdered orange peel combined carboxymethyl chitosan and its acylated derivative for the emulsification of marine diesel and 2T-oil with different qualities of water. *Journal of Molecular Liquids*, 291, 111327, pp. 1-13.

The publications are numbered throughout this thesis using Roman numerals as mentioned above. Reprints of each publication are included at the end of this thesis.

Author’s contribution

Bhairavi Doshi is the principal and corresponding author in papers I-IV. The author carried out all of the experimental work, analysed the data and had the main responsibility of writing the manuscript.

Other related publication

1. Doshi, B., Sillanpää, M. and Kalliola, S. (2018). A review of bio-based materials for oil spill treatment. *Water Research*, 135, pp. 262-272.

Nomenclature

In the present work, variables and constants are denoted using *slanted style*, and abbreviations are denoted using regular style.

List of symbols and units

$V_{initial}$	Volume of NaOH used in blank titration	ml
V_{used}	Volume of NaOH used in sample titration	ml
W	Weight of sample	g
N	Molarity of NaOH	mol kg^{-1}
$V_{i,}$	Respective volumes of NaOH ($i=1,2,3$)	ml
C	Concentration of NaOH	mmol L^{-1}
V	Volume of NaOH to neutralize the carboxylate group	L
C_i	Initial amount of oil	ml
C_s	Separated amount of oil	ml
C_r	Recovered amount of oil	ml
Dx	Equivalent volume diameters	µm
R	Recovery of oil	%
T_{CA}	Amount of carboxylic acid content	mmol g^{-1}

Abbreviations

^{1}H NMR	Proton nuclear magnetic resonance spectroscopy
BAC	Benzalkonium chloride
BET	Brunauer-Emmett-Teller
BZT	Benzethonium chloride
Ch-A	Chitosan from crab shells
Ch-B	Chitosan from shrimp shells
Ch-C	Chitosan having high molecular weight
CPC	Cetylpyridinium chloride
CSOP-A	Hydrophobically modified carboxymethyl chitosan-orange peels
CTAB	Cetyl trimethylammonium bromide
CTAC	Cetyl trimethylammonium chloride
DDA	Degree of deacetylation
DI	Deionised water
DOSS	Dioctyl sodium sulfosuccinate
DS	Degree of substitution
DTAC	Dodecyl trimethyl ammonium chloride
ECH	Epichlorohydrin
EDS	Energy dispersive X-ray spectroscopy
FTIR	Fourier transform infrared spectrophotometer
GC-FID	Gas Chromatography

Glu	Glutaraldehyde
HCl	Hydrochloric acid
IFT	Interfacial tension
IPA	Isopropanol
ITOPF	The International Tanker Owners Pollution Federation Ltd
LABs	Linear alkylbenzene sulfonates
MB	Methylene blue
NaOH	Sodium hydroxide
Na-CS[b]	Sodium salt of carboxymethyl chitosan (from shrimp shells chitosan)
Na-CS[c]	Sodium salt of carboxymethyl chitosan (from high molecular weight chitosan)
NaO-CS	Sodium salt of oleoyl carboxymethyl chitosan
NO-CS	N,O-carboxymethyl chitosan
NPOC	Non-purge organic carbon
OP-A	Hydrophobically modified orange peels powder
O/W	Oil-in-water
O/W/O	Oil-in-water-in-oil
PFOS	Perfluorooctanesulfonate
RT	Room temperature
SaO	Safranin O
SDS	Sodium dodecyl sulfate
SEM	Scanning electron microscopy
SLS	Sodium lauryl sulfate
SW	Seawater
Tart	Tartrazine
TOC	Total organic carbon
XRD	X-ray diffraction spectroscopy
W/O	Water-in-oil
W/O/W	Water-in-oil-in-water
ZP	Zeta potential

List of figures

List of tables

1 Introduction

Global entry of oil into the water stream is either through accidental spills from oil tankers and/or underwater pipelines, through the waste disposal from factories and industrial facilities, through offshore drilling and production operations, or by increased in transportation (Farrington and McDowell, 2004). An oil spill is the release of liquid petroleum hydrocarbon into the environment. Since approx. 13% of oil entering the oceans is the resultant of oil spill, oceans are considered as the world's largest water resource getting polluted by oil. In addition, the changing climate made a revolution in the arctic regions through expansion of the industrial activities along with maritime traffic (Wassmann et al., 2011; Arrigo, 2013), which also increased the oil spill rate.

As per ITOPF, the spills are generally categorised by size as <7 tonnes, 7-700 tonnes and >700 tonnes, respectively, among which the majority of spill incidents fall into the smallest category. Table 1.1 presents a history of the oil entered the water resources since 1970 (ITOPF, 2018). After the number of oil spills incidents, various regulations and strategies, such as trained crew and appropriate damage control materials must be on boarded, have been incorporated to prevent spills in the future (Arctic Council, 2009; Carriger and Barron, 2011; Environmental Protection Agency, 2018). Some of the largest catastrophic tankers oil spills in past few years were Atlantic Empress (1979), Castillo de Bellver (1983), Exxon Valdez (1987) and Deep Horizon (2010), that not only affected the water surface, but also trapped marine creatures (Peterson et al., 2003; DeLeo et al., 2016; Sagerup et al., 2016) and offshore landfills (Jernelöv, 2010).

Table 1.1: Perspective of oil spills from 1979-2017.

Year	Number of spills		Quantity (in tonnes)
	7-700 tonnes	>700 tonnes	
1970-1979	543	245	3195000
1980-1989	360	94	1175000
1990-1999	281	77	1134000
2000-2009	149	32	196000
2010-2017	39	14	47000

Generally during the clean-up operations only few percent of the total spilled oil was successfully recovered, whereas, the bulk of clean-up was carried out by oil-eating microbes in the water (Hoff, 1993; Atlas, 1995; Röling et al., 2002; Atlas and Hazen, 2011). In addition to this, the type of oil and geographical conditions plays a significant role in the determination of oil spills impacts and recovery rates (Dicks, 1998; Dahlmann, 2003). Nevertheless, for Arctic regions, clean-up was difficult due to the remoteness and harsh environmental conditions.

Although there are predefined methods such as mechanical/physical, chemical, and biological, for the oil spill response (Tewari and Sirvaiya, 2015; Environmental Protection Agency, 2017), until the date there is a huge gap between the available techniques and its applicability in reality. Figure 1.1 shows the functionalisation of spilled oil in the marine ecosystem together with their treatment methods. The methods associated with the recovery of spilled oil from the water surfaces without

any physical change in the property of oil are classified as physical/mechanical methods. It mainly includes booms, barriers, and skimmers, for the removal and recovery of spilled oil. Booms are the stationary floating objects which absorb the spilled oil and prevent the movement of slicked oil. Barriers are the materials that prevent the movement and dispersal of spilled materials. Skimmers are stationary or mobile devices used to remove floating and/or emulsified oil from the water surface. In addition to this, in-situ burning is feasible using high-temperature booms (Evans et al., 2001; Fingas, 2011) and this is mostly used in Arctic conditions along with skimmers. Hydrophobic sorbents and meshes could be utilised in skimmers for enhanced oil recovery (EOR) (Doshi et al., 2018).

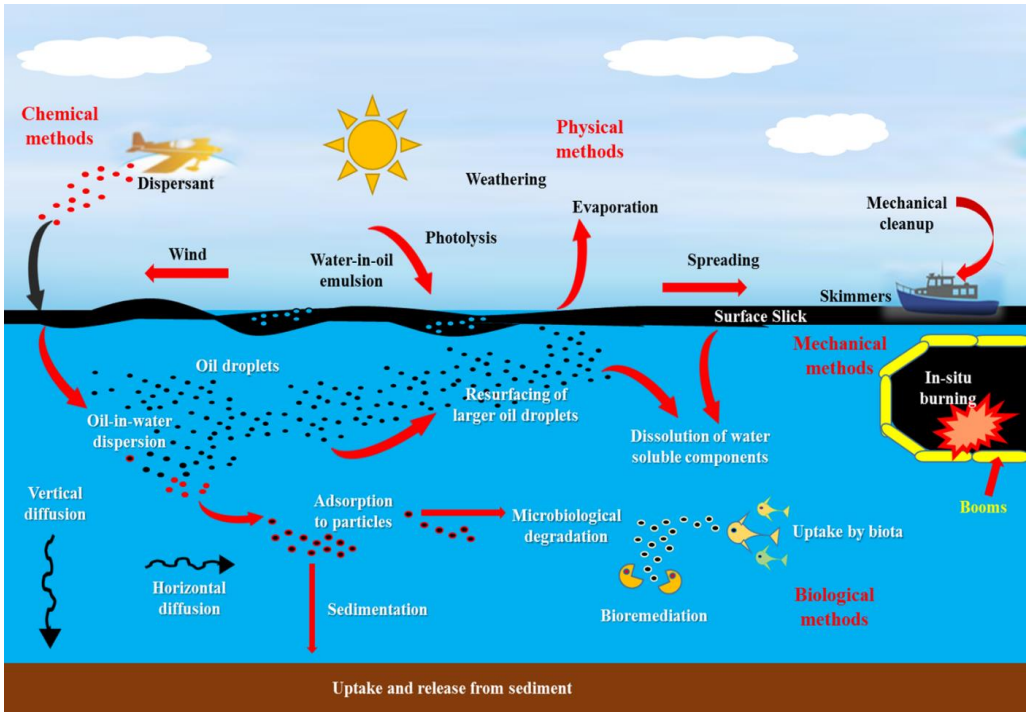

Figure 1.1: Ideal behaviour of spilled oil in the marine environment along with its response techniques.

Other than mechanical methods, weathering i.e. certain naturally occurring processes such as oxidation, evaporation, and biodegradation, are also taken into account for the oil spill response. Generally, these are too slow to provide adequate environmental recovery and, hence, wiping with sorbent materials, pressure washing, and raking and bulldozing can be used to assist these natural processes. Sorbents materials that can soaked oil either by absorption or adsorption are also used to treat spilled oil. Chemical methods include dispersants sprayed on the oil spill to break it up into

small droplets (ITOPF, 2014; Graham et al., 2016; John et al., 2016). These small droplets of oil then disperse or mix with water. However, the other side of using dispersants is their toxicity towards marine life (Zheng et al., 2014; Wise et al., 2014). In addition, sorbent materials may be used in small-scale oil spills. Biological methods include the addition of microbes and/or nutrients and/or oxygen to stimulate bacterial growth and the resultant biodegradation as well as the bioremediation of the spilled oil (Azubuike et al., 2016). However, physiochemical methods have limitations in terms of crude oil clean-up and, therefore, recently biological methods have held sway (Das and Chandran, 2011; Dave and Ghaly, 2011). Moreover, the nature of the oil spill determines the techniques and the materials (Teas et al., 2001) to be used.

On the basis of chemical and mechanical clean-up, sorbents, gelators, surfactants, aerogel and separators were used in past ten years for treating the spilled oil. These materials are either bio-based or synthetic, but there is a growing demand for green and sustainable materials for the treatment of oil spill (Doshi et al., 2018). Recently, biopolymers such as cellulose, chitin, chitosan, gum agar, xanthan gum and agarose, were widely used in the treatment of oil spills (Venkataraman et al., 2013; Chaudhary et al., 2014; Chaudhary et al., 2015; Paul et al., 2016; Pi et al., 2016; Dai et al., 2017; Laitinen, Suopajärvi, et al., 2017; Laitinen, Ojala, et al., 2017; Mohy Eldin et al., 2017). In addition to this, many alternative eco-friendly dispersants based on food-grade amphiphilies (Athas et al., 2014; Riehm et al., 2015; Riehm et al., 2017), bio-polymeric blends (Fouad et al., 2016) and magnetic nano-particles (Zhang et al., 2017; Soares et al., 2017) have been studied for the removal and/or separation of oil from water resources.

The main objective of this work was to develop chitosan-based materials, as an oil sorbent or as an oil emulsifier or as a surfactant for the oil spill treatment. Chitosan is an effective macromolecule consisting of hydroxyl and amino groups, which provides hydrophilicity and adsorptive characteristics. Generally, the oil-in-water emulsions is feasible, when the chitosan particles gets adsorb at oil-water interface. However, the native chitosan was insoluble at pH>6.5, but protonation of amino groups of chitosan in acidic solutions make it soluble. So, the functionality of amino groups with changing pH might affect the stabilization of emulsions along with the hydrophilicity and hydrophobicity of modified chitosan. Mostly, water available in the nature is seawater with salinity up to 3.5% and pH of approximately 8. Hence, effectiveness of chitosan-based materials to stabilize oil-in-water emulsions in presence of ionic strength is also an important factor prior to its applicability. The emulsification of oil stepped down the spreading of the oil on the water after oil spill and enhanced the natural biodegradability.

The main aim of this study was to demonstrate the application of bio-polymer, chitosan, in breaking of the oil present on the water surface to form emulsion. In addition, the type of emulsion formed and its stability with changing pH and salinity after application of chitosan-based material was also studied as follows (Papers I-II, IV)

- Development of water soluble chitosan derivative and its applicability in the formation of emulsion with marine diesel, diesel and marine 2T-oil
- Development of amphiphilic chitosan as a surfactant or an emulsifier for removal of marine diesel from water surface

- Study the effect of pH, salinity and temperature in the behaviour of emulsion
- Recovery of oil from emulsified oil using different quality of water
- Development of bio-based surfactant use in the formulation of dispersants to enhance the sustainability and bio-remediation

The suitability of chitosan-based materials was also tested for the removal of dyes such as methylene blue (MB), safranin O (SaO) and Tartrazine (Tart) along with divalent metal ions from the water resources (Paper III). In this study, effect of pH, ionic strength, temperature, contact time and presence of competing ions were examined. In addition to these, adsorption behaviour (kinetics, isotherms and thermodynamics) and corresponding experimental data were also estimated with different theoretical models such as Bangham, Weber-Morris, Langmuir, Freundlich, Tekmin, Dubinin-Radushkevich, and Sips, along with pseudo-first and -second order.

2 State of the art

2.1 Emulsions

An emulsion is a thermodynamically unstable system consisting of at least two immiscible liquid phases, one of which is dispersed as globules in the other liquid phase. In an ideal emulsion system, small volume fraction is classified as dispersed phase (oil) and larger as continuous phase (aqueous/water) or in other ways, the droplet phase is called the dispersed phase and the liquid in which the droplets are dispersed is called a continuous phase. The boundary between these two phases is known as an interface. Interfacial tension (IFT) is the amount of energy required to increase the interfacial area between two immiscible liquids, i.e. oil and water. In other words, IFT is the force per unit length existing at the interface between two immiscible liquid phases. Generally, the IFT of oil-water interfaces are higher, but the presence of some polar groups in the organic liquid might reduce the IFT. For example, IFT of oleic acid is ~15.7 mN m^{-1}, whereas that of octanol is ~8.5 mN m^{-1} (Barnes and Gentle, 2011). The substances stabilised these two immiscible phases are called emulsifying agents.

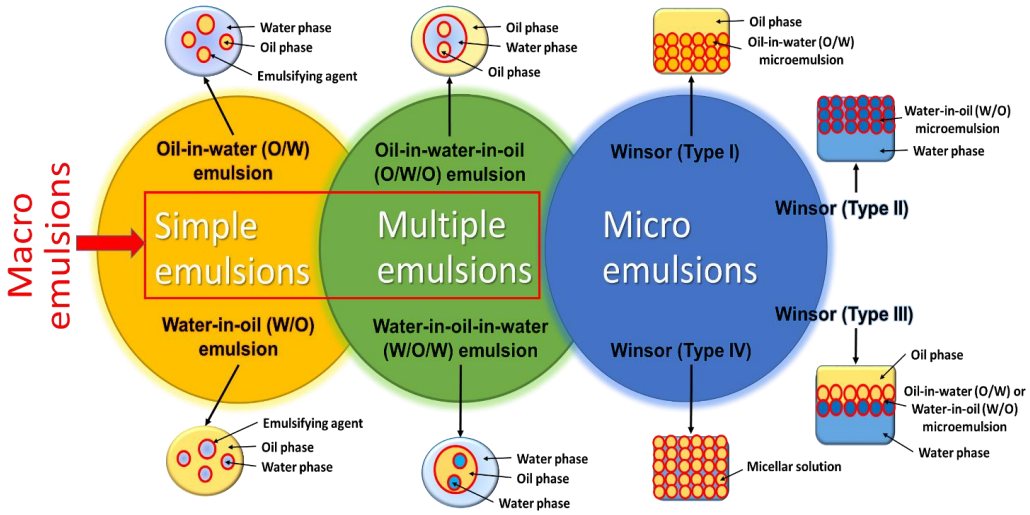

Figure 2.1: Classification of emulsion systems based on dispersed phase and size of liquid droplets.

The classification of different types of emulsion is mainly based on dispersed phase and size of liquid droplets (Figure 2.1). The dispersed phase emulsions are either simple or multiple emulsions. The emulsion in which oil is the dispersed phase and water as the continuous phase is called oil-in-water (O/W) emulsion and vice-versa is called water-in-oil (W/O) emulsion. Multiple emulsions are the complex polydispersed systems, where o/w and w/o emulsions exhibit simultaneously which are stabilised by the surfactants. These emulsions which comprise two water layers with a centre oil layer is water-in-oil-water (W/O/W) emulsion and vice versa is oil-in-water-in-oil

(O/W/O) emulsion. Moreover, in macro-emulsions (simple and multiple emulsions), the droplets size is 0.2–50 mm, whereas in micro-emulsions it is 0.01–0.2 mm (Eastoe, 2003), respectively. Micro-emulsions are thermodynamically stable, clear, isotropic liquid mixtures of oil, water and surfactant, frequently in combination with co-surfactant (Sharma and Shah, 1985; Wennerström et al., 1997).

Winsor proposed four types of microemulsions (see Figure 2.1, right most part) based on the behaviour of surfactant (Winsor, 1947). In type I, the surfactant is soluble in water and co-exist with oil phase to form O/W microemulsion as the bottom layer, and the excess of oil as the upper layer. In type II, the surfactant is present in the oil phase and co-exist with aqueous phase to form W/O microemulsion as the upper layer, leaving the excess aqueous layer at the bottom. In type III, the surfactant co-exist with the aqueous and oil phase, which resulted either in O/W or W/O microemulsions at the middle, leaving excess of oil as the upper layer and excess of aqueous layer at the bottom. In type IV, there is a formation of single phase (isotropic) micellar solution, due to the addition of surfactant and alcohol.

Pickering emulsions are emulsions stabilised by solid particles, with similar properties to classical emulsions stabilised by surfactant, which can be either o/w-, w/o- or multiple emulsions (see Figure 2.2). So far, the Pickering emulsions have attracted more interest in the field of nanoparticles, as they form kinetically stable emulsions through a physical barrier and not by decreasing the tension between the phases. In other ways, particles undergo Pickering emulsions via irreversible adsorption at the liquid-liquid interface to stabilize emulsions (Rayner et al., 2014; Yang et al., 2017; Calabrese et al., 2018) . The exchange of particles between the droplets in Pickering emulsion is also presented (French et al., 2015). The particles must be small enough for effective Pickering emulsion and to regulate the size of the oil droplets, while larger particles will improve steric hindrance and prevent coalescence (Aveyard et al., 2003; Kalashnikova et al., 2013; Matos et al., 2017).

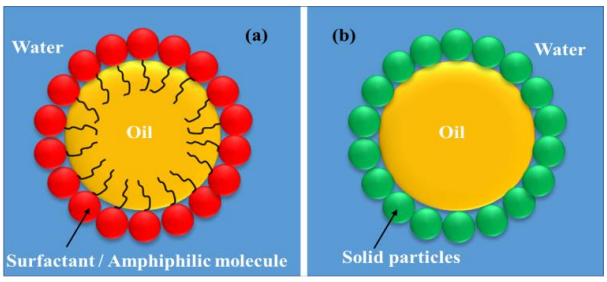

Figure 2.2: Schematics of (a) o/w classical emulsion and (b) o/w Pickering emulsion.

2.2 Emulsion stability

Emulsifiers are typically amphiphilic molecules that have both hydrophilic and hydrophobic groups on their surfaces, and the nature and effectiveness of the emulsifier influence the stability of emulsion. The primary source of attraction between the colloidal particles of similar composition

is Van der Waals forces (see Figure 2.3), and emulsion remains stable only when the strong repulsive forces counteracts the Van der Waals attraction. Furthermore, interparticle forces existing among particles in aqueous phase also includes repulsive hydration/solvation force caused by water or other water-interacting molecules adsorbed on the surfaces, attractive or repulsive electrostatic force due to ions on the surfaces, and attractive hydrophobic force imposed by hydrophobic polymer chains that are anchored to the particle surfaces along with attractive Van der Waals forces. However, the attractive and repulsive interactions between the droplets in oil-in-water emulsions are determined by the type of emulsifier, i.e. when the attractive interactions dominate, the droplets in the emulsion will adhere each other towards coalescence, whereas, if the repulsive interactions increases, the droplet remains stable in an emulsion (McClements and Gumus, 2016).

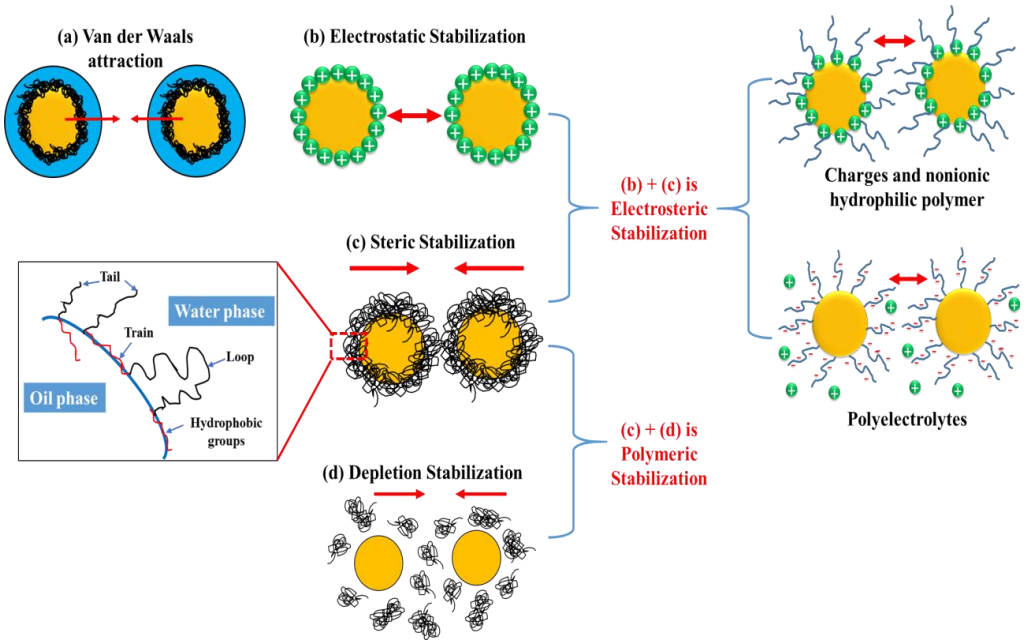

Figure 2.3: Schematics of (a) Van der Waals attraction, (b) electrostatic stabilization (c) steric stabilization and (d) depletion stabilization. Schematics of electrosteric stabilization for charged and nonionic hydrophilic polymers as well as polyelectrolytes.

Electrostatic stabilization is attained via the electrostatic repulsion between net surface charges caused by ionization of surface atoms, binding of solution ions, and ion exchange between surface and solution (McClements and Gumus, 2016). So, the particle will be surrounded by an equal number of oppositely charged counterions in the dispersion media to form charge-neutral double layers, which provides stability (Schatz et al., 2004). Generally, particles with an electrical double layer attain stability by electrostatic or charge stabilization (Hierrezuelo et al., 2010). However, with polymeric emulsifier, the stabilization mechanism also includes steric stabilization (particles

with adsorbed or chemically attached polymeric molecules) and depletion stabilization (particles with free polymer in the dispersion medium) as presented in Figure 2.3. The combination of electrostatic and steric stabilization is called electrosteric stabilization, whereas, the combination of steric and depletion stabilization is referred as polymeric stabilization (Barnes and Gentle, 2011).

Oil-in-water emulsions, along with thermodynamic instability, also become physically unstable due to physiochemical processes such as gravitational separation (creaming/sedimentation), flocculation, coalescence and phase separation (refer Figure 2.4). This instability is mainly dependent on the nature of the emulsifier.

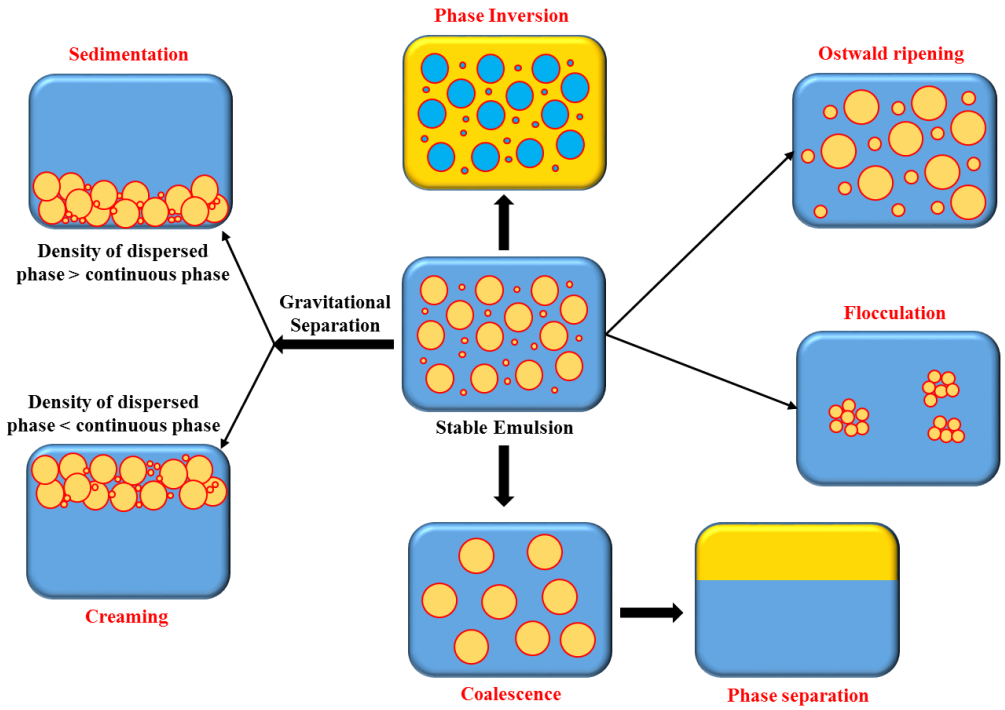

Figure 2.4: Emulsion instability mechanisms in the emulsion system.

2.3 Surface-active agents

The surface-active agents (surfactants) reduce the interfacial tension between the dispersed and continuous phase, by orienting the hydrophilic groups towards aqueous phase and the hydrophobic groups towards oil phase. This forms a layer around the droplets of dispersed phase, which might be either rigid interfacial film or double electrical layer that prevents the coalescence of the droplets. Moreover, the interfacial film can be either mono molecular, multi molecular or solid particle films. The emulsifying agents have both hydrophilic part (called head) and lipophilic part

(called tail) in their chemical structure, which can be easily adsorbed onto the oil and water interface to form stable emulsions. The spontaneity of emulsions mainly depends on the type and structure of the surfactant. For W/O/W emulsions, at least two surfactants are required, out of which one is predominantly lipophilic for stabilising the primary O/W emulsion and the other is hydrophilic for the secondary O/W emulsion.

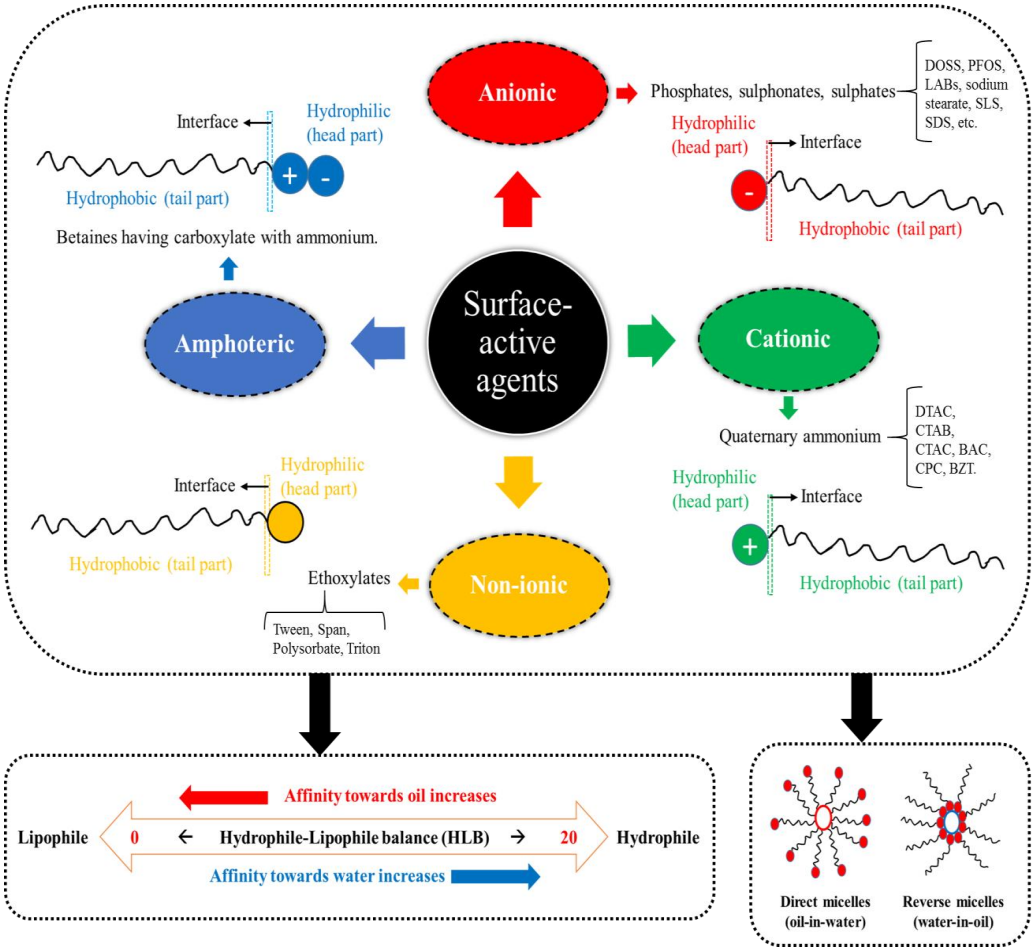

Figure 2.5: Classification of surface-active agents (surfactants) based on polarity of hydrophiles along with hydrophile-lipophile balance and micelles formation.

Surfactants mainly acts as wetting agents, emulsifiers, foaming agents and dispersants. They are classified on the basis of the molecular composition and the polarity of their head groups, as anionic, cationic, non-ionic and amphoteric (zwitterionic) (Oldehhove de Guertechin, 2001). As

mentioned in Figure 2.5, the hydrophobic part (tail) is always non-polar, that has no affinity for aqueous solvents, whereas, the hydrophilic part (head) always has affinity towards water. Anionic surfactants comprised of negative charge head, cationic surfactants comprised of positive charge head, and, for non-ionic surfactant there is no charged groups on the head. Moreover, the amphoteric (zwitterionic) surfactants have both positive and negative charged centres attached to the same molecule and so they are pH sensitive.

In addition to this, gemini-surfactant was introduced, which composed of two identical single chain surfactants covalently bonded by a spacer (Menger and Littau, 1991). This type of surfactant is generally cationic in nature and used in detergents, cosmetics, paint industry, pharmaceuticals, textile, enhanced oil recovery and many other branches of life (Brycki et al., 2017). Therefore, in case of ionic (cationic, anionic and amphoteric) together with a single hydrocarbon chain, microemulsion is formed in the presence of co-surfactant and/or electrolyte, whereas, for non-ionic and double chain ionics surfactants, co-surfactant is not required (Eastoe, 2003).

The selection of surfactant/emulsifier mainly depends on its hydrophile-lipophile balance (HLB), since they consist of hydrophilic and lipophilic groups (Griffin, 1947). The ratio of these groups determines the HLB number. For non-ionic surfactants, the HLB values ranges from 0–20, where, HLB value >10 have affinity towards water (hydrophilic) and HLB value <10 have an affinity for oil (lipophilic). For W/O emulsion, the HLB value should be 3.5–6, while for an O/W emulsion it should be 8–18 (Barnes and Gentle, 2011).

The self-assemble of surfactant molecules dispersed in a liquid colloid is known as micelle (Bordel and Giesecke, 2007). For the water and oil phase, the micelles formation is either direct or reverse/inverse (as shown in Figure 2.5). When the hydrophilic head is in the shell and the hydrophobic tail is pointed in the core region, the obtained segment is known as direct micelles (for the oil-in-water micelle), whereas, when the head groups are at the core with tails extending out are called as the inverse/reverse micelles (for water-in-oil micelle). The process of forming micelle is known as micellization. Sometimes, the solubility of the sparingly soluble substances increases in the solution containing micelles, as these molecules gets trapped in the micelles, and this process is called solubilisation. The lowest concentration at which the formation of micelles begins is called as the critical micelle concentration (CMC), or in other way, the CMC is the point at which the surfactant molecules aggregates together in the liquid to form micelles. The CMC is determined by plotting the graph of surface tension, conductivity or turbidity as a function of concentration. Despite that, CMC is mainly affected by the solubility of surfactant, but the chain length of the hydrophobic groups in the amphiphile, electrolyte concentration, temperature and the presence of other polar additives also affecting CMC (Barnes and Gentle, 2011). The CMC decreases with the increase in the alkyl chain of the surfactant. Cationic surfactants have slightly higher CMC compared to anionic, but for non-ionic, the CMC increases as the polar head becomes larger. Furthermore, ionic surfactants bearing inorganic counter-ions have higher CMC compared to organic counter-ions.

The surfactants, which are amphiphilic can be used as the oil-spill response in two different ways: either as dispersing agents, which can break down the oil into small droplets to enhance the natural

biodegradability (Lessard and DeMarco, 2000), or as herding agents, which can thicken the thin oil slick sufficiently to enable the in-situ burning of the oil (Buist et al., 2011). Their efficacy has been demonstrated also in the Arctic oil-spill response using synthetic surfactants. (Belore et al., 2009; Wang et al., 2013) Hence, in the field of oil spill, there is a major role of surfactants. Furthermore, synthetic dispersing agents, such as Corexit 9500 and 9527 (whose main surfactant was DOSS), were used during the Exxon Valdez oil spill in Alaska followed by Deepwater Horizon in Gulf of Mexico. Despite of their effectiveness, traces of these dispersants in water left negative impact on human and marine ecosystem, which had questioned their formulation (Zheng et al., 2014; Almeda et al., 2014). Consequently, countries such as the United Kingdom, Denmark and Sweden have banned the use of the type of synthetic dispersing agents used during Exxon Valdez and Deepwater Horizon oil spills. Therefore, nowadays, bio-surfactants or biopolymer-based surfactants are focused more than synthetic surfactants for the oil spill response, due to their non-toxicity, biodegradability and sustainability.

2.4 Chitosan

Chitin is the second most abundant natural polymer obtained from cell walls of fungi and exoskeletons of various organisms such as crustaceans (e.g. crabs, lobsters and shrimps) and insects (Kurita, 2006; Rinaudo, 2006), which is a major source of surface pollution in coastal areas (FAO, 2016). Therefore, utilisation of leftover chitin would reduce the amount of sea-waste (Yan and Chen, 2015). Chitosan is obtained from the deacetylation of chitin (Figure 2.6), and typically the degree of deacetylation is >60%. Chitosan is composed primarily of glucosamine or 2-amino-2-deoxy-β-D-glucose, which is also known as (1→4)-2-amino-2-deoxy-(D-glucose). Moreover, the deacetylated amino groups of chitosan undergo protonation and enhance the solubility of chitosan in acidic medium (pH < 6.5). However, the biggest challenge is to improve the solubility of chitosan at pH > 6.5, as in alkaline condition, it tends to agglomerate and form gels. Hence, the solubility of chitosan can be modified by introducing functional moieties into the polymer. Despite of chemical modification, the fundamental skeleton remains intact in modified chitosan, which retaines the original physicochemical and biochemical properties, and incorporate improved properties.

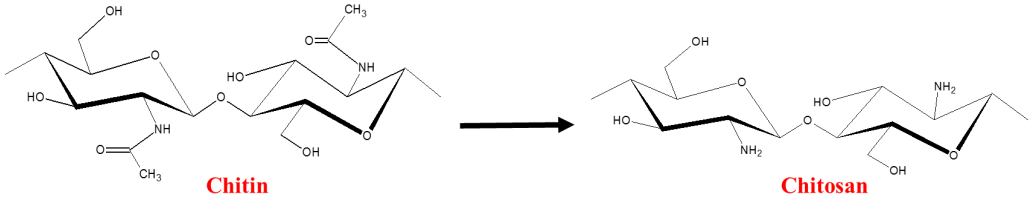

Figure 2.6: Structure of chitin and chitosan.

Chitosan, because of its abundance, versatility, non-toxicity and biodegradability (Khor and Lim, 2003), is widely used in the field of biomedicine, cosmetics, pharmaceuticals, and food industry

(Shahidi et al., 1999; Majeti, 2000; Suh and Matthew, 2000; Di Martino et al., 2005; Muzzarelli, 2009; Dash et al., 2011) as a biomaterial as well as in wastewater treatment (Guibal, 2004; Crini and Badot, 2008; Bhatnagar and Sillanpää, 2009; Ngah et al., 2011) as a sorbent. Generally, the oily wastewater is in complex acidic, alkaline or saline-conditions, and, therefore, it might be challenging to develop material for the removal of oil from the water in such a complex environment. Chitosan has many hydrophilic sites (hydroxyl and amine groups) and randomly distributed limited hydrophobic sites (acetyl amine groups) (Klinkesorn, 2013). The surface-active functional groups of chitosan can be modified by various methods (refer Figure 2.7), such carboxyalkylation, acylation, alkylation, cross-linking, grafting, ionic-gelation, etc. to produce particles, beads, microspheres, aerogels, hydrogels, foams and membranes. These materials can be effectively used for the oil spill treatment.

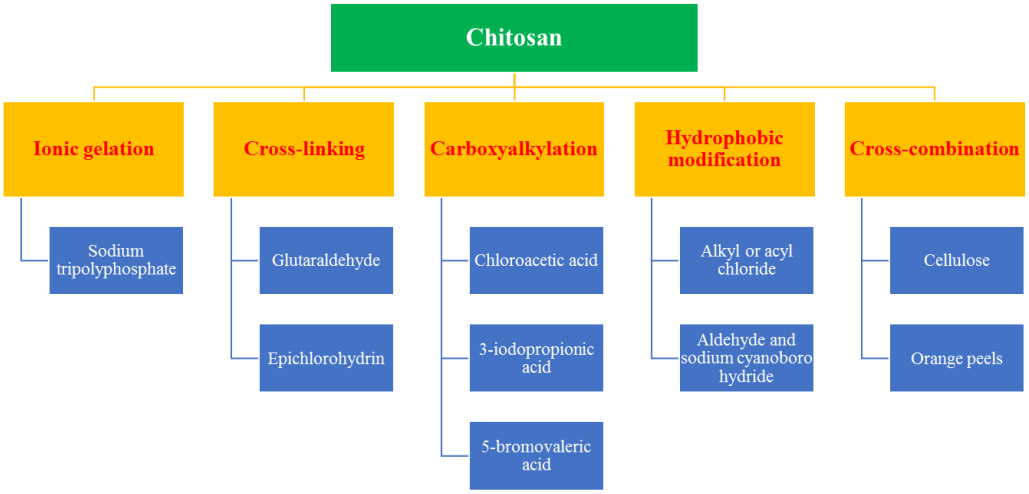

Figure 2.7: Schematic representation of various methods for the modification of chitosan.

Ionic gelation of chitosan with reticulating agent (sodium tripolyphosphate, STP) was formed between the amino groups of chitosan and negatively charged phosphate ions and successfully used to remove oil from the water at acidic pH (Grem et al., 2013). Although such type of ionic cross-linking is non-toxic, the reverse reaction might degrade the chitosan backbone. Simultaneously, the aggregation of STP-linked chitosan in neutral and alkaline solutions, limit its potential for surfactant application. On the other hand, the covalent cross-linking agents (i.e. glutaraldehyde, epichlorohydrin) improve its stability by preventing the dissolution of crosslinked material in acidic solutions. The aldehyde ends of glutaraldehyde crosslink with amine moieties of chitosan to form imine via Schiff's base reaction, whereas the epichlorohydrin (ECH) crosslink with hydroxyl moieties of chitosan. Although the amino groups were eliminated in ECH-crosslinked chitosan, the Glu-crosslinked chitosan was more effective than ECH-crosslinked chitosan in the removal of oil from water, because of its molecular mass and charge density (Farias et al., 2015). Despite of

effectivity, the toxic characteristics of the above described materials restrict their applicability, and hence, introducing oppositely charged moieties into the polymer is more practical for the oil spill applications.

Introducing carboxyl group onto the backbone of chitosan macromolecule through carboxyalkylation enhance the solubility of chitosan even at neutral and alkaline pH. In the carboxymethylation of chitosan (Chen et al., 2003; Chen and Park, 2003; Kalliola et al., 2016), the alkaline medium attributed in the swelling of chitosan for better diffusion of chloroacetate ion into its structure, and alcoholic medium facilitates the reaction (Paper I-II). The reactive functional groups (hydroxylic and amino groups) on the backbone, make chitosan a charged biopolymer, which via electrostatic attraction is capable of adsorbing oppositely charged emulsion droplets. However, the formation of protonated amino groups enhanced the solubility of chitosan in acidic solutions (Bée et al., 2017). This variable functionality of amino groups at a different pH tends to form aggregates through the hydrogen of amino groups and hydrophobic interaction, and hence, can be used as an emulsifier to stabilise oil-in-water emulsions (Aranaz et al., 2010; Colombo et al., 2015). However, the emulsion stability depends on the hydrophilicity and hydrophobicity of the modified chitosan.

Amphiphilic chitosan consists of polar and non-polar groups with its structure, where the polar part shows its affinity towards the aqueous phase and non-polar towards oil phase. Hydrophobic moiety was introduced onto the chitosan backbone either by alkylation, acylation, or grafting, which mainly interact with amino groups of chitosan. It has been observed that hydrophobically modified chitosan stabilised marine diesel (Paper II and Paper IV) and crude oil emulsions (Venkataraman et al., 2013) with saline water. Furthermore, the longer hydrophobic chains and the larger hydrophilic groups in amphiphilic copolymers, supports the enhancement of the micelles stability (Li et al., 2011). Therefore, amphiphilic chitosan can be used as a surfactant, either in the form of dispersing agent or herding agent. Furthermore, to expand the applicability and to minimise the hazardous effects/toxicity of chemicals in the marine ecosystem, a new approach of using bio-based blends have also developed. Recently, chitosan-based bio-polymeric blends (Fouad et al., 2016) and magnetic nanoparticles (Zhang et al., 2017; Soares et al., 2017) have also been studied for the removal and/or separation of oil from water resources. Chitosan-based materials used for the oil spill treatment are presented in Table 2.1. However, there are not much studies existing about the interactive chemistry between the modified chitosan in sodium form and oils for the oil spill treatment.

Table 2.1: Different form of chitosan-based materials used for the oil spill treatment

Materials *(Method)*	**Oils**	**Observations**	**References**
Biomass- M.Rouxii having 32.7% chitosan *(Shaking flask method)*	Mineral oil Vegetable oil Cutting Oil	77.2 mg g^{-1} (77%) 95.5 mg g^{-1} (93%) 84 mg g^{-1} (84%)	(Srinivasan and Viraraghavan, 2010)
H-Oleoyl-Carboxymethyl chitosan	Wastewater of oil extraction	>95% residual oil adsorption	(Sun et al., 2010)

(Carboxymethylation and acylation)			
Chitin Chitosan *(Powder form)*	Toluene	1.6 mg g^{-1} 2.2 mg g^{-1}	(Mohamed and Ouki, 2011)
Chitosan based polyacrylamide hydrogel *(Graft Polymerization)*	Crude oil	2.3 g g^{-1}	(Sokker et al., 2011)
Octyl carboxymethyl chitosan *(Carboxymethylation, acylation and reduction)*	Waxy Crude oil Fresh asphaltenic oil	Dispersion efficiency is 90% and 53%	(Al-Sabagh et al., 2012)
Chitosan microspheres *(Crosslinking with STP)*	Oil in water effluents of oil industry	90% removal	(Grem et al., 2013)
Copper mesh coated with CS-PVA-GA *(Immersing)*	Hexane	>99.0% separation efficiency	(Zhang et al., 2013)
Chitosan flakes Chitosan powder	Crude Oil	~0.379 g g^{-1} ~0.281 g g^{-1}	(Barros et al., 2014)
Stainless Steel (SS) with CTS-PFO/SiO_2 *(Gun spraying)*	Hexadecane	>99.0% separation	(Yang et al., 2014)
Aerogel membrane from Chitosan, Agarose, and Genipin *(Blending + Lyophilization)*	Bio-diesel, Oil-spill wastewater	>99% pure water	(Chaudhary et al., 2015)
Blends of poly (vinyl alcohol) nanoparticles with chitosan *(Emulsion polymerization)*	Toluene Kerosene Hydraulic oil	48.7 g g^{-1} 39.3 g g^{-1} 22.7 g g^{-1}	(Fouad et al., 2016)
Chitosan grafted with n-butyl acrylate *(Copolymerization grafting)*	Gasoil Mobil-1 oil Light crude oil Heavy Crude oil	~45% ~60% ~75% ~80%	(Mohy Eldin et al., 2016)
Stainless Steel (SS) coated with CS-SiO_2-GA composite *(Spraying)*	Gasoline Rapseed oil Petroleum Ether Toluene Bean Oil	>99.0% separation efficiency	(Liu et al., 2016)
Chitosan-silica hybrid *(Sol-gel encapsulation)*	Toluene, Cyclohexane	>90% removal efficiency	(Soares et al., 2017)

	n-heptane Chloroform		
Hydrophobically modified carboxymethyl chitosan (*Carboxymethylation, alkylation and reduction*)	Dodecane	pH switchable emulsification from free flowing to gel-like	(Kalliola et al., 2018)
Engineered clay from the mixture of kaolinite and chitosan *(Carbonization)*	Anadarko crude oil	Biodegradation of stable oil-in-seawater emulsions by alkane-degrading organism *Alcanivorax borkumensis.*	(Omarova et al., 2018)

3 Materials and Methods

3.1 Synthesis of Chitosan-based surface-active materials

Carboxymethylation, acylation and cross-linking methods were used for the preparation of chitosan-based surface-active materials. Three different types of chitosan, such as chitosan from crab shells (Ch-A, Paper I), chitosan from shrimp shells (Ch-B, Papers II and IV) and chitosan having high molecular weight (Ch-C) Paper III) were used for synthesising the materials. The scheme of the synthesis is shown in Figure 3.1 below.

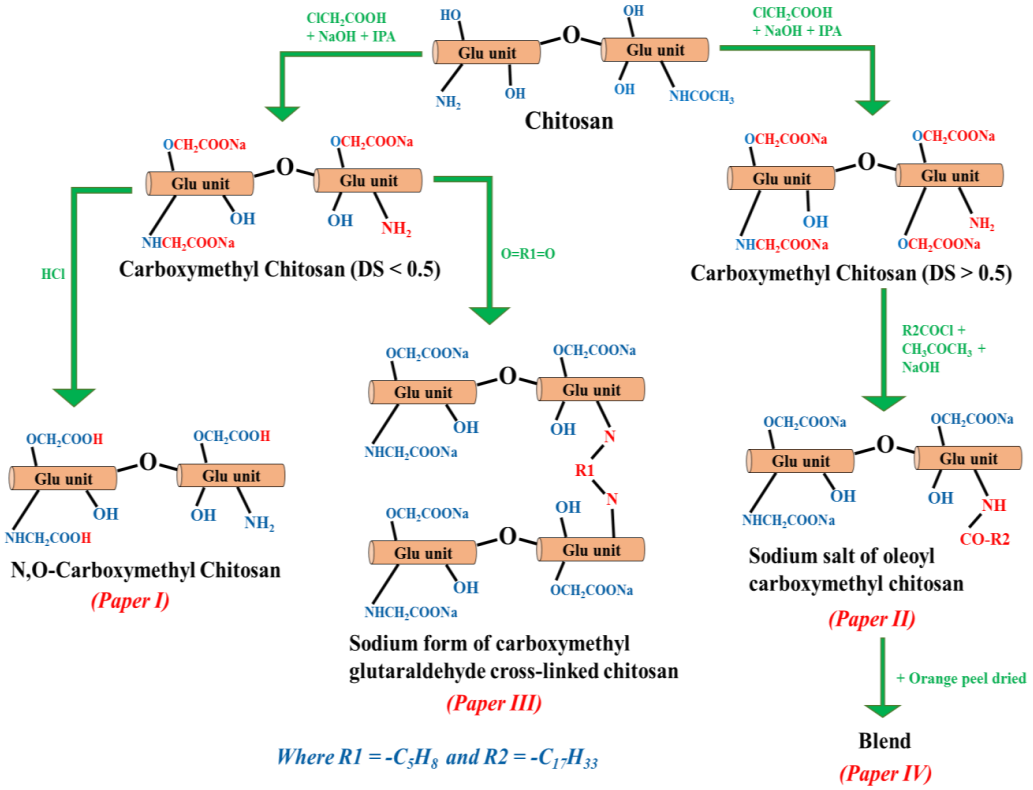

Figure 3.1: Synthesis of chitosan-based surface-active materials. The modification of functional groups is marked in red. The reagents used during the synthesis are marked in green.

3.1.1 Synthesis of N,O-Carboxymethyl chitosan

Carboxymethyl chitosan was synthesized using chloroacetic acid in hydro-alkaline reaction medium. Typically, Ch-A (5 g) was mixed with NaOH (5 g), IPA (40 ml) and water (100 ml) for

1 h at 50°C. After which chloroacetic acid in IPA (7.5 g in 10 ml) was added dropwise to it for 30 min and stir for 4 h at 50°C. Then after ethanol (70%, 100 ml) was added and washed with 70–90% ethanol. The product (Na-CS) was dried overnight at room temperature (RT). Na-CS (2 g) was mixed with ethanol (80%, 200 ml) and HCl (37%, 20 ml) for 1 h. The solid product was washed with 70–90% ethanol and dried overnight at RT. The final product is N,O-Carboxymethyl chitosan (NO-CS) (Paper I).

3.1.2 Synthesis of sodium salt of oleoyl carboxymethyl chitosan

The synthesis of carboxymethyl chitosan (Na-CS^{b}) is quite similar as described in section 3.1.1 with some modification. Typically, Ch-B (4 g) was mixed with NaOH (5.6 g), IPA (96 ml), and water (24 ml) at 50-55°C for 1 h. To this mixture, chloroacetic acid (6 g) dissolved in IPA (8 ml) was added over a period of 30 min, and the stirring was continued for 3 h at the same temperature. Then after (70%, 50 ml) was added and washed with 70–90% ethanol. The product (Na-CS^{b}) was dried overnight at RT. Na-CS^{b} (2.3 g) was soaked in acetone (10 ml) for 1 h at 5°C, after which oleoyl chloride (2.6 ml) dissolved in acetone (2.6 ml) was added along with 4M NaOH solution (10 ml) to the reaction mixture dropwise over a period of 30 min. Then after acetone (20 ml) was added and the reaction was continued for 3 h with same temperature. Finally, ethanol (70%, 60 ml) was added, and the washing and drying was performed as per the procedure mentioned in section 3.1.1. The final product is sodium salt of oleoyl carboxymethyl chitosan (NaO-CS) (Paper II).

3.1.3 Synthesis of sodium form of carboxymethyl glutaraldehyde cross-linked chitosan

Carboxymethyl chitosan (Na-CS^{c}) was synthesized as per method described in section 3.1.1. Here high molecular weight chitosan (Ch-C) was used instead of Ch-A. The obtained Na-CS^{c} (1 g) was mixed with glutaraldehyde solution (10%, 30 ml) and stirred for 30 min at RT. The product was washed with water and dried at RT for overnight. The obtained product is sodium form of carboxymethyl glutaraldehyde cross-linked chitosan (NaCS-GL) (Paper III).

3.1.4 Synthesis of orange peel combined carboxymethyl chitosan and its hydrophobic derivative

The details about the synthesis route for the powdered orange peels combined carboxymethyl chitosan and its hydrophobic derivatives cross-combination of chitosan with orange peel powder (Paper IV) has been mentioned in Figure 3.2. Orange peels were washed and dried at RT for 48 h. These dried orange peels were ground with tubemill and again dried for 24 h at 60°C giving the product OP-D. For the Blend, equal portions of OP-D and NaO-CS (Paper II) were mixed. For hydrophobically modified carboxymethyl chitosan-orange peels (CSOP-A), the mixture of Na-CS (1.2 g) (Paper II) and OP-D (1.1 g) was soaked in acetone (20 mL) for 1 h at 5°C. To this mixture, lauroyl chloride in acetone (1:1, 2.6 mL each) and NaOH solution (4 M) were added simultaneously after 30 min, and mixed continuously for 4 h at the same temperature. Ethanol (70%) was then added to the reaction mixture. The obtained solid was washed three times with ethanol (70–90%), dried overnight at RT and ground with tubemill. This obtained dried solid is CSOP-A (Paper IV).

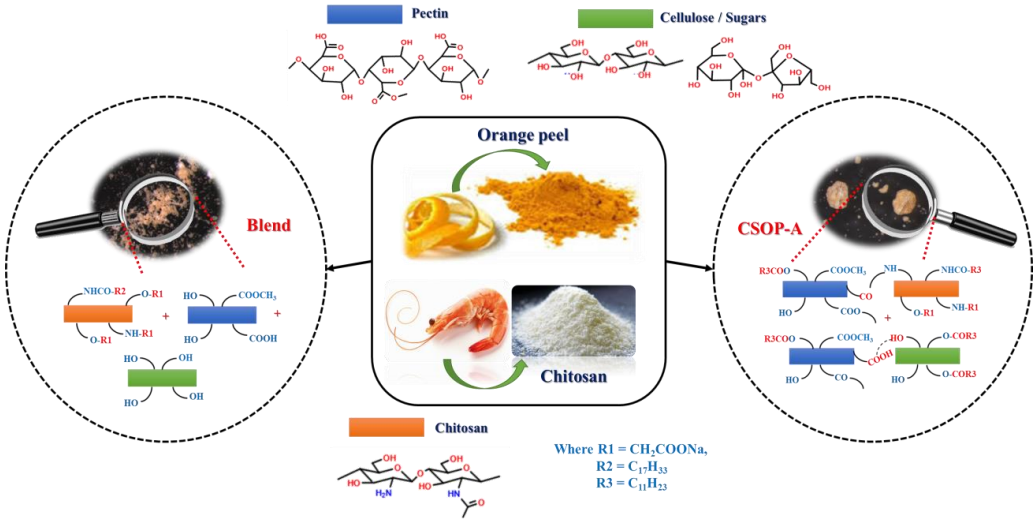

Figure 3.2: Synthesis of the Blend and CSOP-A along with the structural and functional change.

3.1.5 Synthesis of hydrophobically modified orange peel

In the synthesis of hydrophobically modified powdered orange peels (OP-A), OP-D (2.3 g) and acetone (20 mL) were mixed at 5°C for 1 h. To this mixture, oleoyl chloride in acetone (1:1, 2.6 mL each) and NaOH solution (4 M) were added simultaneously after 30 min, and mixed continuously for 4 h at the same temperature. Ethanol (70%) was then added to the reaction mixture. The obtained solid was washed three times with ethanol (70–90%), dried overnight at RT and ground with tubemill. This dried and ground solid is OP-A.

3.2 Characterisation

The degree of deacetylation (DDA) of chitosan was determined by acid-base titration. Briefly, 0.1 g of chitosan was dissolved in 25 ml 0.1 M HCl solution and titrated against 0.1 M NaOH solution using methyl red as an indicator. For blank reading, the same titration was performed without addition of chitosan. The DDA was calculated (Paper I) as follows:

$$DDA = \frac{(V_{initial} - V_{used}) * 0.162 * N * 100}{W * (1.00 - LOD)} \qquad (3.1)$$

where $V_{initial}$ (ml) is the volume of NaOH used in blank titration, V_{used} (ml) is the volume of NaOH used in sample titration, N is the molarity of NaOH, W (g) is the weight of sample, LOD is the loss on drying in chitosan sample.

Two different approaches were considered for the calculation of degree of substitution (DS). In the first approach, DS was calculated by the first order differential method using potentiometric titration mentioned in equation 3.2 as follows (refer Paper I for more details):

$$DS = \frac{(V_2 - V_1) * DDA}{(V_3 - V_2)} \quad (3.2)$$

Where V_1, V_2 and V_3 are the volumes of NaOH for neutralization of excess of HCl, followed by deprotonation of carboxylate ion and then deprotonation of ammonium ion, respectively.

In the second approach, DS was calculated from the CHNS elemental analysis using equations 3.3 and 3.4 as follows (refer Paper II for more details):

$$DS_1 = \frac{\left(\frac{C}{N}\right)_{Na-CS} - \left(\frac{C}{N}\right)_{Chitosan}}{estimated\ no.\ of\ carbon\ atoms\ in\ Na-CS} \quad (3.3)$$

$$DS_2 = \frac{\left(\frac{C}{N}\right)_{NaO-CS} - \left(\frac{C}{N}\right)_{Na-CS}}{estimated\ no.\ of\ carbon\ atoms\ in\ NaO-CS} \quad (3.4)$$

Where DS_1 and DS_2 are the degree of substitution of Na-CS and NaO-CS, respectively. C/N are the mol. ratio of carbon to nitrogen obtained from CHNS analysis.

Surface morphology of chitosan and its derivatives were studied by scanning electron microscopy (SEM) analysis using Hitachi SU3500 at an accelerating voltage of 10kV. Elemental distribution and composition were examined by EDS (Thermo Scientific UltraDry SDD EDS, dual detector with Software NSS at 15.0 kV accelerating voltage using Aluminium sample holder) and CHNS-Elemental Analyzer (Thermo Flash 2000 using tin sample holder). The Brunauer-Emmett-Teller (BET) surface area of chitosan and its derivatives was determined by nitrogen (N_2) adsorption-desorption method at 77.35 K using Micromeritics Tristar II plus instrument. The samples were degassed using Vac Prep 061 degassing unit with nitrogen at 30 °C for 18 h prior to the measurements. The total pore volume and average pore diameter were determined by the amount of nitrogen adsorbed at the relative pressure of 0.95 and BET (4V/A), respectively (Paper II-IV).

The functional group changes in chitosan and its derivatives were investigated using FTIR (ATR-FTIR, Bruker Vertex 70 model) in the range of 400 to 4000 cm^{-1} with a resolution of 4 cm^{-1} for 60 scans. Samples were measured without any further treatment (Paper I-IV). For ^1H NMR measurements, samples were dissolved in D_2O containing 0.7% of DCl and placed in 5 mm NMR tubes. The ^1H NMR spectra were recorded by using Bruker Ascend 400 MHz spectrometer and standard proton parameters with the delay time (d1) of 6 s at 70 ºC (Paper I-II). ^1H NMR spectrum was recorded with a Bruker Avance III spectrometer operating at 500 MHz for protons. Samples were dispersed in deuterium oxide doped with 1 m-% deuterated trifluoric acid and measured at room temperature (Paper IV). XRD patterns were recorded on a PANalytical X-ray diffractometer using Co Kα radiation (λ = 1.790 Å) operated at 40 kV and 40 mA in the 2θ range of 5–60° (Paper IV).

The zeta potential of chitosan-based materials was studied using Malvern Zetasizer (Nano ZS, Malvern UK) at 25.0 ± 0.1 °C. The presence of free amino groups in carboxymethylated chitosan was determined through potentiometric titration of 0.25% of chitosan solution (acidic) with 0.01M NaOH. The pH was measured by InoLab pH meter (WTW, calibrated before use). Moreover, the carboxylic acid content was determined by conductometric titration of 0.25% of chitosan solution (acidic) with 0.01M NaOH. The conductivity was measured using InoLab_IDS Multi 9310P equipment (WTW, Germany) and the amount of carboxylic acid content T_{CA} (mmol g^{-1}) was determined using equation 3.5 as follows (Paper III):

$$T_{CA} = \frac{C * V}{W} \tag{3.5}$$

where C (mmol L^{-1}) is the concentration of NaOH, V (L) is the NaOH volume to neutralize the carboxylate group and W (g) is the weight of sample.

3.3 Oil and its properties

The constituents of crude oil are saturates, aromatics, resins, and asphaltenes, in which light crude oil contains a higher percentage of saturated hydrocarbons and aromatics, while heavy oil contains more resins and asphaltenes (Fan and Buckley, 2002). Diesel fuel being a refined petroleum product, consists of either branched and/or linear hydrocarbon from C8-C26, whereas, marine diesel and diesel contains about 1.2% and 2% of polyaromatics, respectively. Marine 2T-oil being a petroleum distillate, consist of hydrocarbons, C11-C14, n-alkanes, isoalkanes, cyclics, solvent-dewaxed heavy paraffinic and polyaromatics (Neste, 2017). A small amount of diesel spills will usually evaporate and disperse naturally within a day or less, whereas, marine diesel persists longer when spilled. On the other hand, marine 2T-oil can easily react with water forming a creamy layer. Moreover, the behaviour of oil fluctuates with respect to environment, in which the oil spill had occurred. The details about the oils used during the studies is mentioned in Table 3.1.

In Arctic cold conditions, for example, the natural weathering process, such as evaporation and the biodegradation rate reduces resulting in increased oil viscosity (Wang and Fingas, 2003). Brandvik et al. demonstrated that the difference in oil film thickness affected the evaporation process, i.e. the evaporative loss for open water, lighter ice coverage and heavier ice coverage were about 30%, 25%, and 19%, respectively (Brandvik and Faksness, 2009). Hence, the climatic conditions and nature of oil plays a significant role in the oil spill response techniques.

Table 3.1: Physiochemical properties of oils.

Type of oil	Grade	Density at 15°C	Viscosity at 40°C	Colour
Marine diesel	Winter grade	828 kg m^{-3}	1.846 mm^2 s^{-1}	Pinkish red
Diesel	Summer grade	803 kg m^{-3}	2.1 mm^2 s^{-1}	Colourless
Marine 2T-oil	-	872 kg m^{-3}	8.5 mm^2 s^{-1}	Green

3.4 Emulsion experiments using water soluble/amphiphilic chitosan materials

3.4.1 Experimental setup

During the studies, different types of oils were used for performing emulsion experiments. The details about the experimental parameters are mentioned in Table 3.2. The oil to water ratio was 1:10 (v/v) throughout the studies. The solution containing chitosan-based material along with oil and water were mixed at 2000 rpm for 30 seconds using vortex mixture (VWR International) to form the o/w emulsion.

Table 3.2: Details about the experimental parameters for the emulsion experiments.

Material	Water	Oil	Experiments	Parameters	Paper
NO-CS	Deionised water	Marine diesel Diesel Marine 2T-oil	Dosage pH Salinity	0–5 g L^{-1} 1–1.5 g L^{-1} (pH 3–9) 1–1.5 g L^{-1} (0–3.5% salinity)	I
NaO-CS	Deionised and seawater	Marine diesel	Dosage pH Salinity Temperature	0–3 g L^{-1} 1 g L^{-1} (pH 5–8) 1 g L^{-1} (0–3.5% salinity) RT and 2 °C	II
OP-D Blend CSOP-A	Deionised and seawater	Marine diesel Marine 2T-oil	Dosage pH Salinity Temperature	0–2.5 g L^{-1} 2 g L^{-1} (pH 3.5–10.5) 2 g L^{-1} (0–4% salinity) RT, 2 °C and -20 °C	IV

After mixing, these solutions were rested for a day to evaluate the stabilization rate, i.e. the emulsion formation rate, as defined in the equation 3.6. The amount of separated oil was measured simultaneously to determine the coalescence rate (see equation 3.7) of oil after mixing and resting.

$$Emulsion\ formation\ rate\ (\%) = \frac{C_i - C_s}{C_s} * 100 \quad (3.6)$$

$$Coalescence\ rate\ (\%) = 100 - \left(\frac{C_i - C_s}{C_s} * 100\right) \quad (3.7)$$

where C_i (g) and C_s (g) are the initial amount of oil taken and the separated amount of oil collected after mixing and resting, respectively.

Firstly, the oil droplet size in o/w emulsion was measured immediately after mixing using optical microscope (Zeiss Axio using 206 the camera unit Axio CamERc5s by ZEN software). Then, the o/w emulsion was allowed to saturate and oil droplet size and stability of emulsion was studied periodically for about six weeks. The oil droplets size was also measured by laser diffraction particle size analyzer (Malvern Mastersizer 3000 with Hydro SV unit, UK). The mean droplet diameter at $D[4,3]$ was taken from five replicate measurements as the volume mean diameter, and the magnitude of the droplet size distribution is expressed by the span, defined in equation 3.8:

$$Span\ value = \frac{\{(Dx(90)) - (Dx(10))\}}{Dx(50)} \quad (3.8)$$

where *Dx(10), Dx(50),* and *Dx(90)* are the equivalent volume diameters at 10%, 50%, and 90% cumulative volume, respectively.

3.4.2 Quality of oil after removal and recovery

Even though the recovery of oil from the emulsified water has a significant value, it is always being challenging for the oil spill response. For these studies, emulsified layer formed using NaO-CS on the water surface was collected. To this collected layer, 10 ml of calcium chloride dihydrate solution (0.1%) was added and the mixtures were kept for 1 h to stabilise naturally. These experiments were performed at RT, and the separated oil was collected and weighed. The recovery of oil was calculated using equation 3.9.

$$R\% = 100 - \left(\frac{C_i - C_r}{C_i} * 100\right) \quad (3.9)$$

where C_i (g) and C_r (g) are the initial and recovered amount of oil.

The recovered oil was characterised using FTIR and GC-FID. The detailed GC parameters are mentioned below in Table 3.3.

Table 3.3: GC parameters for measuring the quality of oil before and after recovery.

Column	VF-5ht Fused Silica (15 m x 0.32 mm x 0.10 µm)
Liner	Split (Split ratio – 100:1)
Inlet Temperature	50 °C
Carrier	H_2, 9.0 psi
Oven	50 °C (1 min), to 180 °C (at 15 °C/min), to 230 °C (at 7 °C/min), to 380 °C (at 30 °C/min)
Injection	1 µL injection in hexane (0.1 mL/mL)
Detector	FID, 350°C
Standard used	C7 - C40 Saturated Alkanes, 1,000 mug/mL each component in hexane

The Ca-crosslinked NaO-CS was collected, dried and characterised using FTIR and SEM.

3.4.3 Water quality after the removal of oil

The determination of surfactant traces in the water resources after the removal of oil is an important factor for the marine ecosystem. For this study, the top oil layer (either emulsified or separate oil)

was removed and the aqueous layer was collected and tested using the NPOC method (TOC Analyzer, Shimadzu) in order to determine the amount of adsorbent traces in the water (Paper IV).

3.5 Adsorption experiments using NaCS-GL

In addition to the removal of oil, the removal of other pollutants such as dyes and divalent metal ions from water using chitosan derivatives was also studied. The details about the experimental parameters are mentioned in Table 3.4. The concentration of dyes and metal ions for the adsorption studies was 20 mg L^{-1}. These solutions along with NaCS-GL were shaken at 100 rpm, and then filtered through 0.45 μm polypropylene membrane filters. The MB, SaO and Tart concentrations were measured by Lambda 45 UV/VIS Spectrometer (Perkin Elmer, USA) at λ_{max} = 664, 520 and 430 nm, respectively. The Pb(II) and Cd(II) concentrations were measured by ICP (Agilent 5110 ICP-OES) (Paper III).

Table 3.4: Details about the experimental parameters for adsorption experiments.

Pollutants	Experiments	Parameters	Paper
Methylene blue (MB)	Dosage	0–2.5 g L^{-1}	III
Safranin O (SaO)	pH	0.8 g L^{-1} (pH 2–12) for dyes	
Tartrazine (Tart)		2.0 g L^{-1} (pH 2–8) for metal ions	
Pb(II) ions	Kinetics	0.8 g L^{-1} (with initial pH for MB and SaO,	
Cd(II) ions	Isotherms	pH < 3 for Tart) and 2.0 g L^{-1} (with initial	
	Thermodynamics	pH for metal ions)	

4 Results and discussions

Chitosan is a multi-nucleophilic polymer due to the presence of hydroxyl and amino groups onto glucosamine backbone. The chemical modification improves the properties of chitosan by keeping the fundamental skeleton of chitosan intact. For example, introducing carboxymethyl moiety onto the surface of chitosan enhances its solubility, which makes this derivative hydrophilic. Similarly, the addition of hydrophobic moiety (long chain hydrocarbon) makes this derivative amphiphilic, and widens its effectivity in a pH range.

4.1 Characterisation of chitosan-based materials

The characterisation of chitosan and its synthesised derivatives determines the nature of physiochemical properties before and after modifications.

4.1.1 Degree of deacetylation, degree of substitution and elemental composition

The process of deacetylation involves the removal of acetyl groups from the molecular structure of chitin, leaving behind the amino groups in the polysaccharides. Moreover, the degree of deacetylation (DDA) of each form of chitosan (Ch-A, Ch-B and Ch-C) slightly differs from each other (see Table 4.1), since the monomer units in different forms of chitosans are not identical.

Depending on the reaction conditions of carboxymethylation, there is a selectivity substitution site for N- versus O- carboxymethyl chitosan derivative. Despite of the enhanced water solubility of carboxymethyl chitosan, changing reaction conditions such as concentration of NaOH and monochloroacetic acid, and reaction time, the solubility was altered due to selectivity of the substitution site. Hence, the degree of substitution (DS) places a significant role in the properties of carboxymethylchitosan. The calculated values of DS are presented in the Table 4.1.

There were two outcomes for DS, first, increasing ratio of water/IPA in the reaction mixture, steeped down the fraction of chloroacetate ions, which, either aggregated the acetylation chain segments or thermal drying led to amide formation. This resulted in decrease of DS, which led to decrease in the solubility of NO-CS at higher pH (Paper I). Whereas, the second outcome reflects that decreasing the water/IPA ratio and increasing the alkaline concentration during carboxymethylation process, increased the fraction of chloroacetate ions and enhanced the DS (Paper II).

The elemental composition of chitosan and modified chitosans are shown in Table 4.1. The C/N ratio had increased from chitosan to modified form of chitosan, indicating the addition of carbon to the chitosan structure. The presence of sodium in the EDS results of chitosan derivatives (such as Na-CS[b], NaO-CS, Na-CS[c], Na-CS-GL, Blend and CSOP-A), and not in chitosan, confirms that the synthesised derivatives were in the sodium form.

Table 4.1: Degree of deacetylation, degree of substitution and elemental composition of unmodified and modified chitosan (Paper I-IV).

	Ch-A	NO-CS	Ch-B	Na-CS[b]	NaO-CS	Ch-C	Na-CS[c]	NaCS-GL	Blend	CSOP-A
DDA (%)	74	-	80	-	-	82	-	-	-	-
DS[a]	-	0.40	-	-	-	-	-	-	-	-
CHNS Elemental analysis (Wt%)										
C	-	-	40.26	27.73	34.98	40.38	39.82	40.85	29.67	32.86
N	-	-	7.85	3.30	1.99	6.86	6.02	4.71	0.43	1.10
H	-	-	6.05	2.39	5.20	6.41	6.88	5.56	4.12	5.08
O	-	-	-	-	-	41.49		30.62	36.71	33.06
C/N	-	-	5.13	8.40	17.61	5.89	6.61	8.67		
DS[b]	-	-	-	1.63	0.51	-	0.36	0.41	-	-
EDS Elemental analysis (Wt%)										
CK	57.3	50.4	47.1	29.0	36.7	45.1	45.31	54.5	65.79	58.65
NK	16.0	7.8				13.0	8.19	9.0	-	
OK	24.2	28.0	40.4	42.8	39.4	41.7	14.45	34.4	19.61	17.76
NaK	-	-	-	**23.4**	**22.4**	**-**	**1.63**	**1.7**	**7.92**	**19.22**
ClK	-	13.8	0.1	4.8	1.0	0.1	-	-	3.35	3.32
AlK	2.6	-	0.1	-	0.6	0.2	2.49	0.1	-	
AgL	-	-					27.35	-	-	

DS[a] and DS[b] are the degree of substitution calculated by titration method and C/N ratio by elemental analysis, respectively. Na-CS[b] and Na-CS[c] are the sodium salt of carboxymethylchitosan obtained from chitosan (shrimp shells) and chitosan (high molecular weight), respectively.

4.1.2 Surface morphology

The surface morphology of chitosan before and after modification was determined by SEM as presented in Figure 4.1. Figures 4.1a-c shows that the surface of chitosans were smooth, and Figures 4.1d-i shows that modification had enhanced the surface roughness of these modified chitosans. Moreover, the surface texture vary in Figures 4.1d-f due to different reaction mixture in the carboxymethylation process. There was a slit-like formation on the surface of NaO-CS after acylation (see Figure 4.1g), which enhanced surface roughness of NaO-CS compared to Na-CS (Figure 4.1e). Similarly, the surface roughness of Na-CS (Figure 4.1f) was enhanced in Na-CS-GL after glutaraldehyde crosslinking (Figure 4.1h). Since the Blend is the mixture of NaO-CS and orange peel, the surface of the Blend (Figure 4.1i) also has a similar slit-like formation as NaO-CS.

Even though the surface roughness of Na-CS was more than that of chitosan, the surface area and porosity dropped down due to the carboxymethylation. The BET surface area, pore volume and average pore diameter of chitosan from shrimps shells was 0.59 m^2/g, 0.0006 cm^3/g and 41.63 Å, respectively. After attachment of the long hydrocarbon chain, these results were 0.36 m^2/g, 0.0011 cm^3/g and 120.49 Å, respectively in NaO-CS (Paper II). The surface porosity in Na-CS-GL was increased after glutaraldehyde crosslinking (Paper III). The BET surface area of OP-D, CSOP-A and Blend was 0.09 m^2/g, 0.39 m^2/g and 0.34 m^2/g, respectively (Paper IV). This shows that

combining OP-D with chitosan derivatives enhances the surface structure of CSOP-A and Blend, so they were rougher and more porous than OP-D. The results are in a good agreement with the SEM results. Thus, the results shows overall enhancement in the BET surface area of modified chitosan by making the surface more porous.

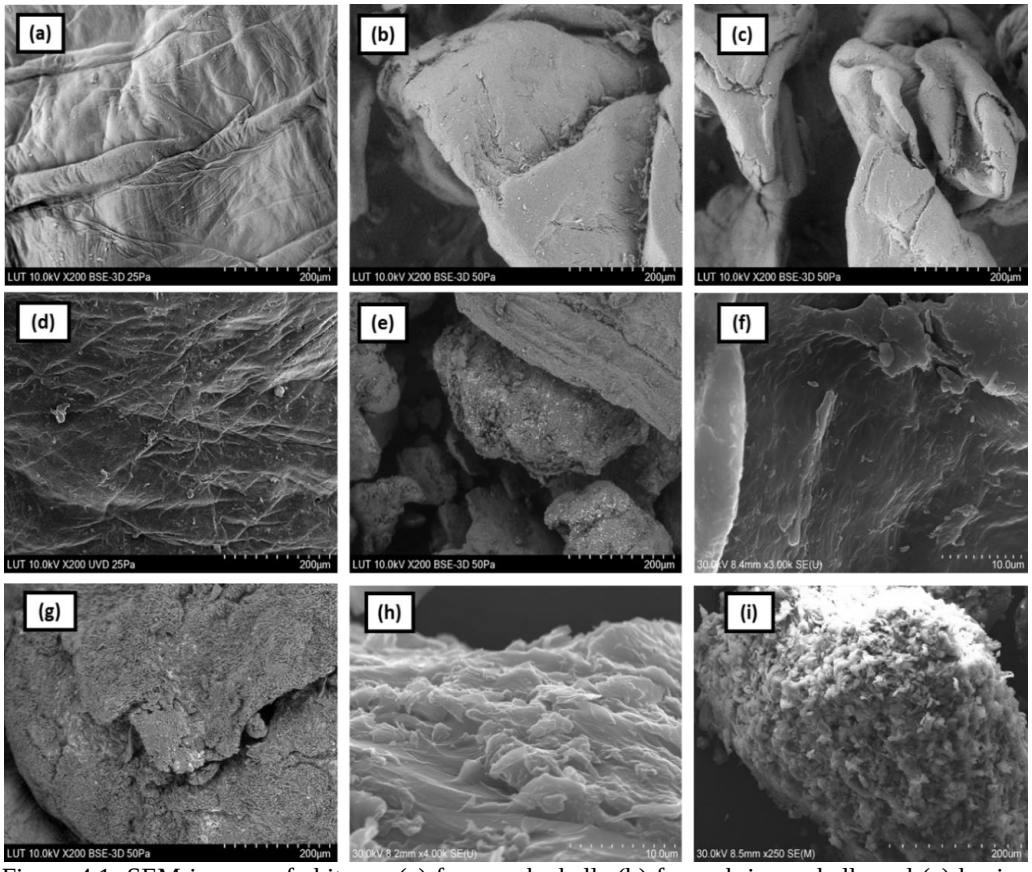

Figure 4.1: SEM images of chitosan (a) from crab shells (b) from shrimps shells and (c) having high molecular weight, (d) N,O-carboxymethyl chitosan obtained from crab shells chitosan, Na-CS after carboxymethylation (e) obtained from shrimp shells chitosan and (f) obtained from chitosan having HMW, (g) NaO-CS, (h) Na-CS-GL, and (i) Blend. All the images except (f), (h) and (i) were taken at accelerating voltage of 10 kV with the scale bars of 200 µm and magnification of x500. SEM images of (f), (h) and (i) were taken at accelerating voltage of 30 kV with the scale bars of 10µm and 200 µm and magnification x3.00K, x4.00K and x250, respectively.

4.1.3 Spectroscopic analysis

FTIR analysis

Table 4.2 summarises the FTIR characteristic bands of the studied chitosan and its synthesised derivatives. The presence of the bands corresponding to the amide/ester bonds and carboxyl groups in the prepared materials indicated the successful carboxymethylation onto the chitosan surface (Paper I-IV). Moreover, the characteristic band of oleoyl chains and amide in NaO-CS confirmed the attachment of oleoyl moiety to primary amine of the carboxymethylated chitosan (Paper II).

Table 4.2: FTIR characteristic bands of chitosan and modified-chitosan derivatives (Paper I- IV).

Materials	Band (cm^{-1})	IR vibration interpretation
Chitosan	3288-3352	O-H and N-H bonds, axial stretching
	2870	C-H bonds, axial stretching
	1650	C=O of the secondary amide (amide I), stretching
	1585	N-H bending of 2-aminoglucose units
	1150-897	C-O and C-O-C of the polysaccharide chain
NO-CS	3301	O-H and N-H bonds, axial stretching
	1734	C=O in the –COOH, symmetric stretching
	1249	C-O in CH_2COOH, stretching vibration
Na-CS[b]	1724	Acid C=O, stretching
	1589	C=O of $–CH_2COONa$ asymmetric stretching
	1416	C=O of –COONa symmetric stretching
NaO-CS	3279	Secondary N-H bond
	2920, 2850, 1442	C-H stretching of oleoyl chains
	1560	N-H (amide II)
CSOP-A	3400	–OH stretching
	2925, 2850	C-H stretching
	1564	Imine bond (C=N)
Blend	1733	–COO– stretching
	1589	–NH– group
	1016	C-O group
	1150-850	C-O, C-C and C-O-C of the polysaccharide chain having glycosidic bond and pyranoid ring
OP-D	1733	–COO– stretching
	1635	C=C stretching
	1150-850	C-O, C-C and C-O-C of the polysaccharide chain having glycosidic bond and pyranoid ring

^{1}H NMR analysis

The ^{1}H NMR spectra of chitosan and NO-CS (from Paper I), and, Na-CS[b] and NaO-CS (Paper II) are presented in Figure 4.2 (Note: refer Paper I and Paper II for magnified images).

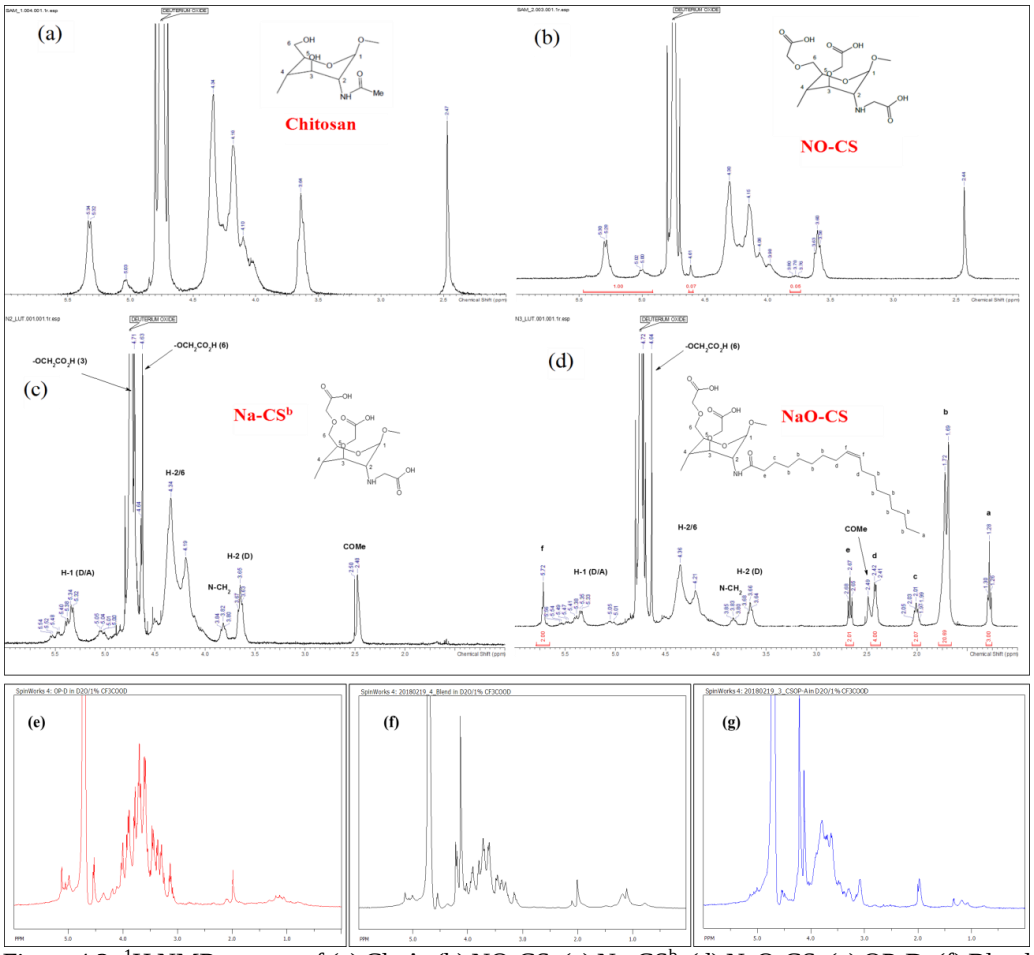

Figure 4.2**:** ^{1}H NMR spectra of (a) Ch-A, (b) NO-CS, (c) Na-CS^b, (d) NaO-CS, (e) OP-D, (f) Blend and (g) CSOP-A.

The spectrum of NO-CS (Figure 4.2a) showed the same characteristic proton signals as can be seen in chitosan spectrum (Figure 4.2b). Two new signals at 3.78 and 4.61 ppm which are assigned to N-CH_2- and -O-CH_2- protons at 2- and 6-positions, respectively, revealing that both the amino and hydroxyl groups are partly carboxymethylated in NO-CS, which was in good agreement with FTIR interpretation. The spectrum of Na-CS^b (Figure 4.2c) shows the similar characteristic proton signals as can be seen in NO-CS from our previous studies (Paper I). Moreover, the two peaks at 4.63 and 4.71 ppm are most likely the signals of -O-CH_2-CO- protons, which got overlapped with the peak of D_2O. The spectrum of NaO-CS (Figure 4.2d) shows the successful attachment of oleoyl substituent to Na-CS^b via amide linkage.

In the ^{1}H NMR spectrum of OP-D (Figure 4.2e), the signals at ~0.8–1.7 ppm are originating from the fatty components and the signals at ~1.9–2.2 ppm shows the presence of O-linked acetate (Bédouet et al., 2005). The spectral region of 3.0–6.0 ppm is associated to ring hydrogen, mainly the presence of sucrose, fructose, and glucose, as witnessed by their respective intensities and earlier literature results (Silva et al., 2012; de Oliveira et al., 2014). In addition to the above peaks, Blend (Figure 4.2f) also shows peaks near 3.7 and 4.1–4.6 ppm, which are attributed to carboxymethyl-protons as N-CH_2-CO- and O-CH_2-CO-, respectively. However, in the CSOP-A spectrum (Figure 4.2g), the reduction of peak intensities in this region compared to OP-D reflects that the –OH groups of sugars moieties present in OP-D might have been substituted during acylation. Moreover, in the CSOP-A spectrum, the peaks in the range of 1.1–2.0 ppm are attributed to the alkyl (CH_2 and CH_3) group of the lauroyl chain. Furthermore, the signal obtained at 2.0 ppm corresponds to –N=CH– linkage (Schiff base), obtained through linkage of –C=O– group of carbohydrate or pectin in OP-D with –NH_2 group of chitosan derivative (Gullón et al., 2016), and also attributed to the CH_2 groups of lauroyl chain. This is in a good agreement with the FTIR results. Moreover, the signals at ~0.8–1.7 ppm in the Blend are originated from the alkane proton of oleoyl chain as well as fatty components present in OP-D. Therefore, FTIR confirms the presence of functional groups in chitosan, before and after modification and the ^{1}H NMR results confirm the position of these functional groups onto the backbone of the chitosan molecule.

XRD analysis

The XRD spectra are shown in Figure 4.3. The intensity of the characteristic peak of chitosan about 23° reduces in Na-CS and NaO-CS after the carboxymethylation and acylation, respectively (refer Figure 4.3a). Furthermore, the peak about 32° is attributed to carboxymethylated part. Moreover, Na-CS and NaO-CS being in sodium form, the XRD pattern does not differ much.

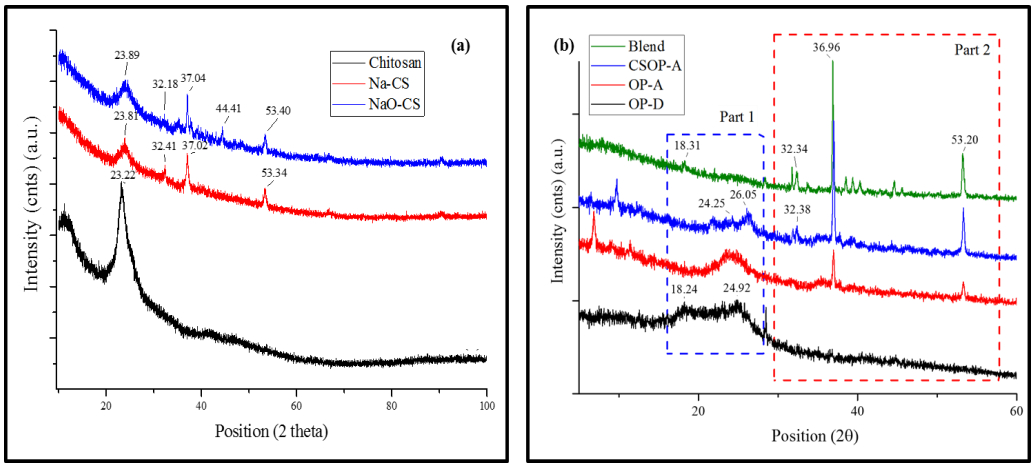

Figure 4.3**:** XRD pattern of (a) Chitosan, Na-CS and NaO-CS and (b) OP-D, OP-A, CSOP-A and Blend.

The XRD spectra of OP-D (Figure 4.3b) did not show any distinguished peak of minerals, concluding the nature of OP-D as amorphous, similar behaviour also observed previously (Mafra et al., 2013). Compared to the XRD pattern of OP-D, the diffractogram of OP-A, CSOP-A and the Blend showed sharper peaks indicating the formation of a new crystalline phase (see Figure 4.3b). The peak around 32° in CSOP-A and the Blend is attributed to the carboxymethylated part present in them, and similar results were observed previously for carboxymethylated chitosan (Patale and Patravale, 2011). After acylation, the peaks around 37° and 53° (see part 2 of Figure 4.3b) were observed in OP-A, CSOP-A and the Blend, which were absent in OP-D. Despite of the similar acylation procedure, the intensities of these peaks in OP-A were lower than the peak intensities of CSOP-A and the Blend. The reason might be that either the carboxymethylated part in CSOP-A and the Blend have influenced the peak intensities or there might be partial acylation in OP-A, or crystallinity in chitosan-based adsorbents, CSOP-A and the Blend might be higher compared to OP-A.

4.1.4 Zeta potential with changing moieties

The electrical properties of the surface play an important role presenting the interactions of surface-active moieties with the surrounding of charged particles. The charge acquired by a particle or molecule in a given medium is its zeta potential and arises from the surface charge and the concentration and types of ions in the solution. Since particles of similar charge will repel each other, those with high charges will resist flocculation and aggregation for longer periods making such samples more stable. This stability can be modified by altering pH, presence of electrolyte, types of ions and by using some additives.

The surface charge of modified chitosan with respect to pH and salinity is presented in Figure 4.4. The initial pH of NaO-CS, NaCS-GL, OP-D, CSOP-A, and Blend were ~10.2, ~9.2, ~5.6, ~10.1 and ~9.0, respectively, and the initial ZP of all these materials was negative. Furthermore, larger negative ZP inhibits the coalescence rate, and make the emulsions more stable (Chansiri et al., 1999; Dickinson, 2017). In case of NaO-CS, the magnitude of the electrical charge at higher pH was highly negative and tended to zero (at isoelectric point) at intermediate pH and then to positive values at lower pH as shown in Figure 4.4a. However, there was a sudden drop in the ZP (–48 mV to –54.8 mV) at pH 9, attributing to the dissociation of almost all Na^+ ions from the sodium carboxylate group of NaO-CS, which made the surface more negative. Moreover, there was protonation of amino groups followed by carboxylate groups by the addition of H^+ ions, which resulted in an increase of the ZP towards the isoelectric point. Furthermore, addition of H^+ ions made the surface more and more positive aligning the deprotonated carboxylate groups to get protonated (from –48 mV to +20.9 mV). On the other hand, Figure 4.4b shows the linear increase in the ZP of NaO-CS in the presence of electrolyte (from –28.1 mV to +4.2 mV), stating that the process of protonation and deprotonation on the surface of NaO-CS did not interfere significantly by the salinity variance except the change in the isoelectric point (Paper II). Furthermore, the glutaraldehyde cross-linked amino groups in NaCS-GL did not take part in the protonation process in the presence of H^+ ions. Hence, the surface ZP of NaCS-GL slightly altered compared to other chitosan derivatives (Paper III).

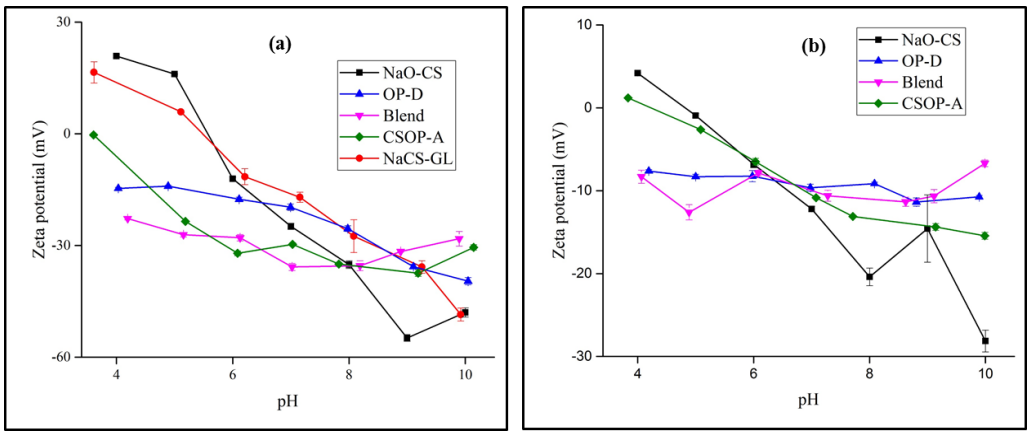

Figure 4.4: Zeta potential of modified chitosan in (a) deionised water and (b) seawater having ~3.5% salinity as a function of pH.

In OP-D, when pH is increased, dissociation of carboxyl group occurs, which then results in decrease in zeta potential value (i.e. more negative zeta potential). On the other hand, when pH decreases, carboxyl groups are associated (i.e. protonated), which results in neutralization of charge, thus increase in zeta potential. In case of CSOP-A and the Blend, simultaneous protonation of carboxyl and amino groups occurred with decrease in pH, which overall increases the ZP by neutralizing the charge. Hence, when pH is decreased to 4, the surface charge in all of the samples seems to be close to zero (i.e. no surface charge). Furthermore, the carboxymethylated groups in Blend and CSOP-A attributes to more negative surface than OP-D. The ZPs were less negative in seawater (SW) than in DI (Figure 4.4b). One reason could be the ions present in SW formed electrical double layer with the surface charges of these materials. Furthermore, there might be ion exchange between the surface charge and electrolyte with decreasing pH (Paper IV). Above mentioned results reflected that the hydrophobic moieties on the chitosan surface led to the formation of more negative surface ZP by inhibiting the protonation of amino groups. Therefore, there is a major role of surface active moieties of these chitosan derivatives in the interaction of other moieties such as oil or metal ions present in the water.

4.2 Oil-in-water emulsions

4.2.1 Interfacial tension (IFT) and wettability

The boundary between two phases is known as an interface. IFT is the amount of energy required to increase the interfacial area between two immiscible liquids, i.e. oil and water. In other words, IFT is the force per unit length existing at the interface between two immiscible liquid phases. IFT results were measured by the pendant drop method (Video-based contact angle instrument,

Dataphysics OCA 15EC Series) as shown in Figure 4.5a. The key parameter for the formation of stable oil droplets in an emulsion is the IFT between the water phase and oil phase.

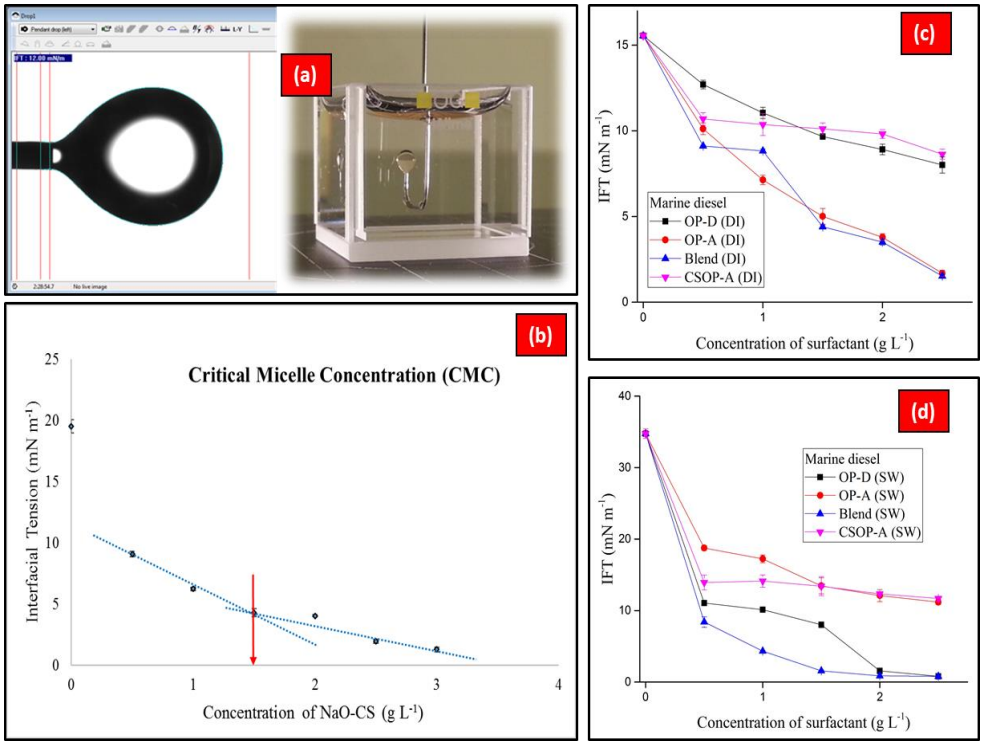

Figure 4.5: (a) Pendant drop method for the calculation of interfacial tension (IFT) using contact angle instrument and image capture by Dataphysics OCA 15EC Series software, (b) determination of CMC of NaO-CS in the presence of marine diesel. IFT between marine diesel and water phase (c) deionised water and (d) seawater in the presence of OP-D, OP-A, CSOP-A and Blend.

For the carboxymethylated chitosan (NO-CS) solution, the IFT obtained at 20 ^{o}C with marine diesel, diesel and Marine 2T-oil were 19.77, 19.01 and 20.45 mN m^{-1}, respectively (Paper I). The IFT between water and marine diesel in absence of NaO-CS was 19.53 ± 0.54 mN m^{-1}. Moreover, a small amount of NaO-CS reduced the IFT to half and the CMC was reached (refer Figure 4.5b) when the IFT was reduced by 70% of its original IFT (Paper II). The results showed that presence of hydrophobic chain in the structure of NaO-CS reduced the IFT drastically as compared to NO-CS, which in turn reduced the free surface energy associated with the formation of droplets. In case of chitosan cross-combined with orange peel, the initial IFT between marine diesel and water phase (DI and SW) without any surface-active material was 15.55 ± 0.08 mN m^{-1} and 34.76 ± 0.68 mN m^{-1}, respectively. A small amount of OP-D, OP-A, CSOP-A and Blend in DI reduced the IFT sequentially (Figure 4.5c), whereas with SW, this reduction was drastic (Figure 4.5d). This shows

that the presence of hydrophobic moieties made OP-A, CSOP-A, and Blend more amphiphilic similar to NaO-CS, which drastically reduced the IFT. At lower IFT, the free surface energy associated with the formation of droplets reduces, which enhanced the emulsion stability of oil and water in the presence of these materials, by forming smaller droplets with greater stability (Paper IV).

Surface chemistry and morphology determine the wettability of the surface, which closely relates to the adsorption of oils. Water contact angle is used to measure wettability. If the contact angle of a water droplet on a flat surface is less than 90°, it is characterized as hydrophilic, if the contact angle is between 90° and 150°, it is characterized as hydrophobic, and if the contact angle is over 150°, it is characterized as superhydrophobic. The wettability of the particles was determined by contact angle with sessile drop method. The contact angle of OP-D, Blend and CSOP-A were 63°, 83° and 113°, respectively. This shows that hydrophobic moieties in Blend and CSOP-A enhanced the contact angle as compared to OP-D. Kaptay also suggested that the optimum contact angle for the stabilization of emulsions by a single or double layer of particles is <90° or <129°, for o/w emulsion (Kaptay, 2006).

4.2.2 Chitosan surface-active moieties versus emulsion stability

The formation of emulsion and its stability was studied as a function of different surface-active moieties on the backbone of chitosan. However, it has been difficult to understand the complete behaviour of emulsion using polymers, as the substitution is not uniform in each monomer unit.

Emulsion stability with NO-CS

Since NO-CS was hydrophilic, increasing concentration enhanced the viscosity of the solution, which resulted in the formation of emulsions with marine diesel, diesel and marine 2T-oil. However, for marine diesel and diesel, the emulsion stability at a lower concentration of NO-CS was weak (refer Figure 4.6a), due to the unavailability of enough NO-CS. At a higher concentration of NO-CS, the emulsions were stable due to the formation of a tighter monolayer with adsorbed species and stronger interparticle interactions surrounding the oil droplets. This had resulted decrease in the coalescence rate of oil droplets due to electrostatic and steric barriers (refer Figure 4.6a). Moreover, there might be some free NO-CS molecules at higher concentration, which probably undergoes depletion stabilization. The case with marine 2T-oil was slightly different than the other two oils because of its composition. The alpha-olefins and paraffins present in Marine 2T-oil form creamy layer with water, and addition of small concentration of NO-CS had converted creamy layer of marine 2T-oil into emulsified precipitates. Although the droplet size was less than 100 µm (refer Figures 4.6b-c), the formation of stabilized oil droplets in the emulsion varied with the concentration of NO-CS. From the obtained results, it was concluded that NO-CS forms stabilized emulsion by adsorbing onto the oil droplets through electrosteric stabilization and the behaviour of emulsion mainly depends on the type of oil. Hence, NO-CS is more effective in the formation emulsions than parent chitosan, because of its hydrophilicity.

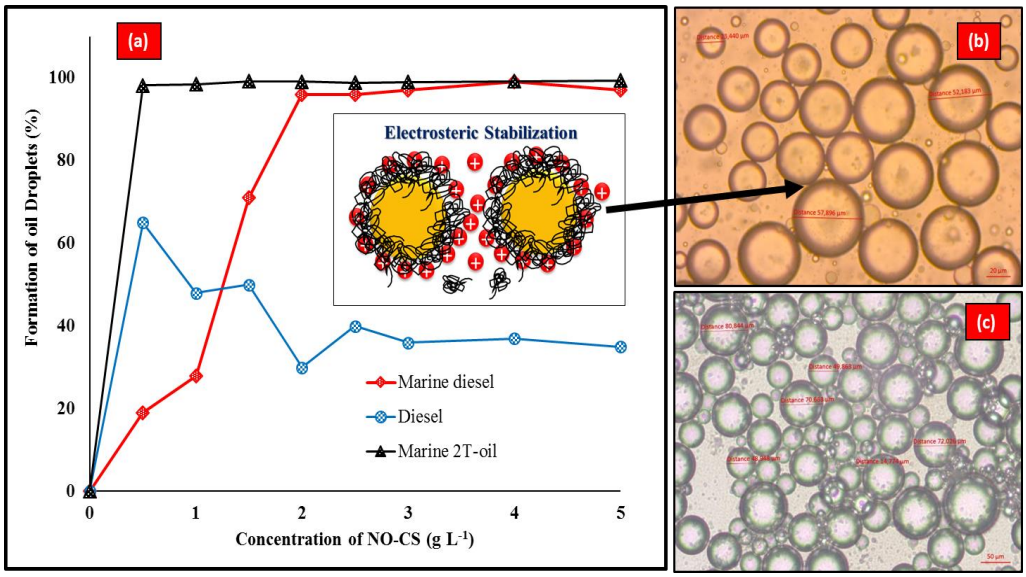

Figure 4.6**:** (a) Effect of NO-CS dosage in formation of oil droplets for marine diesel, diesel and marine 2T-oil along with stabilization mechanism. The microscopic images of emulsion (b) with diesel having 4 g L^{-1} of NO-CS and (c) with marine 2T-oil having 1 g L^{-1} of NO-CS.

Emulsion stability after hydrophobic modification of chitosan

The emulsion stability was studied by adding hydrophobic long carbon chain (oleoyl moiety) to the chitosan backbone. NaO-CS being amphoteric, can easily interact with aqueous and oil phase, and reduced the IFT. Figure 4.7 shows that the hydrophobic oleoyl tails interacted with the oil leaving the hydrophilic end to interact with water and resulted in the formation of stable creamy emulsion. Here the hydrophobic oleoyl moieties of NaO-CS got adsorbed onto the oil droplets and build up the steric repulsive barrier, so that the droplets in the emulsion did not adhere each other towards coalescence. Furthermore, the orientation of electrical charged groups of NaO-CS towards the aqueous phase generated electrostatic hindrance between droplets. These repulsive barriers reflected the stability of droplets in the formed emulsion. Hence, NaO-CS formed stable emulsion with marine diesel by a combination of electrostatic and steric stabilization. The emulsion mechanism is shown in Figure 4.7. Thus, the results confirmed that the hydrophobic modification of NaO-CS had enhanced the overall emulsification ability compared to NO-CS. The formation of creamy emulsion at the top indicates that the particles density in the dispersed phase is less than that in the continuous (aqueous) phase. The stability of this emulsion retained for more than 6 weeks and the average oil droplets size was ≤ 30 µm at RT (see Figure 4.7).

Moreover, the span value was 18.44 immediately after mixing, revealing a wide range of size distribution in the emulsion. Nevertheless, the span value decreased with time, i.e. the span value for o/w emulsion after 2 hours of mixing and after 6 weeks were 2.05 and 1.70, respectively, which

also favours the stability of creamy o/w emulsion (Paper II). The robustness of emulsion in the wave action was also verified by shaking the existing emulsion periodically, which retained the similar emulsion after few hours. The result concluded that addition of hydrophobic moiety onto the chitosan backbone enhanced the emulsion stability and this amphiphilic chitosan might act as an emulsifier for oil spill treatment. Therefore, in case of an oil spill, this type of the stable creamy emulsion can be skimmed away easily from the water surface.

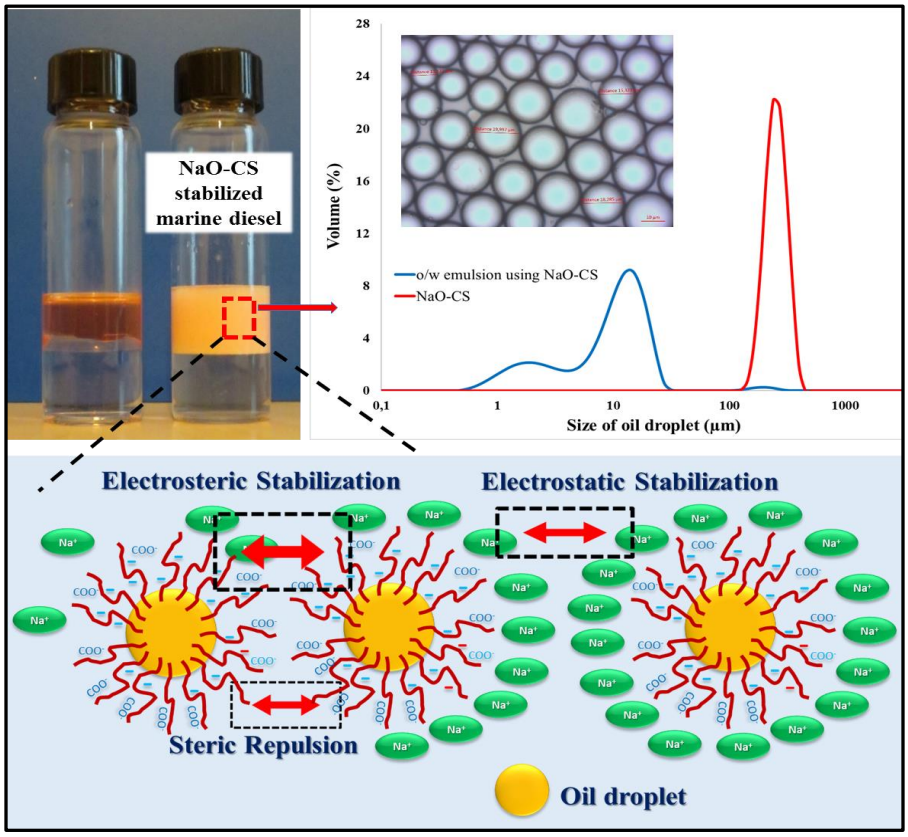

Figure 4.7**:** Stable o/w emulsion formation by NaO-CS along with emulsion mechanism, microscopic images of droplets and droplet size distribution in the emulsion.

Emulsion behaviour and stability for OP-D, Blend, CSOP-A and OP-A

Further studies show the effectiveness of chitosan derivatives combined with bio-waste such as orange peels in the formation of emulsion with oils. Figure 4.8a shows an increase in OP-D concentration in DI enhanced the emulsion formation rate from 5% to 70%, i.e. more and more oil molecules are broken down into oil droplets, which were stabilized by OP-D. This suggests the

adsorption of OP-D at the interface which resist against droplets coalescence via electrosteric stabilization. On the other hand, OP-D particles being smaller in size provides a barrier against droplets coalescence, resulting in solid-stabilized (Pickering) emulsion. Moreover, the effectiveness of the Blend and OP-A was more than 80% even with a low dosage (0.5 g L^{-1}). This reveals that the orientation of hydrophobic hydrocarbon segments (oleoyl groups) of the Blend and OP-A at oil-water interface have generated steric repulsion between the oil droplets. Furthermore, the magnitude of this steric repulsion between the droplets was enhanced with the increasing concentration of the Blend and OP-A, due to the dense packing and thick interface of the molecules around the oil droplets (see Figure 4.8b, mechanism part). This resulted in the enhancement of the oil droplets stabilization rate through the formation of stable emulsion.

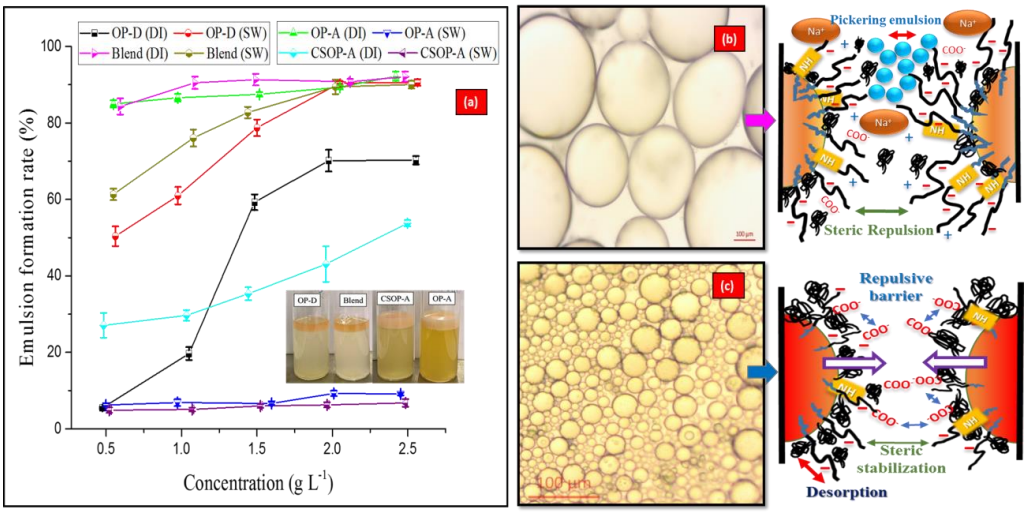

Figure 4.8**:** (a) Effect of OP-D, OP-A, CSOP-A and the Blend dosage in the emulsion formation of marine diesel with deionised water and seawater, along with the o/w emulsion with marine diesel image having 2.0 g L^{-1} of dosage in DI water. The microscopic images of o/w emulsion along with mechanism for (b) the Blend and (c) CSOP-A with marine diesel in DI water taken at a magnification of 100 µm.

Despite of hydrophobic moieties in CSOP-A, the maximum formation of o/w emulsion was about 50%. The reason could be the exposure of non-polar region to the surrounding water, which had started generating the hydrophobic attraction between the droplets (McClements and Gumus, 2016) due to rapturing of the steric repulsive interactions of CSOP-A from the oil droplets. This resulted in the aggregation of oil droplets and destabilized the emulsion (see Figure 4.8c, mechanism part). Although CSOP-A and Blend have a negative surface ZP in DI, the oil droplets stabilization rate (emulsion formation rate) varied in them due to the presence of different hydrocarbon segments. The effect of the hydrocarbon chain on oil droplets stabilization or emulsion formation was demonstrated previously (Shiao et al., 1998). In addition, lengthening the hydrocarbon chain also

enhanced ions exchange and hydrophobic interactions (Valandro et al., 2013; Benner et al., 2015). Hence, the interaction of CSOP-A with marine diesel differs from the Blend and OP-A.

The o/w emulsion behaviour was gel-like in a Blend due to the presence of OP-D, whereas with CSOP-A creamy emulsions were observed. Hence, the oil droplet size in the Blend (Figure 4.8b) and OP-D was >100 µm, whereas in OP-A (Figure 4.8c) and CSOP-A, it was <100 µm. The coalescence rate dominated the droplets stabilization rate with OP-A and CSOP-A in SW, whereas the presence of OP-D in the Blend showed more than 90% conversion of oil into emulsion, even at a very small dosage. This shows that water salinity decreases the critical micelle concentration of the Blend. Similar results were observed previously (Jiao et al., 2016). However, about 2.0 g L^{-1} of NaO-CS was required to form stable emulsion with seawater (Paper II). On the other hand, this study addresses that addition of OP-D to NaO-CS reduces the dosage to half with the same seawater.

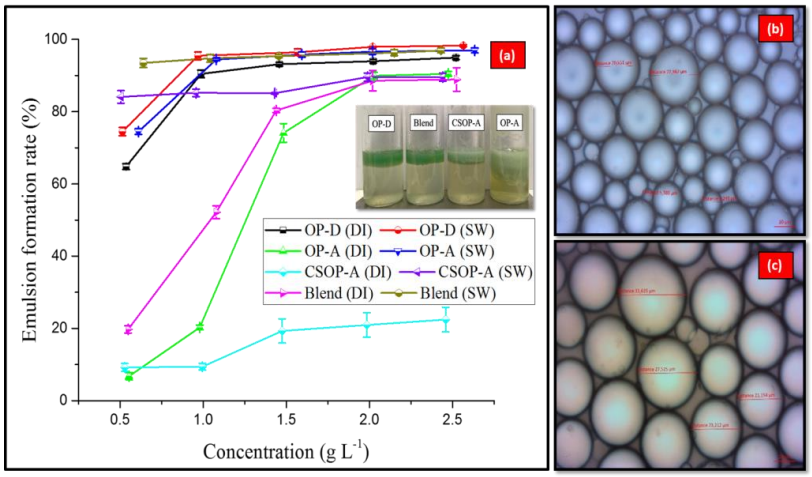

Figure 4.9**:** (a) Effect of dosage of OP-D, OP-A, CSOP-A and the Blend in emulsion formation of 2T-oil with deionised water and seawater, along with the o/w emulsion with 2T-oil image having 1.5 g L^{-1} of dosage in SW. The microscopic images of o/w emulsion for (b) OP-D and (c) CSOP-A with 2T in SW taken at a magnification of 10 µm.

Figure 4.9 shows the effect of dosage OP-D, OP-A, CSOP-A and the Blend on the emulsion formation rate with 2T-oil. The emulsion formation with 2T-oil (Refer Figure 4.9a) differs from marine diesel, because of its composition. 2T-oil being viscous, consists of solvent-dewaxed heavy paraffinic and polyaromatics, that can easily form a creamy layer with water even in the absence of oil emulsifier/surfactants. Furthermore, a small addition of either OP-A, OP-D, the Blend or CSOP-A converts this creamy layer to an emulsified layer. However, the droplets stabilization rate to formed emulsion is more likely to be dependent on the type of water for CSOP-A, as with DI the rate was approx. 22%, whereas with SW it was about 90%. This also shows that the presence of different hydrocarbon chains in CSOP-A might have affected the emulsion stability and

behaviour as discussed earlier. However, for the remaining materials, the droplets stabilization rate (emulsion formation) was more than 80% with DI and SW. Although the emulsion behaviours were not identical, the oil droplet sizes in the emulsions were <100 µm (Figures 4.9b-c). The result also presented that if the emulsion is gel-like, the oil droplet size would be greater than 100 µm, whereas, for creamy emulsion, the droplet size always falls under 100 µm (Paper IV).

4.2.3 Emulsion behaviour with different solution pH

The pH of the wastewater-containing oil or spilled oil plays a significant role in the applicability of the surface-active materials, especially organic sorbent used for the oil sorption (Rajaković-Ognjanović et al., 2008).

For NO-CS

NO-CS is hydrophilic and provides mainly steric barrier between the oil droplets to coalescence, however, the charge and conformation of the polymer affects the emulsion stability. The initial pH of the NO-CS solution was ~3.5–4.5, and when pH was slightly increased the oppositely charged groups (amino and carboxyl groups) of NO-CS underwent interchain interactions (Refer left most part of Figure 4.10). Excess of protonated amino groups of NO-CS provided electrostatic barrier to the oil droplets to coalescence along with the steric barrier. This resulted in stable o/w emulsion (Figure 4.10a).

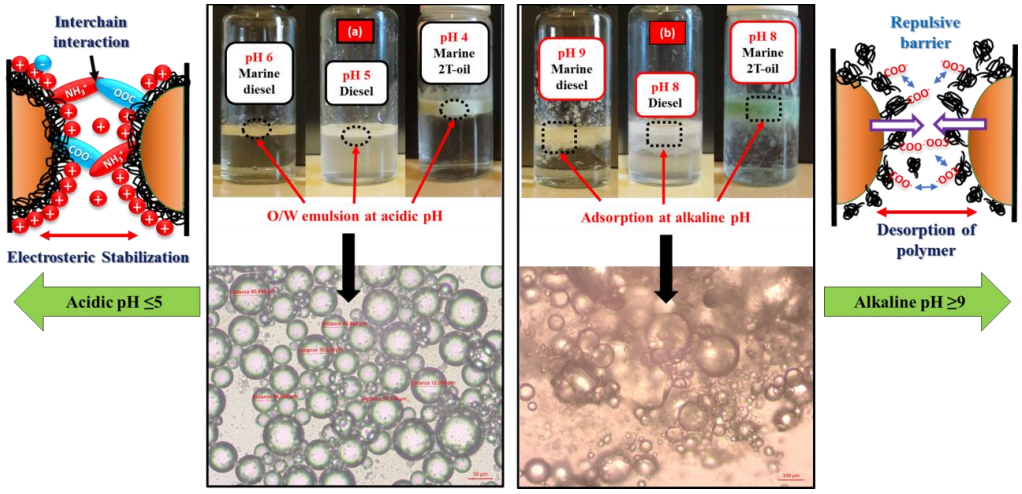

Figure 4.10**:** Effect of pH on the behaviour of stabilized oil droplets (a) o/w emulsions at acidic pH along with microscopic image of emulsion formed by diesel at pH 6 (b) adsorption of oil droplets on the surface of NO-CS at alkaline pH with a microscopic image of adsorbed marine diesel at pH 8. Left most part shows the interchain interaction and stabilization of oils at pH ≤5 and the right most part presents the open-chain conformation of the polymers at pH ≥9.

Increasing the pH started the deprotonation of amino groups, which resulted in the precipitation of NO-CS at pH >6.5, and hence started reducing the electrostatic barrier. In such case, the electrosteric interaction between the NO-CS and oils resulted in the stabilization of oil droplets through adsorption (Figure 4.10b). Furthermore, the negative charge of hydrocarbon present in oils will pull the positive charge of the non-substituted amino groups of NO-CS, by enhancing adsorption at oil and water interface in the presence of NO-CS, and similar behaviour was also observed previously (Lusiana et al., 2014). In addition, since the electrostatic barrier was reduced, NO-CS molecules were desorbed from the droplet surfaces, and resulted in extensive droplet flocculation or bridging flocculation. At pH ≥9, all the amino groups are deprotonated and neutral, and no further interchain interaction occurs between the amino and carboxyl groups. Since, all the carboxyl groups are negatively charged and there exists repulsive barrier between the polymer chains, NO-CS adopts open-chain conformation (Refer right most part of Figure 4.10). This resulted in the adhering of the oil droplets towards each other and enhanced the destabilization rate of the emulsion.

For NaO-CS

Long hydrocarbon chains were introduced into carboxymethylchitosan surfaces, in order to study its effect on emulsion stabilization as a function of pH. The long oleoyl chains grafted into the polymer-chain allow the NaO-CS to get attached to the liquid–liquid interface. These long chains also creates the repulsive forces between them, and being hydrophobic in nature easily interacted with the oil. Despite of the repulsive barrier between the deprotonated carboxyl groups, adsorption of long hydrocarbon chains of NaO-CS to the oil droplets provides additional stabilization even at pH ~10 (Figure 4.11). Such stabilization was not feasible in case of NO-CS at higher pH. Moreover, the electrical charge of oil droplets in an emulsion is always identical resulting in the repulsive electrostatic interactions among the oil droplets (Klinkesorn, 2013). This suppressed the coalescence rate and hence a stable emulsion was formed. Since, NaO-CS was in the sodium form, addition of HCl started to build up ion exchange effect between Na^+ and NH_3^+ groups of NaO-CS along with H^+ ions present in the aqueous phase. This resulted in the strong attraction of hydrophilic moiety of NaO-CS towards the aqueous phase.

As the pH decreased, there was more interchain interaction between the oppositely charged amino and carboxyl groups, which resulted in the denser packing of the NaO-CS at the oil-water interface. This favors effective stabilization against coalescence near to pH 8 via chain interaction, and similar behavior was also observed previously (Kalliola et al., 2018). Furthermore, decrease in the pH started building positive charges surrounding the droplets, and this electrical layers enhanced the repulsive barrier between the oil droplets. Therefore, the o/w emulsion was formed via electrosteric stabilization. The overall mechanism is presented in the Figure 4.11. However, the o/w emulsion formed at alkaline pH ~8 was creamy and decreasing pH build a positive surface (refer Figure 4.4a), which had changed the creamy emulsion into clear emulsion (pH ~5). Furthermore, the addition of positive charge made the emulsion unstable. Therefore, from the observed results, it was concluded that the emulsion was found to be stable at the aqueous phase

pH >4. (Paper II) Although the emulsion behaviour of NaO-CS was similar to NO-CS, the effect of pH was hindered by the hydrophobic modification.

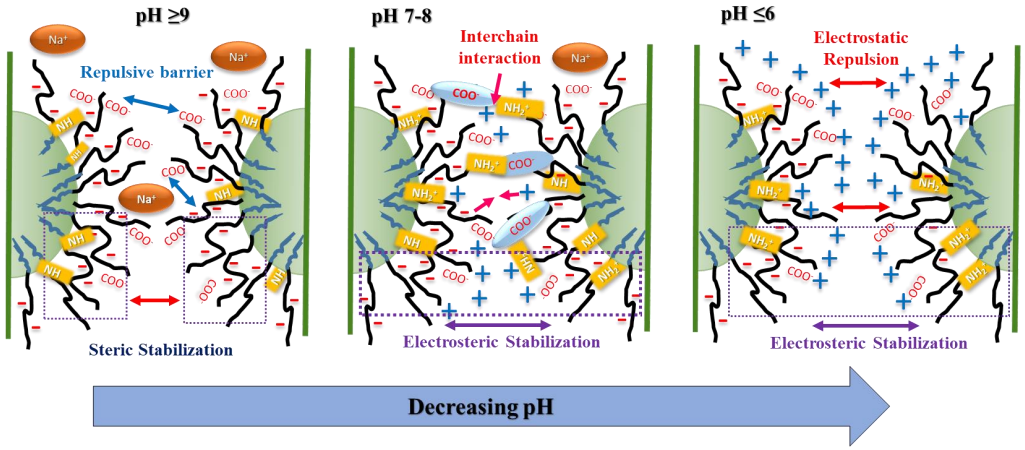

Figure 4.11**:** Effect of pH on the stabilization behaviour of oil droplets in emulsion using NaO-CS.

For OP-D, Blend, CSOP-A and OP-A

Furthermore, coordination between carboxymethyl chitosan derivatives and OP-D changed the behaviour of emulsion as a function of pH. When OP-D interacted with marine diesel at its initial pH (pH was 5.5), there was a formation of gel-like emulsion, suggested the bridging of particles between droplets and particle-particle interaction. So the obtained emulsion is because of the hydrogen bonding as well as due to bonds between hydrophobic groups and oil droplets via steric barriers (Schmidt et al., 2015).

In addition to steric stabilization, the electrostatic contribution to this stabilization is quantified by the electrophoretic mobility (EM) which is proportional to the surface charge. When pH decreases to 4, there was association (i.e. protonation) of carboxyl groups, which resulted in the neutralization of charges, and thus increased the zeta potential. Hence, the EM value of OP-D at pH 4 was -1.14 µmcm/Vs, and resulted in thick gel-like layer with oil via electrosteric barriers. However, increasing pH had decreased the EM values (Figure 4.12a), which attributed to the dissociation of carboxyl groups present in it and resulted in the formation of o/w emulsion mainly due to steric stabilization. Furthermore, repulsive barriers are also generated by negative charged carboxyl groups, which could resist against droplets coalescence. The electrolyte in SW, increased the EM (Figure 4.12b) compared to OP-D in DI water, by shielding the negative charges and enhancing the emulsion rate (Schmidt et al., 2017) through electrostatic barriers of electrical charges. Hence, overall obtained emulsion was due to steric and electrostatic stabilization. OP-A with DI water formed creamy emulsion at pH 9–10 similar to NaO-CS, but the coalescence rate was enhanced in

the presence of SW. Moreover, the EM value in OP-A was less negative than OP-D at pH 4, due to the presence of the hydrophobic hydrocarbon chain in OP-A, and thus resulted in o/w emulsion but not a gel-like.

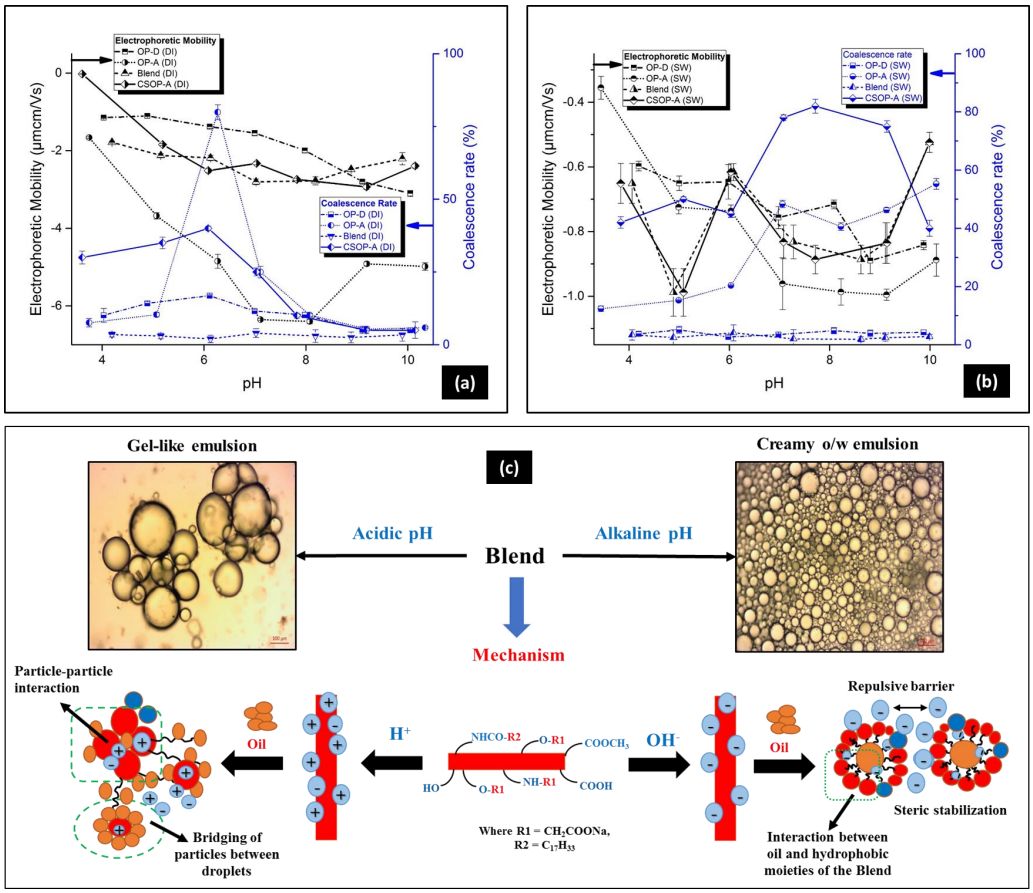

Figure 4.12**:** Effect of solution pH of OP-D, OP-A, CSOP-A and the Blend on the electrophoretic mobility and coalescence rate of (a) marine diesel with deionised water, (b) marine diesel with seawater, (c) Emulsion mechanism of marine diesel with 2.0 g L^{-1} of Blend in DI at acidic and alkaline pH. Electrophoretic mobility is represented with black lines with symbols and the coalescence rate is represented with blue lines with a symbol.

Since CSOP-A possessed a glucosamine backbone along with OP-D, the EM values differed from OP-A at a different pH range, and so did the oil droplet stabilization rate (emulsion formation rate). In addition to this, the incremental of EM values from alkaline to the acidic pH region implied the adsorption of surfactant via hydrophobic bonding, distributed on the external surfaces of

aggregates. Although there was the presence of long hydrocarbon segments in CSOP-A, the simultaneous protonation of amino and carboxyl groups occurred in CSOP-A with decreasing pH and mitigated the oil droplets' resistance to coalescence by stepping down the emulsion rate. The Blend bearing hydrophobic glucosamine backbone and OP-D, however, did not affect the oil droplets stabilization rate much with pH change, but rather changed the nature of the emulsion, i.e. gel-like emulsion at acidic pH and creamy emulsion at alkaline pH (refer Figures 4.12c along with its mechanism). In addition, the emulsion formation with the Blend was autonomous of the water quality, as some of the hydrophobically modified chitosan present in the Blend was effective in DI (Paper II) and some of OP-D present in the Blend was effective in SW.

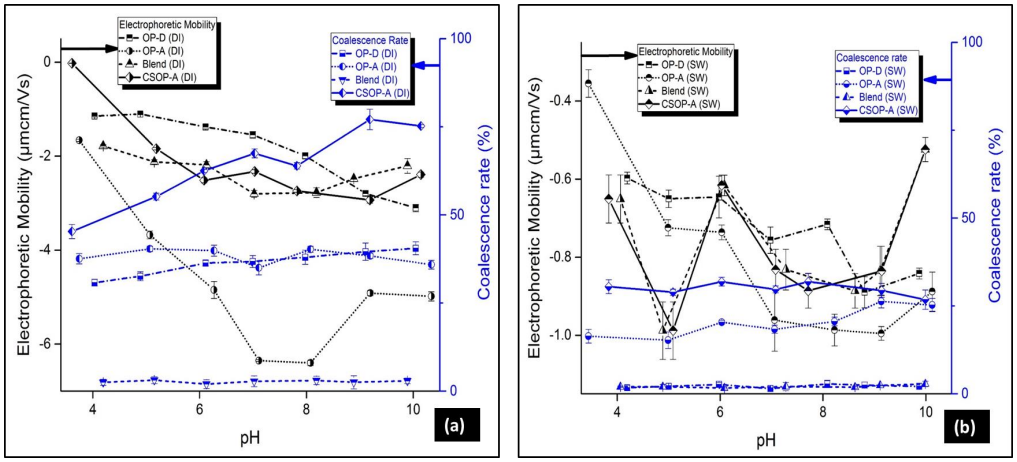

Figure 4.13**:** Effect of solution pH of OP-D, OP-A, CSOP-A and the Blend on the electrophoretic mobility and coalescence rate of (a) 2T-oil with deionised water, and (b) 2T-oil with seawater. Electrophoretic mobility is represented with black lines with symbols and the coalescence rate is represented with blue lines with a symbol.

The droplets stabilization rate of 2T-oil in DI was more dependent on pH, than that in SW (Figures 4.13a-b). The reason was the cation exchange from SW with H^+ of surface-active moieties (−COOH and –OH) of OP-D and the Blend, which resulted in bulky o/w emulsion. In addition, the IFT of 2T-oil was less in SW than DI, which resulted in dissolution of some compounds of 2T-oil in SW, and similar result was reported previously (Ghorbanizadeh and Rostami, 2017). Furthermore, 2T-oil swells easily in SW, resulting in spontaneous oil-in-water emulsification, which diffuses the surfactants across the interface and forms bulky emulsion (Riehm et al., 2017). Nevertheless, for OP-D and Blend, the decreasing pH formed the interfacial monolayer that contributed to the prevention of dispersed 2T-oil droplets to coalescence, resulting in a creamy and gel-like emulsion. Even though the EM values of the Blend and CSOP-A do not differ much in SW with changing pH, the emulsion behaviour changes in them due to the presence of OP-D and crosslinked OP-D. Despite of the long hydrocarbon chains in Blend, CSOP-A and OP-A, the pH gradient at the interface in DI prevents the adsorption of long chains towards 2T-oil due to the

presence of free surface-active groups (such as –OH and –COOH), which might have enhanced the coalescence rate. Moreover, the protonation of amino groups in the CSOP-A with decreasing pH provides a repulsive barriers, which slightly resist against the aggregation of droplets. Hence, the coalescence rates of these hydrophobically modified materials varied in DI.

4.2.4 Salinity variance versus the behaviour of emulsion

The interaction of NO-CS with oils in the presence of electrolyte was studied by measuring the oil droplets size. It has been shown that emulsion is more stable when the ionic strength of the solution is lower (Wang and Alvarado, 2012). In contrast, presence of salt induced the formation of more rigid interfacial film i.e. stronger interfacial activity (Alves et al., 2014).

For NO-CS, addition of ionic strength reduces the IFT and forms electrical double layer surrounding the positively charged surface on NO-CS, which provides additional electrostatic barrier to the sterically stabilized droplets against coalescence. However, further increase in the salinity shields the surface charges of NO-CS and reduces the electrostatic repulsive barrier. This facilitates the adsorption of NO-CS onto the oil-water interface and favors the hydrophobic interactions among the NO-CS polymer via steric barriers. The formation of oil droplets with diesel dropped significantly with an increase in salinity from 0.5% to 2% compared to marine diesel (refer Figures 4.14a-b). However, the hydrophilicity of NO-CS decreased with increase in salinity from 2% to 3%, and thus reduces the emulsion stability. This resulted in slight more drop in the formation of oil-droplets for marine diesel compared to diesel. The average droplet size for marine diesel was less than 50 µm, whereas for diesel, it was less than 75 µm. In case of marine-2T oil, a small addition of electrolyte quickly dropped the rate of oil droplets formation with average droplet size less than 35 µm (refer Figure 4.14c). Increase in salinity changes the formation of oil droplets but it does not affect the oil droplets size significantly.

For NaO-CS, there was a strong affinity of NaO-CS towards aqueous phase due to an ion exchange effect among the amino groups and the Na^+ of NaO-CS with H^+ ions in the aqueous phase. The increase in electrolyte concentration, narrowed down the electrically charged double layer near the hydrophilic part of NaO-CS through neutralization of charges. Furthermore, the repulsive force among the hydrophobic groups in NaO-CS quickly grabbed the marine diesel (hydrophobic effect) and provided steric hindrance to the droplets against coalescence. Moreover, the oil droplets had the same electrical charge in the emulsion as they were stabilized by the same stabilizer, showing repulsive electrostatic interaction between the oil droplets in an emulsion (Klinkesorn, 2013) by inhibiting coalescence. Since NaO-CS got adsorbed onto the surface of more than one droplet, there was a formation of bridging flocculation between the NaO-CS and emulsion droplets and an increase in salinity accelerated this rate by making the emulsion droplets denser (see Figure 4.14d). The formation of bridging flocculation was maximum for pH 6–7 up to 3.5% salinity, due to slightly negatively charged NaO-CS. However, decreasing pH with variable salinity tended towards the instability of o/w emulsion, i.e. at pH 5 the stability of o/w emulsion suppressed the coalescence because of the positively charged NaO-CS.

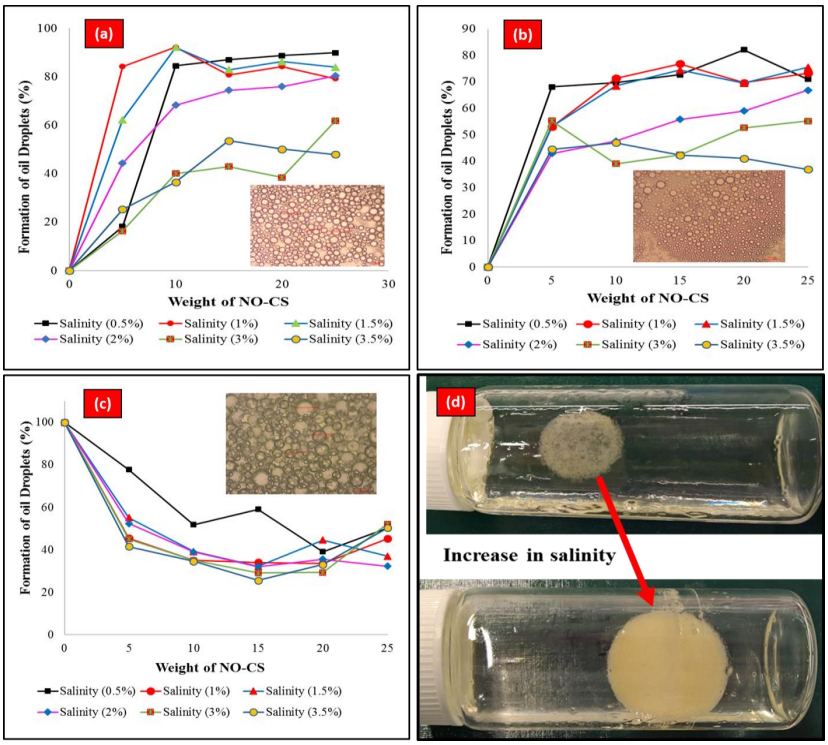

Figure 4.14**:** Effect of salinity on formation of oil droplets using NO-CS (a) for marine diesel (b) for diesel and (c) for marine 2T-oil along with the microscopic images of oil droplets, (d) formation of bridging flocculation between the NaO-CS and emulsion droplets with increase in salinity.

In the formed emulsion, droplets stabilization rate of marine diesel with OP-D was enhanced with increased in electrolyte concentration, whereas the orange peels powder combined chitosan derivatives showed the stabilization of this oil in a different way (refer Figure 4.15a). One reason was that the electrolyte prevented water hydration around OP-D molecules, which resulted in the reduction of electrostatic repulsion between the intermolecular hydrophilic groups, and, thus, enhanced the hydrophobicity of OP-D. Similar behaviour was observed previously (Jiao et al., 2016). Furthermore, crosslinking of metal ions with carboxyl and hydroxyl groups present in OP-D might have reduced intermolecular electrostatic repulsion. Kasprzak et al. demonstrated the coordination of metal ions with flavonoids to form complexes (Kasprzak et al., 2015). In CSOP-A, the unavailability of carboxylic acid, have declined the crosslinking activity with ions, and thus reduced its effectiveness in the emulsion stability at seawater salinity. Although CSOP-A possesses hydrocarbon chains, an increase in electrolyte concentration strengthened the electrostatic interaction of unreacted hydroxyl groups towards water, which enhanced the aggregation of oil droplets and destabilized the emulsion of marine diesel. In case of the Blend, the stabilization rate was not affected much with salinity variance in DI, due to the steric forces.

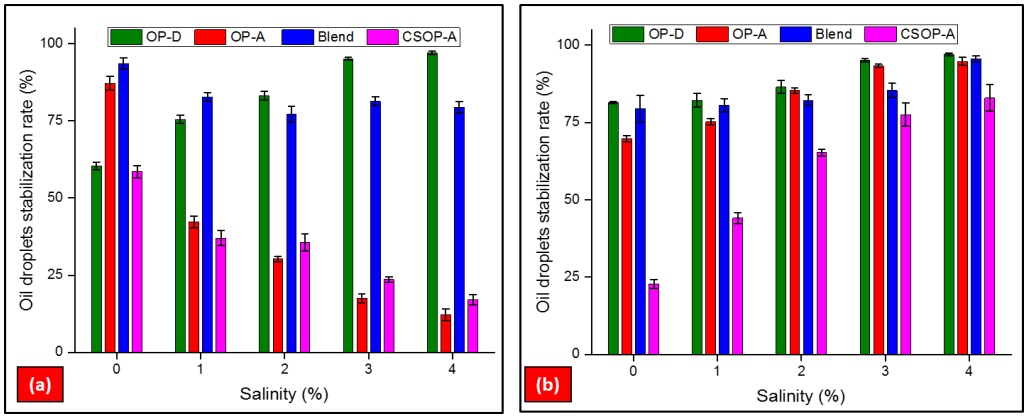

Figure 4.15**:** Effect of salinity on stabilization of oil droplets to formed emulsion (a) Marine diesel and (b) 2T-oil using OP-D, OP-A, CSOP-A and the Blend.

2T-oil consists of solvent-dewaxed heavy paraffinic and polyaromatics along with hydrocarbons, which immediately form clusters when mixed with seawater. Even though the stabilization rate of the oil droplets or emulsion formation rate was similar (Figure 4.15b), the nature of emulsion with respect to these materials was different. OP-D formed stable emulsion that could be skimmed easily, whereas OP-A, CSOP-A and the Blend formed bulky lumps due to the long hydrocarbon chain present in these derivatives. Secondly, the presence of electrolyte led to a stronger interfacial activity with these surface-active species, by limiting the coalescence effect and then the stabilization (Alves et al., 2014).

4.2.5 Effect of temperature on emulsion stability

There was a direct influence of temperature on the behaviour of emulsions. Therefore, three different temperatures (RT, 2 °C and -20 °C) were considered to analyse the behaviour of oil droplets in the emulsions.

For NaO-CS, the oil droplets size of marine diesel at RT was ≤30 µm for more than 6 weeks (refer Figure 4.16a), whereas, at 2 °C, the droplet size in the emulsion became ≤60 µm for higher concentration of NaO-CS (more than 1.5 g L^{-1}) and was extended up to 100 µm for the lower concentration of NaO-CS (refer Figure 4.16b). These results reflect the enhancement of the interaction between water and the hydrophilic moiety of NaO-CS at a lower temperature, which resulted in the increased mean droplet diameter of the o/w emulsion and similar behaviour was also observed earlier (Shinoda and Saito, 1969). Moreover, the coalescence rate showed up a slight separation of oil from the emulsion at lower concentration of NaO-CS but increasing the dosage had reduced the coalescence rate. Nevertheless, the concentration of NaO-CS also affected the emulsion stability with a fluctuating temperature.

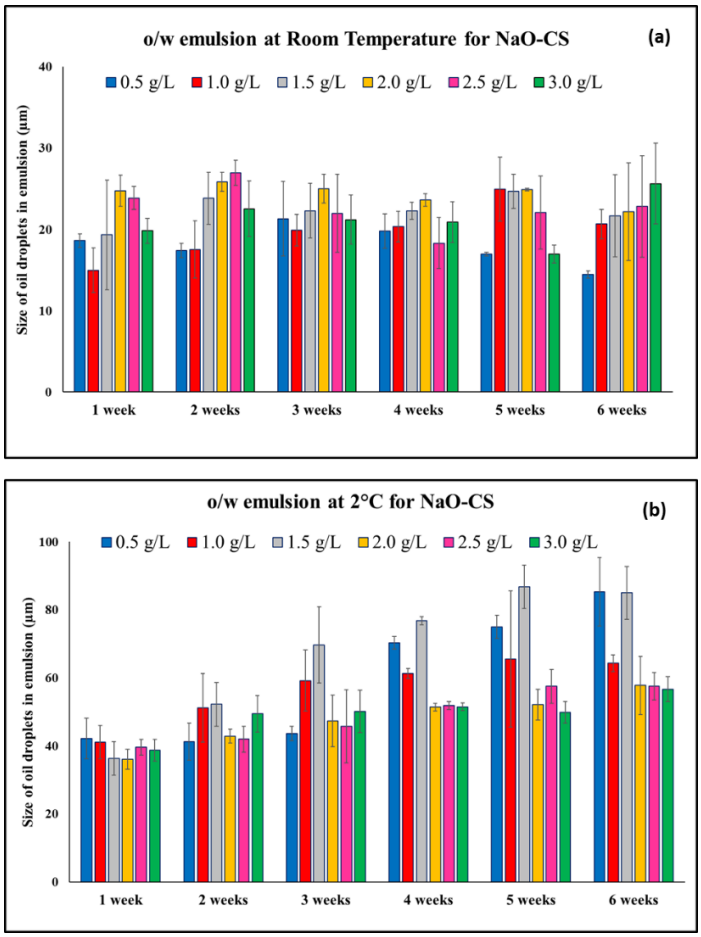

Figure 4.16**:** Oil droplet size in the emulsion with different dosage of NaO-CS (a) at RT and (b) at 2°C measured weekly by optical microscope.

The oil droplet size for different materials such as OP-D, OP-A, CSOP-A and Blend were also studied as a function of pH and water salinity with optimised concentration. The results showed that the emulsion rate of the oils at RT and 2 °C did not fluctuate much apart from the size of oil droplets in the emulsion, but water quality affected the oil droplet size (refer Figure 4.17). Furthermore, at (-20 °C) the water quality did not play a significant role in the formation of o/w emulsion due to the ice, rather more dependent on surface-active materials concentration. Therefore, the oil droplets stabilization rate (emulsion formation) on the surface of ice in the presence of these surface-active materials steeped down to less than 10%. Despite hydrophobic moieties in OP-A, CSOP-A and the Blend, the absence of the liquid-dispersed phase suppressed the hydrophilic properties of these materials, which in turn inhibited the formation of o/w emulsion.

Secondly, in such cold conditions, the biodegradation rate decreases with an increase in the viscosity of oils, which might be one reason for the ineffectiveness of these materials in the formation of emulsion. These particle-formed surfactants were effective for spilled oil above 0 °C, due to their dispersion in water, but below 0 °C there was a decline in the dispersion rate and particle effectiveness in the stabilization of oil droplets or formation of emulsion also declined (Paper IV).

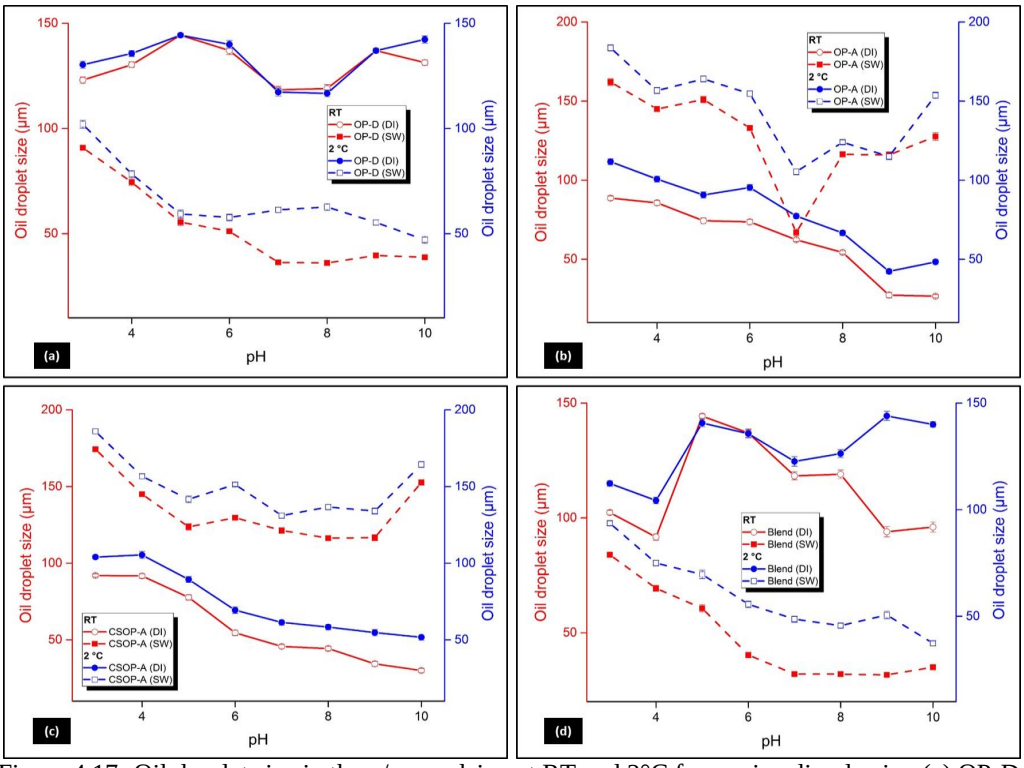

Figure 4.17**:** Oil droplet size in the o/w emulsion at RT and 2°C for marine diesel using (a) OP-D, (b) OP-A, (c) CSOP-A and (d) Blend.

4.3 Recovery of oil from the emulsified oil

The significant step in the oil spill treatment is the recovery of oil. Using NaO-CS, the recovery of oil was feasible simply by the addition of Ca^{+2} ($CaCl_2$ solution). Two carboxylic acid groups of the NaO-CS cross-linked with Ca^{+2} ions (Figure 4.18), which reduced the effect of electrostatic barrier and might also affect the steric barrier in the stabilized emulsion. This affected the interaction between the long carbon chain of NaO-CS and oil in the o/w emulsion, as a result of which the Ca-

crosslinked NaO-CS was pulled out from the stable emulsion. From the obtained results, it was concluded that Ca-crosslinked NaO-CS acted as an emulsion destabiliser, by enhancing the coalescence rate of the oil droplets within the stable emulsion. Although NaO-CS forms stable emulsion, the oil recovery rate was also dependent on the quality of the water. One reason for this might be the presence of multiple ions along with sodium ions in the seawater, which maintained the electrical double layer through electrostatic stabilization and suppressed the coalescence rate. Therefore, the recovery rate of oil from emulsification was about 75–85% and 19–49% using deionised water and seawater, respectively (Paper II).

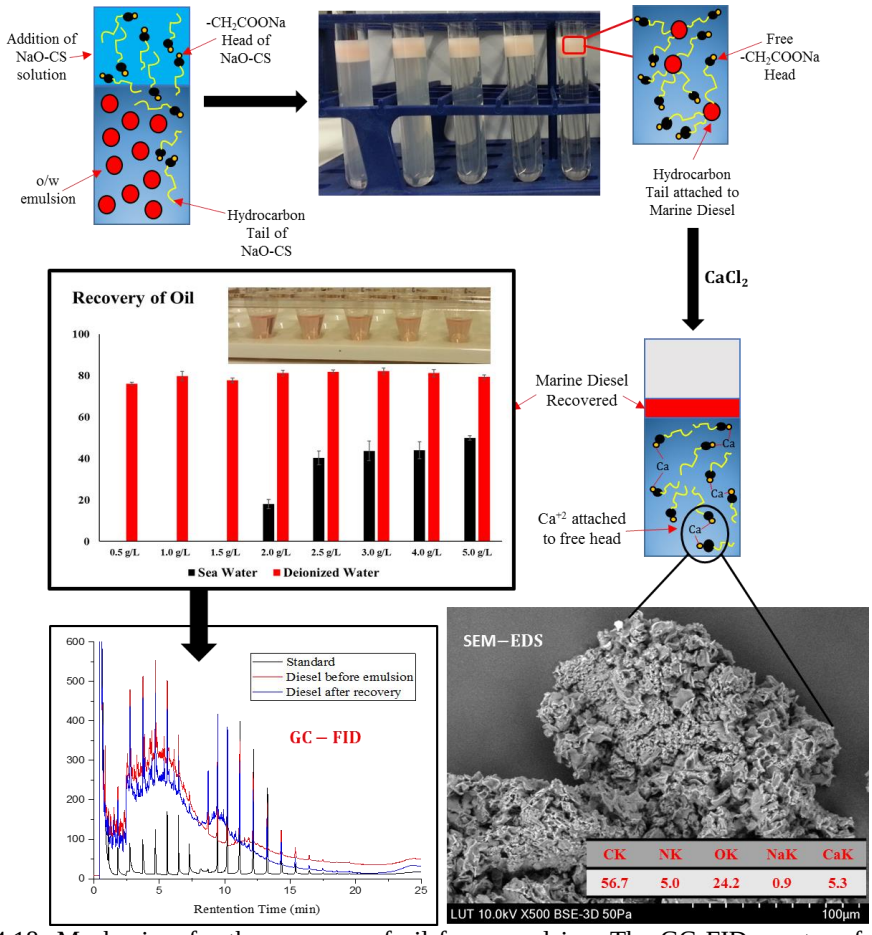

Figure 4.18**:** Mechanism for the recovery of oil from emulsion. The GC-FID spectra of marine diesel before emulsion and after recovery along with the SEM-EDS results of Ca-crosslinked NaO-CS.

The recovered oil was characterised qualitatively using GC-FID and FTIR. The retention time of the saturated hydrocarbon in the standard diesel remained the same in recovered marine diesel (Figure 4.16). Moreover, from the FTIR spectra the peak intensities at 2854 cm^{-1}, 2922 cm^{-1} and 2954 cm^{-1} of C-H stretching, and at 1377 cm^{-1} and 1457 cm^{-1} of C-H bending of the marine diesel below emulsion and after recovering remained unaltered (Paper II). This resemblance of FTIR and GD-FID results with each other shows that the marine diesel recovered from the emulsion was in the pure form. The surface morphology and EDS results also confirmed the crosslinking of Ca^{2+} ions with the two carboxylic acid groups of NaO-CS. Hence the amount of sodium was reduced in Ca-crosslinked NaO-CS after the recovery of oil.

4.4 Water quality after the removal of oil

The maximum consumption of dispersants, Corexit, was done during a Gulf of Mexico oil spill without studying their post-application effect. Recent research changes the scenario, as the found traces of Corexit, due to its poor biodegradability, turned to be more harmful for the marine creatures. Hence, to study the water quality after application of dispersants for oil spill response is mandatory.

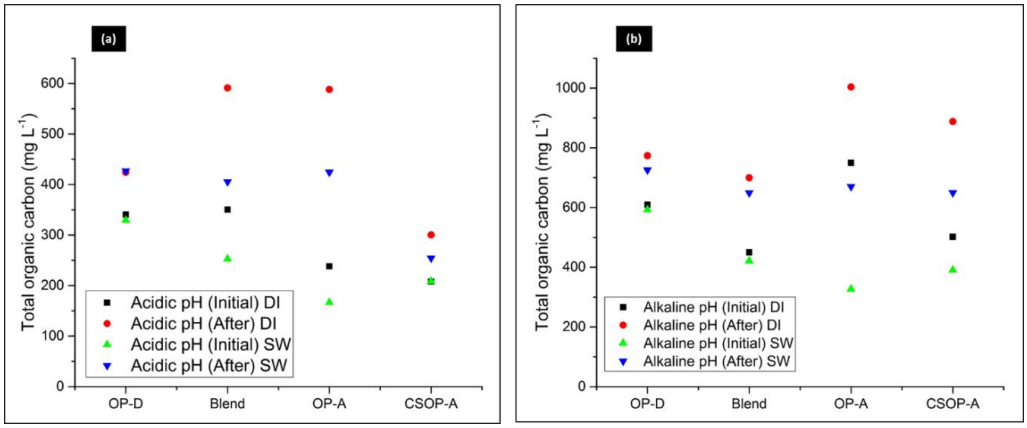

Figure 4.19**:** Total organic carbon content after removal of marine diesel (a) at acidic pH and (b) at alkaline pH.

Traces of organic matter (left over of OP-D, CSOP-A, OP-A and the Blend) after the removal of emulsified/separated oil were investigated using TOC through the NPOC method. As we see from Figures 4.8a and 4.9a, the aqueous layer was not cleared, which indicates the traces of unreacted surfactants. Figure 4.19 shows the traces of OP-D, the Blend, CSOP-A and OP-A after removal of the oil/emulsified marine diesel layer in acidic and alkaline conditions. Despite the removal of the oil layer, the increase in the amount of organic carbon was attributed to either the adsorption of oil molecules on the surface-active moieties or the presence of degraded oil in the continuous aqueous phase along with the surfactants. Especially for 2T-oil, the spontaneous oil-in-water emulsification

implies the leaching of surfactant from oil to the aqueous phase (Riehm et al., 2017). However, the amount of increased TOC was less than that obtained from marine diesel due to the formation of bulky emulsion, in which the surface-active materials were trapped. Various biosurfactants derived from varied microbial sources are present in the water, enhancing the biodegradation of the dispersed crude oil through bioremediation (Mohanram et al., 2016). Moreover, earlier studies demonstrate orange peel as a substrate for Bacillus Licheniformis biosurfactant production and the biodegradation of hydrocarbons (Arthala et al., 2016), so that the traces of OP-D in the water phase proved to be non-toxic. Chitosan being non-toxic and biodegradable, its derivatives, CSOP-A and the Blend could not have many adverse effects, if found in water resources.

4.5 Other applications of surface-active chitosan

Although NaCS-GL was partially carboxymethylated, the glutaraldehyde crosslinking inhibited the attractive power towards oil. In other words, since a partial amount of amino groups underwent carboxymethylation and partial were cross-linked with glutaraldehyde, the hydrophobic interaction of this derivative (NaCS-GL) was not efficient with oil. However, NaCS-GL as surface-active material was used for the removal of other pollutants from water. Paper III deals with the functionalities of chitosan moieties in the adsorptive removal of cationic and anionic dyes along with divalent metal ions. Figure 4.20 shows the adsorption mechanism of dyes such as MB, Tart and SaO, and metal ions such as Pb(II) and Cd(II), on the surface of NaCS-GL (Paper III).

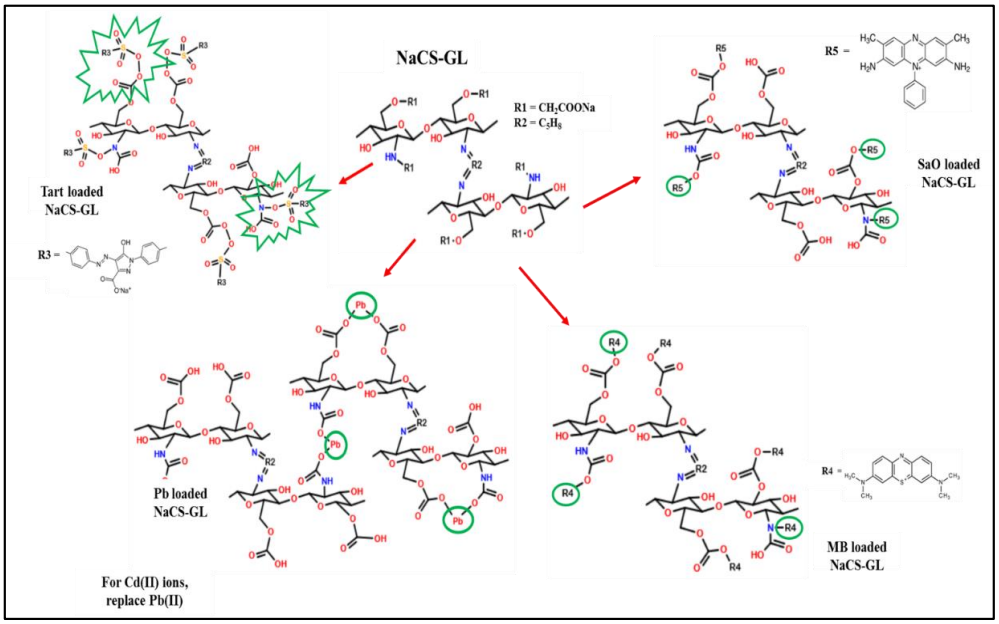

Figure 4.20**:** Adsorption mechanism of dyes and ions on the surface of NaCS-GL.

The maximum adsorption capacities of MB, SaO and Tart were 365.77, 126.80 and 609.26 mg g^{-1}, whereas, for Pb(II) and Cd(II) ions they were 51.93 and 36.43 mg g^{-1}, respectively. Initially, film diffusion or chemical reaction controlled the rate of the adsorption followed by the pore diffusion. From the experimental data, Langmuir isotherm model was best fitted for the adsorptive removal of dyes, whereas, for metals, the surface heterogeneity of NaCS-GL fitted the Freundlich and Temkin isotherm models better than Langmuir. Hence, this surficial properties of NaCS-GL resulted in the simultaneous removal of dyes and metal ions from the water resources, and the spontaneity of Pb(II) was the most and MB was the least. Bio-based materials can be considered also safe to use in production of drinking water. Therefore, in future such functionalized biopolymer are extended for the water remediation of the industrial effluents.

5 Other bio-based materials for oil spill treatment

Beside chitosan various other materials based on biopolymers such as cellulose, chitin, gum agar, xanthan gum, and agarose, food-grade amphiphiles, bio-polymeric blends and magnetic nano-particles have been studied for the oil spill treatment. Some examples are presented in Table 5.1. Other bio-based materials in the form of aerogel, separators, and gelators used in oil spill treatment are available in the review paper (Doshi et al., 2018).

Table 5.1: Different bio-based materials for oil spill treatment.

Materials *(Method)*	**Oils**	**Observations**	**References**
Walnut shells *(Media preparation)*	Mineral oil Vegetable oil	0.56 g g^{-1} 0.58 g g^{-1} *(sorption of oil)*	(Srinivasan and Viraraghavan, 2008)
Silkworm cocoon waste *(Drying, Cutting and Milling)*	Motor oil Vegetable oil	42 – 52 g g^{-1} 37 – 60 g g^{-1} *(sorption of oil)*	(Moriwaki et al., 2009)
Rice husks *(Pyrolysis)*	Gasoline Diesel Light crude oil Motor oil Heavy Crude oil	3.7 kg kg^{-1} 5.5 kg kg^{-1} 6.0 kg kg^{-1} 7.5 kg kg^{-1} 9.2 kg kg^{-1} *(sorption of oil)*	(Angelova et al., 2011)
Oil palm leaves *(Blending and hydrophobic modification with lauric acid)*	Crude oil	1.2 g g^{-1}	(Sidik et al., 2012)
Food-Grade Amphiphiles, Soyabean lecithin and Tween 80 *(Blending)*	Crude oil	Acts as an emulsifier and effectiveness depends on the amphiphiles ratio	(Athas et al., 2014)
Foam membrane from Agarose, Gelatin and Genipin (*Blending and Lyophilization)*	Crude oil, Hexane, Toluene, Oil-spill wastewater	>97% of pure water obtained after removal of separation of oil	(Chaudhary et al., 2014)
Cellulose-based aerogel from waste newspaper *(Dissolution, Gelation, Solvent exchange and Freeze drying)*	Waste engine oil	16 g g^{-1} *(sorption of oil)*	(Jin et al., 2015)
Polyvinylpyrrolidone-coated magnetite nanoparticles *(Hydrothermal)*	MC252 oil	~100% *(magnetic separation)*	(Mirshahghassemi and Lead, 2015)

Hexadecyl-trimenthyl-ammoinum-bromide modified eggshell *(Mixing and drying)*	Crude oil	6.493 mg g^{-1} *(Removal of oil)*	(Muhammad et al., 2015)
Stainless steel mesh with waste potato residues and polyurethane *(Spraying)*	Light/ heavy oil Kerosene	>96.5% 98.0% *(Separation of oil)*	(Li et al., 2016)
Bifunctionalized cellulose rod-like nanocrystals *(Oxidation and amination)*	Marine diesel	Dispersion of oil up to seawater salinity	(Ojala et al., 2016)
Ostrich bone waste-loaded a cationic surfactant *(Mixing and drying)*	Benzene Toluene Ethylbenzene p-Xylene	85.9 mg g^{-1} 119.5 mg g^{-1} 114.1 mg g^{-1} 137.7 mg g^{-1} *(sorption of oil)*	(Shakeri et al., 2016)
Cellulose nanofibril and polyvinyl alcohol aerogel microspheres *(Emulsification and Freeze drying)*	Crude oil	54–140 g g^{-1} *(sorption of oil)*	(Zhai et al., 2016)
Cellulose foam *(Drop-casting and heating)*	Paraffin Motor oil	~100% *(absorption of oil)*	(Calcagnile et al., 2017)
Liquidambar formosana (Pyrolysis)	Paraffin Turpentine oil	~100% *(extraction of oil)*	(Feng et al., 2017)
Cellulose membrane coated with block co-polymer of silane and myrcene monomers *(RAFT polymerization)*	Crude oil	>99% *(Separation of oil)*	(Kollarigowda et al., 2017)

6 Conclusions and future prospective

For the huge oil spill, when booms and skimmers are ineffective, dispersants are the best option. However, the biggest challenge of these materials is their effectiveness in terms of behaviour of oil, i.e. their effectiveness with change in density of oil, evaporation of oil or emulsification of oil over a period of time. From an environmental point of view, the removal of the oil from the environment is always the best solution, but economic aspects may restrict the methods available for the oil spill treatment.

This thesis demonstrates the application of bio-polymer, chitosan, in the breaking of oils present on the water surface to form emulsion. Chitosan-based materials are rather environmental friendly, but economically expensive. The characterisation of chitosan and its synthesised derivatives determines the nature of physiochemical properties before and after modifications. The degree of substitution was altered on the chitosan polymer by changing the reaction parameters of the carboxymethylation process, which in turn affected the solubility of the produced derivative. Partially substituted hydrophilic NO-CS broke the dispersed phase (marine diesel, diesel and marine 2T-oil) into droplets and formed stable emulsion through electrosteric stabilization, with droplet size less than 100 µm. In acidic condition, there was a formation of oil-in-water emulsion via electrosteric stabilization (combination of electrostatic and steric stabilization), whereas, at alkaline pH, NO-CS stabilized the emulsion by adsorbing onto the oil droplets. Presence of ionic strength in NO-CS solution had enhanced the oil adsorption rate, and formation of bridging flocculation clumps of these adsorbed oil occurred in the presence of H^+ ions, which can be easily skimmed off from water surface.

Hydrophobic modification of chitosan backbone had enhanced the stability of emulsion with smaller average droplet size than hydrophilic chitosan. NaO-CS being amphoteric, the hydrophobic oleoyl tails interacted with the oil leaving the hydrophilic end to interact with water and resulted in the formation of stable creamy emulsion through steric hindrance. The emulsion was stable for more than 6 weeks with the average oil droplets size $\leq$ 30 µm at RT. At alkaline pH, there was formation of creamy o/w emulsion, and decreasing pH, there was more interchain interaction between the oppositely charged amino and carboxyl groups. This resulted in the denser packing of the NaO-CS at the oil-water interface and also led to formation of electrical layers, which enhanced the repulsive barrier between the oil droplets. Hence, clear o/w emulsion were formed via electrosteric stabilization at acidic condition. Increase in electrolyte concentration accelerates the bridging flocculation between the NaO-CS and oil droplets in emulsion, which could be easily skimmed. Recovery of emulsified oil was feasible using calcium chloride solution. However, the recovery with deionized water was more than with seawater. Increasing temperature expanded the oil droplet size in the emulsion up to 100 µm. Amphiphilic chitosan in sodium form not only reduced the synthesis steps, but also enhanced the affinity of hydrophilic segments towards continuous phase through electrostatic stabilization along with steric stabilization.

A new approach of combining orange peel powder with NaO-CS have effectively formed stable emulsion by breaking marine diesel and 2T-oil present on the water surface. Different chitosan derivatives were hydrophobically modified in presence of OP-D via acylation. The efficiency of OP-D to form o/w emulsion was maximum with seawater, however, with the Blend, the emulsion formation was independent on the water quality due to the presence of hydrophobically modified chitosan together with OP-D. For chitosan-based materials, the oil droplet size was greater than 100 µm in gel-like emulsion, whereas, for creamy emulsion the droplet size always fell under 100 µm. Use of bio-waste such as orange peel together with chitosan facilitated the oil droplet breakup through faster adsorption of the surface-active moieties at the oil-water interface. The droplets stabilization rate or emulsion formation of marine diesel followed the order of the Blend > OP-D > OP-A > CSOP-A, whereas for 2T-oil the order was OP-D > Blend > OP-A > CSOP-A. Since these surfactants are originated from the bio-based materials, their hazardousness is minimal compared to commercially available dispersants.

The biodegradation or bioremediation of chitosan-based materials is more feasible than their regeneration after the separation of oil/emulsified oil. However, the cytotoxicity of chitosan on marine species needs further attention, as this cationic polymer may interact negatively with biodegrading organisms. Addition to this, the challenge is still to find environmental friendly and sustainable pathway to modify chitosan, which retains the green properties of chitosan, i.e. non-toxicity and biodegradability. The scope of using hydrophobically modified materials in the stabilization of emulsions could be extended to other natural polymers. The future prospective is to reutilize more bio-waste as surfactants in the formulation of dispersants for the oil spill response. Use of bio-based surfactants in the formulation of dispersants minimise the hazardousness of the commercially available dispersants for oil spill. Although, the use of dispersants is banned in Arctic region, the bio-based formulation may open a way towards a revolutionary sustainability.

References

Al-Sabagh, A.M., Morsi, R.E., Elsabee, M.Z., Naguib, H.F. and Moustafa, Y.M. 2012. Petroleum Oil Dispersion Efficiency and Stability Using Eco-Friendly Chitosan-Based Surfactant and Nanoparticles. *Journal of Dispersion Science and Technology*. **33**(11), pp.1661–1666.

Almeda, R., Hyatt, C. and Buskey, E.J. 2014. Toxicity of dispersant Corexit 9500A and crude oil to marine microzooplankton. *Ecotoxicology and Environmental Safety*. **106**, pp.76–85.

Alves, D.R., Carneiro, J.S.A., Oliveira, I.F., Façanha, F., Santos, A.F., Dariva, C., Franceschi, E. and Fortuny, M. 2014. Influence of the salinity on the interfacial properties of a Brazilian crude oil–brine systems. *Fuel*. **118**, pp.21–26.

Angelova, D., Uzunov, I., Uzunova, S., Gigova, A. and Minchev, L. 2011. Kinetics of oil and oil products adsorption by carbonized rice husks. *Chemical Engineering Journal*. **172**(1), pp.306–311.

Aranaz, I., Harris, R. and Heras, A. 2010. Chitosan Amphiphilic Derivatives. Chemistry and Applications. *Current Organic Chemistry*. **14**, pp.308–330.

Arctic Council 2009. *Arctic Marine Shipping Assessment 2009 Report* [Online]. Arctic Council's Protection of the Arctic Marine Environment (PAME). Available from: http://hdl.handle.net/11374/54.

Arrigo, K.R. 2013. The changing Arctic Ocean. *Elementa: Science of the Anthropocene*. **1: 000010**, pp.1–5.

Arthala, P.K., Avilala, J., Buddolla, V., Kallubhai, M., Jung, J.-Y. and Golla, N. 2016. Evaluation of orange peel for biosurfactant production by Bacillus licheniformis and their ability to degrade naphthalene and crude oil. *3 Biotech*. **6**, pp.1–10.

Athas, J.C., Jun, K., McCafferty, C., Owoseni, O., John, V.T. and Raghavan, S.R. 2014. An Effective Dispersant for Oil Spills Based on Food-Grade Amphiphiles. *Langmuir*. **30**(31), pp.9285–9294.

Atlas, R.M. 1995. Petroleum biodegradation and oil spill bioremediation. *Marine Pollution Bulletin*. **31**, pp.178–182.

Atlas, R.M. and Hazen, T.C. 2011. Oil biodegradation and bioremediation: a tale of the two worst spills in U.S. history. *Environmental science & technology*. **45**, pp.6709–6715.

Aveyard, R., Binks, B.P. and Clint, J.H. 2003. Emulsions stabilised solely by colloidal particles. *Advances in Colloid and Interface Science*. **100**–**102**, pp.503–546.

Azubuike, C., Chikere, C. and Okpokwasili, G. 2016. Bioremediation techniques–classification based on site of application: principles, advantages, limitations and prospects. *World Journal of Microbiology and Biotechnology*. **32**, pp.1–18.

Barnes, G.T. and Gentle, I.R. 2011. *Interfacial Science: An Introduction* Second. New York: Oxford University Press Inc.

Barros, F.C.F., Vasconcellos, L.C.G., Carvalho, T.V. and Ronaldo, F. do N. 2014. Removal of petroleum spill in water by chitin and chitosan. *Orbital: The Electronic Journal of Chemistry*. **6**, pp.70–74.

Bédouet, L., Courtois, B. and Courtois, J. 2005. Methods for obtaining neutral and acid oligosaccharides from flax pectins. *Biotechnology Letters*. **27**(1), pp.33–40.

Bée, A., Obeid, L., Mbolantenaina, R., Welschbillig, M. and Talbot, D. 2017. Magnetic

chitosan/clay beads: A magsorbent for the removal of cationic dye from water. *Journal of Magnetism and Magnetic Materials*. **421**, pp.59–64.

Belore, R.C., Trudel, K., Mullin, J. V and Guarino, A. 2009. Large-scale cold water dispersant effectiveness experiments with Alaskan crude oils and Corexit 9500 and 9527 dispersants. *Marine Pollution Bulletin*. **58**, pp.118–128.

Benner, S.W., John, V.T. and Hall, C.K. 2015. Simulation Study of Hydrophobically Modified Chitosan as an Oil Dispersant Additive. *The Journal of Physical Chemistry B*. **119**(23), pp.6979–6990.

Bhatnagar, A. and Sillanpää, M. 2009. Applications of chitin- and chitosan-derivatives for the detoxification of water and wastewater — A short review. *Advances in Colloid and Interface Science*. **152**, pp.26–38.

Bordel, S. and Giesecke, M. 2007. Micelles, the simplest example of self assembling system. Main features and thermodynamic properties *In*: *Colloid and Surface Research Trends*. New York: Nova Science Publishers, Inc.

Brandvik, P.J. and Faksness, L.-G. 2009. Weathering processes in Arctic oil spills: Meso-scale experiments with different ice conditions. *Cold Regions Science and Technology*. **55**, pp.160–166.

Brycki, B.E., Kowalczyk, I.H., Szulc, A., Kaczerewska, O. and Pakiet, M. 2017. Chapter 4: Multifunctional Gemini Surfactants: Structure, Synthesis, Properties and Applications *In*: *Application and Characterization of Surfactants*. Intechopen.

Buist, I., Potter, S., Nedwed, T. and Mullin, J. 2011. Herding surfactants to contract and thicken oil spills in pack ice for in situ burning. *Cold Regions Science and Technology*. **67**, pp.3–23.

Calabrese, V., Courtenay, J.C., Edler, K.J. and Scott, J.L. 2018. Pickering emulsions stabilized by naturally derived or biodegradable particles. *Current Opinion in Green and Sustainable Chemistry*. **12**, pp.83–90.

Calcagnile, P., Caputo, I., Cannoletta, D., Bettini, S., Valli, L. and Demitri, C. 2017. A bio-based composite material for water remediation from oily contaminants. *Materials & Design*. **134**, pp.374–382.

Carriger, J.F. and Barron, M.G. 2011. Minimizing risks from spilled oil to ecosystem services using influence diagrams: the Deepwater Horizon spill response. *Environmental Science & Technology*. **45**, pp.7631–7639.

Chansiri, G., Lyons, R.T., Patel, M. V and Hem, S.L. 1999. Effect of surface charge on the stability of oil/water emulsions during steam sterilization. *Journal of Pharmaceutical Sciences*. **88**, pp.454–458.

Chaudhary, J.P., Nataraj, S.K., Gogda, A. and Meena, R. 2014. Bio-based superhydrophilic foam membranes for sustainable oil-water separation. *Green Chemistry*. **16**, pp.4552–4558.

Chaudhary, J.P., Vadodariya, N., Nataraj, S.K. and Meena, R. 2015. Chitosan-Based Aerogel Membrane for Robust Oil-in-Water Emulsion Separation. *ACS Applied Materials & Interfaces*. **7**, pp.24957–24962.

Chen, L., Du, Y. and Zeng, X. 2003. Relationships between the molecular structure and moisture-absorption and moisture-retention abilities of carboxymethyl chitosan: II. Effect of degree of deacetylation and carboxymethylation. *Carbohydrate Research*. **338**, pp.333–340.

Chen, X.-G. and Park, H.-J. 2003. Chemical characteristics of O-carboxymethyl chitosans related to the preparation conditions. *Carbohydrate Polymers*. **53**, pp.355–359.

Colombo, E., Cavalieri, F. and Ashokkumar, M. 2015. Role of Counterions in Controlling the Properties of Ultrasonically Generated Chitosan-Stabilized Oil-in-Water Emulsions. *ACS Applied Materials & Interfaces*. **7**, pp.12972–12980.

Crini, G. and Badot, P.-M. 2008. Application of chitosan, a natural aminopolysaccharide, for dye removal from aqueous solutions by adsorption processes using batch studies: A review of recent literature. *Progress in Polymer Science*. **33**, pp.399–447.

Dahlmann, G. 2003. *Characteristic features of different oil types in oil spill identification*. Hamburg ; Rostock: BSH.

Dai, L., Wang, B., An, X., Zhang, L., Khan, A. and Ni, Y. 2017. Oil/water interfaces of guar gum-based biopolymer hydrogels and application to their separation. *Carbohydrate Polymers*. **169**, pp.9–15.

Das, N. and Chandran, P. 2011. Microbial Degradation of Petroleum Hydrocarbon Contaminants: An Overview. *Biotechnology research international*. **2011**, p.13.

Dash, M., Chiellini, E., Chiellini, F. and Ottenbrite, R.M. 2011. Chitosan—A versatile semi-synthetic polymer in biomedical applications. *Progress in Polymer Science*. **36**, pp.981–1014.

Dave, D. and Ghaly, A.E. 2011. Remediation Technologies for Marine Oil Spills: A Critical Review and Comparative Analysis. *American Journal of Environmental Sciences*. **7**, pp.423–440.

DeLeo, D.M., Ruiz-Ramos, D. V, Baums, I.B. and Cordes, E.E. 2016. Response of deep-water corals to oil and chemical dispersant exposure. *Deep Sea Research Part II: Topical Studies in Oceanography*. **129**, pp.137–147.

Dickinson, E. 2017. Biopolymer-based particles as stabilizing agents for emulsions and foams. *Food Hydrocolloids*. **68**, pp.219–231.

Dicks, B. 1998. The environmental impact of marine oil spills - Effects, Recovery and Compensation. Available from: https://www.itopf.org/fileadmin/data/Documents/Papers/environ.pdf.

Doshi, B., Sillanpää, M. and Kalliola, S. 2018. A review of bio-based materials for oil spill treatment. *Water Research*. **135**, pp.262–277.

Eastoe, J. 2003. Chapter 3 : Microemulsions *In*: *Surfactant Chemistry*. Bristol UK.

Environmental Protection Agency 2017. Oil Spill Response Techniques, EPA's Response Techniques. Available from: https://www.epa.gov/emergency-response/epas-response-techniques.

Environmental Protection Agency 2018. Overview of the Spill Prevention, Control, and Countermeasure (SPCC) Regulation. Available from: https://www.epa.gov/oil-spills-prevention-and-preparedness-regulations/overview-spill-prevention-control-and.

Evans, D.D., Mulholland, G.W., Baum, H.R., Walton, W.D. and McGrattan, K.B. 2001. In Situ Burning of Oil Spills. *Journal of research of the National Institute of Standards and Technology*. **106**, pp.231–278.

Fan, T. and Buckley, J.S. 2002. Rapid and Accurate SARA Analysis of Medium Gravity Crude Oils. *Energy & Fuels*. **16**, pp.1571–1575.

FAO 2016. *The state of World Fisheries and Aquaculture 2106. Contributing to food security and nutrition for all,*.

Farias, P.V.S., Aragão, D.C., Farias, M. V, Correia, L.M., Carvalho, T. V, Aguiar, J.E. and Vieira,

R.S. 2015. Natural and Cross-Linked Chitosan Spheres as Adsorbents for Diesel Oil Removal. *Adsorption Science & Technology*. **33**, pp.783–792.

Farrington, J.W. and McDowell, J.E. 2004. Mixing Oil and Water, Tracking the sources and impacts of oil pollution in the marine environment. *Oceanus Magazine*.

Feng, Y., Liu, S., Liu, G. and Yao, J. 2017. Facile and fast removal of oil through porous carbon spheres derived from the fruit of Liquidambar formosana. *Chemosphere*. **170**, pp.68–74.

Fingas, M. 2011. Chapter 23 - An Overview of In-Situ Burning *In*: *Oil Spill Science and Technology*. Elsevier Inc, pp.737–903.

Fouad, R.R., Aljohani, H.A. and Shoueir, K.R. 2016. Biocompatible poly(vinyl alcohol) nanoparticle-based binary blends for oil spill control. *Marine Pollution Bulletin*. **112**(1–2), pp.46–52.

French, D.J., Taylor, P., Fowler, J. and Clegg, P.S. 2015. Making and breaking bridges in a Pickering emulsion. *Journal of Colloid and Interface Science*. **441**, pp.30–38.

Ghorbanizadeh, S. and Rostami, B. 2017. Surface and Interfacial Tension Behavior of Salt Water Containing Dissolved Amphiphilic Compounds of Crude Oil: The Role of Single-Salt Ionic Composition. *Energy & Fuels*. **31**(9), pp.9117–9124.

Graham, L., Hale, C., Maung-Douglass, E., Sempier, S., Swann, L. and Wilson, M. 2016. *Oil Spill Science: Chemical dispersants and their role in oil spill response. MASGP-15-015* [Online]. Available from: http://masgc.org/oilscience/oil-spill-science-dispersant-bkgrnd.pdf.

Grem, I.C.S., Lima, B.N.B., Carneiro, W.F., Queirós, Y.G.C. and Mansur, C.R.E. 2013. Chitosan microspheres applied for removal of oil from produced water in the oil industry. *Polímeros Ciência e Tecnologia*. **23**, pp.705–711.

Griffin, W.C. 1947. Classification of Surface-Active Agents by "HLB". *The Journal of the Society of Cosmetic Chemists*. **1**, pp.311–326.

Guibal, E. 2004. Interactions of metal ions with chitosan-based sorbents: a review. *Separation and Purification Technology*. **38**, pp.43–74.

Gullón, B., Montenegro, M.I., Ruiz-Matute, A.I., Cardelle-Cobas, A., Corzo, N. and Pintado, M.E. 2016. Synthesis, optimization and structural characterization of a chitosan–glucose derivative obtained by the Maillard reaction. *Carbohydrate Polymers*. **137**, pp.382–389.

Hierrezuelo, J., Sadeghpour, A., Szilagyi, I., Vaccaro, A. and Borkovec, M. 2010. Electrostatic Stabilization of Charged Colloidal Particles with Adsorbed Polyelectrolytes of Opposite Charge. *Langmuir*. **26**(19), pp.15109–15111.

Hoff, R.Z. 1993. Bioremediation: an overview of its development and use for oil spill cleanup. *Marine Pollution Bulletin*. **26**, pp.476–481.

ITOPF 2018. *Oil Tanker Spill Statistics 2017* [Online]. The International Tanker Owners Pollution Federation Limited. Available from: https://www.itopf.org/fileadmin/data/Photos/Statistics/Oil_Spill_Stats_2017_web.pdf.

ITOPF 2014. Use of dispersants to treat oil spills. Available from: http://www.itopf.com/knowledge-resources/documents-guides/document/tip-4-use-of-dispersants-to-treat-oil-spills/.

Jernelöv, A. 2010. The Threats from Oil Spills: Now, Then, and in the Future. *AMBIO*. **39**, pp.353–366.

Jiao, T., Liu, X. and Niu, J. 2016. Effects of sodium chloride on adsorption at different interfaces and aggregation behaviors of disulfonate gemini surfactants. *RSC Advances*. **6**(17), pp.13881–

13889.

Jin, C., Han, S., Li, J. and Sun, Q. 2015. Fabrication of cellulose-based aerogels from waste newspaper without any pretreatment and their use for absorbents. *Carbohydrate Polymers*. **123**, pp.150–156.

John, V., Arnosti, C., Field, J., Kujawinski, E. and McCormick, A. 2016. The Role of Dispersants in Oil Spill Remediation: Fundamental Concepts, Rationale for Use, Fate, and Transport Issue . *Oceanography*. **29**, pp.108–117.

Kalashnikova, I., Bizot, H., Bertoncini, P., Cathala, B. and Capron, I. 2013. Cellulosic nanorods of various aspect ratios for oil in water Pickering emulsions. *Soft Matter*. **9**(3), pp.952–959.

Kalliola, S., Repo, E., Sillanpää, M., Singh Arora, J., He, J. and John, V.T. 2016. The stability of green nanoparticles in increased pH and salinity for applications in oil spill-treatment. *Colloids and Surfaces A: Physicochemical and Engineering Aspects*. **493**, pp.99–107.

Kalliola, S., Repo, E., Srivastava, V., Zhao, F., Heiskanen, J.P., Sirviö, J.A., Liimatainen, H. and Sillanpää, M. 2018. Carboxymethyl Chitosan and Its Hydrophobically Modified Derivative as pH-Switchable Emulsifiers. *Langmuir*. **34**(8), pp.2800–2806.

Kaptay, G. 2006. On the equation of the maximum capillary pressure induced by solid particles to stabilize emulsions and foams and on the emulsion stability diagrams. *Colloids and Surfaces A: Physicochemical and Engineering Aspects*. **282**–**283**, pp.387–401.

Kasprzak, M.M., Erxleben, A. and Ochocki, J. 2015. Properties and applications of flavonoid metal complexes. *RSC Advances*. **5**(57), pp.45853–45877.

Khor, E. and Lim, L.Y. 2003. Implantable applications of chitin and chitosan. *Biomaterials*. **24**, pp.2339–2349.

Klinkesorn, U. 2013. The Role of Chitosan in Emulsion Formation and Stabilization. *Food Reviews International*. **29**, pp.371–393.

Kollarigowda, R.H., Abraham, S. and Montemagno, C.D. 2017. Antifouling Cellulose Hybrid Biomembrane for Effective Oil/Water Separation. *ACS applied materials & interfaces*. **9**(35), pp.29812–29819.

Kurita, K. 2006. Chitin and Chitosan: Functional Biopolymers from Marine Crustaceans. *Marine Biotechnology*. **8**(3), pp.203–226.

Laitinen, O., Ojala, J., Sirviö, J. and Liimatainen, H. 2017. Sustainable stabilization of oil in water emulsions by cellulose nanocrystals synthesized from deep eutectic solvents. *Cellulose*. **24**, pp.1679–1689.

Laitinen, O., Suopajärvi, T., Österberg, M. and Liimatainen, H. 2017. Hydrophobic, Superabsorbing Aerogels from Choline Chloride-Based Deep Eutectic Solvent Pretreated and Silylated Cellulose Nanofibrils for Selective Oil Removal. *ACS Applied Materials & Interfaces*. **9**, pp.25029–25037.

Lessard, R.R. and DeMarco, G. 2000. The Significance of Oil Spill Dispersants. *Spill Science and Technology Bulletin*. **6**, pp.59–68.

Li, Jian, Li, D., Yang, Y., Li, Jianping, Zha, F. and Lei, Z. 2016. A prewetting induced underwater superoleophobic or underoil (super) hydrophobic waste potato residue-coated mesh for selective efficient oil/water separation. *Green Chemistry*. **18**(2), pp.541–549.

Li, Y., Zhang, S., Meng, X., Chen, X. and Ren, G. 2011. The preparation and characterization of a novel amphiphilic oleoyl-carboxymethyl chitosan self-assembled nanoparticles.

Carbohydrate Polymers. **83**, pp.130–136.

Liu, J., Li, P., Chen, L., Feng, Y., He, W., Yan, X. and Lü, X. 2016. Superhydrophilic and underwater superoleophobic modified chitosan-coated mesh for oil/water separation. *Surface & Coatings Technology*. **307**, pp.171–176.

Lusiana, R.A., Siswanta, D. and Mudasir 2014. Modifying Surface Charge of Chitosan Membrane by N,O-Carboxymethyl chitosan Blended with Poly(vinylalcohol). *International Journal of Advances in Chemical Engineering and Biological Sciences*. **1**.

Mafra, M.R., Igarashi-Mafra, L., Zuim, D.R., Vasques, É.C. and Ferreira, M.A. 2013. Adsorption of remazol brilliant blue on an orange peel adsorbent. *Brazilian Journal of Chemical Engineering*. **30**(3), pp.657–665.

Majeti, N.V.R. 2000. A review of chitin and chitosan applications. *Reactive and Functional Polymers*. **46**, pp.1–27.

Di Martino, A., Sittinger, M. and Risbud, M. V 2005. Chitosan: A versatile biopolymer for orthopaedic tissue-engineering. *Biomaterials*. **26**, pp.5983–5990.

Matos, M., Marefati, A., Bordes, R., Gutiérrez, G. and Rayner, M. 2017. Combined emulsifying capacity of polysaccharide particles of different size and shape. *Carbohydrate Polymers*. **169**, pp.127–138.

McClements, D.J. and Gumus, C.E. 2016. Natural emulsifiers — Biosurfactants, phospholipids, biopolymers, and colloidal particles: Molecular and physicochemical basis of functional performance. *Advances in Colloid and Interface Science*. **234**, pp.3–26.

Menger, F.M. and Littau, C.A. 1991. Gemini surfactants: synthesis and properties. *Journal of the American Chemical Society*. **113**, pp.1451–1452.

Mirshahghassemi, S. and Lead, J.R. 2015. Oil Recovery from Water under Environmentally Relevant Conditions Using Magnetic Nanoparticles. *Environmental Science & Technology*. **49**(19), pp.11729–11736.

Mohamed, M. and Ouki, S. 2011. Removal Mechanisms of Toluene from Aqueous Solutions by Chitin and Chitosan. *Industrial & Engineering Chemistry Research*. **50**(16), pp.9557–9563.

Mohanram, R., Jagtap, C. and Kumar, P. 2016. Isolation, screening, and characterization of surface-active agent-producing, oil-degrading marine bacteria of Mumbai Harbor. *Marine Pollution Bulletin*. **105**(1), pp.131–138.

Mohy Eldin, M.S., Ammar, Y.A., Tamer, T.M., Omer, A.M. and Ali, A.A. 2017. Development of low-cost chitosan derivatives based on marine waste sources as oil adsorptive materials: I. Preparation and characterization. *Desalination and Water Treatment*. **72**, pp.41–51.

Mohy Eldin, M.S., Ammar, Y.A., Tamer, T.M., Omer, A.M. and Ali, A.A. 2016. Development Of Oleophilic Adsorbent Based On Chitosan- Poly (Butyl Acrylate) Graft Copolymer For Petroleum Oil Spill Removal. *International Journal of Advanced Research*. **4**(11), pp.2095–2111.

Moriwaki, H., Kitajima, S., Kurashima, M., Hagiwara, A., Haraguchi, K., Shirai, K., Kanekatsu, R. and Kiguchi, K. 2009. Utilization of silkworm cocoon waste as a sorbent for the removal of oil from water. *Journal of Hazardous Materials*. **165**(1), pp.266–270.

Muhammad, I.M., El-Nafaty, U.A., Surajudeen, A. and Makarfi., Y.I. 2015. Oil removal from Produced Water Using Surfactant Modified Eggshell. *2015 4th International Conference on Environmental, Energy and Biotechnology*. **85**, pp.84–92.

Muzzarelli, R.A.A. 2009. Chitins and chitosans for the repair of wounded skin, nerve, cartilage and

bone. *Carbohydrate Polymers*. **76**, pp.167–182.

Neste 2017. Safety Data Sheet Neste Marine 2T. Available from: https://www.neste.fi/static/ktt/19000_eng.pdf.

Ngah, W.S.W., Teong, L.C. and Hanafiah, M.A.K.M. 2011. Adsorption of dyes and heavy metal ions by chitosan composites: A review. *Carbohydrate Polymers*. **83**, pp.1446–1456.

Ojala, J., Sirviö, J.A. and Liimatainen, H. 2016. Nanoparticle emulsifiers based on bifunctionalized cellulose nanocrystals as marine diesel oil–water emulsion stabilizers. *Chemical Engineering Journal*. **288**, pp.312–320.

Oldehhove de Guertechin, L. 2001. Chapter 37: Classification of Surfactants *In*: A. Barel, M. Payne and H. I. Maibach, eds. *Handbook of Cosmetic Science and Technology*. New York: Taylor & Francis.

de Oliveira, C.R., Carneiro, R.L. and Ferreira, A.G. 2014. Tracking the degradation of fresh orange juice and discrimination of orange varieties: An example of NMR in coordination with chemometrics analyses. *Food Chemistry*. **164**, pp.446–453.

Omarova, M., Swientoniewski, L.T., Tsengam, I.K.M., Panchal, A., Yu, T., Blake, D.A., Lvov, Y.M., Zhang, D. and John, V. 2018. Engineered Clays as Sustainable Oil Dispersants in the Presence of Model Hydrocarbon Degrading Bacteria: The Role of Bacterial Sequestration and Biofilm Formation. *ACS Sustainable Chemistry & Engineering*. **6**(11), pp.14143–14153.

Patale, R.L. and Patravale, V.B. 2011. O,N-carboxymethyl chitosan–zinc complex: A novel chitosan complex with enhanced antimicrobial activity. *Carbohydrate Polymers*. **85**(1), pp.105–110.

Paul, U., Fragouli, D., Bayer, I. and Athanassiou, A. 2016. Functionalized Cellulose Networks for Efficient Oil Removal from Oil–Water Emulsions. *Polymers*. **8**, pp.1–12.

Peterson, C.H., Rice, S.D., Short, J.W., Esler, D., Bodkin, J.L., Ballachey, B.E. and Irons, D.B. 2003. Long-term ecosystem response to the Exxon Valdez oil spill. *Science*. **302**, pp.2082–2086.

Pi, G., Li, Y., Bao, M., Mao, L., Gong, H. and Wang, Z. 2016. Novel and Environmentally Friendly Oil Spill Dispersant Based on the Synergy of Biopolymer Xanthan Gum and Silica Nanoparticles. *ACS Sustainable Chemistry & Engineering*. **4**(6), pp.3095–3102.

Rajaković-Ognjanović, V., Aleksić, G. and Rajaković, L. 2008. Governing factors for motor oil removal from water with different sorption materials. *Journal of Hazardous Materials*. **154**, pp.558–563.

Rayner, M., Marku, D., Eriksson, M., Sjöö, M., Dejmek, P. and Wahlgren, M. 2014. Biomass-based particles for the formulation of Pickering type emulsions in food and topical applications. *Colloids and Surfaces A: Physicochemical and Engineering Aspects*. **458**, pp.48–62.

Riehm, D.A., Neilsen, J.E., Bothun, G.D., John, V.T., Raghavan, S.R. and McCormick, A. V. 2015. Efficient dispersion of crude oil by blends of food-grade surfactants: Toward greener oil-spill treatments. *Marine Pollution Bulletin*. **101**(1), pp.92–97.

Riehm, D.A., Rokke, D.J., Paul, P.G., Lee, H.S., Vizanko, B.S. and McCormick, A. V. 2017. Dispersion of oil into water using lecithin-Tween 80 blends: The role of spontaneous emulsification. *Journal of Colloid and Interface Science*. **487**, pp.52–59.

Rinaudo, M. 2006. Chitin and chitosan: Properties and applications. *Progress in Polymer Science*.

31(7), pp.603–632.

Röling, W.F.M., Milner G, M., Jones, D.M., Lee, K., Daniel, F., Swannell, R.J.P. and Head, I.M. 2002. Robust Hydrocarbon Degradation and Dynamics of Bacterial Communities during Nutrient-Enhanced Oil Spill Bioremediation. *Applied and Environmental Microbiology*. **68**, pp.5537–5548.

Sagerup, K., Nahrgang, J., Frantzen, M., Larsen, L.-H. and Geraudie, P. 2016. Biological effects of marine diesel oil exposure in red king crab (Paralithodes camtschaticus) assessed through a water and foodborne exposure experiment. *Marine Environmental Research*. **119**, pp.126–135.

Schatz, C., Domard, A., Viton, C., Pichot, C. and Delair, T. 2004. Versatile and Efficient Formation of Colloids of Biopolymer-Based Polyelectrolyte Complexes. *Biomarcomolecules*. **5**(5), pp.1882–1892.

Schmidt, U.S., Schmidt, K., Kurz, T., Endreß, H.-U. and Schuchmann, H.P. 2015. Pectins of different origin and their performance in forming and stabilizing oil-in-water-emulsions. *Food Hydrocolloids*. **46**, pp.59–66.

Schmidt, U.S., Schütz, L. and Schuchmann, H.P. 2017. Interfacial and emulsifying properties of citrus pectin: Interaction of pH, ionic strength and degree of esterification. *Food Hydrocolloids*. **62**, pp.288–298.

Shahidi, F., Arachchi, J.K.V. and Jeon, Y.-J. 1999. Food applications of chitin and chitosans. *Trends in Food Science & Technology*. **10**, pp.37–51.

Shakeri, H., Arshadi, M. and Salvacion, J.W.L. 2016. Removal of BTEX by using a surfactant – Bio originated composite. *Journal of Colloid and Interface Science*. **466**, pp.186–197.

Sharma, M.K. and Shah, D.O. 1985. Chapter 1: Introduction to Macro- and Microemulsions *In*: *Macro- and Microemulsions*. ACS Symposium Series, pp.1–18.

Shiao, S.., Chhabra, V., Patist, A., Free, M.., Huibers, P.D.., Gregory, A., Patel, S. and Shah, D.. 1998. Chain length compatibility effects in mixed surfactant systems for technological applications. *Advances in Colloid and Interface Science*. **74**(1–3), pp.1–29.

Shinoda, K. and Saito, H. 1969. The Stability of O/W type emulsions as functions of temperature and the HLB of emulsifiers: The emulsification by PIT-method. *Journal of Colloid and Interface Science*. **30**, pp.258–263.

Sidik, S.M., Jalil, A.A., Triwahyono, S., Adam, S.H., Satar, M.A.H. and Hameed, B.H. 2012. Modified oil palm leaves adsorbent with enhanced hydrophobicity for crude oil removal. *Chemical Engineering Journal*. **203**, pp.9–18.

Silva, L.M.A., Alves Filho, E.G., Choze, R., Lião, L.M. and Alcantara, G.B. 2012. 1H HRMAS NMR spectroscopy and chemometrics for evaluation of metabolic changes in citrus sinensis Caused by Xanthomonas axonopodis pv. citri. *Journal of the Brazilian Chemical Society*. **23**(6), pp.1054–1061.

Soares, S.F., Rodrigues, M.I., Trindade, T. and Daniel-da-Silva, A.L. 2017. Chitosan-silica hybrid nanosorbents for oil removal from water. *Colloids and Surfaces A: Physicochemical and Engineering Aspects*. **532**, pp.305–313.

Sokker, H.H., El-Sawy, N.M., Hassan, M.A. and El-Anadouli, B.E. 2011. Adsorption of crude oil from aqueous solution by hydrogel of chitosan based polyacrylamide prepared by radiation induced graft polymerization. *Journal of Hazardous Materials*. **190**(1), pp.359–365.

Srinivasan, A. and Viraraghavan, T. 2010. Oil removal from water using biomaterials. *Bioresource*

Technology. **101**(17), pp.6594–6600.
Srinivasan, A. and Viraraghavan, T. 2008. Removal of oil by walnut shell media. *Bioresource Technology*. **99**(17), pp.8217–8220.
Suh, F.J.K. and Matthew, H.W.T. 2000. Application of chitosan-based polysaccharide biomaterials in cartilage tissue engineering: a review. *Biomaterials*. **21**, pp.2589–2598.
Sun, G.Z., Chen, X.G., Zhang, J., Feng, C. and Cheng, X.J. 2010. Adsorption characteristics of residual oil on amphiphilic chitosan derivative. *Water Science & Technology*. **61**(9), pp.2363–2374.
Teas, C., Kalligeros, S., Zanikos, F., Stournas, S., Lois, E. and Anastopoulos, G. 2001. Investigation of the effectiveness of absorbent materials in oil spills clean up. *Desalination*. **140**, pp.259–264.
Tewari, S. and Sirvaiya, A. 2015. Oil Spill Remediation and its Regulation. *International Journal of Research In Science & Engineering*. **1**, pp.1–7.
Valandro, S.R., Lombardo, P.C., Poli, A.L., Posakoda, C.E. and Cavalheiro, C.C.S. 2013. Effect of Hydrocarbon Chain Length Surfactants on Particle Size of SWy-1 Montmorillonite Suspensions. *International Journal of Basic & Applied Sciences*. **13**(6), pp.1–6.
Venkataraman, P., Tang, J., Frenkel, E., McPherson, G.L., He, J., Raghavan, S.R., Kolesnichenko, V., Bose, A. and John, V.T. 2013. Attachment of a hydrophobically modified biopolymer at the oil-water interface in the treatment of oil spills. *ACS Applied Materials & Interfaces*. **5**, pp.3572–3580.
Wang, W., Zheng, Y. and Lee, K. 2013. Chemical dispersion of oil with mineral fines in a low temperature environment. *Marine Pollution Bulletin*. **72**, pp.205–212.
Wang, X. and Alvarado, V. 2012. Effects of Aqueous-Phase Salinity on Water-in-Crude Oil Emulsion Stability. *Journal of Dispersion Science and Technology*. **33**, pp.165–170.
Wang, Z. and Fingas, M.F. 2003. Development of oil hydrocarbon fingerprinting and identification techniques. *Marine Pollution Bulletin*. **47**, pp.423–452.
Wassmann, P., Duarte, C.M., Agust, S. and Sejr, M.K. 2011. Footprints of climate change in the Arctic marine ecosystem. *Global Change Biology*. **17**(2), pp.1235–1249.
Wennerström, H., Söderman, O., Olsson, U. and Lindman, B. 1997. Macroemulsions versus microemulsions. *Colloids and Surfaces A: Physicochemical and Engineering Aspects*. **123**, pp.13–26.
Winsor, P.A. 1947. Hydrotropy, Solubilisation and related Emulsification Processes. Part I. *Transactions 583 of the Faraday Society*. **44**, pp.376–398.
Wise, C.F., Wise, J.T.F., Wise, S.S., Thompson, W.D., Wise, J.P. and Wise, J.P. 2014. Chemical dispersants used in the Gulf of Mexico oil crisis are cytotoxic and genotoxic to sperm whale skin cells. *Aquatic Toxicology*. **152**, pp.335–340.
Yan, N. and Chen, X. 2015. Sustainability: Don't waste seafood waste. *Nature*. **524**(7564), pp.155–157.
Yang, J., Song, H., Yan, X., Tang, H. and Li, C. 2014. Superhydrophilic and superoleophobic chitosan-based nanocomposite coatings for oil/water separation. *Cellulose*. **21**(3), pp.1851–1857.
Yang, Y., Fang, Z., Chen, X., Zhang, W., Xie, Y., Chen, Y., Liu, Z. and Yuan, W. 2017. An Overview of Pickering Emulsions: Solid-Particle Materials, Classification, Morphology, and

Applications. *Frontiers in Pharmacology*. **8**, p.287.

Zhai, T., Zheng, Q., Cai, Z., Xia, H. and Gong, S. 2016. Synthesis of polyvinyl alcohol/cellulose nanofibril hybrid aerogel microspheres and their use as oil/solvent superabsorbents. *Carbohydrate Polymers*. **148**, pp.300–308.

Zhang, S., Lu, F., Tao, L., Liu, N., Gao, C., Feng, L. and Wei, Y. 2013. Bio-inspired anti-oil-fouling chitosan-coated mesh for oil/water separation suitable for broad pH range and hyper-saline environments. *ACS Applied Materials & Interfaces*. **5**(22), pp.11971–11976.

Zhang, S., Lü, T., Qi, D., Cao, Z., Zhang, D. and Zhao, H. 2017. Synthesis of quaternized chitosan-coated magnetic nanoparticles for oil-water separation. *Materials Letters*. **191**, pp.128–131.

Zheng, M., Ahuja, M., Bhattacharya, D., Clement, T.P., Hayworth, J.S. and Dhanasekaran, M. 2014. Evaluation of differential cytotoxic effects of the oil spill dispersant Corexit 9500. *Life Sciences*. **95**(2), pp.108–117.

Publication I

Doshi, B., Repo, R., Heiskanen, J. P., Sirviö, J. A., Sillanpää, M.

Effectiveness of N,O-carboxymethyl chitosan on destabilization of Marine Diesel, Diesel and Marine-2T oil for oil spill treatment

Reprinted with permission from

Carbohydrate Polymers

Vol 167, pp. 326-336, 2017

Carbohydrate Polymers 167 (2017) 326–336

Contents lists available at ScienceDirect

Carbohydrate Polymers

journal homepage: www.elsevier.com/locate/carbpol

Effectiveness of N,O-carboxymethyl chitosan on destabilization of Marine Diesel, Diesel and Marine-2T oil for oil spill treatment

Bhairavi Doshi[a,*], Eveliina Repo[a], Juha P. Heiskanen[b], Juho Antti Sirviö[c], Mika Sillanpää[a]

[a] Laboratory of Green Chemistry, Lappeenranta University of Technology, Sammonkatu 12, Mikkeli 50130, Finland
[b] Research Unit of Sustainable Chemistry, University of Oulu, P.O. Box 3000, FI-90014, Finland
[c] Fibre and Particle Engineering Research Unit, University of Oulu, P.O. Box 4300, FI-90014, Finland

ARTICLE INFO

Article history:
Received 24 October 2016
Received in revised form 16 March 2017
Accepted 19 March 2017
Available online 21 March 2017

Chemical compound studied in this article:
Chitosan (PubChem CID: 71853)

Keywords:
N,O-carboxymethyl chitosan
Oil droplets
Micro emulsions
Oil spill treatment
Marine diesel
Adsorption

ABSTRACT

Oil spills are the significant sources of hydrocarbons entering in the receiving aquatic environment. An efficient method to remove hydrocarbons from water resources is adsorption. In this study, water soluble N,O-carboxymethyl chitosan (NO-CS) was synthesized by carboxymethylation of chitosan in a hydro-alcoholic medium at 50 °C by chloroacetic acid. The polymer was characterized through degree of deacetylation, degree of substitution, FTIR and ^{1}H NMR. Effectiveness of NO-CS as an adsorbent was studied as a function of dosage, salinity and pH to destabilize the Marine diesel (Oil-1), Diesel (Oil-2) and Marine-2T oil (Oil-3) into small oil droplets of less than 100 μm. Optical microscope was used for studying the size of oil droplets and adsorption effect of the oils on this polymer. The destabilization of marine diesel was the most effective among the studied three oils, which showed excellent adsorption at sea water alkalinity and salinity.

1. Introduction

Oil entering the natural water resources originates from the accidental spills or leaks from ships or tankers, storm water drainage from cities and farms, untreated waste disposal from factories and industrial facilities, unregulated recreational boating, offshore drilling and production operations (Farrington and McDowll, 2004). Climatic change (Wassmann, Duarte, Agust, & Sejr, 2011) enables increase in transportation (Arrigo, 2013) and industrial activities in arctic regions by enhancing the oil spill rate (Nevalainen, Helle, & Vahnatalo, 2017). Oil spilled from the ships and tankers including the transportation fuel used by the vessels themselves or their cargos, such as crude oil, fuel oil, or heating oil are the significant sources of hydrocarbon inputs into the oceans, lakes, rivers, etc. These spills, not only destroy the marine life (DeLeo, Ruiz-Ramos, Baums, & Cordes, 2016; Sagerup, Nahrgang, Frantzen, Larsen, & Geraudie, 2016) and wetland, but also affects the estuarine habitat (Klemas, 2010).

Behavior of oil varies in different environments and, therefore it is important to know the type of oil spill (Dahlmann, 2003). The constituents of crude oil are saturates, aromatics, resins, and asphaltenes. Light crude oil contains a higher percentage of saturated hydrocarbons and aromatics, while heavy oil contains more resins and asphaltenes (Fan & Buckley, 2002). Diesel fuel is most often a light, refined petroleum product consists of hydrocarbon from C8-C26 which are either branched and/or linear. A small amount of diesel spills will usually evaporate and disperse naturally within a day or less. But marine diesel is often a heavier fuel oil that persist longer when spilled and in-situ burning may not be possible under Arctic conditions even though it is designed for combustion. Marine diesel and diesel contains about 1.2% and 2% of polyaromatics, respectively. Marine 2T-oil is the petroleum distillates consist of hydrocarbons, C11-C14, n-alkanes, isoalkanes, cyclics, butene, solvent-dewaxed heavy paraffinic and polyaromatics, and it is used in ships and, boats as a lubricant can easily react with water forming a creamy layer. A small amount of oil spill affects the marine ecosystem due to its toxicity (Peterson et al., 2003). In extreme cold conditions, natural weathering process such as evaporation and biodegradation (Wang & Fingas, 2003) rates reduce with increase in viscosity of oil. There is evaporative loss of about 30% for open water, 25% for the lighter ice coverage, and 19% for the heavier ice

* Corresponding author. Tel.: +358 504356962.
E-mail address: Bhairavi.doshi@lut.fi (B. Doshi).

http://dx.doi.org/10.1016/j.carbpol.2017.03.064

coverage, due to differences in oil film thicknesses (Brandvik and Faksness, 2009). To clean up oil in the coastal environment, various spill containment methods such as use of booms, hard booms, sorbent booms, fire booms, skimmers, vacuum trucks, in situ burning, dispersants (Brakstad et al., 2014), and chemical cleaners are used.

A mixture of oil and water is generally unstable and addition of surfactants reduces the interfacial tension between the oil and water by breaking the oil into oil droplets and preventing coalescence of dispersed oil droplets. A surfactant used in oil spill treatment can either be adsorbed at the oil-water interfaces or form thicker slicks with oil. However, prolonged use of synthetic surfactants reflects toxic effects on the marine ecosystems (Claireauxa et al., 2013; Lewis & Pryor, 2013; Smit et al., 2009). Nowadays, replacement of these hazardous chemicals has been studied, either by using bio-surfactants (Silva et al., 2014) or biopolymers (Venkataraman et al., 2013) due to their biocompatibility, non-toxicity and sustainability in the oil-spill treatment.

Biopolymer chitosan is a deacetylated form of chitin used widely as a biomaterial in drug delivery and tissue engineering (Martinoa, Sittingerc, & Risbud, 2005), as a sorbent in waste water treatment for removal of metals (Bhatnagar & Sillanpää, 2009; Crini, 2005; Ngaha, Teonga, & Hanafiaha, 2010; Repo, Warchol, Bhatnagar, & Sillanpää, 2011), and in food industry as it is abundant, versatile, non-toxic, biocompatible and biodegradable (Khora & Lim, 2003). Chitosan has excellent adsorption characteristics due to the presence of large number of hydroxyl groups, which gives hydrophilicity and large number of amino groups with high activity as adsorption sites (Mourya, Inamdar, & Tiwari, 2010). However, the formation of protonated amino group contributes to the solubility of chitosan in acidic solutions (Bee, Obeid, Mbolantenaina, Welschbillig, & Talbot, 2016). This variable functionality of amino groups at different solution pH, can be used to stabilize oil-in-water emulsions (Colombo, Cavakieri, & Muthupandian, 2015). Emulsion stability also depends on the hydrophobicity and hydrophilicity of the particles, so to get oil-in-water emulsion, particles should be hydrophilic (Tsabet & Fradette, 2015).

Carboxymethylation is a reaction of an alkaline pre-treated chitosan with chloroacetic acid in the presence of isopropanol as a solvent. The presence of sodium hydroxide in the reaction mixture results in swelling of chitosan and consequently better diffusion of chloroacetic acid into the rigid structure of chitosan (Chen, Du, & Zeng, 2003) and, appropriate amounts of isopropanol together with water facilitates the reaction (Chen & Park, 2003). Reaction time and amount of chloroacetic acid and sodium hydroxide have a significant effect on the solubility of the carboxymethyl chitosan in water (Bidgoli, Zamani, & Taherzadeh, 2010). Depending of the reaction conditions, there is a selectivity substitution site for N- versus O-carboxymethyl chitosan derivative. Hence, the overall properties of carboxymethylation is structural dependent and mainly on degree of substitution (An, Thien, Dong, & Dung, 2009). Carboxymethyl chitosan is used in waste water treatment (Boricha & Murthy, 2010), in cosmetics (Jimtaisong & Saewan, 2014), in biomedical and pharmaceuticals (Chen, Wang, Chen, Ho, & Sheu, 2006) due to its biological properties, and as a sorbent for removal of metals (Sun & Wang, 2006) and dyes (Wang & Wang, 2008), etc. N,O-carboxymethyl chitosan (NO-CS) is a water soluble derivative of chitosan, enhancing biodegradability and biocompatibility, physiochemical and biological properties (Upadhyaya, Singh, Agarwal, & Tewari, 2013), in comparison to chitosan. However, the applicability of NO-CS with degree of substitution lower than 0.5, has not been studied much for in oil spill treatment.

This study was carried out to investigate the effectiveness of NO-CS on three different oils by considering dosage, salinity, and pH. As NO-CS was hydrophilic, the effect of dosage was limited only to destabilization of oil inhibiting coalescence due to electrostatic interaction between negatively charged carboxylate ion attached to amino group of NO-CS and hydrocarbons presented in oil with oil droplets size less than 100 μm. Here the amino groups which were not carboxymethylated remains unaffected. Sodium chloride was used as an electrolyte to study the salinity effect on NO-CS solution on oil. Ionic strength of the NO-CS solution increased due to increase in the salinity. This decreases the critical micelle concentration (CMC) of NO-CS for the formation of oil droplets for oil-1 and oil-2 compared to oil-3. Therefore, the amount of NO-CS dosage decreases with increases in salinity.

The pH effect of NO-CS leading to destabilization of oil droplets was also studied. At acidic pH, the amino groups (free as well as carboxymethylated both) were protonated and the negatively charged carboxylate ions attached to amino groups underwent electrostatic repulsion towards negatively charged hydrocarbons forming Winsor type-III (Winsor, 1947) micro emulsions. Whereas at alkaline pH, those protonated amino groups of NO-CS undergoing electrostatic attraction with the hydrocarbons of oils enhancing adsorption over formation of oil droplets. The pH of seawater before industrial era began was about 8.2 (slightly basic) and nowadays it is about 8.1. So it was important to study the effect of NO-CS on oil-1, oil-2 and oil-3 at alkaline pH in presence of salinity. The destabilization of oils using NO-CS was investigated by this study.

2. Materials and methods

2.1. Materials

Chitosan from crab shells (CAS No. 9012-76-4, Lot #BCBP6349V, highly viscous, viscosity >400 mPa.s in 1% acetic acid at 20 °C), chloroacetic acid (CAS No. 79-11-8, Lot #SHBD8969V, ≥99%), hydrochloric acid (CAS No. 7647-01-0, Lot #SZBF2070V, 37%) and sodium chloride (CAS no. 7647-14-5, Lot #SZBB0170V) were purchased from Sigma-Aldrich Finland Oy. Sodium hydroxide (CAS No. 1310-73-2, Lot #SZBE1130V) and methyl red (CAS No. 493-52-7, Lot 80950) were purchased from Fluka. Isopropanol (CAS No. 67-63-0, Lot #K40448334) was purchased from Merck. Ethanol (99.5%) was purchased from Altia Oyj. All chemicals were used without further purification. Oil-1 is a sulfur-free marine diesel oil (winter grade) with a density of 828 kg/m^3 at 15 °C and viscosity of 1.846 mm^2/s at 40 °C, which was received from Fibre and Particle Engineering Research Unit, University of Oulu, whereas Oil-2 is the diesel (summer grade) with a density of 803 kg/m^3 at 15 °C and viscosity of 2.1 mm^2/s at 40 °C and Oil-3 is the Neste Marine-2T oil with a density of 872 kg/m^3 at 15 °C and viscosity of 8.5 mm^2/s at 40 °C were purchased from Neste Oyj, Finland. Deuterium chloride solution (35 wt.% in D_2O, 99 atom-% D, CAS No 7698-05-7, Lot #MBB1157 V) was obtained from Sigma Aldrich. D_2O was obtained from Eurisotop (99.96% atom-% D, CAS No 7789-20-0, Lot #D215FL0701). During all the experiments deionized water (Siemens Ultra Clear RO with Conductivity 0.055 μS/cm) was used. All the experiments were carried out at room temperature (21 °C).

2.2. Synthesis and characterization

2.2.1. Degree of deacetylation

One of the important chemical characterization of chitosan is the degree of deacetylation (DDA), which determines the content of free amino groups in the polysaccharides. The degree of deacetylation of chitosan from crab shells was determined by acid-base titration as mentioned in (Barros, Vasconcellos, Carvalho, & Nascimento, 2014) with some modification. 0.1 g of chitosan from crab shells was dissolved in 25 ml 0.1 M HCl solution. This solution was titrated against 0.1 M NaOH solution using methyl red as an indicator. For blank reading, the same titration was performed

without addition of chitosan. This titration was carried out in triplicate. The degree of deacetylation is given by

$$DDA = \frac{(V_{initial} - V_{used}) * 0.162 * N * 100}{W * (1.00 - LOD)},$$

where, $V_{initial}$ is the volume of NaOH used in blank titration, V_{used} is the volume of NaOH used in sample titration, N is the molarity of NaOH, W is the weight of sample, LOD is the loss on drying in chitosan sample.

2.2.2. Synthesis of N,O-carboxymethyl chitosan

N,O-carboxymethyl chitosan (NO-CS) was synthesized based on previously reported method (Sun et al., 2008) with some modification. Briefly, chitosan from crab shells (5 g), sodium hydroxide (5 g), isopropanol (40 ml), and water (100 ml) were added in a reaction flask and allowed to alkalize and swell for 1 h in water bath (IKA C-MAG HS 7 Digital) at 50 °C. Dissolved chloroacetic acid (7.5 g) in isopropanol (10 ml) was added dropwise in the reaction mixture during the next 30 min. The reaction was allowed to continue at the same temperature for 4 h in order to complete the reaction between chitosan and chloroacetate which rapidly forms from the reaction between sodium hydroxide and chloroacetic acid. Then 100 ml ethyl alcohol (70%) was added to stop the reaction. The product was washed with 70–90% ethyl alcohol and dried overnight at room temperature to give the sodium salt of carboxymethyl chitosan (Na-NO-CS). Na-NO-CS (2 g) was suspended in 200 ml ethyl alcohol (80%), 20 ml hydrochloric acid (37%) was added, and the mixture was stirred for 1 h. The solid was washed with 70–90% ethyl alcohol and dried overnight at room temperature to give the product (NO-CS). SEM (Hitachi SU3500) was used to study the surface of the chitosan before and after carboxymethylation at accelerating voltage of 10 kV.

2.2.3. Degree of substitution

The degree of substitution (DS) also depends on the degree of deacetylation. The degree of substitution of NO-CS was determined by using potentiometric titration (Bidgoli et al., 2010; Ge & Luo, 2005) with some modifications. 0.2 g of NO-CS was dissolved in 40 ml water and the pH was adjusted below 2 by adding 0.1 M HCl detected by pH meter (WTW pH 341S). The solution was titrated against 0.1 M NaOH solution and simultaneously the pH was measured for each addition of NaOH solution. The amount of NaOH was determined using the first order differential method. The degree of substitution was calculated by

$$DS = \frac{(V_2 - V_1) * DDA}{(V_3 - V_2)}$$

where, V_1, V_2 and V_3 are the respective volumes of NaOH.

2.2.4. Characterization of NO-CS by FTIR and ^{1}H NMR

Chitosan from crab shells and NO-CS were characterized using Bucker FTIR (Vertex 70) from the range of 400–4000 cm^{-1} with a resolution of 4 cm^{-1} for 60 scans. For NMR measurement, samples of chitosan and NO-CS were dissolved in D_2O containing 0.7% of DCl and placed in 5 mm NMR tubes. The ^{1}H NMR spectra were recorded by using Bruker Ascend 400 MHz spectrometer and standard proton parameters with the delay time (d1) of 6 s at 70 °C.

2.3. Effect of dosage

For this study, different dosages of NO-CS (0–50 mg) were dissolved in water. Oil-1 was added in each and every NO-CS dosage solution, so that the concentration of NO-CS to oil was about 0–65 mg/g. The ratio of oil to water was 1:10, which remained constant throughout the study. The same procedure was repeated for oil-2 and oil-3. All the solutions were shaken at 2000 rpm with vortex mixture (VWR International) for 30 s and then 300 rpm for 30 min with shaker (using KS 4000 ic control from IKA) in order to study the formation of oil droplets with respect to NO-CS dosage. The mixture was allowed to saturate for 2 h and then centrifuged (Eppendorf 5810R) for 5 min at 1500 rpm. After centrifugation, separated oil was removed and weighed again. This procedure was repeated in triplicate. Oil droplet size was measured using optical microscope (Zeiss Axio using the camera unit Axio CamERc5s by ZEN software).

2.4. Effect of salinity

Different dosages of NO-CS (0–25 mg) were dissolved in saline water having concentration from 0 to 3.5%. Oil-1 was added to each concentration having different dosage of NO-CS (so that the concentration of NO-CS to oil was about 0–35 mg/g). The ratio of oil to water was 1:10, which remained constant throughout the study. The same procedure was repeated for oil-2 and oil-3. All the solutions were shaken at 2000 rpm with vortex mixture (VWR International) for 30 s and then 300 rpm for 30 min with shaker (using KS 4000 ic control from IKA) in order to study the behavior of NO-CS in the presence of salinity in destabilizing the oils. The oil-in-water solution was saturated for 2 h and then centrifuged (Eppendorf 5810R) for 5 min at 1500 rpm. The separated oil was removed and weighed again. The same was repeated in triplicate. Oil droplet sizes were measured using optical microscope (Zeiss Axio using the camera unit Axio CamERc5s by ZEN software) in order to show the effect of salinity.

2.5. Effect of pH

Effect of hydrophilic NO-CS was studied with respect to pH. NO-CS (10–15 mg) was dissolved in water and pH of the solution was adjusted with either 0.1 M HCl solution or 0.1 M NaOH solution by using pH meter (WTW pH 341S). Oil-1 was added to each NO-CS solution having different pH (3–9). The ratio of oil to water was 1:10, which remained constant throughout the study. The same procedure was repeated for oil-2 and oil-3. All the solutions were shaken at 2000 rpm with vortex mixture for 30 s and allowed to saturate for 2 h. The effect of different pH solution of NO-CS on oils was studied using Optical microscope (Zeiss Axio using the camera unit Axio CamERc5 s by ZEN software).

2.6. Adsorption of oil

Adsorption was studied from the optimized conditions of dosage and pH with different salinity for NO-CS polymer. Sea water has a salinity of about 3.5% of dissolved salts, mainly in the form of sodium and chloride ions. Hence, this study was carried out to show the behavior of NO-CS in presence of salinity up to 3%. NO-CS solutions (0.10–0.15%) were prepared with different salinity (0–3.5%) with pH about 9. pH was adjusted using 0.1 M NaOH by pH meter (WTW pH 341S). Oils were separately added to NO-CS solutions and shaken at 2000 rpm with vortex mixture for 15 s. After that, the pH was adjusted to 7.5–8 by addition of 0.1 M HCl and mixed for 15 s with the same speed. The mixture was allowed to saturate for 2 h and adsorption was studied using Optical microscope (Zeiss Axio using the camera unit Axio CamERc5s by ZEN software).

3. Results

3.1. Degree of deacetylation and degree of substitution

The measured degree of deacetylation of chitosan from crab shells was 74%, with reproducibility of less than 5% of standard deviation. The process of deacetylation involves the removal of acetyl

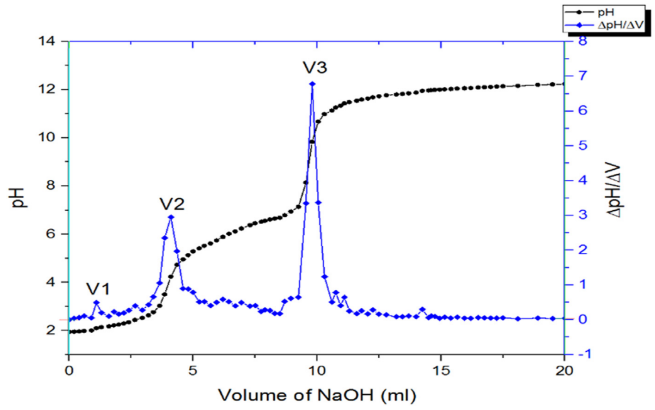

Fig. 1. Potentiometric titration for NO-CS with three inflection points.

groups from the molecular chain of chitin, leaving behind amino group (-NH_2) (Khan, Peh, & Ch'ng, 2002) and chitosan versatility depends mainly on this highly reactive amino groups. Therefore, it was essential to determine degree of deacetylation prior to its utilization for oil spill treatment.

The degree of substitution was 0.40, which indicates that by increasing the ratio of water/isopropanol in the reaction solvent, the fraction of carboxymethylation decreases by increasing the insolubility of NO-CS at higher pH range (Chen & Park, 2003). This insoluble region was either due to aggregation of highly acetylated chain segments or to amide formation subsequent to thermal drying. Three inflection points in the titration curve of NO-CS as shown in Fig. 1, is due to the oppositely ionizable carboxyl and amino groups, which coexist onto the same polysaccharide chains because of the carboxymethylation (Wang, Chen, Liu, Liu, & Zhou, 2008). First inflection point in Fig. 1, occurs due to neutralization of excess of HCl, followed by deprotonation of carboxylate ion and then deprotonation of ammonium ion of NO-CS.

The overall potentiometric titration of NO-CS can be expressed as follows:

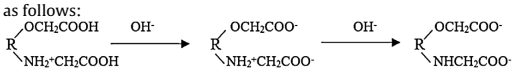

Where R is the glucopyranose unit of NO-CS.

In NO-CS, part of —NH_2 or —$NHCH_2COOH$ groups exists in the form of —NH_3^+ or —$NH_2^+CH_2COOH$ and so increase in carboxylic acid content in NO-CS, lowers the degree of substitution (Kong, 2012).

3.2. Structural characterization of NO-CS

3.2.1. SEM analysis

The surface morphology of chitosan before and after carboxymethylation was studied. SEM images of the chitosan surface before and after carboxymethylation are shown in Fig. 2.

3.2.2. FTIR analysis

The FTIR spectra for chitosan from crab shells (Fig. 3A) and NO-CS (Fig. 3B) were analyzed to determine the carboxymethylation process and possible substitution site of carboxymethylation in NO-CS as shown in Fig. 3. For NO-CS, the wide band at 3301 cm^{-1} corresponds to the axial stretching of the O—H and N—H bonds (An et al., 2009) which shows more hydrophilic character of NO—CS compared to chitosan (Lusiana, Siswanta, & Mudasir, 2014). The peaks at 2887 cm^{-1} corresponds to the axial stretching of the C—H bonds (Kong, 2012) and 1734 cm^{-1} corresponds to the symmetric stretching vibration of C=O in the —COOH groups, which was not found in chitosan. Two bands at 1624 cm^{-1} and 1519 cm^{-1} assigned to NH_3^+, indicates that the carboxymethylation occurred at OH position only (Mourya et al., 2010). In contrast, the peak at 3301 cm^{-1} of NO-CS (Fig. 3A) is broader than chitosan (Fig. 3B), shows the presence of secondary amine indicating the carboxymethylation had also occurred at NH position in NO-CS. The peak at 1377 cm^{-1} was related to the symmetric angular deformation of C—H bonds. The stretching vibration of C—O in CH_2COOH group gives rise to the peak at 1249 cm^{-1}, which was not observed in chitosan. The peaks, in the range of 1150–897 cm^{-1} are the results of vibrations of C—O and C—O—C of the polysaccharide chain also observed in chitosan. From FTIR, it is confirmed that the carboxymethylation takes place only at both amino groups and hydroxyl groups.

3.2.3. ^1H NMR analysis

The ^1H NMR spectra of chitosan and NO-CS are presented in Fig. 4. The spectrum of NO-CS shows the same characteristic proton signals as can be seen in chitosan spectrum. However, two new signals can be found in the spectrum of NO-CS compared to chitosan. The peaks at 3.78 and 4.61 ppm are assigned to N—CH_2- and —O—CH_2- protons at 2- and 6-positions, respectively (Chen & Park, 2003; Abreu & Campana-Filho, 2005). Thus, the NMR data also supports the interpretation of FTIR data that both the amino and hydroxyl groups at the 2- and 6-positions are partly carboxymethylated. Based on the integrals of peaks at 3.78 and 4.61 ppm, the ratio of carboxymethyl substituents at 2-N position to carboxymethyl substituents at 6-OH position is 5:7.

3.3. Effectiveness of NO-CS as a function of dosage

NO-CS is hydrophilic chitosan derivative and increase in the dosage leads to crowding effect of micelles, which increases the

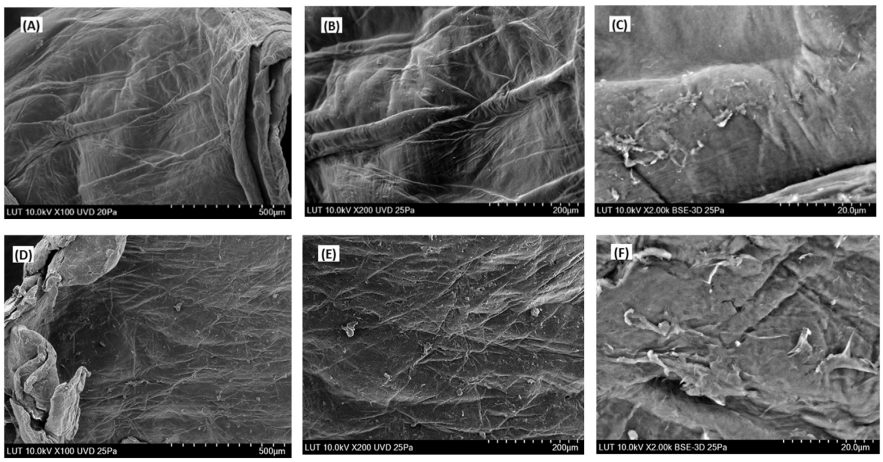

Fig. 2. SEM images of chitosan surface before and after carboxymethylation were taken at accelerating voltage of 10 kV. (A), (B), (C) are Chitosan images taken at 500 μm, 200 μm and 20 μm of magnifications and (D), (E), (F) are NO-CS images taken at 500 μm, 200 μm and 20 μm of magnifications.

viscosity of the solution. Fig. 5A shows the effect of dosage on the formation of oil droplets for all three oils. Fig. 5B and C show that, in the absence of NO-CS, oil-in-water emulsion was not stable as it undergoes coalescence forming two separate phase with oil-1 and oil-2 after saturation. Initial interfacial tension between NO-CS (0.1% solution) and oils was 19.77, 19.01 and 20.45 mN/m at 20 °C respectively, which was measured by pendant drop method (Optical contact angle measuring instrument, DataPhysics OCA 15EC Series). In the presence of NO-CS, oils undergo the Winsor type-III micro emulsions by destabilization of oil into droplets with less than 100 μm measured by Optical microscope. NO-CS, with dosage of 20 mg/g destabilized 96% of oil-1 into small droplets, whereas 25 mg/g was needed to destabilize oil-2 with 37% of oil separation (Fig. 5A), which is critical micelle concentration (CMC) for oil-1 and oil-2 after which interfacial tension is independent of the concentration. This was because at lower concentration, the o/w emulsion was not very stable, as the amount of amphiphilies was not enough to cover the interface. For concentrated solutions, the stabilization of emulsion occurs because of the formation of a tighter monolayer with adsorbed species and stronger interparticle interactions inhibiting the coalescence of emulsion droplets in highly viscous medium. Oil-3, being highly viscous among the three, consists of alpha-olefins and paraffins which forms creamy layer with water even though NO-CS is absent, and small amount of NO-CS (5 mg) converts creamy layer to emulsified precipitates (Fig. 5D). Oil droplets formation for oil-3 with 10 mg/g of NO-CS is shown in Fig. 5E.

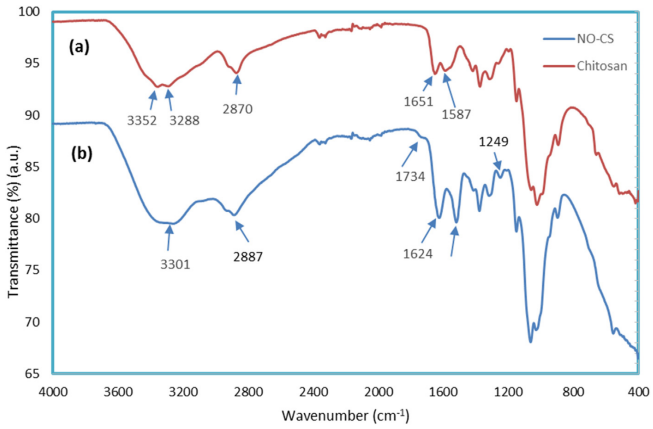

Fig. 3. FTIR Spectra (A) Chitosan and (B) NO-CS.

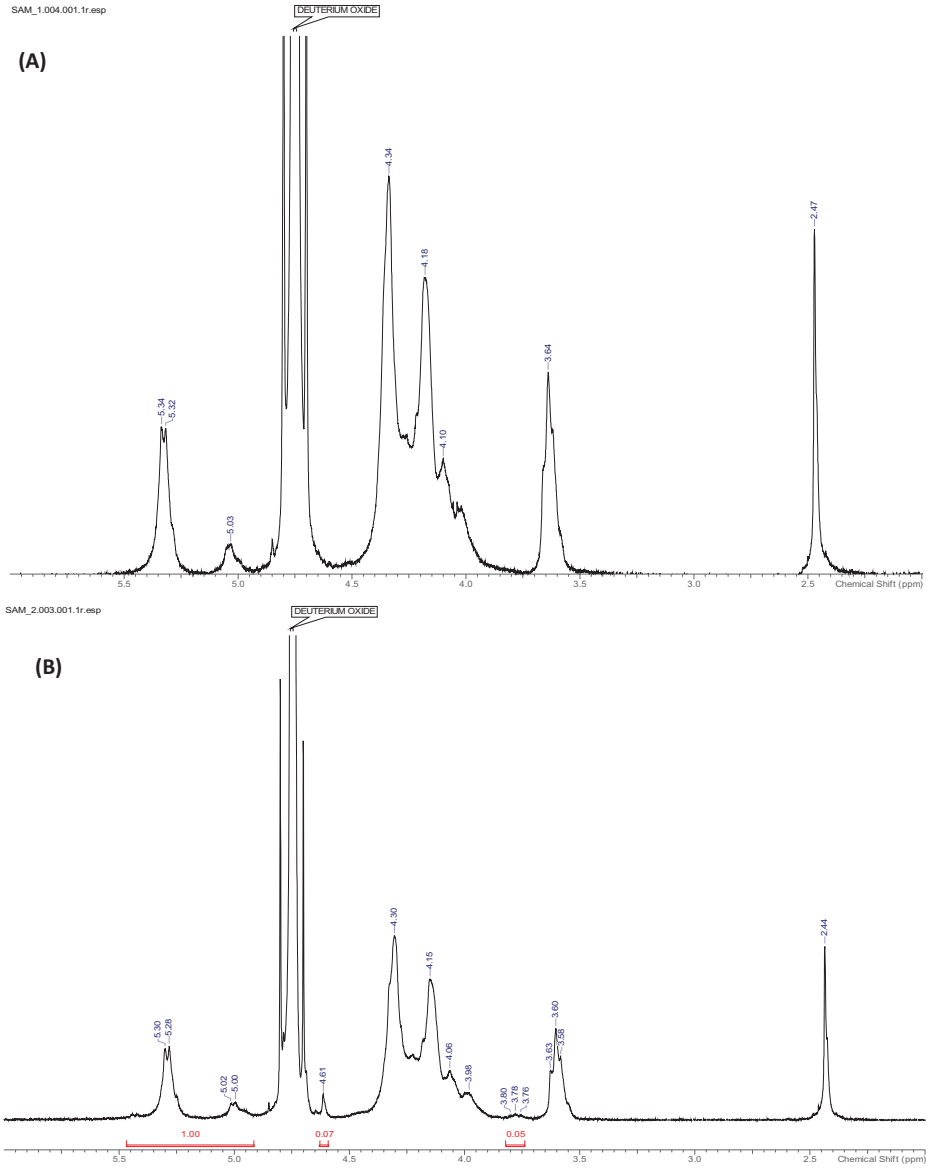

Fig. 4. ^{1}H NMR Spectra (A) Chitosan and (B) NO-CS.

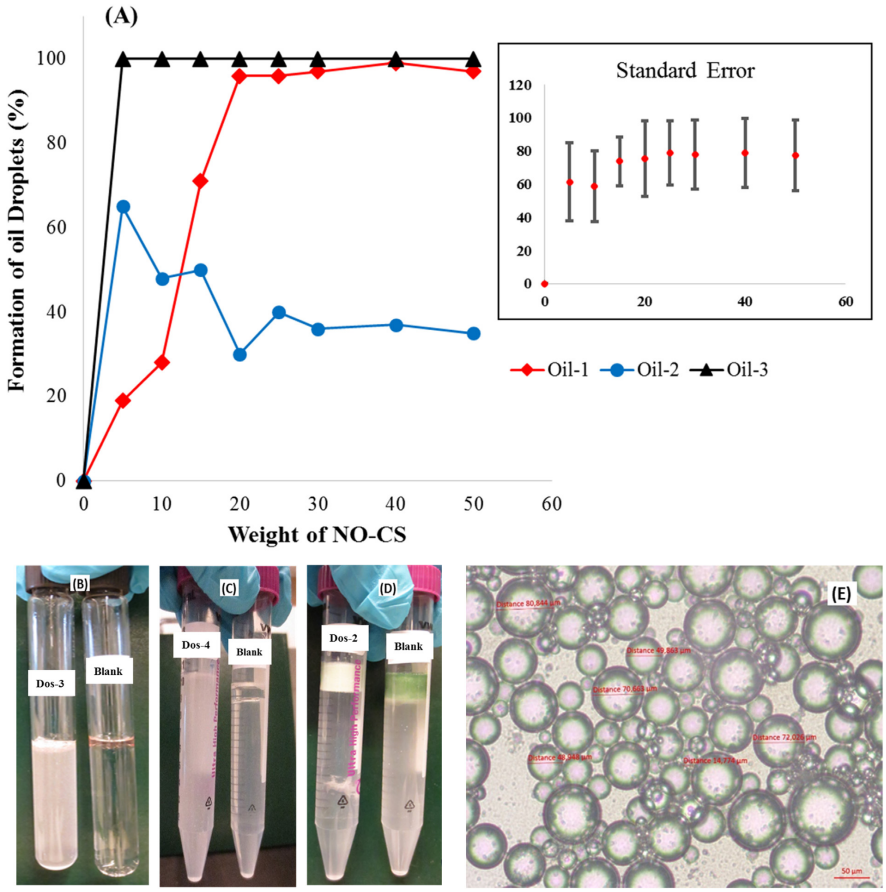

Fig. 5. (A) Effect of dosage in formation of oil droplets for oil-1, oil-2 and oil-3, (B) Oil-1 with 15 mg NO-CS (Dos-3) and without NO-CS in water (C) Oil-2 with 20 mg NO-CS (Dos-4) and without NO-CS in water (D) Oil-3 with 5 mg NO-CS (Dos-2) and without NO-CS in water (E) Oil-3 with 10 mg NO-CS.

3.4. *Effectiveness of NO-CS as a function of salinity*

Destabilization of the oil with increasing salinity was studied by measuring the size of the droplets after mixing. As the salinity increases, the solubility of NO-CS drops the CMC. Hence, lower ionic strength solutions favor emulsion stability (Wang & Alvarado, 2012). In contrast, increase in salinity forms electric double layer due to presence of ions in the aqueous phase and forming electrostatic repulsion with the carboxylic ions favoring hydrophobic interactions among the NO-CS polymer. With increase in salinity from 0.5% to 2%, there was a significant drop in formation of oil-droplets for oil-2 (Fig. 6B) compared to oil-1 (Fig. 6A). Whereas, the increase in salinity from 2% to 3%, shows slight more drop in the formation of oil-droplets for oil-1 compared to oil-2 may be because of the insolubility of NO-CS. For 3.5% salinity, the oil-droplets formation for oil-1 was about 48% and that of oil-2 was about 37%. Overall droplet size was less than 40 μm for oil-1 and Fig. 6D shows that in 1.5% saline solution 25 mg of NO-CS destabilized oil to form droplets of less than 30 μm whereas oil droplets of less than 50 μm were formed in 1% saline solution of 15 mg NO-CS. Overall droplet size was less than 75 μm for oil-2. Oil-3 consists of unsaturated hydrocarbons, and addition of electrolyte in small portion undergoes addition reaction, inhibiting the oil droplets formation more than 50% drop in comparison with 0% salinity. Droplet size with 1% salinity of 10 mg NO-CS was less than 35 μm as shown in Fig. 6F. Increase in salinity changes the formation of oil droplets but it does not affect the oil droplets size significantly.

3.5. *Effectiveness of NO-CS as a function of pH*

NO-CS was soluble in deionized water and pH of this solution was 3.5–4.5. It has been found that oil sorption on organic sorbent is highly affected by pH value (Rajakovic-Ognjanovic, Aleksic, & Rajakovic, 2008), as pH has a strong influence on the surface of

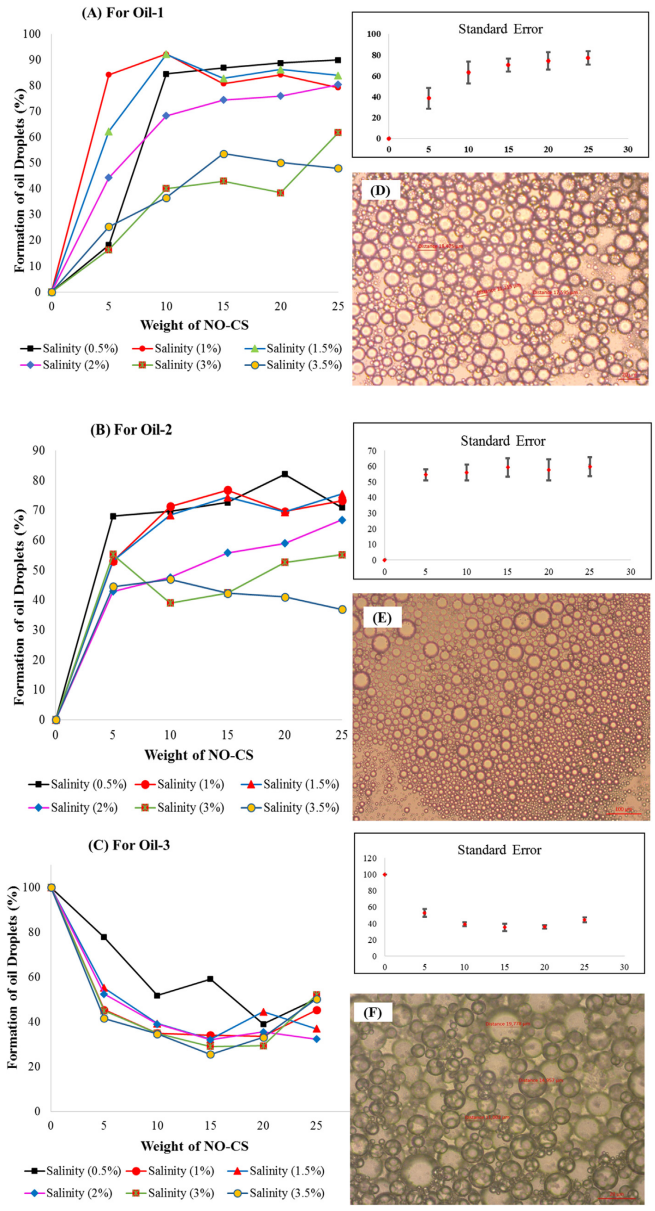

Fig. 6. Effect of salinity on formation of oil droplets (A) for Oil-1 (B) for Oil-2 (C) for Oil-3 and Microscopic images for o/w emulsion were (D) for 25 mg NO-CS with 1.5% Salinity for Oil-1 (E) for 15 mg NO-CS with 1% Salinity for Oil-2 (F) for 10 mg NO-CS with 1% Salinity for Oil-3.

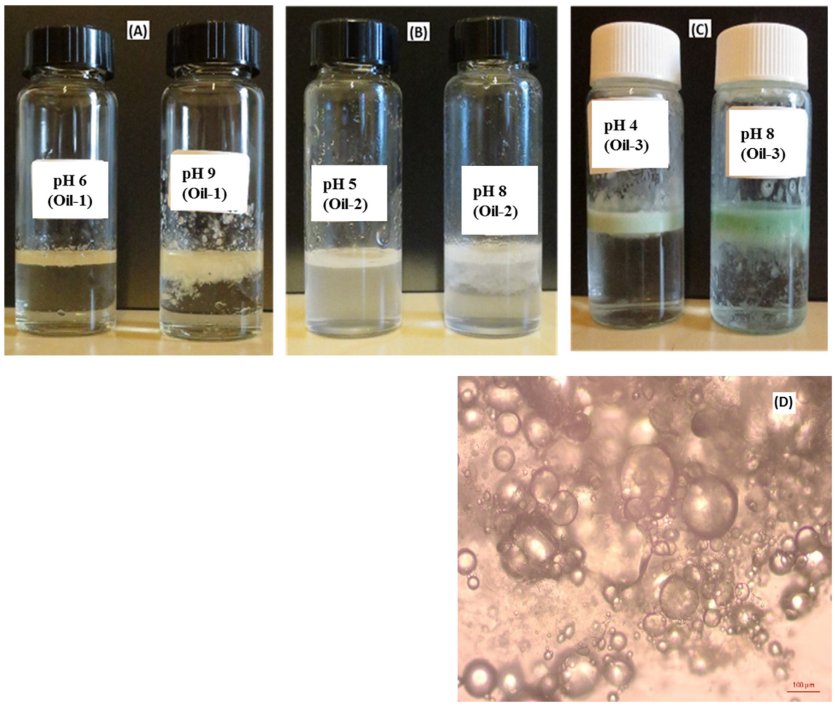

Fig. 7. Effect of pH on oil droplets (A) Oil droplets formation at pH 6 followed by adsorption at pH 9 for Oil-1 (B) Oil droplets formation at pH 5 followed by adsorption at pH 8 for Oil-2 (C) Oil droplets formation at pH 4 followed by adsorption at pH 8 for Oil-3 (D) Microscopic image for Oil-1 at pH 8.

NO-CS due to active amino groups. In acidic conditions, a positive charge on the surface of NO-CS is formed due to protonation of the amino group, leading to interaction with negative charge of the hydrocarbon present in oils (Lusiana et al., 2014). Hence, Winsor type-III micro emulsions of oils was observed at acidic pH with oil-1 (Fig. 7A), oil-2 (Fig. 7B) and oil-3 (Fig. 7C). Increasing pH has a strong influence on the surface of NO-CS. Due to low DS, NO-CS starts to precipitate at pH > 6.5. At alkaline pH, deprotonation of amino groups of NO-CS leads to destabilization of oil-1 (Fig. 7A), oil-2 (Fig. 7B) and oil-3 (Fig. 7C) and enhancing adsorption due to electrostatic attraction of NO-CS with hydrocarbon of oils. Additionally, the negative charge of hydrocarbon present in oils will pull the positive charge of the amino groups of NO-CS, not substituted completely (Lusiana et al., 2014) by enhancing adsorption at oil and water interface in presence of NO-CS. Fig. 7D is the microscopic image showing the adsorption of oil-1 at pH 8.

3.6. Adsorption of oils by NO-CS

Adsorption is the one of the important step for the removal of oil from water. At alkaline pH the polymer re-precipitates because of lower carboxymethylation rate and decrease in ionic strength of the solution. Addition of salinity, increases the ionic strength of the solution and protonates the amino groups of NO-CS and hence enhances the adsorption rate. The presence of positively charged surface on NO-CS lowers the interfacial tension between two phases by stabilizing the droplets against coalescence by electrostatic repulsion. Fig. 8A shows the adsorption of oil-1 with 0.10% NO-CS solution with 2% salinity at pH 8 after drying the adsorbed oil. The adsorption of oil-2 was less than that of oil-1, due to presence of higher rate of polyaromatics and lower density. Fig. 8B shows the adsorption of oil-2 with 0.10% NO-CS solution with 0.5% salinity and Fig. 8C shows the adsorption of oil-3 with 0.15% NO-CS solution with 3% salinity. Addition of few drops of 0.1 M HCl gives lumps of oil as shown in Fig. 8D. This addition of HCl shows the ion exchange effect in o/w emulsion, which leads to NO-CS adsorption on to the surface of more than one droplet and linking them together to form bridging flocculation between the NO-CS and o/w emulsion droplets. This was studied to show the acidification effect on to oil-in-water emulsion and to extend its applicability to ocean acidification as this could affect most fundamental biological and chemical processes of the sea in coming decades.

4. Conclusions

This study explains how water soluble NO-CS with degree of substitution 0.40, breaks the dispersed phase into droplets by rising them to the surface resisting droplets to coalescence. For marine Diesel and Diesel, oil droplets of less than 100 μm were formed with 20–25 mg/g of NO-CS, whereas only 5 mg/g of NO-CS was needed for Marine 2T oil to form oil droplets of less than 100 μm. Addition of salinity reduces the dose of NO-CS to about 10–15 mg/g for marine Diesel and Diesel to form oil droplets and there was a reduction in formation of oil droplets with increasing salinity, but

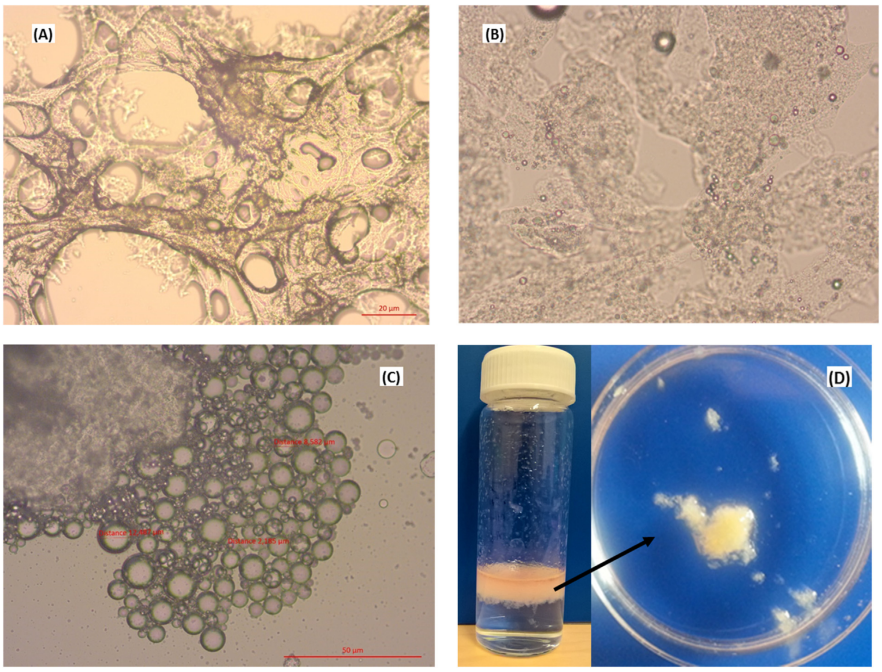

Fig. 8. Microscopic Images for Adsorption of Oil (A) 0.1% NO-CS with 2% Sal Oil-1 (B) 0.1% NO-CS with 0.5% Sal Oil-2 (C) 0.15% NO-CS with 3% Sal Oil-3 (D) Lumps of oil after addition of 0.1 M HCl for 0.15% NO-CS with 2% Sal Oil-1.

it does not affect the oil droplets size significantly NO-CS behavior differs in acidic and alkaline medium. In acidic pH, NO-CS forms Winsor type-III micro emulsions in a separate phase between oil and water, which contains NO-CS, water and dissolved hydrocarbons from oils enhancing oil recovery process. Whereas in alkaline pH, it shows destabilization of oil followed by adsorption because of the removal of carboxylate ion by deprotonating the amino groups. This derivative was most effective with marine diesel and at the least with diesel, because density of marine Diesel > Marine 2T oil > Diesel. Therefore, the applicability of the synthesized NO-CS, can be extended to sea-water for the removal of marine diesel as a part of oil spill response.

Acknowledgement

This work was funded by the European Union Structural Funds as a part of VIKE project (A70963: Improvement of the oil spill prevention and response with the green chemicals).

References

Abreu, F. R., & Campana-Filho, S. P. (2005). Preparation and characterization of carboxymethylchitosan. *Polimeros*, *15*, 79–83.
An, N. T., Thien, D. T., Dong, N. T., & Dung, P. L. (2009). Water-soluble N-carboxymethylchitosan derivatives: Preparation, characteristics and its application. *Carbohydrate Polymers*, *75*, 489–497.
Arrigo, K. R. (2013). The changing Arctic ocean. *Elementa: Science of the Anthropocene*,. 1:10.
Barros, F. C. F., Vasconcellos, L. C. G., Carvalho, T. V., & Nascimento, R. F. (2014). Removal of petroleum spill in water by Chitin and Chitosan. *The Electronic Journal of Chemistry*, *6*(1). ISSN 1984-6428.
Bee, A., Obeid, H., Mbolantenaina, R., Welschbillig, M., & Talbot, D. (2016). Magnetic chitosan/clay beads: A magsorbent for the removal of cationic dye from water. *Journal of Magnetism and Magnetic Materials*, *421*, 59–64.
Bhatnagar, A., & Sillanpää, M. (2009). Applications of chitin- and chitosan-derivatives for the detoxification of water and wastewater – A short review. *Advances in Colloid and Interface Science*, *152*, 26–38.
Bidgoli, H., Zamani, A., & Taherzadeh, M. J. (2010). Effect of carboxymethylation conditions on the water-binding capacity of chitosan-based superabsorbents. *Carbohydrate Research*, *345*, 2683–2689.
Boricha, A. G., & Murthy, Z. V. P. (2010). Preparation of N,O-carboxymethyl chitosan/cellulose acetate blend nanofiltration membrane and testing its performance in treating industrial wastewater. *Chemical Engineering Journal*, *157*, 393–400.
Brakstad, O. G., Daling, P. S., Faksness, L., Almås, I. K., Vang, S., Syslak, L., et al. (2014). Depletion and biodegradation of hydrocarbons in dispersions and emulsions of the Macondo 252 oil generated in an oil-on-seawater mesocosm flume basin. *Marine Pollution Bulletin*, *84*, 125–134.
Brandvik, P. J., & Faksness, L. G. (2009). Weathering processes in Arctic oil spills: Meso-scale experiments with different ice conditions. *Cold Regions Science and Technology*, *55*, 160–166.
Chen, X. G., & Park, H. J. (2003). Chemical characteristics of O-carboxymethyl chitosans related to the preparation conditions. *Carbohydrate Polymers*, *53*, 355–359.
Chen, L., Du, Y., & Zeng, X. (2003). Relationships between the molecular structure and moisture-absorption and moisture-retention abilities of carboxymethyl chitosan II. Effect of degree of deacetylation and carboxymethylation. *Carbohydrate Research*, *338*, 333–340.
Chen, R. N., Wang, G. M., Chen, C. H., Ho, H. O., & Sheu, M. T. (2006). Development of N,O-(Carboxymethyl) chitosan/collagen matrixes as a wound dressing. *Biomacromolecules*, *7*, 1058–1064.
Claireauxa, G., Théronb, M., Prineauc, M., Dussauzeb, M., Merlind, F. X., & Flochd, S. L. (2013). Effects of oil exposure and dispersant use upon environmental

adaptation performance and fitness in the European sea bass, Dicentrarchus labrax. *Aquatic Toxicology*, *130–131*, 160–170.
Colombo, E., Cavakieri, F., & Muthupandian, A. (2015). Role of counterions in controlling the properties of ultrasonically generated chitosan-stabilized oil-in-water emulsions. *Applied Materials & Interfaces*, *7*, 12972–12980.
Crini, G. (2005). Recent developments in polysaccharide-based materials used as adsorbents in wastewater treatment. *Progress in Polymer Science*, *30*, 38–70.
Dahlmann, G. (2003). Characteristic features of different oil types in oil spill identification. *Berichte des BSH*, (31), 48. ISSN 0946-6010.
DeLeo, D. M., Ruiz-Ramos, D. V., Baums, I. B., & Cordes, E. E. (2016). Response of deep-water corals to oil and chemical dispersant exposure. *Deep-Sea Research II*, *129*, 137–147.
Fan, T., & Buckley, J. S. (2002). Rapid and accurate SARA analysis of medium gravity crude oils. *Energy & Fuels*, *16*, 1571–1575.
Farrington, J. W., & McDowll, J. E. (2004). Mixing Oil and Water, tracking the sources and impacts of oil pollution in the marine environment. *Oceanus Magazine*, *42*(3).
Ge, H. C., & Luo, D. K. (2005). Preparation of carboxymethyl chitosan in aqueous solution under microwave irradiation. *Carbohydrate Research*, *340*, 1351–1356.
Jimtaisong, A., & Saewan, N. (2014). Utilization of carboxymethyl chitosan in cosmetics. *International Journal of Cosmetic Science*, *36*, 12–21.
Khan, T. A., Peh, K. K., & Ch'ng, H. S. (2002). Reporting degree of deacetylation values of chitosan: The influence of analytical methods. *Journal of Pharmacy & Pharmaceutical Sciences*, *5*(3), 205–212.
Khora, E., & Lim, L. Y. (2003). Implantable applications of chitin and chitosan. *Biomaterials*, *24*, 2339–2349.
Klemas, V. (2010). Tracking oil slicks and predicting their trajectories using remote sensors and models: Case studies of the sea princess and deepwater horizon oil spills. *Journal of Coastal Research*, *25*(5), 789–797.
Kong, X. (2012). Simultaneous determination of degree of deacetylation, degree of substitution and distribution fraction of COONa in carboxymethyl chitosan by potentiometric titration. *Carbohydrate Polymers*, *88*, 336–341.
Lewis, M., & Pryor, R. (2013). Toxicities of oils, dispersants and dispersed oils to algae and aquatic plants: Review and database value to resource sustainability. *Environmental Pollution*, *180*, 345–367.
Lusiana, R. A., Siswanta, D., & Mudasir, M. (2014). Modifying surface charge of chitosan membrane by N,O-Carboxymethyl chitosan blended with poly(vinylalcohol). *International Journal of Advances in Chemical Engineering and Biological Sciences (IJACEBS)*, *1*(1).
Martinoa, A. D., Sittingerc, M., & Risbud, M. V. (2005). Chitosan: A versatile biopolymer for orthopaedic tissue-engineering. *Biomaterials*, *26*, 5983–5990.
Mourya, V. K., Inamdar, N. N., & Tiwari, A. (2010). Carboxymethyl chitosan and its applications. *Advanced Materials Letters*, *1*(1), 11–33.
Nevalainen, M., Helle, I., & Vahnatalo, J. (2017). Preparing for the unprecedented — Towards quantitative oil risk assessment in the Arctic marine areas. *Marine Pollution Bulletin*, *114*, 90–101.
Ngaha, W. S. W., Teonga, L. C., & Hanafiaha, M. A. K. M. (2010). Adsorption of dyes and heavy metal ions by chitosan composites: A review. *Carbohydrate Polymers*, *83*, 1446–1456.
Peterson, C. H., Rice, S. D., Short, J. W., Esler, D., Bodkin, J. L., Ballachey, B. E., et al. (2003). Long-term ecosystem response to the exxon valdez oil spill. *Science*, *302*, 2082–2086.
Rajakovic-Ognjanovic, V., Aleksic, G., & Rajakovic, L. (2008). Governing factors for motor oil removal from water with different sorption materials. *Journal of Hazardous Materials*, *154*, 558–563.
Repo, E., Warchol, J. K., Bhatnagar, A., & Sillanpää, M. (2011). Heavy metals adsorption by novel EDTA-modified chitosan–silica hybrid materials. *Journal of Colloid and Interface Science*, *358*, 261–267.
Sagerup, K., Nahrgang, J., Frantzen, M., Larsen, L. H., & Geraudie, P. (2016). Biological effects of marine diesel oil exposure in red crab (Paralithodes camtschaticus) assessed through a water and food borne exposure experiment. *Marine Environmental Research*, *119*, 126–135.
Silva, R. S. F. S., Almeida, D. G., Rufino, R. D., Luna, J. M., Santos, V. A., & Sarubbo, L. A. (2014). Applications of biosurfactants in the petroleum industry and the remediation of oil spills. *International Journal of Molecular Science*, *15*, 12523–12542.
Smit, M. G. D., Bechmann, R. K., Hendriks, A. J., Skadsheim, A., Larsen, B. K., Brussant, T., et al. (2009). Relating biomarkers to whole-organism effects using species sensitivity distributions: A pilot study for marine species exposed to oil. *Environmental Toxicology and Chemistry*, *28*(5), 1104–1109.
Sun, S., & Wang, A. (2006). Adsorption kinetics of Cu (II) ions using N,O-carboxymethyl-chitosan. *Journal of Hazardous Materials*, *131*, 103–111.
Sun, G. Z., Chen, X. G., Li, Y. Y., Liu, C. S., Liu, C. G., Zheng, B., et al. (2008). Preparation and properties of Amphiphilic chitosan derivative as a Coagulation Agent. *Environmental Engineering Science*, *25*(9), 1325–1332.
Tsabet, E., & Fradette, L. (2015). Effect of processing parameters on the production of Pickering Emulsions. *Industrial & Engineering Chemistry Research*, *54*, 227–2236.
Upadhyaya, L., Singh, J., Agarwal, V., & Tewari, R. P. (2013). Biomedical applications of carboxymethyl chitosans. *Carbohydrate Polymers*, *91*, 452–466.
Venkataraman, P., Tang, J., Frenkel, E., McPherson, G. L., He, J., Raghavan, S. R., et al. (2013). Attachment of a hydrophobically modified biopolymer at the oil-water interface in the treatment of oil spills. *Applied Materials and Interfaces*, *5*, 3572–3580.
Wang, X., & Alvarado, V. (2012). Effects of Aqueous-phase salinity on water-in-crude oil emulsion stability. *Journal of Dispersion Science and Technology*, *33*, 165–170.
Wang, Z., & Fingas, M. F. (2003). Development of oil hydrocarbon fingerprinting and identification techniques. *Marine Pollution Bulletin*, *47*, 423–452.
Wang, L., & Wang, A. (2008). Adsorption properties of congo red from aqueous solution onto N,O-carboxymethyl-chitosan. *Bioresource Technology*, *99*, 1403–1408.
Wang, L. C., Chen, X. G., Liu, C. S., Liu, P. W., & Zhou, Y. M. (2008). Dissociation behaviors of carboxyl and amine groups on Carboxymethyl-Chitosan in Aqueous System. *Journal of Polymer Science Part B Polymer Physics*, *46*, 1419–1429.
Wassmann, P., Duarte, C. M., Agust, S., & Sejr, M. K. (2011). Footprints of climate change in the Arctic Marine ecosystem. *Global Change Biology*, *17*, 1235–1249.
Winsor, P. A. (1947). Hydrotropy, solubilisation and related emulsification processes. Part I. *Transactions of the Faraday Society*, *44*, 376–398.

Publication II

Doshi, B., Repo, R., Heiskanen, J. P., Sirviö, J. A., Sillanpää, M.

Sodium salt of oleoyl carboxymethyl chitosan: A sustainable adsorbent in the oil spill treatment

Reprinted with permission from

Journal of Cleaner Production

Vol 170, pp. 339-350, 2018

Journal of Cleaner Production 170 (2018) 339–350

Contents lists available at ScienceDirect

Journal of Cleaner Production

journal homepage: www.elsevier.com/locate/jclepro

Sodium salt of oleoyl carboxymethyl chitosan: A sustainable adsorbent in the oil spill treatment

Bhairavi Doshi [a, *], Eveliina Repo [a], Juha P. Heiskanen [b], Juho Antti Sirviö [c], Mika Sillanpää [a, d]

[a] Laboratory of Green Chemistry, Lappeenranta University of Technology, Sammonkatu 12, Mikkeli, 50130, Finland
[b] Research Unit of Sustainable Chemistry, University of Oulu, P.O. Box 3000, FI-90014, Finland
[c] Fibre and Particle Engineering Research Unit, University of Oulu, P.O. Box 4300, FI-90014, Finland
[d] Department of Civil and Environmental Engineering, Florida International University, Miami, FL 33174, USA

ARTICLE INFO

Article history:
Received 24 May 2017
Received in revised form
25 August 2017
Accepted 16 September 2017
Available online 17 September 2017

Keywords:
Oleoyl carboxymethyl chitosan
o/w emulsion
Adsorbent
Oil spill
Calcium chloride
Recovery of oil

ABSTRACT

Spills due to the floating oil on the surface of sea water shows a significant alteration in the natural phenomenon of the marine ecosystem. Hence, amphiphilic sodium salt of oleoyl carboxymethyl chitosan (NaO-CMCS) was synthesized, characterized and studied as a sustainable adsorbent for the removal of floating oil in the oil spill treatment. Successful chemical modification of chitosan was confirmed by chemical analysis using Fourier Transform Infrared (FTIR), ^{1}H Nuclear Magnetic Resonance (^{1}H NMR), Scanning electron microscopy (SEM), Energy dispersive X-ray spectroscopy (EDS) and Elemental Analyzer. The effect of pH and salinity on the surface charge of NaO-CMCS was studied. Marine diesel was chosen as an oil phase for the emulsion studies. Hydrophobically modified NaO-CMCS shows the oil-in-water (o/w) emulsion stability for more than 6 weeks with droplet size $\leq$ 30 μm which increases with decreasing temperature. The behavior of emulsion with different salinity shows phase separation at pH 5, bridging flocculation at pH 6–7 and o/w emulsion at pH 8. Calcium ions act as a cross-linker between two carboxylic acid groups of NaO-CMCS, enhancing the removal of oil from the creamy emulsion. The recovery of oil was 75–85% and 19–49% from deionized water and sea water, respectively. Oil was not chemically altered during the recovery, demonstrating the effectiveness of this derivative in the oil spill response for the removal and recovery of floating oil from the sea water.

1. Introduction

Oceans are the world's largest water resource getting polluted by oil either in the form of routine shipping or industrial run-offs or oil spills, which become a severe environmental threat. Out of these, about 12% of oil entering the oceans is due to oil spill. In past 37 years, Exxon Valdez in 1987 and Deep Horizon in 2010 were among the largest oil spill disasters in the history. Not only the water surface, but also the marine creatures (U.S. Fish and Wildlife Service, 2004) and seashores were trapped through this spilled oil (Hong and Yanjie, 2009; Jernelöv, 2010). Scientists studying the fate of the oil estimated that 20% evaporated, 50% biodegraded, 14% was cleaned up, 13% remained in subtidal sediments, 2% remained on shorelines, and less than 1% remained in the water (Wolfe et al., 1994). Cleanup is the first step towards the recovery process and therefore, various spill contaminant methods such as use of booms, skimmers, vacuum trucks, in-situ burning, dispersants, and chemical cleaners were used for the cleaning up of the spilled oil. Amongst them, use of oil dispersants such as Corexit 9500A and Corexit 9527A were commonly used for the Deep Horizon oil spill. However, these materials turned out to be toxic and had adverse effect on the aquatic life (Graham et al., 2016), which has led the researchers to develop more and more non-toxic and biodegradable biomaterials for the oil spill response (Zhang et al., 2013b; Zhang et al., 2014).

Chitosan, being a deacetylated form of chitin obtained from the crustaceans of crabs and shrimp shells, is an effective biomacromolecule consisting both reactive amino and hydroxyl groups. In addition, chitosan is a charged biopolymer that is capable of adsorbing oppositely charged emulsion droplets via electrostatic attraction. This behavior of chitosan is based on the presence of both the main polysaccharide backbone and the N-acetyl groups at

* Corresponding author.
E-mail address: bhairavi.doshi@lut.fi (B. Doshi).

https://doi.org/10.1016/j.jclepro.2017.09.163

C2 position. Therefore, fully protonated chitosan tends to form aggregates through hydrogen of amino groups and hydrophobic interactions in acidic conditions (Aranaz et al., 2010), and hence, acts as a good emulsifier (Liu et al., 2012). The water solubility of chitosan was improved through chemical modifications of these functional groups either by Michael addition reaction (Jianga et al., 2010), or by enzymatic and chemical grafting, and similar property of chitosan was also reviewed (Pillai et al., 2009; Shukla et al., 2013). Physically and chemically modified chitosan either in the form of beads (Mubarak et al., 2017), coated (Nawi et al., 2010), or cross-linked (Repo et al., 2011; Jawad and Nawi, 2012; Jawad et al., 2017) has been widely studied and reviewed (Bhatnagar and Sillanpää, 2009; Pintor et al., 2016; Kyzas and Bikiaris, 2015) for the removal of pollutants from water, in food industry (No et al., 2007; Ngo et al., 2015), in biomedical (Sonia et al., 2010; Dash et al., 2011), and in cosmetics (Rinaudo, 2006).

Many factors such as type of oil, thickness of the oil deposition, geographical parameters, biological communities and type of cleanup have been considered for the determination of oil spills impacts and recovery rates (Dicks, 1999). Some oils with volatile chemicals can easily be evaporated, some oil components can be broken by sunlight through photochemical reaction and some can be biodegraded by microbes (Farrington and McDowll, 2004). However, viscous and heavy oils like petroleum crude oil and heavy fuel oil, which cannot be evaporated easily, may form the blanket covering areas on the water surface causing a significant threat to the birds and mammals. So, spilled oil spread out on the water surface forming a thin layer, from which some lighter components evaporate whereas some water soluble components dissolve, and some transform to droplets through wave action by forming emulsion. The formation and stability of emulsion also depends on the nature of oil used, e.g., its interfacial tension, polarity, water solubility, and rheology (Jumaa and Müller, 1998; Langevin et al., 2004). A mixture of oil and water is generally unstable for emulsion and hence addition of surfactants, which reduce the interfacial tension between the oil and water to form a stable emulsion by preventing coalescence of dispersed oil droplets is mandatory. A surfactant used in oil spill treatment can either be adsorbed at the oil-water interfaces or form thicker slicks with oil. However, prolonged use of synthetic surfactants is not feasible as it reflects toxic effects on the marine ecosystems (Smit et al., 2009). Thus, nowadays, bio-surfactants or biopolymers, due to their biocompatibility, non-toxicity and sustainability, are focused more in the oil-spill response rather than synthetic surfactants.

Amphiphilic chitosan derivative comprise of both polar and non-polar groups along with the glucosamine backbone, so when adsorbed to the oil droplet surface, the polar part extends towards the aqueous phase and non-polar part towards the oil phase (McClements and Gumus, 2016). Various methods such as alkylation (Auzèly and Rinaudo, 2003; Huo et al., 2011), acylation (Sun et al., 2008), and grafting (Sun et al., 2003; Yang et al., 2012; Jena and Sangamwar, 2016) have been used to prepare amphiphilic chitosan by introducing hydrophobic moieties onto the carboxymethylated chitosan backbone. For an amphiphilic copolymers, longer hydrophobic chains along with larger hydrophilic groups helps to stabilize the micelle structure (Li et al., 2011). Therefore, from past few years naturally occurring biopolymers such as chitosan present in sea food waste (Ummadisingu and Gupta, 2012) or fungal biomass (Srinivasan and Viraraghavan, 2010) along with their derivatives either in the form of hydrogel/aerogel (Sokkera et al., 2011; Chaudhary et al., 2015) or microspheres (Grem et al., 2013) or grafted (Zhang et al., 2013a; Lü et al., 2015) have been studied more for oil spill. But as per our knowledge, the sodium form of amphiphilic chitosan for oil spill has not yet been studied.

The aim of this study was to investigate effectiveness of sodium form of amphiphilic chitosan obtained by carboxymethylation and acylation as an emulsion stabilizer for floating oil onto the water surface through minimization of one synthesis step. Sodium salt of oleoyl carboxymethyl chitosan (NaO-CMCS) was synthesized by introducing hydrophobic groups on amino groups of hydrophilic sodium salt of carboxymethylchitosan (Na-CMCS). After the modifications, amphiphilic NaO-CMCS was hydrophilic in nature. The solubility of this synthesized polymer was reversed than that of chitosan, i.e. it was insoluble at pH < 6. The molecular structure was analyzed by Fourier Transform Infrared (FTIR), ^{1}H Nuclear Magnetic Resonance (^{1}H NMR), Scanning electron microscopy (SEM), Energy dispersive X-ray spectroscopy (EDS) and Elemental Analyzer. Binks et al., 2006 had explained that the particle wettability at the oil-water interface alters by changing the pH or salt concentration. Therefore, surface charge of NaO-CMCS was investigated at different pH with different ionic strength.

Oil-in-water (o/w) emulsion was obtained using marine diesel as a dispersed phase. Interfacial tension (IFT) between the aqueous phase and dispersed phase was investigated by the addition of NaO-CMCS. The formation of o/w emulsion and its stability was studied at room temperature (about 22 °C) for six weeks by measuring the average oil droplet size periodically as well as at lower temperature (2 °C) to extent its applicability for arctic oil spill also. Addition of hydrophobic moiety to Na-CMCS alters the average oil droplet size in comparison to our previous work (Doshi et al., 2017) by making the o/w emulsion more stable. Furthermore, the stability of o/w emulsions was studied with the optimized dosage of NaO-CMCS at pH range (5–8) with different salinity (0–3.5%) to build equivalent condition as seawater oil spill. Recovery of oil from the stabilized o/w emulsions was investigated by using calcium chloride as a cross-linker to show the effectiveness of NaO-CMCS as a biopolymer cleaner for the floating oil. Recovered oil was further studied by FTIR and Gas Chromatography using Flame ionization detector (GC-FID). The chitosan derivative after cross-linking was investigated by SEM and EDS analysis.

2. Experimental

2.1. Materials

Chitosan from shrimp shells (practical grade, MW 190000–375000 Da; ≥75% deacetylated; viscosity >200 cP, CAS No. 9012-76-4, Lot # SLBL3564V, PubChem CID: 71853), chloroacetic acid (≥99%, CAS No. 79-11-8, Lot #SHBD8969V, PubChem CID: 300), oleoyl chloride (≥89%, CAS No. 112-77-6, Lot #SHBF3232V, PubChem CID: 5364783), sodium chloride (CAS no. 7647-14-5, Lot #SZBB0170V, PubChem CID: 300), acetone (≥99.5%, CAS No. 67-64-1, Lot #STBG1776V, PubChem CID: 180), and calcium chloride dihydrate (≥99%, CAS No. 10035-04-8, Lot #SLBM8013V, PubChem CID: 329775159) were purchased from Sigma-Aldrich Finland Oy. Sodium hydroxide (NaOH) (CAS No. 1310-73-2, Lot #SZBE1130V, PubChem CID: 14798) was purchased from Fluka. Isopropanol (IPA) (CAS No. 67-63-0, Lot #K40448334, PubChem CID: 3776) was purchased from Merck. Ethanol (99.5%) was purchased from Altia Oyj. Deuterium chloride solution (35 wt. % in D_2O, 99 atom-% D, CAS No 7698-05-7, Lot #MBB1157V, PubChem CID: 122198780) was obtained from Sigma Aldrich. D_2O was obtained from Euriso-top (99.96% atom-% D, CAS No 7789-20-0, Lot #D215FL0701, PubChem CID: 24602). All chemicals were used without further purification. The marine diesel (sulfur-free oil with a density of 828 kg/m^3 at 15 °C and viscosity of 1.846 mm^2/s at 40 °C) was received from Fibre and Particle Engineering Research Unit, University of Oulu. Deionized water (Siemens Ultra Clear RO with Conductivity 2.1 μS/cm at 23.8 °C) was used throughout the experiments. Sea water (Conductivity 8.46 mS/cm and pH 7.844 at

22.3 °C) collected from the area near to Matinkylä Espoo, Finland was used only for the recovery of oil experiments.

2.2. Synthesis of NaO-CMCS

Carboxymethylated chitosan was crosslinked with long chained hydrocarbon, to form amphiphilic chitosan having hydrophilic and hydrophobic groups. The two steps reaction is shown in Fig. 1.

2.2.1. Synthesis of sodium salt of carboxymethyl chitosan (Na-CMCS)

Na-CMCS was synthesized based on previously reported method (Doshi et al., 2017; Chen and Park, 2003) with some modification. Briefly, chitosan from shrimp shells (4 g) was alkalized at 50–55 °C for 1 h with the mixture of NaOH (5.6 g), IPA (96 ml), and water (24 ml) using water bath (IKA C-MAG HS 7 Digital). Chloroacetic acid (6 g) dissolved in IPA (8 ml) was added to the reaction mixture over a period of 30 min, and the reaction was continued for 3 h at the same temperature. Then, 70% ethanol (50 ml) was added to stop the reaction. The solution was centrifuged at 1500 rpm for 2 min (using Centrifuge 5810R from Eppendorf). The supernatant was removed and the solid was washed with increasing concentration of ethanol (70–90%) for three times using same centrifugation method, and dried overnight at room temperature. The obtained product was Na-CMCS as shown in step-1 of Fig. 1.

2.2.2. Synthesis of sodium salt of oleoyl carboxymethyl chitosan (NaO-CMCS)

NaO-CMCS was synthesized based on previously reported method (Sun et al., 2008) with some modifications. Na-CMCS (2.3 g) was soaked in acetone (10 ml) for 1 h at 5 °C. Dissolved oleoyl chloride (2.6 ml) in acetone (2.6 ml) was added along with 4M NaOH solution (10 ml) to the reaction mixture dropwise over a period of 30 min. Acetone (20 ml) was added to the reaction mixture and the reaction was continued for 3 h at same temperature. To stop the reaction, 70% ethanol (60 ml) was added. The workup was carried out as mentioned in section 2.2.1. The product NaO-CMCS shown in step-2 of Fig. 1 was grounded in the tube mill to remove lumps of particles formed during the drying process.

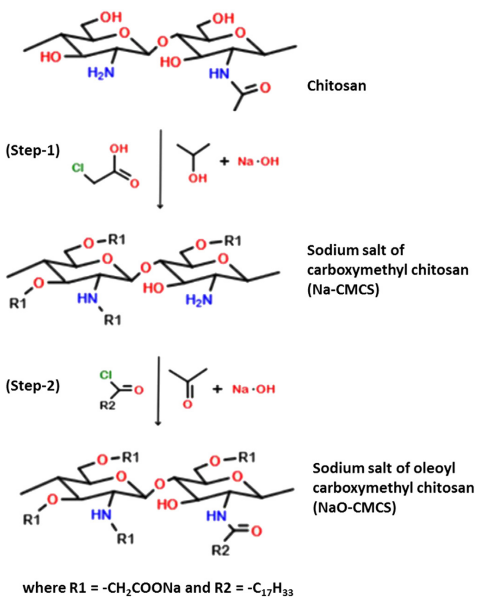

Fig. 1. Shows the two steps synthesis of NaO-CMCS from chitosan.

2.3. Characterizations

FTIR images of chitosan, Na-CMCS and NaO-CMCS were recorded in the range of 400–4000 cm^{-1} with a resolution of 4 cm^{-1} for 60 scans (ATR-FTIR, Bruker Vertex 70 model) to investigate the functional groups changes in chitosan due to modifications with chloroacetic acid and oleoyl chloride. Samples were measured without any further treatment. For ^1H NMR measurements, samples of Na-CMCS and NaO-CMCS were dissolved in D_2O containing 0.7% of DCl and placed in 5 mm NMR tubes. The ^1H NMR spectra were recorded by using Bruker Ascend 400 MHz spectrometer and standard proton parameters with the delay time (d1) of 6 s at 70 °C. Surface morphology of chitosan and its derivatives were studied by SEM analysis using Hitachi SU3500 at accelerating voltage of 10 kV. Elemental distribution and composition were examined by EDS (Thermo Scientific UltraDry SDD EDS, dual detector with Software NSS at 15.0 kV accelerating voltage using Aluminium sample holder) and CHNS-Elemental Analyzer (Thermo Flash 2000 using tin sample holder). The degree of substitution was calculated from the CHNS elemental analysis as follows:

$$DS_1 = \frac{\left(\frac{C}{N}\right)Na-CMCS - \left(\frac{C}{N}\right)Chitosan}{estimated\ no.\ of\ carbon\ atoms\ in\ Na-CMCS} \quad (1)$$

$$DS_2 = \frac{\left(\frac{C}{N}\right)NaO-CMCS - \left(\frac{C}{N}\right)Na-CMCS}{estimated\ no.\ of\ carbon\ atoms\ in\ NaO-CMCS} \quad (2)$$

where DS_1 and DS_2 are the degree of substitution of Na-CMCS and NaO-CMCS, respectively. (C/N) are the mol. ratio of carbon to nitrogen obtained from CHNS analysis. The BET surface area of chitosan and NaO-CMCS was determined by nitrogen (N_2) adsorption-desorption method at 77.35 K using Micromeritics Tristar II plus instrument. The samples were degassed using Vac Prep 061 degassing unit with nitrogen at 30 °C for 18 h prior to the measurements. The total pore volume and average pore diameter were determined by the amount of nitrogen adsorbed at the relative pressure of 0.95 and BET (4V/A), respectively.

2.4. Effect of pH and salinity on surface charge

The amount of charge on the particle surface is the important characteristic of the particles as it determines the behavior of the emulsion. Therefore, the effect on surface charge of NaO-CMCS was studied as a function of pH with increasing salinity. Firstly, solid NaCl was added to NaO-CMCS solution (1 g/L) to increase the salinity from 0% to 3.5%. This solution was mixed for 5 min and pH was adjusted with 0.01 M HCl using pH meter (WTW InoLab, calibrated before use). The studied pH range was in between 4 and 10. All the measurements were recorded in triplicate using Malvern Zetasizer (Nano ZS, Malvern UK) at 25.0 ± 0.1 °C.

2.5. o/w emulsion stability

For this study, different dosage of NaO-CMCS (0.5–3 g/L) were used. Simultaneously, marine diesel was mixed with water at

2000 rpm using vortex mixture (VWR International) to form the o/w emulsion. The oil to water ratio was 1:1 (v/v). To this o/w emulsion, solution of NaO-CMCS was added. This was again mixed at 2000 rpm for 30 s. The oil droplet size of o/w emulsion was measured immediately after mixing using optical microscope (Zeiss Axio using 206 the camera unit Axio CamERc5s by ZEN software). Then the o/w emulsion was allowed to saturate and oil droplet size and stability of emulsion was studied periodically for six weeks. The oil droplets size after mixing, after 2 h stability and 6 weeks saturation was also measured by laser diffraction particle size analyzer (Malvern Mastersizer 3000 with Hydro SV unit, UK). The mean droplet diameter at D[4,3] was taken from five replicate measurements as the volume mean diameter, and the magnitude of the droplet size distribution is expressed by the span, defined as

$$Span = \frac{[Dx(90) - Dx(10)]}{Dx(50)} \quad (3)$$

where $Dx(10)$, $Dx(50)$, and $Dx(90)$ denote the equivalent volume diameters at 10%, 50%, and 90% cumulative volume. The same procedure was repeated by storing all the solutions at lower temperature (2 °C).

2.6. Effect of pH and salinity on o/w emulsion

The 10 mL of optimized dosage of NaO-CMCS (1 g/L) was used through the study. To the optimized NaO-CMCS solution, solid NaCl (0–350 mg) was added. These solutions were mixed for 5 min with magnetic stirrer (2 mag MIX 15, Germany) and pH was adjusted with 0.01 M HCl using a pH meter (WTW InoLab, Germany). The studied pH were from 5 to 8. Simultaneously, marine diesel and water (1:1 v/v) were mixed at 2000 rpm using a vortex mixture (VWR International) to form the o/w emulsion. To this o/w emulsion, previously prepared NaO-CMCS solution was added separately. These were again mixed at 2000 rpm for 30 s. The emulsions were kept for about one month. All the experiments were carried out at room temperature.

2.7. Recovery of marine diesel

Recovery of oil from the emulsified water has a significance value for the oil spill response. Here both, deionized water and sea water were used for the o/w emulsion (oil:water is 1:1 v/v). The o/w creamy emulsions were prepared as per section 2.5 with different dosage of NaO-CMCS (0.5–5 g/L). The stabilized o/w creamy emulsion was collected and 10 ml calcium chloride dihydrate solution (0.1%) was added to it. The mixtures were kept for 1 h to stabilize naturally. All the experiments were carried out at room temperature in triplicate. The separated oil was collected (using micropipette from Sartorius), weighed and the recovery of the oil (R %) was calculated as follows:

$$R\% = 100 - \left(\frac{C_i - C_r}{C_i} * 100\right) \quad (4)$$

where C_i and C_r are the initial and recovered amount of oil. Recovered oil was characterized using FTIR and GC-FID. GC-FID parameters are mentioned in Supplementary Material (SM8). The NaO-CMCS crosslinked with calcium was collected and dried, and SEM and EDS analysis were performed (using the same instruments as mentioned earlier in section 2.3).

3. Results and discussion

Chitosan is a multi-nucleophilic polymer due to the presence of the hydroxyl and amino functional groups. Introduction of carboxymethyl groups (−CH_2COO−) to chitosan, makes Na-CMCS pH-sensitive, so that in acidic pH, this group exists in non-ionized form, whereas in alkaline pH it exists in ionized form, which makes the derivative hydrophilic in nature. Nucleophilic acyl substitution takes places between the free amino groups of the carboxymethylated polymer and oleoyl chloride through an addition/elimination type mechanism. The reaction driven towards amide formation by the low reaction temperature, had favors N-acylation over O-acylation (Chiandotti et al., 2010). The sizes of chitosan, Na-CMCS and NaO-CMCS particles are available in the SM1 (Supplementary Material).

3.1. Structural characterization of NaO-CMCS

3.1.1. FTIR analysis

Structural changes of chitosan and its derivatives were confirmed by FTIR spectra. In Fig. 2A, peaks at 3351 cm^{-1} and 3286 cm^{-1} express the N–H and O–H group, 2866 cm^{-1} shows C–H stretching, 1650 cm^{-1} and 1585 cm^{-1} indicates C=O stretching of the secondary amide (amide I) and N–H bending of 2-aminoglucose units, 1150 cm^{-1}, 1060 cm^{-1} and 1026 cm^{-1} attributed to asymmetric stretching of the C–O–C stretching and the skeletal vibration of C–O stretching, respectively in chitosan. In

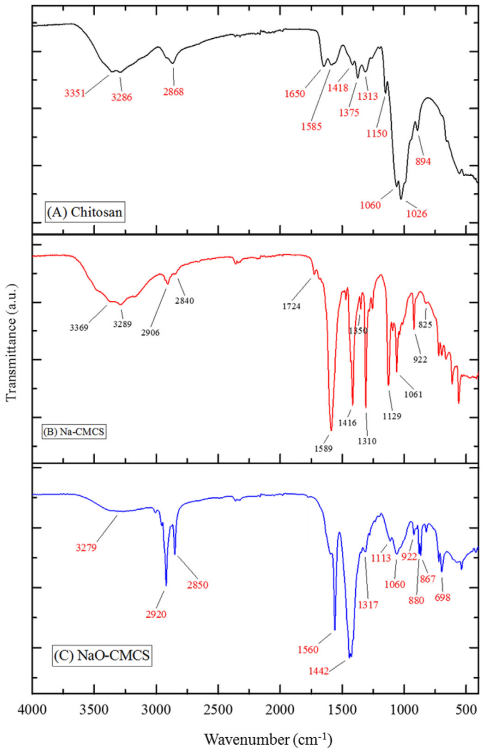

Fig. 2. FTIR spectra of (A) Chitosan (B) Na-CMCS and (C) NaO-CMCS.

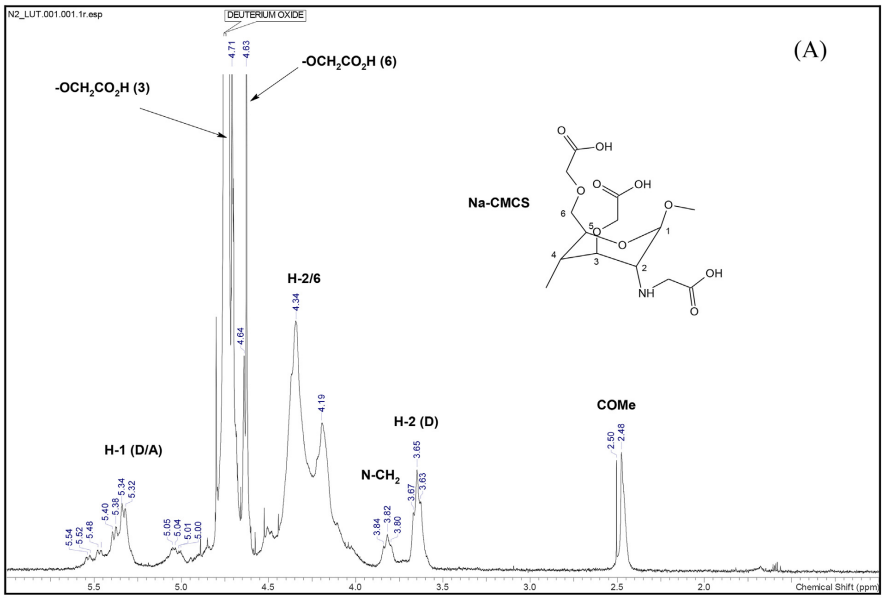

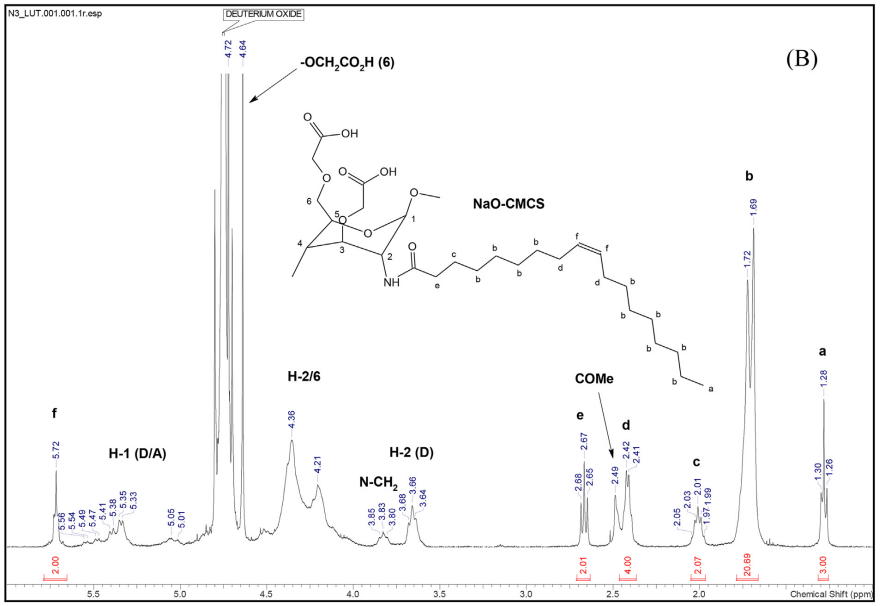

Fig. 3. ^{1}H NMR spectra of (A) Na-CMCS and (B) NaO-CMCS.

Fig. 2B, peaks at 3369 cm^{-1} and 3289 cm^{-1} express the N–H and O–H group, 2906 cm^{-1} and 2840 cm^{-1} attributes to the C–H stretching, 1724 cm^{-1} (acid C=O, stretch), which was absent in chitosan conforming carboxymethylation of chitosan. The characteristic bands of Na-CMCS found at 1589 cm^{-1} (C=O of –COONa asymmetric stretching) had overlapped the N–H peak of chitosan at 1585 cm^{-1} which corresponds to the previously observed results (Kong, 2012) and 1416 cm-1 (C=O of –COONa symmetric stretching). In Fig. 2C, the 3279 cm^{-1} indicates secondary N–H, intensified peaks at 2920 cm^{-1}, 2850 cm^{-1} and 1442 cm^{-1} attributes to C–H stretching of oleoyl chains. After acylation, the 1585 cm^{-1} peak of primary amine disappeared, while the prominent band bands at 1560 cm^{-1} for N–H (amide II) was observed similar to earlier findings (Tiena et al., 2003), which indicates the incorporation of oleoyl moiety onto the primary amine of Na-CMCS. The peaks, in the range of 1150–850 cm^{-1} are the results of vibrations of C–O and C–O–C of the polysaccharide chain also observed in chitosan and Na-CMCS.

3.1.2. ^1H NMR analysis

The ^1H NMR spectra of Na-CMCS and NaO-CMCS are presented in Fig. 3A and 3B, respectively. The spectrum of NaO-CMCS shows the similar characteristic proton signals as can be seen in the spectrum of Na-CMCS which was assigned according to our previous studies (Kalliola et al., 2017). In addition in the spectrum of NaO-CMCS, the successful attachment of oleoyl substituent to Na-CMCS can be clearly seen. The triplet (a) ($J = 6.6$ Hz) at 1.28 ppm is assigned to CH_3 unit of oleoyl chain. Signals of 20 protons of CH_2 units (b) can be observed at around 1.69 ppm. The protons of CH_2 unit (e) next to the carbonyl group appear as a clear triplet with a coupling constant of 7.4 Hz at 2.67 ppm. The protons of CH_2 unit in a position c appear as a multiplet at around 2.01 ppm. The protons of double bond (f) show the peak at 5.72 ppm which corresponds a typical shift of alkene type protons. The protons of CH_2 units (d) next to alkene protons appear at around 2.42 ppm. The assignments are consistent with the previous assignments of a similar type oleoyl amide structure (Niu et al., 2010).

3.1.3. SEM/EDS analysis

The SEM images of raw and treated chitosan are shown in Fig. 4. The surface morphology of chitosan (Fig. 4A and B) has been altered after carboxymethylation (Fig. 4C and D) followed by acylation (Fig. 4E and F). The surface roughness increases in Na-CMCS as compared to that of chitosan. The attachment of hydrocarbon long chain to Na-CMCS, makes the surface of NaO-CMCS rougher compared to Na-CMCS. These alterations on the surface topography were likely to result from the long hydrocarbon chain attached to the Na-CMCS. Thus, chitosan after carboxymethylation and acylation, appears to be rough and more porous. This was further confirmed by the BET analysis by considering the porosity.

Elemental analysis for chitosan, Na-CMCS and NaO-CMCS are shown in Table 1. The increasing C/N ratio from chitosan to its derivatives indicates the addition of carbon atoms to chitosan. The degree of substitution (DS) in Na-CMCS was 1.63, which confirms that both hydroxyl and amino groups might have been substituted after carboxymethylation. Reduction of nitrogen (%) shows that addition of long carbon chain groups took place during the acylation and the DS of 0.51 was obtained. The presence of sodium in EDS results of Na-CMCS and NaO-CMCS, and not in chitosan, concludes that the synthesized derivatives were in the sodium form. The EDS results of Na-CMCS and NaO-CMCS were also taken at 1.0 kV accelerating voltage to confirm the presence of nitrogen as mentioned in Table T1. At 1.0 kV, heavier elements other than oxygen cannot be detected. From the results, it was concluded that the carbon (%) increases from Na-CMCS to NaO-CMCS indicating that the hydrocarbon long chain was attached to the backbone of chitosan after acylation. The C/N ratio of EDS (at 1.0 kV) is also in a good resemblance to the CHNS results.

3.1.4. BET analysis

N_2 adsorption and desorption isotherms at 77.35 K plotted as a function of P/P^0 is shown in Fig. S2 (Supplementary Material). The isothermal curve of NaO-CMCS can be classified as IUPAC type IV showing type H3 hysteresis loop between 0.45 and 0.95, which is associated with the capillary condensation taking places in mesopores. The type H3 hysteresis loop in NaO-CMCS, also reveals to the

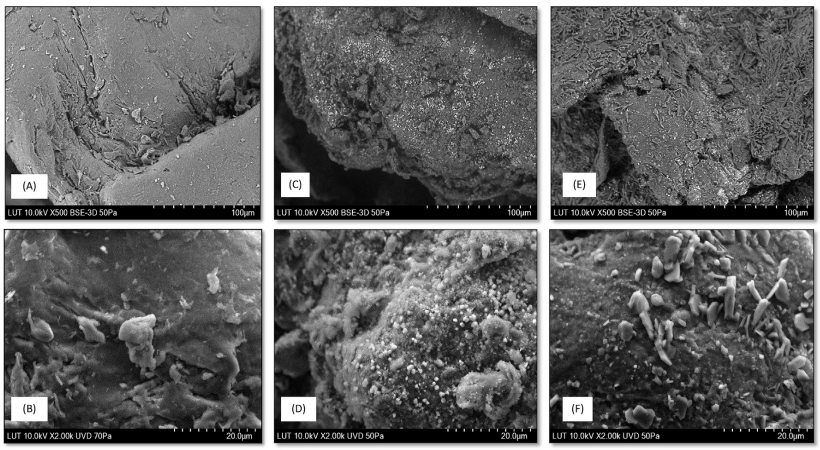

Fig. 4. SEM images of chitosan (A and B), Na-CMCS (C and D) after carboxymethylation, and NaO-CMCS (E and F) after addition of long hydrocarbon chain. All the images were taken at accelerating voltage of 10 kV with the scale bars of 100 µm and 20 µm and magnification ×500 and ×2.00K.

Table 1
Elemental analysis of chitosan, Na-CMCS and NaO-CMCS by CHNS Analyzer and EDS.

CHNS				EDS (15.0 kV)				EDS (1.0 kV)		
Wt.%	Chitosan	Na-CMCS	NaO-CMCS	Wt.%	Chitosan	Na-CMCS	NaO-CMCS	Wt.%	Na-CMCS	NaO-CMCS
C	40.26	27.73	34.98	C K	47.1	29.0	36.7	C K	52	71
N	7.85	3.30	1.99	N K	12.3	–	–	N K	6	4
H	6.05	2.39	5.20	O K	40.4	42.8	39.4	O K	43	26
C/N	5.13	8.40	17.61	Na K	–	23.4	22.4	C/N	8.67	17.75
DS	**-**	**1.63**	**0.51**	Cl K	0.1	4.8	1.0	**DS**	**-**	**0.50**
				Al k	0.1	–	0.6			

aggregates of plate-like particles which give rise to slit-shaped pores similar to previously observed results (Sing et al., 1985). These results were in a good resemblance to the SEM interpretation. The BET surface area of chitosan and NaO-CMCS were 0.3603 m^2/g and 0.5874 m^2/g, respectively. The pore volume and pore diameter of NaO-CMCS were 0.0011 cm^3/g and 120.49 Å, whereas 0.0006 cm^3/g and 41.63 Å for chitosan. This concludes that NaO-CMCS is more porous than chitosan and there is a decrease in surface area of NaO-CMCS, compared to that of chitosan due to addition of long hydrocarbon chain attached to the amino group of Na-CMCS.

3.2. Effect of salinity and pH on surface charge of NaO-CMCS

The influence of salinity and pH on the electrical characteristics and solubility of NaO-CMCS were studied. In order to investigate this effect, the pH of NaO-CMCS solution (1 g/L) was studied with different salinity (0–3.5%) in the pH range (4–10). The initial conductivity of NaO-CMCS solution was 0.670 mS/cm, which shows that the carboxylate groups ($-COO^-Na^+$) of NaO-CMCS were ionized easily in water. Increase in conductivity to 54.80 mS/cm at 3.5% salinity (Fig. 5A) confirms that the ionized particles in the water were significantly affected by the addition of the salt. So, there was a formation of a net charge at the surface of NaO-CMCS, which affected the distribution of ions in the surrounding of its interfacial region. This resulted in an increased concentration of Na^+ ions close to the surface forming an electrical double layer around NaO-CMCS. Thus, increasing salt concentration reduces the charged density of NaO-CMCS by altering the interactions between the NaO-CMCS and negatively charged components (Klinkesorn, 2013). On the other hand, the conductivity significantly lowered down, but did not reach zero even after the surface was neutralized, which shows the presence of free ions in the solutions.

The prime and important factor affecting zeta potential is pH. The natural pH of NaO-CMCS solution was ~10.2, and declined to ~9.6 with increasing salinity (3.5%). Initially the zeta potential of NaO-CMCS particle was negative and addition of HCl started building up the positive charges. Hence, the magnitude of the electrical charge in NaO-CMCS at higher pH was highly negative and tended to zero (at isoelectric point) at intermediate pH and then to positive values at lower pH as shown in Fig. 5B. At pH 9, there was a sudden drop in the zeta-potential, which shows that almost all Na^+ ions from the sodium carboxylate group of NaO-CMCS were dissociated by making the surface more negative. The addition of H^+ ions, firstly protonates the free amino groups followed by the protonation of some carboxylate groups causing the increase of zeta-potential up to zero where the amount on positive and negative charges on the surface of NaO-CMCS were either equal or neutralized. The acylated amino groups remained unaffected. Further addition of H^+ ions made the surface more and more positive aligning the deprotonated carboxylate groups to get protonated. The zeta-potential of NaO-CMCS in the presence of electrolyte was observed to increase linearly which states that the process of protonation and deprotonation on the NaO-CMCS surface was not interfered significantly by the salinity variance except the change in the isoelectric point. Therefore, the optimal pH for the formation of emulsion can be in the range of 6–8, were the zeta potential is negative irrespective of the salinity.

3.3. Interfacial tension

IFT between the water phase and oil phase is the key parameter for the formation of oil droplets followed by the stability of o/w emulsion. IFT was measured by the pendant drop method (Video-based contact angle instrument, Dataphysics OCA 15 EC Series). The initial IFT between these two (water and oil) phases without NaO-CMCS, was 19.53 ± 0.54 mN/m and a small addition of NaO-CMCS reduced the IFT by 50%. However, at the critical micelle concentration (CMC), the IFT reduction was up to 70%. The IFT was affected by the increasing concentration of NaO-CMCS (Fig. S3 in Supplementary Material SM3). Thus, the result confirms that the attachment of hydrophobic hydrocarbon chain made NaO-CMCS more amphiphilic, which drastically reduced the interfacial tension. At lower interfacial tensions, the free surface energy associated with the formation of droplets reduces, enhancing the formation of smaller emulsion droplets with greater stability.

3.4. Emulsion stability

Amphiphilic NaO-CMCS was mixed within the aqueous phase, and when the oil and aqueous phase were combined and mixed, there was an instant formation of o/w emulsion. Firstly, the oil phase deformed and disrupted into small droplets forming the new interface, which reduced the IFT followed by the adsorption of NaO-CMCS on that interface forming creamy o/w emulsion. After standing, this creamy emulsion formed a layer at the top, by removing the extra water from the emulsion at the bottom. The stability of this emulsion retained for more than 6 weeks, due to the strong interaction between the non-polar carbon chains (attached to the amino groups) in NaO-CMCS and oil through Van der Waals attractive forces, which had enhanced the o/w emulsion stability. On the other hand, emulsion was stable when the repulsive interactions dominates, and when the attractive forces dominate, the oil droplets in an emulsion tend to aggregate (McClements and Gumus, 2016). Increasing concentration of NaO-CMCS creates more and more hydrophobic atmosphere surrounding the oil surface and lowers the IFT by creating denser creamy emulsion. Moreover, sodium carboxylate (−COONa), being the hydrophilic part of the polymer, is attached strongly towards the aqueous phase and inhibits the o/w emulsion to coalescence. Metastable emulsion (0% salinity) formed immediately after mixing (Fig. 6A), and after saturation, creamy emulsion of dispersed phase (Fig. 6C) was obtained. Whereas, in the absence of NaO-CMCS, higher IFT between the water phase and oil phase showed faster phase separation in an hour. This was because the intermolecular forces among the oil phase and aqueous phase were significantly lower than the

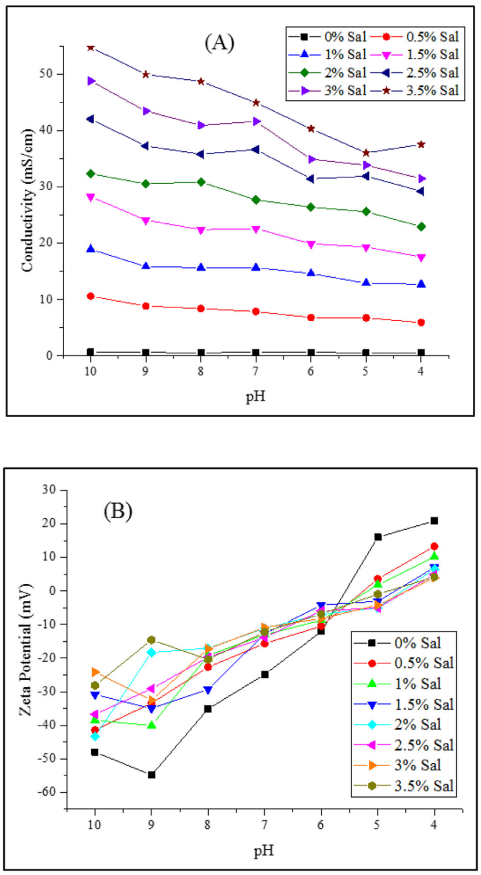

Fig. 5. Effect of salinity and pH on (A) Conductivity and (B) Zeta-potential of NaO-CMCS.

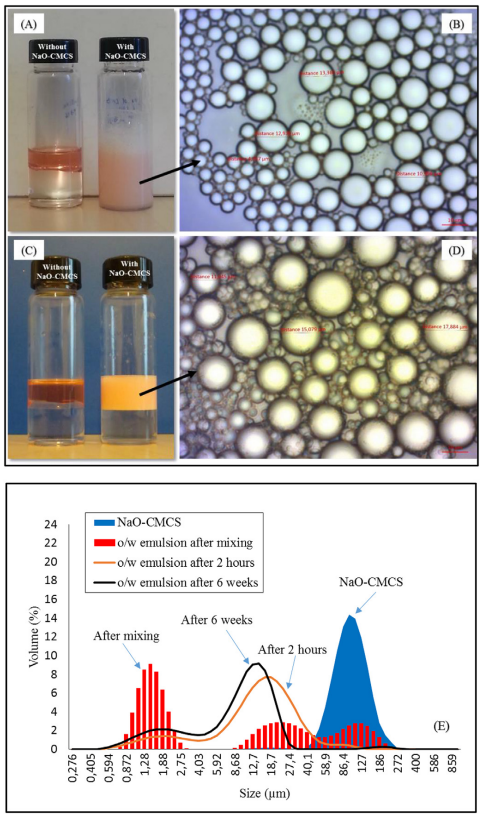

Fig. 6. o/w emulsion at room temperature (A) after mixing without and with NaO-CMCS (B) Microscopic images of o/w emulsion with NaO-CMCS after mixing (C) after 6 weeks of stabilization without and with NaO-CMCS (D) Microscopic images of o/w emulsion with NaO-CMCS after 6 weeks of stabilization (E) Size distributions of NaO-CMCS, oil droplet from o/w emulsions after mixing, after 2 h and after 6 weeks. Scale bar for microscopic images is 10 μm.

intramolecular forces, which makes these phases to be liable to interact themselves but not with each other. Imaging of droplets was conducted periodically using optical microscope. Fig. 6B and 6D are the images of the emulsion after mixing and saturation. The oil droplets sizes were measured weekly (Fig. S4 in Supplementary Material SM4). The average oil droplets size was ≤30 μm for the room temperature emulsions.

The measured size of NaO-CMCS along with the oil droplets of emulsion by laser diffraction is shown in Fig. 6E. The particle size of NaO-CMCS is 113 μm which was in a good resemblance of the microscopic measured values. The o/w emulsion after mixing shows variety of size range due to the presence of water along with NaO-CMCS and oil. However, by increasing the stability time of emulsion the measured droplet diameter became 19.2 μm after 2 h stability and to 13.4 μm after 6 weeks stability, respectively, which were in a good resemblance with the droplet diameter measured by optical microscope (which was ≤30 μm). The oil droplet size at Dx (10), Dx (50) and Dx (90) are shown in Table T1 (in Supplementary Material SM4). The particle size >100 μm at Dx (90) for the emulsion after mixing, reveals that the NaO-CMCS was not completely soluble in water. However, insoluble NaO-CMCS being at the interface between aqueous phase and emulsion, shows partial formation of oil droplets on its surface (Fig. S5 in Supplementary Material SM4). The span value measured for the o/w emulsion after mixing is 18.44 showing a wide range of size distribution, as the size of NaO-CMCS were in μm. However, the decrease in the span value measured for o/w emulsion after 2 h of mixing and after 6 weeks to 2.05 and 1.70, respectively also favors the stability of creamy o/w emulsion.

The o/w emulsion stability was also studied at lower temperature (2 °C) with different dosages of NaO-CMCS. At lower temperature, the interaction between water and hydrophilic moiety of NaO-CMCS increased, which was seen from the increase of the

mean droplet diameter of the o/w emulsion and similar behavior was also observed earlier (Shinoda and Saito, 1969). Hence, there was a size expansion of droplets in the o/w emulsion at lower temperature compared to that at room temperature (Fig. 7). However, at lower concentration of NaO-CMCS, the coalescence rate showed up a slight separation of oil from the emulsion, but increasing the dosage had slower coalescence rate and made a stable o/w emulsion. Therefore, the mean volume diameter in the emulsion was $\leq$60 μm for higher concentration of NaO-CMCS (>1.5 g/L), and was extended up to 100 μm for the lower concentration of NaO-CMCS. The peak with >100 μm mean volume obtained for lower dosage might be due to the size of NaO-CMCS particles (Fig. S6 in Supplementary Material SM4). The results conclude that the o/w emulsions were stable at lower temperature with higher concentration of NaO-CMCS.

The changes in emulsified layer, turbid layer, and clear layer were studied with respect to time after mixing (Fig. S7 in Supplementary Material SM4). The height of the emulsified layer almost remained uniform, whereas the turbid layer and clear layer competed with each other. With time span, the intensity of the turbid layer decreased with increase in the clear layer. In the case of an oil spill, this type of the stable creamy emulsion can be skimmed away from the water surface, demonstrating a presence of very small amount of NaO-CMCS in the aqueous phase. Additionally, the stability of the o/w emulsion was verified by shaking it periodically, with the same reformation of creamy layer after few hours as before. Hence, NaO-CMCS was robust to remain stable even in the wave action.

3.5. Emulsion behavior with pH and salinity variance

Ionic strength along with pH, also plays an important role in the enhancement of the stability of o/w emulsion. Hence, the o/w emulsion behavior was studied for the salinity (0–3.5%) in the pH range of 5–8, i.e. before and after the isoelectric point. Increasing concentration of the electrolyte makes the electrically charged double layer near the hydrophilic part of NaO-CMCS narrower. Addition of HCl shows the ion exchange effect among the amino groups and the Na^+ and H^+ ions present in the NaO-CMCS and aqueous phase, respectively, by making the hydrophilic part (−COONa) attracted more strongly towards the aqueous phase. The repulsive forces among the hydrophobic long carbon chain attached to the amino groups in NaO-CMCS, increase the area in between the hydrophobic long carbon chain of NaO-CMCS by making its way to interact with the oil. Furthermore, the oil droplets have same electrical charge in the emulsion as they were stabilized by the same stabilizer, showing repulsive electrostatic interaction between the oil droplets in an emulsion (Klinkesorn, 2013) by inhibiting the coalescence. After saturation, it was observed that, NaO-CMCS adsorbs onto the surface of more than one droplet and links them together by forming bridging flocculation between the NaO-CMCS and emulsion droplets. Decreasing pH with variable salinity tended towards the instability of o/w emulsion. About pH 6–7 with salinity (0–3.5%), the formation rate of bridging flocculation was maximum (Fig. S8 in Supplementary Material SM5) due to slightly negatively charged NaO-CMCS, whereas, at pH 8 only o/w emulsion was observed, and at pH 5 the stability of o/w emulsion suppressed the coalescence because of the positively charged NaO-CMCS. Increasing salinity accelerates the turbidity of the NaO-CS solution and this builds the bridging flocculation between the NaO-CMCS making the emulsion droplets denser.

3.6. Recovery of oil from emulsified oil

The significant step in the oil spill treatment is the recovery of oil. The stable creamy emulsion with deionized water was gained at lower concentration of NaO-CMCS (below CMC), whereas with sea water, this stability was acquired at higher concentration of NaO-CMCS (above CMC) as shown in Fig. S9 (Supplementary Material SM6). One reason for this might be the presence of multiple ions along with sodium ions in the seawater, which has altered the stability of emulsion below CMC of NaO-CMCS by suppressing the coalescence rate. Addition of Ca^{+2} ($CaCl_2$ solution) to the emulsified oil causes the crosslinking of Ca^{+2} ions with two carboxylic acid groups of the NaO-CMCS. This cross-linking reduces the water solubility of NaO-CMCS through precipitation, which depresses the interaction between the long carbon chain of NaO-CMCS and oil in the o/w emulsion, and pulls out calcium cross-linked NaO-CMCS from the stable emulsion. Hence, stable o/w emulsion breaks, and increasing coalescence rate of the oil droplets concludes that the calcium cross-linked NaO-CMCS lost its property as a stabilizer.

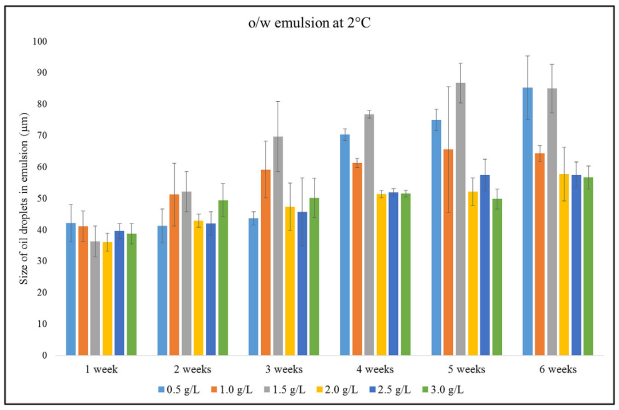

Fig. 7. Droplet size of o/w emulsion at 2 °C with different dosage of NaO-CMCS measured weekly by optical microscope.

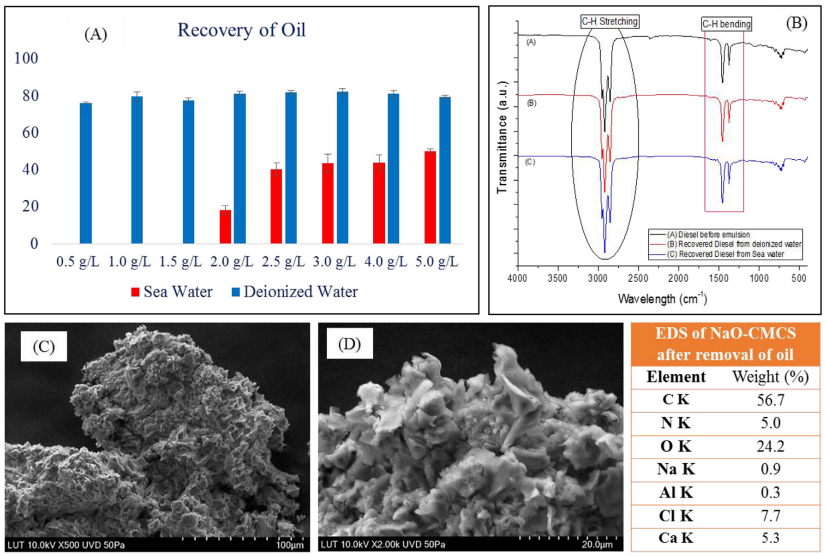

EDS of NaO-CMCS after removal of oil	
Element	Weight (%)
C K	56.7
N K	5.0
O K	24.2
Na K	0.9
Al K	0.3
Cl K	7.7
Ca K	5.3

Fig. 8. (A) Recovery of oil from the emulsified oil using deionized water and sea water with different dosage of NaO-CMCS, (B) FTIR images of oil before emulsion, after recovery of diesel using deionized water with 1 g/L of NaO-CMCS and sea water with 2.5 g/L of NaO-CMCS, (C) and (D) are the SEM images of NaO-CMCS cross-linked with $CaCl_2$ after removal of oil along with the EDS results.

Table 2
Comparison between NaO-CMCS and other adsorbents for the removal or separation of different types of oil.

Adsorbents	Different type of Oils	Removal/ Separation/ Recovery of oil	References
M. rouxii biomass (Chitosan content – 32.7%)	Mineral oil Vegetable oil Cutting oil	77–93%	Srinivasan and Viraraghavan, 2010
Chitosan based polyacrylamide hydrogel	Crude oil	2.3 g/g	H.H. Sokkera et al., 2011
Chitosan microspheres	Total oil and grease (TOG) in oily water	>90%	Grem et al., 2013
Chitosan-coated mesh	Hexane Gasoline Diesel Crude oil	>99% >99% >99% >99%	Zhang et al., 2013a
Polyurethane foam	Gasoline Crude oil Hexane Petroleum ether	96% 98% 95.5% 97%	Zhang et al., 2013,b
Chitosan based aerogel membrane	Crude oil in water emulsion	99%	Chaudhary et al., 2015
Chitosan-poly(vinyl alcohol) blend	Hydraulic oil Kerosene Toluene	33.6 g/g 73.96 g/g 73.96 g/g	Fouad et al., 2016
NaO-CMCS	Marine Diesel	75–85%	This work

Therefore, the recovery of oil was feasible at lower concentrations of NaO-CMCS with deionized water, whereas with sea water it was above CMC of NaO-CMCS due to the instability of o/w emulsion below CMC. The collected oil was weighed and its characteristics compared with those of the initial oil. From the results (Fig. 8A), it was concluded that there was about 75–85% and 19–49% recovery of oil from the emulsified oil using deionized water and sea water, respectively. The recovered oil was characterized using FTIR (Fig. 8B) which shows that the peak intensities at 2854 cm^{-1}, 2922 cm^{-1} and 2954 cm^{-1} of C–H stretching, and at 1377 cm^{-1} and 1457 cm^{-1} of C–H bending remained unaltered, concluding that the recovered diesel was identical to the original one. The detailed of FTIR spectra for each concentration are available in Figs. S10 and S11 (Supplementary Material SM7). The recovered oil was also characterized by GC-FID (Supplementary Material SM8). The SEM images (Fig. 8C and D) show the morphological change in the surface of NaO-CMCS after the recovery of the oil. The presence of calcium in the EDS results confirms the crosslinking of Ca^{2+} ions with the two carboxylic acid groups of NaO-CMCS, which in turn reduces the amount of sodium.

Performance comparison between NaO-CMCS and other adsorbents for the removal and recovery of oil is shown in Table 2.

4. Conclusions

The amphiphilic sodium salt of oleoyl carboxymethyl chitosan (NaO-CMCS) was successfully used as a stabilizer for o/w emulsion. NaO-CMCS forms emulsion when mixed with oil, because of the hydrophobic groups in NaO-CMCS, which reached the surface of the solution and decreased the interfacial tension. The o/w emulsion obtained using NaO-CMCS was stable over 6 weeks. The average oil droplets size was $\leq$30 µm at room temperature and increased with decreasing temperature. The oil droplets were surrounded by the hydrophobic part of NaO-CMCS making the oil intact by reducing the coalescence of oil droplets. Although the surface area for NaO-CMCS was lower than that of unmodified chitosan, the oil affinity of NaO-CMCS was rather impressive due to

its porosity. The salinity and pH of water played a significant role in the deformation of oil to oil droplets. NaO-CMCS being charged showed a strong dependence of o/w emulsion on the pH. At lower pH (<5.5), there was a loss of electrostatic repulsion between the charged groups, which decreased the solubility of NaO-CMCS by forming insoluble NaO-CMCS aggregates. Whereas at higher pH (>5.5), the negative charged groups of NaO-CMCS dominated the rate of the formation of bridging flocculation causing o/w creamy emulsion at pH 8. Oil was recovered from creamy o/w emulsion using calcium ions (Ca^{+2}), which acts as a cross-linker between the two carboxylic acid groups of NaO-CMCS. The recovery of oil was 76% from deionized water with 0.5 g/L concentration of NaO-CMCS and 20% from sea water with 2 g/L concentration of NaO-CMCS. This derivative of chitosan proves to be an effective material for the oil spill removal from the sea water. Increasing the chain of hydrophilic part through carboxy-acylation and its effectiveness in o/w emulsion stability should be studied in the future.

Acknowledgements

This work was funded by the European Union Structural Funds as a part of VIKE project (A70963: Improvement of the oil spill prevention and response with the green chemicals). Chemical structures were drawn using ChemSpider and graphs were plotted using Origin software.

Appendix A. Supplementary data

Supplementary data related to this article can be found at https://doi.org/10.1016/j.jclepro.2017.09.163.

References

U.S. Fish & Wildlife Service, 2004. Effects of oil spills on Wildlife and habitat. http://okaloosa.ifas.ufl.edu/MS/OilSpillFactSheetAlaska.pdf.
Aranaz, I., Harris, R., Heras, A., 2010. Chitosan amphiphilic derivatives. Chemistry and applications. Curr. Org. Chem. 14, 308–330.
Auzèly, R., Rinaudo, M., 2003. Controlled chemical modifications of chitosan. Characterization and investigation of original properties. Macromol. Biosci. 3, 562–565.
Bhatnagar, A., Sillanpää, M., 2009. Applications of chitin- and chitosan-derivatives for the detoxification of water and wastewater — a short review. Adv. Colloid Interfac. 152, 26–38.
Binks, B.P., Murakami, R., Armes, S.P., Fujii, S., 2006. Effects of pH and salt concentration on oil-in-water emulsions stabilized solely by nanocomposite microgel particles. Langmuir 22, 2050–2057.
Chaudhary, J.P., Vadodariya, N., Nataraj, S.K., Meena, R., 2015. Chitosan-based aerogel membrane for robust oil-in-water emulsion separation. ACS Appl. Mater. Inter. 7, 24957–24962.
Chen, X.G., Park, H.J., 2003. Chemical characteristics of O-carboxymethyl chitosans related to the preparation conditions. Carbohyd. Polym. 53, 355–359.
Chiandotti, R.S., Rodrigues, P.C., Akcelrud, L., 2010. Grafting of chitosan with fatty acyl derivatives. J. Braz. Chem. Soc. 21, 1910–1916.
Dash, M., Chiellini, F., Ottenbrite, R.M., Chiellini, E., 2011. Chitosan—a versatile semi-synthetic polymer in biomedical applications. Prog. Polym. Sci. 36, 981–1014.
Dicks, B., 1999. The environmental impact of marine oil spills - effects, recovery and compensation. http://www.itopf.com/fileadmin/data/Documents/Papers/enviro n.pdf.
Doshi, B., Repo, E., Heiskanen, J.P., Sirviö, J.A., Sillanpää, M., 2017. Effectiveness of N,O-carboxymethyl chitosan on destabilization of Marine Diesel, Diesel and Marine-2T oil for oil spill treatment. Carbohyd. Polym. 167, 326–336.
Farrington, J.W., McDowll, J.E., 2004. Mixing Oil and Water, tracking the sources and impacts of oil pollution in the marine environment. Ocean. Mag. 42 (3), 1–4. http://www.whoi.edu/cms/files/dfino/2005/4/v42n3-farrington_2285.pdf.
Fouad, R.R., Aljohani, H.A., Shoueir, K.R., 2016. Biocompatible poly(vinyl alcohol) nanoparticle-based binary blends for oil spill control. Mar. Pollut. Bull. 112, 46–52.
Graham, L., Hale, C., Maung-Douglass, E., Sempier, S., Swann, L., Wilson, M., 2016. Oil Spill Science: Chemical Dispersants and Their Role in Oil Spill Response. MASGP-15–015. http://masgc.org/oilscience/oil-spill-science-dispersant-bkgrnd.pdf.
Grem, I.C.S., Lima, B.N.B., Carneiro, W.F., Queirós, Y.G.C., Mansur, C.R.E., 2013. Chitosan microspheres applied for removal of oil from produced water in the oil industry. Polímeros 23, 705–711.
Hong, M., Yanjie, Y., 2009. Studies on marine oil spills and their ecological damage. J. Ocean Univ. China Oceanic Coast. Sea Res. 8, 312–316.
Huo, M., Zhang, Y., Zhou, J., Zou, A., Li, J., 2011. Formation, microstructure, biodistribution and absence of toxicity of polymeric micelles formed by N-octyl-N,O-carboxymethyl chitosan. Carbohyd. Polym. 83, 1959–1969.
Jawad, A.H., Islam, Md A., Hameed, B.H., 2017. Cross-linked chitosan thin film coated onto glass plate as an effective adsorbent for adsorption of reactive orange 16. Int. J. Biol. Macromol. 95, 743–749.
Jawad, A.H., Nawi, M.A., 2012. Characterizations of the photocatalytically-oxidized cross-linked chitosan-glutaraldehyde and its application as a sub-layer in the TiO_2/CS-GLA bilayer photocatalyst system. J. Polym. Environ. 20, 817–829.
Jena, S.K., Sangamwar, A.T., 2016. Polymeric micelles of amphiphilic graft copolymer of α-tocopherol succinate-g-carboxymethyl chitosan for tamoxifen delivery: synthesis, characterization and *in vivo* pharmacokinetic study. Carbohyd. Polym. 151, 1162–1174.
Jernelöv, J., 2010. The threats from oil spills: now, then, and in the future. AMBIO 39, 353–366.
Jianga, M., Wanga, K., Kennedy, J.F., Niec, J., Yua, Q., Mac, G., 2010. Preparation and characterization of water-soluble chitosan derivative by Michael addition reaction. Int. J. Biol. Macromol. 47, 696–699.
Jumaa, M., Müller, B.W., 1998. The effect of oil components and homogenization conditions on the physicochemical properties and stability of parenteral fat emulsions. Int. J. Pharm. 163, 81–89.
Kalliola, S., Repo, E., Srivastava, V., Heiskanen, J.P., Sirviö, J.A., Liimatainen, H., Sillanpää, M., 2017. The pH sensitive properties of carboxymethyl chitosan nanoparticles cross-linked with calcium ions. Colloid. Surf. B 153, 229–236.
Klinkesorn, U., 2013. The role of chitosan in emulsion formation and stabilization. Food Rev. Int. 29, 371–393.
Kong, X., 2012. Simultaneous determination of degree of deacetylation, degree of substitution and distribution fraction of –COONa in carboxymethyl chitosan by potentiometric titration. Carbohyd. Polym. 88, 336–341.
Kyzas, G.Z., Bikiaris, D.N., 2015. Recent modifications of chitosan for adsorption applications: a critical and systematic review. Mar. Drugs 13, 312–337.
Langevin, D., Poteau, S., Hénaut, I., Argillier, J.F., 2004. Crude oil emulsion properties and their application to heavy oil transportation. Oil Gas. Sci. Technol. 59, 511–521.
Li, Y., Zhang, S., Meng, X., Chen, X., Ren, G., 2011. The preparation and characterization of a novel amphiphilic Oleoyl-carboxymethyl chitosan self-assembled nanoparticles. Carbohyd. Polym. 83, 130–136.
Liu, H., Wang, C., Zou, S., Wei, Z., Tong, Z., 2012. Simple, reversible emulsion system switched by pH on the basis of chitosan without any hydrophobic modification. Langmuir 28, 11017–11024.
Lü, T., Zhao, H., Qi, D., Chen, Y., 2015. Synthesis of a novel amphiphilic and cationic chitosan-based flocculant for efficient treatment of oily wastewater. Adv. Polym. Tech. 34 (21502), 1–7.
McClements, D.J., Gumus, C.E., 2016. Natural emulsifiers — biosurfactants, phospholipids, biopolymers, and colloidal particles: molecular and physicochemical basis of functional performance. Adv. Colloid Interfac. 234, 3–26.
Mubarak, N.S.A., Jawad, A.H., Nawawi, W.I., 2017. Equilibrium, kinetic and thermodynamic studies of Reactive Red 120 dye adsorption by chitosan beads from aqueous solution. Energy Ecol. Environ. 2, 85–93.
Nawi, M.A., Sabar, S., Jawad, A.H., Sheilatina, Ngah, W.S.W., 2010. Adsorption of Reactive Red 4 by immobilized chitosan on glass plates: towards the design of immobilized TiO_2–chitosan synergistic photocatalyst-adsorption bilayer system. Biochem. Eng. J. 49, 317–325.
Ngo, D.H., Vo, T.S., Ngo, D.N., Kang, K.H., Je, J.Y., Pham, H.N., Byun, H.G., Kim, S.K., 2015. Biological effects of chitosan and its derivatives. Food Hydrocoll. 51, 200–216.
Niu, W., Wu, S., Zhang, S., 2010. A facile and general approach for the multicolor tuning of lanthanide-ion doped NaYF4 upconversion nanoparticles within a fixed composition. J. Mater. Chem. 20, 9113–9117.
No, H.K., Meyers, S.P., Prinyawiwatkul, W., Xu, Z., 2007. Applications of chitosan for improvement of quality and shelf life of foods: a review. J. Food Sci. 72, R87–R100.
Pillai, C.K.S., Paul, W., Sharma, C.P., 2009. Chitin and chitosan polymers: chemistry, solubility and fiber formation. Prog. Polym. Sci. 34, 641–678.
Pintor, A.M.A., Vilar, V.J.P., Botelho, C.M.S., Boaventura, R.A.R., 2016. Oil and grease removal from wastewaters: sorption treatment as an alternative to state-of-the-art technologies. A critical review. Chem. Eng. J. 297, 229–255.
Repo, E., Warchoł, J.K., Bhatnagar, A., Sillanpää, M., 2011. Heavy metals adsorption by novel EDTA-modified chitosan–silica hybrid materials. J. Colloid Interf. Sci. 358, 261–267.
Rinaudo, M., 2006. Chitin and chitosan: properties and applications. Prog. Polym. Sci. 31, 603–632.
Shinoda, K., Saito, H., 1969. The stability of O/W type emulsions as functions of temperature and the HLB of emulsifiers: the emulsification by PIT method. J. Colloid Interf. Sci. 30, 258–263.
Shukla, S.K., Mishra, A.K., Arotiba, O.A., Mamba, B.B., 2013. Chitosan-based nanomaterials: a state-of-the-art review. Int. J. Biol. Macromol. 59, 46–58.
Sing, K.S.W., Everett, D.H., Haul, R.A.W., Moscou, L., Pierotti, R.A., Rouquerol, J., Siemieniewska, T., 1985. Reporting physisorption data for gas/solid systems with special reference to the determination of surface area and porosity. Pure Appl. Chem. 57, 603–619.
Smit, M.G.D., Bechmann, R.K., Hendriks, A.J., Skadsheim, A., Larsen, B.K., Brussant, T., Bamber, S., Sanni, S., 2009. Relating biomarkers to whole-organism effects using species sensitivity distributions: a pilot study for marine species exposed to oil.

Environ. Toxicol. Chem. 28, 1104–1109.
Sokkera, H.H., El-Sawy, N.M., Hassan, M.A., El-Anadouli, B.E., 2011. Adsorption of crude oil from aqueous solution by hydrogel of chitosan based polyacrylamide prepared by radiation induced graft polymerization. J. Hazard. Mater. 190, 359–365.
Sonia, T.A., Rekha, M.R., Sharma, C.P., 2010. Bioadhesive hydrophobic chitosan microparticles for oral delivery of insulin: in vitro characterization and in vivo uptake studies. J. Appl. Polym. Sci. 119, 2902–2910.
Srinivasan, A., Viraraghavan, T., 2010. Oil removal from water using biomaterials. Bioresour. Technol. 101, 6594–6600.
Sun, T., Xu, P., Liu, Q., Xue, J., Xie, W., 2003. Graft copolymerization of methacrylic acid onto carboxymethyl chitosan. Eur. Polym. J. 39, 189–192.
Sun, G.Z., Chen, X.G., Li, Y.Y., Liu, C.S., Liu, C.G., Zheng, B., Gong, Z.H., Sun, J.J., Chen, H., Li, J., Lin, W.X., 2008. Preparation and properties of amphiphilic chitosan derivative as a coagulation agent. Environ. Eng. Sci. 25, 1325–1332.
Tiena, C.L., Lacroixb, M., Ispas-Szaboa, P., Mateescu, M.A., 2003. N-acylated chitosan: hydrophobic matrices for controlled drug release. J. Control. Release 93, 1–13.
Ummadisingu, A., Gupta, S., 2012. Characteristics and kinetic study of chitosan prepared from seafood industry waste for oil spills cleanup. Desalin. Water Treat. 44, 44–51.
Wolfe, D., Michel, J., Hameedi, M.J., Payne, J.R., Galt, J.A., Watabayashi, G., Braddock, J., Short, J., O'Clarie, C., Rice, S., 1994. The fate of the oil spilled from the Exxon Valdez. Environ. Sci. Technol. 28, 560A–568A.
Yang, Z., Yuan, B., Huang, X., Zhou, J., Cai, J., Yang, H., Li, A., Cheng, R., 2012. Evaluation of the flocculation performance of carboxymethyl chitosan-graft-polyacrylamide, a novel amphoteric chemically bonded composite flocculant. Water Res. 46, 107–114.
Zhang, S., Lu, F., Tao, L., Liu, N., Gao, C., Feng, L., Wei, Y., 2013a. Bio-inspired anti-oil-fouling chitosan-coated mesh for oil/water separation suitable for broad pH range and hyper-saline environments. ACS Appl. Mater. Inter. 5, 11971–11976.
Zhang, X., Li, Z., Liu, K., Jiang, L., 2013b. Bioinspired multifunctional foam with self-cleaning and oil/water separation. Adv. Funct. Mat. 23, 2881–2886.
Zhang, Z., Sèbe, G., Rentsch, D., Zimmermann, T., Tingaut, P., 2014. Ultralightweight and flexible silylated nanocellulose sponges for the selective removal of oil from water. Chem. Mater. 26, 2659–2668.

Publication III

Doshi, B., Ayati, A., Tanhaei, B., Repo, E. and Sillanpää, M.

Partially carboxymethylated and partially cross-linked surface of chitosan versus the adsorptive removal of dyes and divalent metal ions

Reprinted with permission from

Carbohydrate Polymers

Vol 197, pp. 586-597, 2018

Carbohydrate Polymers 197 (2018) 586–597

Contents lists available at ScienceDirect

Carbohydrate Polymers

journal homepage: www.elsevier.com/locate/carbpol

Partially carboxymethylated and partially cross-linked surface of chitosan versus the adsorptive removal of dyes and divalent metal ions

Bhairavi Doshi[a,*], Ali Ayati[b], Bahareh Tanhaei[b], Eveliina Repo[c], Mika Sillanpää[a,d]

[a] Department of Green Chemistry, School of Engineering Science, Lappeenranta University of Technology, Sammonkatu 12, FI-50130 Mikkeli, Finland
[b] Department of Chemical Engineering, Quchan University of Advanced Technology, Quchan, Iran
[c] Department of Separation and Purification, School of Engineering Science, Lappeenranta University of Technology, Skinnarilankatu 34, FI-53850, Finland
[d] Department of Civil and Environmental Engineering, Florida International University, FL-33174 Miami, USA

ARTICLE INFO

Keywords:
Carboxymethyl chitosan
Glutaraldehyde crosslinked
Dyes and metal ions
Adsorption
Sodium leaching
Modeling

ABSTRACT

Industrial wastes and their effluents containing dyes and heavy metals are a tremendous threat to the environment, and to treat these toxic waste streams, effective and environmentally benign methods are needed. In this study, NaCS-GL was used as an effective adsorbent, for the removal of dyes and metal ions from their aqueous solution. The presence of carboxylate groups on the NaCS-GL surface has altered the protonation of amino groups. The adsorption kinetics of dyes on NaCS-GL was initially controlled by the film diffusion or chemical reaction after which the intra-particle or pore diffusion started to govern the rate. Leaching of sodium ion confirmed the crosslinking of two carboxylate groups of NaCS-GL with the metal ions. Modeling of the adsorption isotherms revealed that the different active surface sites of NaCS-GL were involved in the adsorption of dyes and metals, suggesting the simultaneous removal of these components from the wastewater.

1. Introduction

The continual use of a variety of dyes such as MB, SaO and Tart, by industries, such as textile, printing, food, pharmaceuticals and cosmetics, usually discharge a large amount of coloured effluents into water resources. Contact with a higher amount of these pollutants can cause harmful effects on human health, such as abnormal urine, hypertension, staining of skin, abdominal pain, nausea, dizziness, asthma, itching, blurred vision and carcinogenic effects. The treatment of these effluents before disposal into the aquatic environment has become a great challenge in recent years (Pereira & Alves, 2011). In a similar manner, the presence of heavy metals, such as lead (Pb) and cadmium (Cd), in water beyond their acceptance limit creates hazardous and carcinogenic effects on living creatures. Various techniques, such as membrane filtration, aerobic and anaerobic biodegradation, coagulation, flocculation, conventional oxidation and adsorption, have been developed for the treatment of effluents containing dyes (Ayati et al., 2014; Ayati, Shahrak, Tanhaei, & Sillanpää, 2016; He et al., 2013; Robinson, McMullan, Marchant, & Nigam, 2001; Särkkä, Bhatnagar, & Sillanpää, 2015). Amongst these methods, adsorption is the most efficient technique for the removal of pollutants from wastewater (Forgacs, Cserháti, & Oros, 2004; Srivastava & Sillanpää, 2017; Zhao et al., 2015). Adsorbents such as activated carbons (Kannan & Sundaram, 2001), clays (Adebowale, Olu-Owolabi, & Chigbundu, 2014; Celis, Hermosin, & Cornejo, 2000; Yi & Zhang, 2008), lignocellulosic wastes and biopolymers (Hokkanen et al., 2014; Tu, Yu, et al., 2017; Zhao et al., 2014) have been used to remove different types of dyes and heavy metals from the waste streams. Carbon based adsorbents show excellent adsorption properties (Alatalo et al., 2016; Chen et al., 2017; Ma et al., 2012), but they can be commercially expensive along with their regeneration.

Chitosan, a deacetylated form of chitin which is naturally occurring biopolymer derived from crustaceans of shrimps and crab shells. Being biodegradable and non-toxic, chitosan was widely used in pharmaceuticals (Martino, Sittinger, & Risbud, 2005), food industry (Khora & Lim, 2003) and water remediation (Bhatnagar & Sillanpää, 2009). Two surface groups, hydroxyl and amino groups, contributes to hydrophilicity and active adsorption sites. One of the important limitations of chitosan in the adsorptive removal of contaminants is its dissolution tendency in acidic effluent (Vakili et al., 2014). The modification of chitosan through chemical cross-linking can improve the mechanical and chemical stability of chitosan in acidic solutions (Chatterjee, Chatterjee, Lim, & Woo, 2011; Vakili et al., 2014). Cross-linking

Abbreviations: DS, degree of substitution; EA, elemental analysis; EDS, energy dispersive X-ray spectroscopy; FTIR, fourier transform infrared spectrophotometer; HCl, hydrochloric acid; IPA, isopropanol; MB, methylene blue; NaCl, sodium chloride; NaOH, sodium hydroxide; Na-CS, sodium form of carboxymethyl chitosan; NaCS-GL, sodium form of carboxymethyl glutaraldehyde cross-linked chitosan; RT, room temperature; SaO, Safranin O; SEM, scanning electron microscopy; Tart, tartrazine

* Corresponding author.
E-mail addresses: bhairavi.doshi@lut.fi, bhairavidoshi3@gmail.com (B. Doshi).

https://doi.org/10.1016/j.carbpol.2018.06.032
Received 22 February 2018; Received in revised form 28 May 2018; Accepted 6 June 2018
Available online 07 June 2018

significantly reduces segment mobility in polymers; meanwhile, a series of interconnected chains appear by creating new inter-chain linkages. Glutaraldehyde, ethyleneglycol diglycidyl ether, formaldehyde and epichlorohydrin are the most common ionic cross-linkers used for the modification of chitosan (Bai et al., 2018; Hsien et al., 2013; Jing, Liu, Yu, Xia, & Yin, 2013; Monier, 2012; Tanhaei, Ayati, Bamoharram, Lahtinen, & Sillanpää, 2016). Even though the hydroxyl groups present on the surface of chitosan are one of the active sites for the adsorbate, Chethan and Vishalakshi demonstrated the amino groups as active sites for the adsorption of metal ions (Chethan & Vishalakshi, 2013).

Chitosan and its derivatives are amongst the low cost adsorbents, which have been extensively studied (Ayati, Tanhaei, & Sillanpää, 2016; Li et al., 2015; Repo, Warchol, Kurniawan, & Sillanpää, 2010; Repo, Warchoł, Bhatnagar, Mudhoo, & Sillanpää, 2013) and reviewed (Ngah, Teong, & Hanafiah, 2011; Vakili et al., 2014) for the dyes removal and metal ions elimination from the waste effluents (Morsy, 2015). Carboxymethyl chitosan consists of surficial active amino and carboxylic acid groups and hence it is widely used in the removal of pollutants from wastewater (Doshi, Repo, Heiskanen, Sirviö, & Sillanpää, 2017; Sarkar, Debnath, & Kundu, 2012; Wu, Dai, Kan, Shilong, & Zhu, 2017). The combination of chitosan beads with Lemna gibba effectively removed Boron from drinking water (Türker & Baran, 2017). Similarly, silica-chitosan hybrid beads were effective in the removal (Ramasamy et al., 2017) and recovery (Ramasamy et al., 2018) of rare earth elements form wastewater effluents. Recent research reveals that chitosan derivatives obtained via electrospinning and electrospraying techniques have enhanced heavy metals adsorption (Huang et al., 2018; Tu, Huang, et al., 2017). However, as per the authors' knowledge, the sodium form of partially carboxymethylated chitosan cross-linked with glutaraldehyde have been not yet studied for the adsorption of dyes and metal ions.

In the present work, we have synthesized and characterized, NaCS-GL, by modifying the chitosan surface through carboxymethylation and cross-linking, to study the adsorptive removal of dyes such as MB, SaO and Tart, and Pb(II) and Cd(II) metal ions from their aqueous solution. The surface charge behaviour of NaCS-GL was investigated with respect to pH, to reflect the protonation and deprotonation of amino groups in the presence of carboxylate group ($-COONa$). The effect of various important parameters, such as adsorbent dosage, solution pH, dye/metal concentration, contact time, and temperature have been investigated, comprehensively along with the competitive adsorption of dyes with metal ions. The NaCS-GL after the adsorption of respective dyes and metal ions were also characterized in order to understand the mechanism of the adsorption of pollutants on the surface of NaCS-GL. Regeneration studies were performed to show the reusability of NaCS-GL and its effectiveness in water remediation.

2. Material and methods

2.1. Chemicals and synthesis

The details of the chemicals used are available in SM1. Na-CS was synthesized based on our previously reported method (Doshi et al., 2017) with some modifications. Briefly, a mixture of 10 g chitosan, 40 mL IPA and 100 mL NaOH (10%) were heated for 1 h in a water bath (C-MAG HS 7 Digital from IKA) at 50 °C. Dissolved monochloroacetic acid (15 g) in isopropanol (20 ml) was added dropwise to above reaction mixture and the reaction was allowed for 4 h at the same temperature. Then, 200 mL ethanol (70%) was added and the product was washed with 70–90% ethanol. It was centrifuged (at 4000 rpm for 5 min) three times and dried overnight at RT. The obtained product was Na-CS. A mixture of 1 g of dried Na-CS in 30 mL glutaraldehyde solution (10%) was stirred for 30 min, and the obtained solid was washed with water and centrifuged (4 times) with overnight drying at RT. The obtained solid is NaCS-GL. The synthesis procedure of NaCS-GL has been presented in Fig. 1.

2.2. Characterization

Chitosan, Na-CS and NaCS-GL has been characterized by FTIR, SEM, EDS and, EA. The DS was calculated from the CHNS elemental analysis (Doshi, Repo, Heiskanen, Sirviö, & Sillanpää, 2018) and unsubstituted amino groups in Na-CS by potentiometric titration, respectively. The surface charge of NaCS-GL was studied as a function of pH ranging from 4 to 10 using Zetasizer Nano ZS (Malvern, UK). The carboxylic acid content in Na-CS and NaCS-GL, were calculated using conductometric titration. Refer to SM2 for the detailed procedure about the characterization methods.

2.3. Adsorption studies as a function of NaCS-GL dosage and solution pH

The dyes and metal ions solutions of the desired concentrations (20 mg L^{-1}) were obtained by the dilution of respective dyes and metal ions stock solution (1000 mg L^{-1}). The adsorption studies were performed with 0.1–2.5 g L^{-1} NaCS-GL, in order to determine the optimum dosage for further studies. With the optimized dosage of NaCS-GL, the effect of pH was studied in the range of 2–12 for the dyes and 2–8 for the metal ions. These solutions were shaken for 24 h at 100 rpm to reach the equilibration, and then filtered through 0.45 µm polypropylene membrane filters. The MB, SaO and Tart concentrations were measured by Lambda 45 UV/VIS Spectrometer (Perkin Elmer, USA) at λ_{max} = 664, 520 and 430 nm, respectively. The Pb(II) and Cd(II) concentrations were measured by ICP (Agilent 5110 ICP-OES). The removal efficiency (R%) and adsorbate uptake at t time (q_t, mg/g) were calculated using Eqs. (1) and (2):

$$R(\%) = \frac{C_0 - C_t}{C_0} * 100 \quad (1)$$

$$q_t = \frac{(C_0 - C_t)}{m} * V \quad (2)$$

Where C_o and C_t (mg L^{-1}) are the pollutant concentrations at initial and t time respectively, m (g) is adsorbent dosage and V (L) is the solution volume.

2.4. Adsorption kinetics on the surface of NaCS-GL

The adsorption mechanism was investigated from the adsorption kinetics using four different models such as pseudo-first-order, pseudo-second-order, Bangham and Weber-Morris (mentioned in Table 1). 10 mL of each dyes and metal ions solutions (20 mg L^{-1}) were shaken with the optimum amount of NaCS-GL at 100 rpm, collected periodically, filtered and analyzed as per Section 2.3.

2.5. Adsorption isotherms and thermodynamics

In order to study the adsorption isotherms, the optimum amount of adsorbent was added to 10 mL of dyes (10–800 mg L^{-1}) and metal ions (5–200 mg L^{-1}) solutions, and the desired concentrations of these pollutants were obtained by the dilution of the respective dyes and metal ions stock solution (1000 mg L^{-1}). These solutions were shaken at 200 rpm for 6 h in controlled temperatures (25–45 °C) using shaker (IKA KS 4000i Control), and analyzed as per Section 2.3. Five well-known isotherms such as Langmuir, Freundlich, Tekmin, Dubinin-Radushkevich and Sips models (mentioned in Table 1), were applied to evaluate the experimental equilibrium data, and MATLAB software was used for the non-linear regression. The adsorption thermodynamics was calculated using the Van't Hoff equation (shown in Table 1).

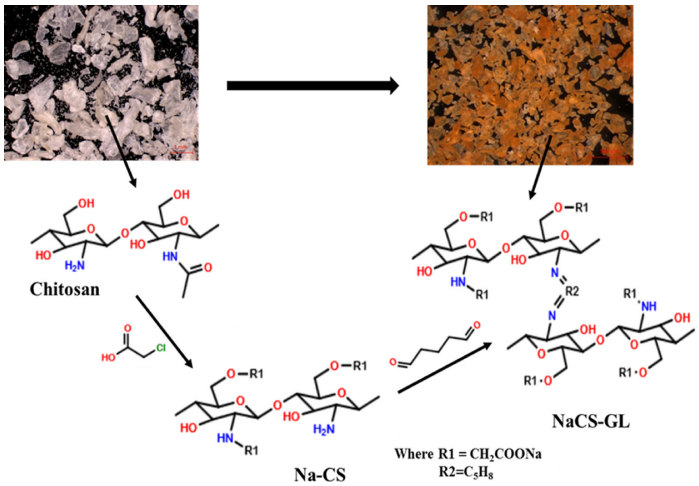

Fig. 1. Synthesis route of NaCS-GL from chitosan.

3. Results and discussion

3.1. Characterization

The off-white coloured chitosan after modification turns into brown colour NaCS-GL, and the shape of NaCS-GL was non-uniform with average particle size ≤ 500 μm (Fig. 1). Two peaks at about 3350 cm^{-1} and 3290 cm^{-1} in the FTIR spectra of chitosan (Fig. 2a) and Na-CS (Fig. 2b) indicates N—H stretching (primary), whereas a peak at 3286 cm^{-1} in NaCS-GL (Fig. 2c) reveals to N—H stretching (secondary). In NaCS-GL, peak intensities at 2869 and 2929 cm^{-1} indicates C—H stretching. The intensity reduction at 1418 cm^{-1} in Na-CS and NaCS-GL

Table 1
Different models for the calculation of adsorption kinetics and adsorption isotherms and thermodynamics.

Models	Parameters
Pseudo-first order (Huang et al., 2014) $\ln(q_e - q_t) = \ln q_e - (k_1 t)$ (3)	q_t and q_e (mg g^{-1}) are the amount of adsorbate at t (min) time and equilibrium state, respectively; k_1 (min^{-1}) = the rate constant of pseudo-first-order
Pseudo-second order (Ho, 2006) $\frac{t}{q_t} = \frac{1}{k_2 q_e^2} + \frac{1}{q_e} t$ (4) $h = k_2 q_e^2$ (5)	k_2 (g mg^{-1} min^{-1}) is the rate constant of pseudo-second order; *h is* the initial adsorption rate.
Bangham (Huang et al., 2014) $\log\log\left[\frac{C_0}{C_0 - m q_t}\right] = \log\left[\frac{k_0 m}{2.303 V}\right] + \alpha_B \log t$ (6)	C_0 (mg L^{-1}) is the initial pollutant concentration; m (g L^{-1}) is the adsorbent dosage; V (mL) is the volume of solution; k_0 and α_B (< 1) are constants.
Weber–Morris (Hosseini, Khan, Malekbala, Cheah, & Choong, 2011) $q_t = k_{id} t^{1/2} + C_i$ (7)	k_{id} (mg g^{-1} min^{-1}) is the intra-particle diffusion rate constant in step i; C_i (mg g^{-1}) is the constant related to the extent of boundary layer thickness in each step.
Langmuir (Ren et al., 2013) $q_e = \frac{q_m K_L C_e}{1 + K_L C_e}$ (8) $R_L = \frac{1}{1 + K_L C_0}$ (9)	K_L is Langmuir constant (L mg^{-1}); R_L value reflects the favourability of adsorption, adsorption is considered as unfavourable if $R_L > 1$, linear for $R_L = 1$ and favourable if $0 < R_L < 1$ and irreversible if $R_L < 0$.
Freundlich (Foo & Hameed, 2010) $q_e = K_F C_e^{1/nF}$ (10)	K_F is Freundlich isotherm constant (L g^{-1}); n_F is Freundlich exponent
Tekmin (Nagy et al., 2017) $q_e = \frac{RT}{b_T} \ln(A_T C_e)$ (11)	A_T is equilibrium binding constant (L mg^{-1}) b_T is Tekmin constant (J/mol)
Dubinin-Radushkevich (Nagy et al., 2017) $q_e = q_m \exp(-\beta \varepsilon^2)$ (12) $\varepsilon = RT \ln(1 + \frac{1}{C_e})$ (13)	β *is* D-R model constant (mol^2 kJ^{-2}) ε is Polanyi potential
Sips (Foo & Hameed, 2010) $q_e = q_m \frac{(K_S C_e)^\gamma}{(1 + (K_S C_e)^\gamma)}$ (14)	K_s is Sips model isotherm constant γ is Sips model exponent
Van't Hoff (Hu et al., 2011) $\Delta G^0 = -RT \ln K_L$ (15) $\Delta G^0 = \Delta H^0 - T\Delta S^0$ (16)	(ΔG°) is standard Gibbs free energy, (ΔH°) is adsorption standard enthalpy, (ΔS°) is entropy, K_L (L mol^{-1}) is the Langmuir constant.

q_e = amount of adsorbate adsorbed at equilibrium; q_m = maximum quantity adsorbed (mg g^{-1}); C_e = equilibrium concentration; R = gas constant (0.008314 kJ $mole^{-1}$); T = absolute temperature.

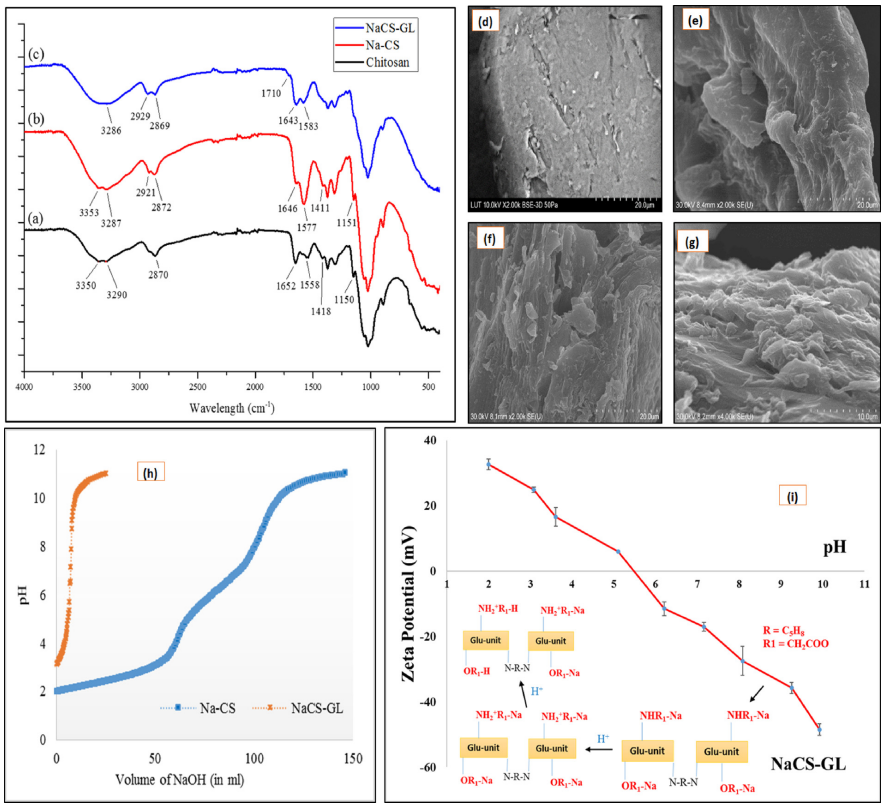

Fig. 2. FTIR spectra of (a) chitosan, (b) Na-CS and (c) NaCS-GL. SEM images of chitosan (d) at accelerating voltage of 10 kV, Na-CS (e) and NaCS-GL (f) at accelerating voltage of 30 kV with 2.0k of magnifications, NaCS-GL (f) at an accelerating voltage of 30 kV with 4.0k of magnification. (h) Potentiometric Titration of Na-CS and NaCS-GL and (i) Surface behaviour of NaCS-GL.

compared to chitosan, shows presence of substituted amino groups, and similar behaviour observed previously (Jabli, Baouab, Sintes-Zydowicz, & Hassine, 2012). The C—O—C bending vibration at 1151 cm^{-1} observed in chitosan and Na-CS, but not in NaCS-GL, indicating the peak hindrance after cross-linking (Li et al., 2013). The characteristic absorption bands at 1577 cm^{-1} (C═O of −COONa asymmetric stretching) and 1411 cm^{-1} (C═O of −COONa symmetric stretching) in Fig. 1b, reveals that, both hydroxyl and amino groups were carboxymethylated.

Fig. 2d–g shows surface morphology of chitosan, Na-CS and NaCS-GL, respectively, whose surface roughness increased after modification. The EA results (Table 2) shows the reduction of nitrogen(%) significantly from chitosan to NaCS-GL, which has increased the C/N ratio (Monteiro & Airoldi, 1999) as carbon(%) was not altered much. The obtained C/N ratio from EDS results were in good agreement with EA results, and conforms the presence of sodium in Na-CS and NaCS-GL (Refer Fig. S1(a–c) in SM2). The DS value < 0.50 suggests the partial carboxymethylation in Na-CS, were few hydroxyl and amino groups remains unaltered and similar behaviour was also observed previously (Doshi et al., 2017). Moreover, the DS results of NaCS-GL (< 0.50) show that the unaltered amino groups of Na-CS might have crosslinked with glutaraldehyde. Fig. 2h shows the presence of unsubstituted amino groups with two range hump in Na-CS but only one range hump in NaCS-GL. The second range hump in Na-CS is due to the deprotonation of free amino groups which was absent in NaCS-GL. This also confirms the crosslinking of free amino groups with glutaraldehyde in NaCS-GL, which confirms the DS interpretation.

According to the IUPAC classification, the N_2 adsorption-desorption graph (Fig. S1d in SM2) is Type-II, representing unrestricted monolayer-multilayered adsorption and the hysteresis H3 suggests the aggregation of plate like particles (Sing et al., 1985). The BET results of NaCS-GL reveals that after modification, the surface area increases and the pore diameter results (Refer Table 2) suggest the formation of mesoporous particles. Even though the surface roughness of Na-CS was more than chitosan, the surface area and porosity dropped down due to the carboxymethylation. Fig. S1e (Refer SM2) suggests that the surface of Na-CS and NaCS-GL possesses a different range of pore size. The carboxylic acid (−COO-) content in Na-CS and NaCS-GL were 2.24 mmol g^{-1} and 0.26 mmol g^{-1}, respectively (Refer Table 2), which reflects the existence of carboxymethylated part in Na-CS as well as in NaCS-GL (Refer SM2). The reduction in the carboxylic acid content of NaCS-GL suggests that a glutaraldehyde molecule has been trapped in between two polymer units via an imine (C═N) bond, which might

Table 2
Elemental composition, DS, surface area, porosity and carboxylic acid content results of chitosan, Na-CS and NaCS-GL. The EDS results of NaCS-GL before and after adsorption.

Element (Wt%)	C	N	O	C/N	DS	BET ($m^2\ g^{-1}$)	Pore Volume ($cm^3\ g^{-1}$)	Pore Diameter (nm)	Carboxylic acid content (mmol g^{-1})
Chitosan	40.38	6.86	6.41	5.89	–	144	0.12	3.41	–
Na-CS	39.82	6.02	6.88	6.61	0.36	92	0.08	4.25	2.24
NaCS-GL	40.85	4.71	5.56	8.67	0.41	178	0.15	3.47	0.26

Element (Wt %)	Before adsorption	After MB adsorption	After SaO adsorption	After Tart adsorption	After Pb(II) adsorption	After Cd(II) adsorption
C K	54.5	65.87	58.81	61.28	75.15	62.31
N K	9.0	8.84	10.11	11.52	11.13	13.40
O K	34.4	14.88	29.39	20.48	11.74	13.23
Na K	**1.7**	–	–	–	–	–
S K	–	**1.06**	–	**0.35**	–	–
Pb K	–	–	–	–	**1.78**	–
Cd K	–	–	–	–	–	**10.26**
Al K	0.1	0.66	0.18	0.52	0.17	0.59
Mg K	–	–	–	0.09	0.03	0.22
Ag K	–	8.69	1.50	5.76	–	–

have expanded the internal polymer structure and increased the surface area of NaCS-GL as compared to Na-CS. Hence, the amount of carboxylic acid per polymer unit might have fallen down as compared to Na-CS. These results were in good agreement with the BET results. The surface charge of NaCS-GL plays an important role in the adsorption of contaminants. The original pH of NaCS-GL solution was around 9.2. The initial surface charge of NaCS-GL was negative (−32.77 mV) as shown in Fig. 2i. The addition of HCl firstly protonated the amino groups of NaCS-GL followed by the protonation of the carboxylate groups. Therefore, decreasing pH has increased the zeta potential towards zero (isoelectric point at pH 5.4) and, furthermore, the addition of HCl made the surface more positive.

3.2. Adsorptive behaviour of NaCS-GL with dyes and metal ions

3.2.1. Effect of adsorbent dosage and solution pH

Fig. 3a shows that, in addition to high colour removal efficiency at very low amount of adsorbent (> 0.4 g L^{-1}), the increase in dosage suggests a removal efficiency from 33.9%, 36.9% and 43.26% to a plateau trend at 97.7%, 91.9% and 96.8% for MB, SaO and Tart, respectively. By increasing the adsorbent dosage, a larger surface area and a higher number of free adsorption sites were available for the dye adsorption. However, beyond 0.6 g L^{-1}, further increasing the amount of the adsorbent did not enhance the removal percentage, due to the excess of adsorption sites for the adsorption process (Naiya, Bhattacharya, & Das, 2009). Moreover, for the metal ions, Pb(II) and Cd (II), the adsorption trend was slightly different than dyes. Pb(II) showed 99.9% removal with 0.8 g L^{-1} NaCS-GL, whereas Cd(II) showed an up to 99.9% removal with 1.5 g L^{-1} of absorbent (Fig. 3a). In addition, the adsorption capacity decreased (Fig. 3b) by an increase in the NaCS-GL dosage, showing that NaCS-GL had lot of active sites even at a smaller amount (0.1 g L^{-1}) (Tanhaei, Ayati, Lahtinen, & Sillanpää, 2015). Hence, the optimum amount of NaCS-GL used for further experiments of dyes is 0.8 g L^{-1} and for metal ions it is 2.0 g L^{-1}.

The pH of the solution plays a key role in the adsorption process due to its strong influence on the surface of NaCS-GL as well as the speciation of dyes and metals. The initial pH of MB, SaO, Tart, Pb(II) and Cd(II) solutions obtained were approx. 5.6, 6.4, 6.3, 5.5 and 6.1, respectively. The results (Fig. 3c) revealed that the cationic dyes MB and SaO removal percentage remained high (> 93%) in the wide pH range of 5–11, whereas for Tart, a similar removal was obtained at pH < 3. At higher pH, both amino and carboxylate groups were deprotonated causing attractive electrostatic forces between the NaCS-GL surface and the cationic dye molecules as well as metal ions. In addition, the charge density of MB and SaO solutions decreased with increasing pH, which in this case led to a decrease of electrostatic repulsion between the cationic dyes and adsorbent surface and consequently enhanced dye adsorption (Monash & Pugazhenthi, 2009). Moreover, the presence of the carboxylate group in NaCS-GL altered the protonation process of amino groups and increased the surface activity by creating more adsorption sites for the cationic dyes and metal ions. For the metal ions Pb (II) and Cd(II), the removal percentage remained high (> 95%) in the pH range of 5–8 (Fig. 3c). Despite the effective removal of metal ions, pH > 6.5 was not considered for metal ions adsorption due to their tendency to form precipitates with OH^- ions (Barakat, 2011; Pejic, Vukcevic, Kostic, & Skundric, 2009; Zhou et al., 2015). However, at a

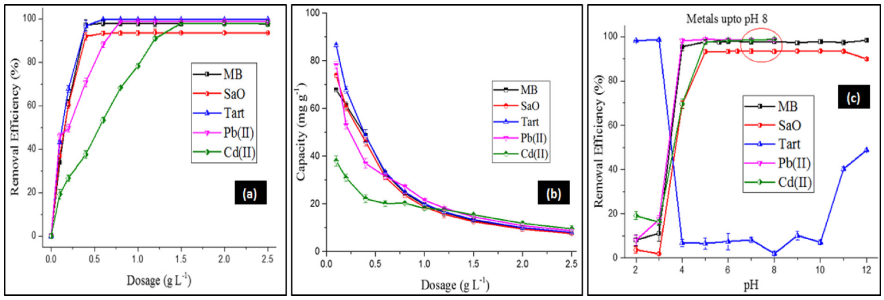

Fig. 3. Effect of NaCS-GL dosage on the (a) adsorptive removal and (b) uptake of dyes and metals, (c) effect of solution pH on the adsorptive removal of dyes and metal ions. The pH range for dyes is 2–12 and for metal ions is 2–8.

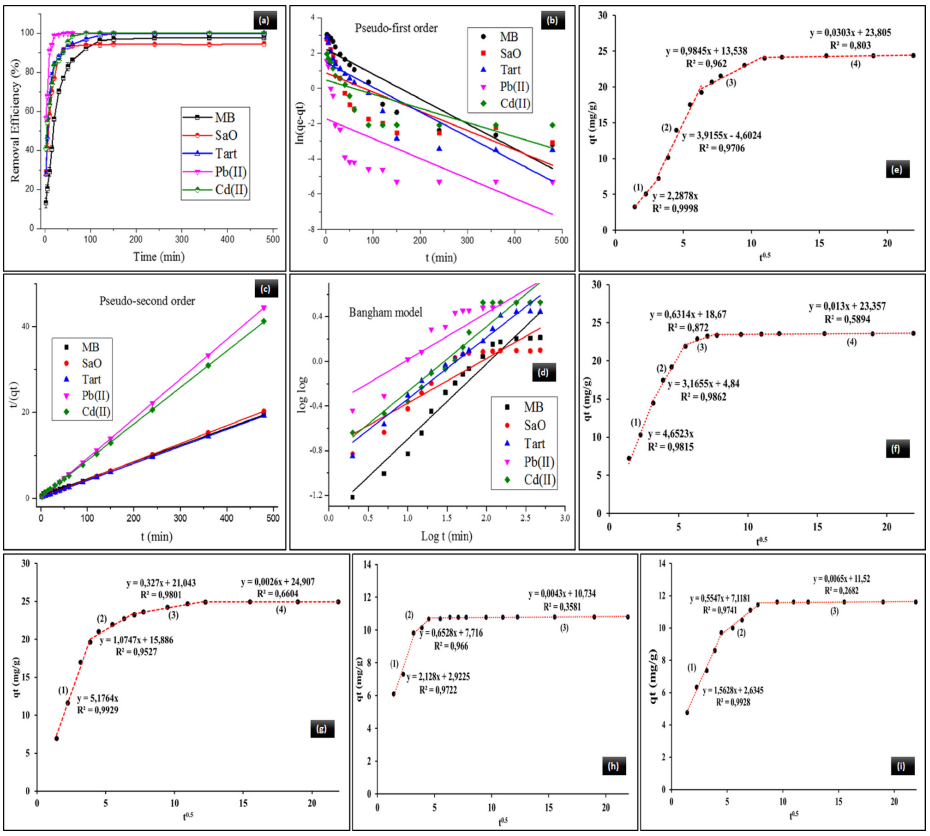

Fig. 4. Effect of contact time on (a) dyes and metal ions adsorption. Kinetic plot for adsorption of dyes and metal ions on NaCS-GL (b) pseudo-first order and (c) pseudo-second order, (d) Bangham adsorption kinetic curve. Intra-particle diffusion curve for the adsorption of (e) MB, (f) SaO, (g) Tart, (h) Pb(II) and (i) Cd(II) on NaCS-GL.

Table 3
Calculated kinetics parameters for cationic and anionic dyes, Pb(II) and Cd(II) adsorption onto the NaCS-GL adsorbent.

Pollutants	$q_{e(exp)}$	Pseudo-first-order (Linear)			Pseudo-second-order (Linear)				Bangham model		
		q_e	k_1	R^2	q_e	k_2	h	R^2	k_0	α_B	R^2
MB	24.46	9.195	0.014	0.842	25.470	0.003	1.750	0.9985	1.225	0.675	0.942
SaO	23.67	2.416	0.011	0.565	23.860	0.012	6.935	0.9998	4.838	0.400	0.822
Tart	24.99	4.326	0.014	0.775	25.263	0.009	5.984	0.9999	3.699	0.552	0.966
Pb(II)	10.81	0.179	0.011	0.426	10.830	0.131	15.397	1.000	1.581	0.420	0.834
Cd(II)	11.76	1.599	0.008	0.514	11.763	0.024	3.328	0.9999	1.580	0.582	0.927

lower pH, the positively charged surface of NaCS-GL created the electrostatic attraction with anionic dye Tart by progressing the rate of adsorption through chemical interactions with NaCS-GL (Dotto, Vieira, & Pinto, 2012). At the same time, at a lower pH, the positively charged H^+ ions competed with Pb(II) and Cd(II) along with MB and SaO for getting adsorbed on NaCS-GL. Thus, cationic dyes and metal ions showed a lower removal percentage below pH 4 due to the repulsive interactions towards the adsorbent surface. Therefore, the pH of MB, SaO, Pb(II) and Cd(II) solutions were unadjusted for the further experiments, whereas, for Tart, all the experiments were carried out at pH < 3.

3.2.2. Effect of contact time and kinetic studies

The kinetics of the adsorption processes were studied (Fig. 4), to investigate the adsorption mechanisms and potential rate-controlling steps. There was a rapid adsorption of dyes and metals (Fig. 4a) during

the early stages of the process due to the abundant availability of the active sites on the NaCS-GL surface, with more than 93% removal efficiency for SaO and Pb(II) until 60 min and, for MB, Tart and Cd(II) it was gained until 120 min. The adsorption kinetics was evaluated and calculated parameters are listed in Table 3 (also refer Table T1 in SM3). The linear fitting of pseudo-first-order (Fig. 4b) and pseudo-second-order (Fig. 4c) reveals that the adsorption of dyes and metal ions onto NaCS-GL was very well correlated to the pseudo-second-order model with high regression coefficients (> 0.998). The pseudo-second-order model suggests that the rate of occupying adsorption sites is proportional to the square of unoccupied sites and the number of occupied sites proportional to the fraction of compound adsorbed on the adsorbent surface. Hence, it can be concluded that the rate-controlling step of the process could be chemisorption i.e. formation of the chemical bond between the adsorbate molecule and the adsorbent (Huang, Li, Chen, Zhang, & Chen, 2014). However, fitting the data by Bangham's model (Fig. 4d and Table 3) with $R^2 > 0.92$ suggests that the adsorption kinetics of MB, Tart and Cd(II) onto NaCS-GL adsorbent could be partially limited by the pore diffusion as well (Mezenner & Bensmaili, 2009).

In this case, the pseudo-first- and -second-order models cannot solely explain the mechanisms of the adsorption, especially due to the porous nature of the adsorbent. Therefore, the intra-particle diffusion model has been applied to examine the relative significance of the two transport mechanisms of intra-particle diffusion and film diffusion for the adsorption of dyes and metal ions onto NaCS-GL (Tanhaei et al., 2015). The multi-linear plot during the sorption process shows four linear regions for dyes (Fig. 4e–g) and three for metals (Fig. 4h and i). The diffusion of dyes and metals from their bulk solution to the NaCS-GL surface cannot be observed only due to the efficient mixing, thus the first linear step describes either the film or surface diffusion or the first pore diffusion stage. As seen from the figures, several pore diffusion steps exist, which attributes to the various pore sizes found in the studied adsorbent (Refer Fig. S1e in SM2), and similar behaviour observed previously (Ren, Abbood, He, Peng, & Huang, 2013). The final region corresponds to the final equilibrium stage, in which the intra-particle or pore diffusion decreases due to decreasing pore volume and a low concentration of adsorbates present in the solution (Wu et al., 2017). In the case of dyes, the first visible diffusion step can be attributed to the film diffusion because the line nearly passes through the origin. However, for the metals, the film diffusion is faster and its rate can be evaluated approximately from the line between origin and the first kinetic point. Based on these findings, it can be concluded that the early stage of adsorption is controlled by the surface reactions and/or film diffusion followed by various pore diffusion steps and due to the size effects the diffusion of dyes is slower compared to that of metals (Qiu et al., 2009). Recently, Albadarin et al. studies also showed similar behaviour (Albadarin et al., 2017).

3.2.3. Sodium leaching

NaCS-GL being in sodium form, the leaching of sodium from NaCS-GL surface along with adsorption of metal ions was investigated using kinetic data. Fig. 5a shows that sodium leaching was higher in the Cd (II) solution compared to Pb(II). The metals loaded NaCS-GL (1.0 g L^{-1} concentration) was used in the removal of 5–30 mg L^{-1} dyes solutions. There was also leaching of sodium from metal loaded NaCS-GL when reacted with dyes (Fig. 5b), which confirms that Pb(II) and Cd(II) were partially adsorbed on the surface of NaCS-GL. This also reveals the presence of free sodium sites on the surface of NaCS-GL, even after metals adsorption. Moreover, the effectiveness of Pb(II) loaded NaCS-GL in the removal of MB and SaO was more than Cd(II) loaded NaCS-GL (Fig. 5c). Even though the removal of Tart was > 95%, it was not considered here due to the leaching of Pb(II) and Cd(II) in acidic condition, which was not observed with cationic dyes MB and SaO. Sodium leaching mechanism and competitive adsorption between Pb(II) and MB in presented in Fig. 5d.

3.3. Adsorption isotherms

Fig. 6a and b shows the effect of the initial concentration of dyes and metal ions on the equilibrium adsorption capacity and the isotherms. Here, a temperature increase provided the faster rate of diffusion of adsorbate molecules from the solution to the NaCS-GL surface but the adsorption capacity did not change significantly with increasing temperature for MB, SaO and Cd(II). However, for Tart and Pb(II) the adsorption capacity slightly stepped up due to the pore enlargement with the increase in the temperature, which exposed more surface sites for the adsorbate interaction. Hence, the adsorption capacity of NaCS-GL sharply increased to reach a plateau trend at high initial concentrations of MB, SaO and Cd(II). At the equilibrium, MB, SaO and Tart uptake by NaCS-GL enhanced from 12.15 to 342.60 mg g^{-1}, 11.98 to 103.72 mg g^{-1} and 11.03 to 550.00 mg g^{-1}, respectively, by increasing their concentrations from 10 to 800 mg L^{-1} at 25 °C. However for the metal ions Pb(II) and Cd(II), the uptake at equilibrium rose up from 2.19 to 47.71 mg g^{-1} and 3.49 to 36.04 mg g^{-1}, respectively by increasing their concentrations from 5 to 200 mg L^{-1} at 25 °C. This reveals that NaCS-GL has been saturated by dyes and metal ions at high initial concentrations, due to the high driving force gradient (Li et al., 2013). The adsorption capacity of NaCS-GL was enhanced compared to the previously studied adsorption behaviour of chitosan for dyes (Dotto et al., 2012; Guo & Wilson, 2012) and metal ions (Bhatnagar & Sillanpää, 2009) removal from water resources. The enhanced pore size and surface area (Refer Table 1) might have enhanced the adsorption of NaCS-GL in comparison to that of chitosan.

3.3.1. Isotherms modeling and mechanism

The isotherm modeling results are summarized in Table 4. From the two-parameter models, the Langmuir model gave the best fitting results generally for the dyes studied (Fig. 6c–e) and the correlation was especially good for MB equilibrium data. This suggests that the adsorption of MB occurred through monolayer formation and the similar active sites (mainly amino groups of NaCS-GL) were involved in the process. In the case SaO, the Langmuir model did not predict the maximum adsorption capacity very well, but generally showed the best apparent fit especially for the curved portion of the isotherms suggesting the amino groups as a prime adsorption sites for SaO as well. However, some carboxylate groups of NaCS-GL also underwent adsorption with cationic dyes due to their negative surface after the leaching of sodium. Whereas with Tart, the isotherm curves (Fig. 6e) showed some hysteresis at a low concentration region, due to the weaker interactions between the Tart and the surface in these conditions, and enhanced adsorption at higher concentrations. This phenomenon also observed earlier for chitosan-based adsorbents at low pH and successfully modeled by the Sips model (Repo et al., 2010).

In the case of metals, the Freundlich and Temkin models obtained the best apparent fittings (Fig. 6f and g). The Sips model gave higher R^2 values for Pb(II) most likely due to better fitting at low concentrations. The Freundlich model suggested that the adsorption process was heterogeneous supported by the fact that the metals most likely interacted with both amino and carboxylic groups on the surface. The fitting of the Temkin model supported the heterogeneity, and simultaneously monolayer adsorption behaviour. In addition, the n values > 1 and R_L values < 1, suggested the favourable adsorption onto NaCS-GL adsorbent surface. Furthermore, the adsorption energy values (D–R model) < 8 kJ/mol indicating physical interactions between the surface and adsorbed compounds. Even if the D–R model did not fit well to the experimental data, the obtained energy values supports similar values obtained from the Temkin isotherm fitting.

The adsorption of pollutants onto the NaCS-GL surface was investigated by FTIR, SEM and EDS analysis. From the FTIR spectra of NaCS-GL after dyes adsorption (Fig. 6i), showed the shifts in the peaks of N—H groups (at 1585 cm^{-1} for NaCS-GL) revealing that the amino groups were the main participant functional groups for interaction and

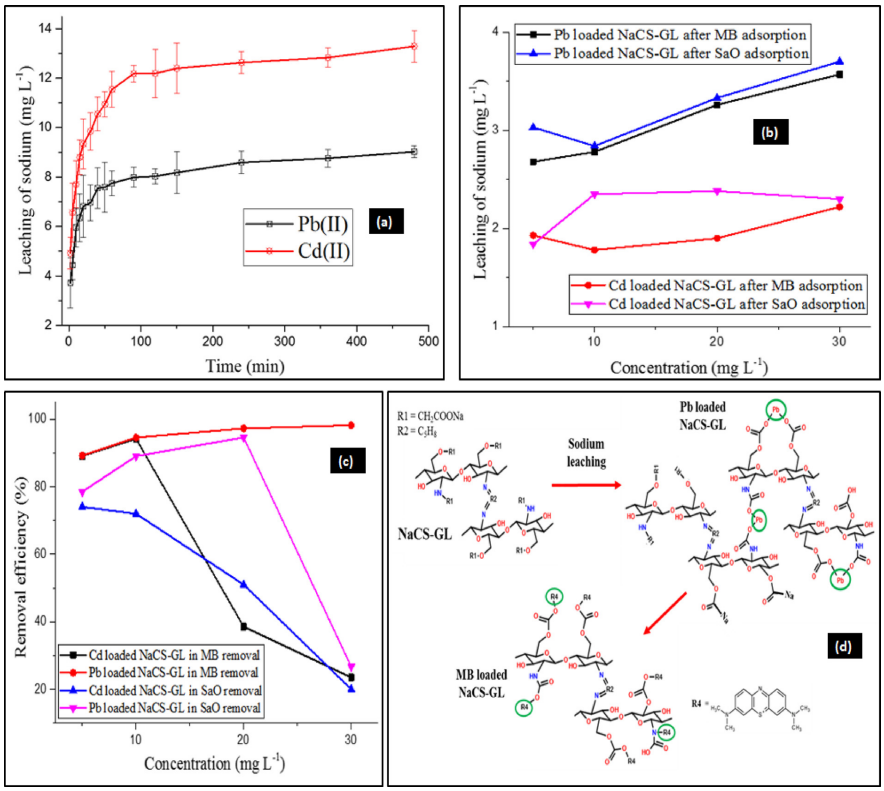

Fig. 5. (a) Sodium leaching from NaCS-GL after Pb(II) and Cd(II) adsorption, (b) Sodium leaching from Pb(II) loaded NaCS-GL and Cd(II) loaded NaCS-GL after MB and SaO adsorption, (c) Removal of MB and SaO from Pb(II) loaded NaCS-GL and Cd(II) loaded NaCS-GL, (d) Mechanism of sodium leaching and competitive adsorption between Pb(II) and MB.

adsorption of dyes. On the other hand, there was no shifting of peak (at 1585 cm^{-1} for NaCS-GL) confirming that the amino groups were not participating in the adsorption of metal ions (Fig. 6h). Moreover, the leaching of sodium ions (Section 3.2.3) also suggested the cross-linking of metal ions with two carboxylate ions and not with the amino groups. Similar crosslinking behaviour of sodium form of chitosan with Ca^{+2} ions was also observed in our previous studies (Doshi et al., 2018). The EDS of NaCS-GL after adsorption (mentioned in Table 2), shows the presence of sulphur in MB and Tart, whereas Pb and Cd in the respective metal ions adsorption. However, sodium was absent after the adsorption of pollutants, suggesting that Na^{+} ions of NaCS-GL (from $-CH_2COONa$) had interacted with the Cl– ions of MB and SaO and respective negative ions of metal ions solution. This also confirmed the leaching of sodium during adsorption. For the SEM images of pollutants after adsorption and the adsorption mechanism of pollutants on the surface of NaCS-GL refer to SM4.

3.3.2. Thermodynamic study

The calculated thermodynamic parameters values of adsorbed pollutants onto the NaCS-GL surface were incorporated in Table T2 (refer SM5). The negative values of ΔG° suggest the feasibility and spontaneity (Pb(II) > SaO > Tart > Cd(II) > MB) of this adsorption process. The decrease in ΔG° values with increasing temperature confirms that cationic and anionic dyes along with Pb(II) and Cd(II) were better adsorbed at higher temperatures (Mezenner & Bensmaili, 2009). Moreover, the negative value of ΔH° for MB, SaO, Tart and Cd(II) adsorption indicates the exothermic nature of adsorption, whereas the positive value of ΔH° for the adsorption of Pb(II) suggests the adsorption as endothermic due to the faster reaction rate compared to other pollutants. A similar behaviour of Pb(II) had observed before (Amer, Khalili, & Awwad, 2010; Alfaro-Cuevas-Villanueva, Hidalgo-Vázquez, Penagos, & Cortés-Martínez, 2014). Furthermore, positive values of ΔS° reveal that an increase in the movement at the solid-liquid interface during adsorption had increased the entropy.

3.3.3. Regeneration study

The recovery and reusability of adsorbent is one of the important industrial applications. The regeneration of NaCS-GL after the adsorption of MB, SaO, Pb(II) and Cd(II) was performed by HCl (0.1 M), whereas for NaCS-GL after the adsorption of Tart, NaOH (0.1 M) was used. The sodium form was retrieve by using $NaCl/Na_2CO_3$ solution. The regeneration studies details can be found in SM6.

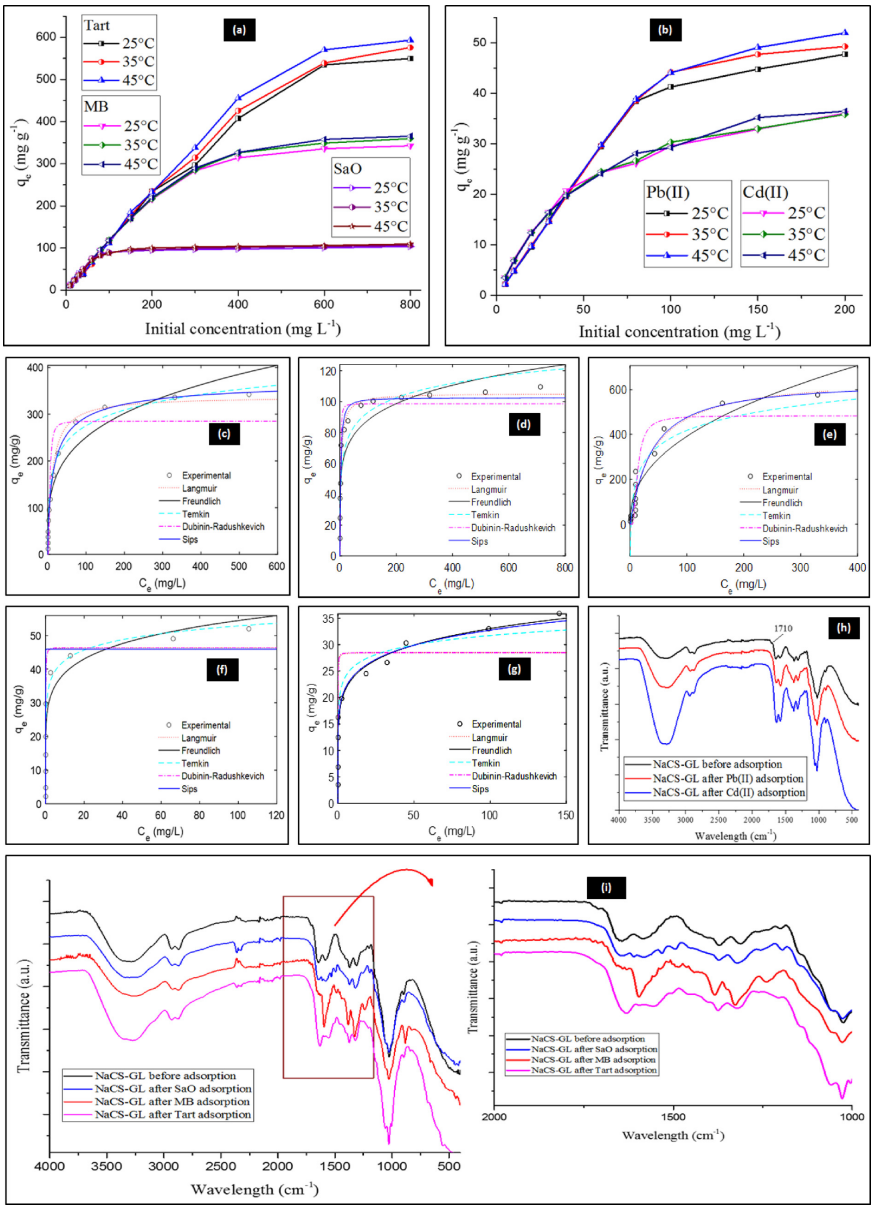

Fig. 6. Effect of initial concentrations on the adsorption of (a) dyes and (b) metal ions. Non-linear regression for isotherm model by Matlab for (c) MB at 25 °C, (d) SaO at 45 °C (e) Tart at 35 °C, (g) Pb(II) at 45 °C and (h) Cd(II) at 35 °C. FTIR spectra of NaCS-GL before and after the adsorption of (h) metal ions and (i) dyes.

Table 4
The calculated adsorption isotherm parameters models for the removal of MB, SaO, Tart, Pb(II) and Cd(II) by NaCS-GL.

Pollutants	T (°C)	Langmuir			Freundlich		Temkin	Dubinin-Radushkevich		Sips	
		q_m	R_L	R^2	n	R^2	R^2	E	R^2	q_m	R^2
MB	25	338.04	0.3648	0.9908	3.742	0.9356	0.9830	0.35	0.8843	376.43	0.9988
	35	353.30	0.3825	0.9896	3.598	0.9374	0.9885	0.36	0.8784	395.28	0.9984
	45	357.37	0.3642	0.9861	3.652	0.9403	0.9892	0.34	0.8822	406.59	0.9971
Sa O	25	97.84	0.0853	0.9476	7.497	0.7749	0.8470	0.97	0.9678	95.29	0.9655
	35	100.9	0.0970	0.9319	6.763	0.7728	0.8471	0.96	0.9622	97.14	0.9556
	45	105.3	0.1641	0.9582	6.049	0.7947	0.8774	0.95	0.9490	102.4	0.9612
Tart	25	628.7	0.6925	0.9506	2.325	0.9072	0.8761	0.90	0.9018	666.6	0.9514
	35	663.1	0.6416	0.9438	2.347	0.8649	0.8573	0.89	0.8875	639.6	0.9443
	45	695.9	0.6197	0.9420	2.394	0.8539	0.8542	0.93	0.9244	610.9	0.9554
Pb(II)	25	43.68	0.0029	0.9323	6.767	0.8138	0.8778	5.65	0.9255	43.12	0.9764
	35	45.51	0.0022	0.9342	6.737	0.8343	0.8932	6.49	0.9203	44.96	0.9705
	45	46.41	0.0023	0.8836	6.831	0.8291	0.8729	1.20	0.8235	45.97	0.9217
Cd(II)	25	28.69	0.0022	0.8522	7.209	0.9131	0.9229	6.41	0.8425	111	0.9136
	35	28.50	0.0016	0.7955	6.993	0.9157	0.9005	0.91	0.8286	214.5	0.9144
	45	32.52	0.0013	0.5497	6.867	0.9185	0.8976	0.79	0.8206	241.9	0.9163

Table 5
Comparison of maximum adsorption capacities (q_m) of MB, SaO, Tart, Pb(II) and Cd(II) using different chitosan adsorbents.

Adsorbent	Pollutants	q_m (mg g^{-1})	Ref.
For removal of dyes			
Chitosan	MB	30.1	Guo and Wilson (2012)
Activated lignin-chitosan	MB	36.25	Albadarin et al. (2017)
Carboxymethyl chitosan-modified magnetic-cored dendrimer	MB	96.31	Kim, Jang, and Park (2016)
Chitosan-crosslinked κ-carrageenan	MB	130.4	Mahdavinia and Mosallanezhad (2016)
Activated oil palm ash zeolite/chitosan	MB	199.20	Khanday, Asif, and Hameed (2017)
Chitosan hydrogel beads	MB	226.24	Chatterjee et al. (2011)
Amino-functionalized attapulgite clay	MB	226.24	Zhou et al. (2015)
Crosslinked O-carboxymethyl chitosan	MB	239.54	Sarkar et al. (2012)
Chitosan	Tart	350	Dotto et al. (2012)
Chitosan films	Tart	413.8	Rêgo, Cadaval, Dotto, and Pinto (2013)
NaCS-GL	MB	365.77	This work
NaCS-GL	SaO	126.80	This work
NaCS-GL	Tart	609.26	This work
For removal of metal ions			
Chitosan	Cd(II)	5.93	Bhatnagar and Sillanpää (2009)
Cross-linked chitosan-Polyphosphate-Epichlorohydrin Beads	Pb(II)	28.42	Jing et al. (2013)
Chitosan-modified polyethylene terephthalate (PET)	Pb(II)	31.25	Niu, Ying, Li, Wang, and Jia (2017)
Ethylene-1,2-diamine-6-deoxy-chitosan	Pb(II)	31.8	Chethan and Vishalakshi (2013)
Ethylenediamine modified chitosan microspheres	Pb(II)	46.51	Chethan and Vishalakshi (2015)
Thiocarbohydrazide cross-linked chitosan-poly(vinyl alcohol)	Pb(II)	47.36	Ahmad, Manzoor, Chaudhari, and Ikram (2017)
Chitosan saturated montmorillonite	Pb(II)	79.92	Hu, Zhu, Cai, Hu, and Fu (2017)
	Cd(II)	23.03	
S. cerevisiae loaded nanofibrous mats (Poly(ε-caprolactone)-Chitosan-Rectorite)	Pb(II)	238	Xin et al. (2017)
NaCS-GL	Pb(II)	51.93	This work
NaCS-GL	Cd(II)	36.43	This work

3.4. Competitive adsorption

The competitive adsorption shows the behaviour and order of pollutants adsorption in the presence of each other. The removal of Pb(II) and Cd(II) was > 95% and > 79%, respectively up to 20 mg L^{-1} solutions for both MB and SaO (Fig. S6a and b in SM7). By increasing the concentration of the solutions to 50 mg L^{-1}, the removal of Pb(II) and Cd(II) drops to 67% and 8%, respectively. This reveals that the adsorption of Pb(II) had ruled over the adsorption of Cd(II) ions, which is in good agreement with the adsorption of metal ions. However, the removal efficiency of MB and SaO was less than Cd(II) for a lower concentration, and from 40 mg L^{-1}, the removal efficiency of MB and SaO exceeds Cd(II), and reaches the flattening plateau. This shows that reactive sites taken up by cationic dyes are much more than metal ions. Therefore, the overall reactivity is Pb(II) > SaO > MB > Cd(II). On the other hand, the adsorption capacity of metal ions with Tart does not show up as high removal (Fig. S6c in SM7), as the pH of the solution was < 3. This shows that all the protonated amino and carboxylate groups of NaCS-GL were attracted towards Tart, and not giving enough vacant sites to metal ions for adsorption onto the NaCS-GL surface. This removal data of the metal ions are in a good resemblance to the removal efficiency of metal ions with respect to pH. Moreover, the adsorption stepped down in saline water, and the effect of electrolyte on the adsorption of MB was investigated and the details can be found in SM8.

3.5. Comparison of the adsorption performance

The maximum adsorption capacity (q_m) of NaCS-GL was compared with some other chitosan adsorbents reported earlier in the literature (refer Table 5). This concludes the effectiveness of NaCS-GL in the removal of dyes and metals was the maximum compared to other adsorbents.

4. Conclusion

In the study, NaCS-GL was synthesized and characterized using various techniques. The carboxymethylated part of the Na-CS remained unaltered after glutaraldehyde crosslinking in NaCS-GL. However, the

decreased amount of carboxylic acid content confirmed the expansion of molecule per gram after crosslinking. NaCS-GL was mesoporous, having a sufficiently high surface area of 178 m^2/g, and the presence of carboxylate groups (−COONa) in NaCS-GL altered the protonation process of amino groups. This increased the surface activity of NaCS-GL, which enhanced the adsorption capacities of dyes and metal ions on its surface. Initially, film diffusion or chemical reaction control the rate of the adsorption followed controlled by the pore diffusion. The Langmuir isotherm model best fitted to the experimental equilibrium data for dyes. However, for metals, the Freundlich and Temkin isotherm models fitted better, suggesting surface heterogeneity. Based on the obtained results NaCS-GL with different surficial chemistry is the potential adsorbent for the removal of cationic and anionic dyes along with heavy metals. The applicability of NaCS-GL could be extended in the future for the water remediation of industrial effluents.

Acknowledgements

The European Union Structural Funds and the City of Mikkeli funded this work.

Appendix A. Supplementary data

Supplementary material related to this article can be found, in the online version, at doi:https://doi.org/10.1016/j.carbpol.2018.06.032.

References

Adebowale, K. O., Olu-Owolabi, B. I., & Chigbundu, E. C. (2014). Removal of Safranin-O from aqueous solution by adsorption onto Kaolinite clay. *Journal of Encapsulation and Adsorption Sciences, 4*, 89–104.

Ahmad, M., Manzoor, K., Chaudhari, R., & Ikram, S. (2017). Thiocarbohydrazide Cross-linked oxidized chitosan and poly(vinyl alcohol): A green framework as efficient Cu (II), Pb(II), and Hg(II) adsorbent. *Journal of Chemical & Engineering Data, 62*, 2044–2055.

Alatalo, S.-M., Mäkilä, E., Repo, E., Heinonen, M., Salonen, J., Kukk, E., ... Titirici, M.-M. (2016). Meso- and microporous soft templated hydrothermal. *Green Chemistry, 18*, 1137–1146.

Albadarin, A. B., Collins, M. N., Naushad, M., Shirazian, S., Walker, G., & Mangwandi, C. (2017). Activated lignin-chitosan extruded blends for efficient adsorption of methylene blue. *Chemical Engineering Journal, 307*, 264–272.

Alfaro-Cuevas-Villanueva, R., Hidalgo-Vázquez, A., Penagos, C., & Cortés-Martínez, R. (2014). Thermodynamic, kinetic, and equilibrium parameters for the removal of lead and cadmium from aqueous solutions with calcium alginate beads. *The Scientific World Journal, 647515*, 1–9.

Amer, M. W., Khalili, F. I., & Awwad, A. M. (2010). Adsorption of lead, zinc and cadmium ions on polyphosphate-modified kaolinite clay. *Journal of Environmental Chemistry and Ecotoxicology, 2*, 001–008.

Ayati, A., Ahmadpour, A., Bamoharram, F. F., Tanhaei, B., Mänttäri, M., & Sillanpää, M. (2014). A review on catalytic applications of Au/TiO2 nanoparticles in the removal of water pollutant. *Chemosphere, 107*, 163–174.

Ayati, A., Shahrak, M. N., Tanhaei, B., & Sillanpää, M. (2016). Emerging adsorptive removal of azo dye by metal-organic frameworks. *Chemosphere, 160*, 30–44.

Ayati, A., Tanhaei, B., & Sillanpää, M. (2016). Lead(II)-ion removal by ethylenediaminetetraacetic acid ligand functionalized magnetic chitosan-aluminum oxide-iron oxide nanoadsorbents and microadsorbents: Equilibrium, kinetics, and thermodynamics. *Journal of Applied Polymer Science, 134*, 44360.

Bai, R., Yang, F., Zhang, Y., Zhao, Z., Liao, Q., Chen, P., ... Cai, C. (2018). Preparation of elastic diglycolamic-acid modified chitosan sponges and their application to recycling of rare-earth from waste phosphor powder. *Carbohydrate Polymers, 190*, 255–261.

Barakat, M. A. (2011). New trends in removing heavy metals from industrial wastewater. *Arabian Journal of Chemistry, 4*, 361–377.

Bhatnagar, A., & Sillanpää, M. (2009). Applications of chitin- and chitosan-derivatives for the detoxification of water and wastewater – A short review. *Advances in Colloid and Interface Science, 152*, 26–38.

Celis, R., Hermosin, M. C., & Cornejo, J. (2000). Heavy metal adsorption by functionalized clays. *Environmental Science & Technology, 34*, 4593–4599.

Chatterjee, S., Chatterjee, T., Lim, S., & Woo, S. (2011). Adsorption of a cationic dye, methylene blue, on to chitosan hydrogel beads generated by anionic surfactant gelation. *Environmental Technology, 32*, 1503–1514.

Chen, J., Shi, X., Zhan, Y., Qiu, X., Du, Y., & Deng, H. (2017). Construction of horizontal stratum landform-like composite foams and their methyl orange adsorption capacity. *Applied Surface Science, 397*, 133–143.

Chethan, P. D., & Vishalakshi, B. (2013). Synthesis of ethylenediamine modified chitosan and evaluation for removal of divalent metal ions. *Carbohydrate Polymers, 97*, 530–536.

Chethan, P. D., & Vishalakshi, B. (2015). Synthesis of ethylenediamine modified chitosan microspheres for removal of divalent and hexavalent ions. *International Journal of Biological Macromolecules, 75*, 179–185.

Doshi, B., Repo, E., Heiskanen, J. P., Sirviö, J. A., & Sillanpää, M. (2017). Effectiveness of N,O-carboxymethyl chitosan on destabilization of marine diesel, diesel and marine-2T oil for oil spill treatment. *Carbohydrate Polymers, 167*, 326–336.

Doshi, B., Repo, E., Heiskanen, J. P., Sirviö, J. A., & Sillanpää, M. (2018). Sodium salt of oleoyl carboxymethyl chitosan: A sustainable adsorbent in the oil spill treatment. *Journal of Cleaner Production, 170*, 339–350.

Dotto, G. L., Vieira, M. L. G., & Pinto, L. A. A. (2012). Kinetics and mechanism of tartrazine adsorption onto chitin and chitosan. *Industrial & Engineering Chemistry Research, 51*, 6862–6868.

Foo, K., & Hameed, B. H. (2010). Insights into the modeling of adsorption isotherm systems. *Chemical Engineering Journal, 156*, 2–10.

Forgacs, E., Cserháti, T., & Oros, G. (2004). Removal of synthetic dyes from wastewaters: A review. *Environment International, 30*, 953–971.

Guo, R., & Wilson, L. (2012). Synthetically engineered chitosan-based materials and their sorption properties with methylene blue in aqueous solution. *Journal of Colloid and Interface Science, 338*, 225–234.

He, X., Male, K. B., Nesterenko, P. N., Brabazon, D., Paull, B., & Luong, J. H. T. (2013). Adsorption and desorption of methylene Blue on porous carbon monoliths and nanocrystalline cellulose. *ACS Applied Materials & Interfaces, 5*, 8796–8804.

Ho, Y. (2006). Review of second-order models for adsorption systems. *Journal of Hazardous Materials, 136*, 681–689.

Hokkanen, S., Repo, E., Suopajärvi, T., Liimatainen, H., Niinimaa, J., & Sillanpää, M. (2014). Adsorption of Ni(II), Cu(II) and Cd(II) from aqueous solutions by amino modified nanostructured microfibrillated cellulose. *Cellulose, 21*, 1471–1487.

Hosseini, S., Khan, M. A., Malekbala, M. R., Cheah, W., & Choong, T. S. Y. (2011). Carbon coated monolith, a mesoporous material for the removal of methyl orange from aqueous phase: Adsorption and desorption studies. *Chemical Engineering Journal, 171*, 1124–1131.

Hsien, K., Futalan, C., Tsai, W., Kan, C., Kung, C., Shen, Y., ... Wan, M. (2013). Adsorption characteristics of copper(II) onto non-cross-linked and cross-linked chitosan immobilized on sand. *Desalination and Water Treatment, 51*, 5574–5582.

Hu, C., Zhu, P., Cai, M., Hu, H., & Fu, Q. (2017). Comparative adsorption of Pb(II), Cu(II) and Cd(II) on chitosan saturated montmorillonite: Kinetic, thermodynamic and equilibrium studies. *Applied Clay Science, 143*, 320–326.

Hu, X., Wang, J., Liu, Y., Li, X., Zeng, G., Bao, Z., ... Long, F. (2011). Adsorption of chromium (VI) by ethylenediamine-modified cross-linked magnetic chitosan resin: Isotherms, kinetics and thermodynamics. *Journal of Hazardous Materials, 185*, 306–314.

Huang, M., Tu, H., Chen, J., Liu, R., Liang, Z., Jiang, L., ... Deng, H. (2018). Chitosan-rectorite nanospheres embedded aminated polyacrylonitrile nanofibers via shoulder-to-shoulder electrospinning and electrospraying for enhanced heavy metal removal. *Applied Surface Science, 437*, 294–303.

Huang, Y., Li, S., Chen, J., Zhang, X., & Chen, Y. (2014). Adsorption of Pb(II) on mesoporous activated carbons fabricated from water hyacinth using H3PO4 activation: Adsorption capacity, kinetic and isotherm studies. *Applied Surface Science, 293*, 160–168.

Jabli, M., Baouab, M. H. V., Sintes-Zydowicz, N., & Hassine, B. (2012). [Dye Molecules/copper(II)/macroporous glutaraldehyde-chitosan] microspheres complex: Surface characterization, kinetic, and thermodynamic investigations. *Journal of Applied Polymer Science, 123*, 3412–3424.

Jing, Y., Liu, Q., Yu, X., Xia, W., & Yin, N. (2013). Adsorptive removal of Pb(II) and Cu(II) ions from aqueous solutions by Cross-linked chitosan-polyphosphate-epichlorohydrin beads. *Separation Science and Technology, 48*, 2132–2139.

Kannan, N., & Sundaram, M. (2001). Kinetics and mechanism of removal of methylene blue by adsorption on various carbons – A comparative study. *Dyes and Pigments, 51*, 25–40.

Khanday, W. A., Asif, M., & Hameed, B. H. (2017). Cross-linked beads of activated oil palm ash zeolite/chitosan composite as a bio-adsorbent for the removal of methylene blue and acid blue 29 dyes. *International Journal of Biological Macromolecules, 95*, 895–902.

Khora, E., & Lim, L. Y. (2003). Implantable applications of chitin and chitosan. *Biomaterials, 24*, 2339–2349.

Kim, H.-R., Jang, J.-W., & Park, J.-W. (2016). Carboxymethyl chitosan-modified magnetic-cored dendrimer as an amphoteric adsorbent. *Journal of Hazardous Materials, 317*, 608–616.

Li, B., Shan, C., Zhou, Q., Fang, Y., Wang, Y., Xu, F., ... Sun, G. (2013). Synthesis, characterization, and antibacterial activity of cross-linked chitosan-glutaraldehyde. *Marine Drugs, 11*, 1534–1552.

Li, K., Gao, Q., Yadavalli, G., Shen, X., Lei, H., Han, B., ... Zhou, C. (2015). Selective adsorption of Gd3+ on a magnetically retrievable imprinted chitosan/carbon nanotube composite with high capacity. *ACS Applied Materials & Interfaces, 7*, 21047–21055.

Ma, J., Yu, F., Zhou, L., Jin, L., Yang, M., Luan, J., ... Chen, J. (2012). Enhanced adsorptive removal of methyl Orange and methylene Blue from aqueous solution by alkali-activated multiwalled carbon nanotubes. *ACS Applied Materials & Interfaces, 4*, 5749–5760.

Mahdavinia, G. R., & Mosallanezhad, A. (2016). Facile and green rout to prepare magnetic and chitosan-crosslinked κ-carrageenan bionanocomposites for removal of methylene blue. *Journal of Water Process Engineering, 10*, 143–155.

Martino, A. D., Sittinger, M., & Risbud, M. V. (2005). Chitosan: A versatile biopolymer for orthopaedic tissue-engineering. *Biomaterials, 26*, 5893–5990.

Mezenner, N. Y., & Bensmaili, A. (2009). Kinetics and thermodynamic study of phosphate adsorption on iron hydroxide-eggshell waste. *Chemical Engineering Journal, 147*, 87–96.

Monash, P., & Pugazhenthi, G. (2009). Adsorption of crystal violet dye from aqueous solution using mesoporous materials synthesized at room temperature. *Adsorption, 15*, 390–405.
Monier, M. (2012). Adsorption of Hg2+, Cu2+ and Zn2+ ions from aqueous solution using formaldehyde cross-linked modified chitosan-thioglyceraldehyde Schiff's base. *International Journal of Biological Macromolecules, 50*, 773–781.
Monteiro, O., Jr, & Airoldi, C. (1999). Some studies of crosslinking chitosan-glutaraldehyde interaction in a homogeneous system. *International Journal of Biological Macromolecules, 26*, 119–128.
Morsy, A. M. A. (2015). Adsorptive removal of uranium ions from liquid waste solutions by phosphorylated chitosan. *Environmental Technology & Innovation, 4*, 299–310.
Nagy, B., Manzatu, C., Maicaneanu, A., Indolean, C., Lucian, B., & Majdik, C. (2017). Linear and nonlinear regression analysis for heavy metals removal using Agaricus bisporus macrofungus. *Arabian Journal of Chemistry, 10*, S3569–S3579.
Naiya, T., Bhattacharya, A., & Das, S. (2009). Adsorption of Cd(II) and Pb(II) from aqueous solutions on activated alumina. *Journal of Colloid and Interface Science, 333*, 14–26.
Ngah, W. S. W., Teong, L. C., & Hanafiah, M. A. K. M. (2011). Adsorption of dyes and heavy metal ions by chitosan composites: A review. *Carbohydrate Polymers, 83*, 1446–1456.
Niu, Y., Ying, D., Li, K., Wang, Y., & Jia, J. (2017). Adsorption of heavy-metal ions from aqueous solution onto chitosan-modified polyethylene terephthalate (PET). *Research on Chemical Intermediates, 43*, 4213–4225.
Pejic, B., Vukcevic, M., Kostic, M., & Skundric, P. (2009). Biosorption of heavy metal ions from aqueous solutions by short hemp fibers: Effect of chemical composition. *Journal of Hazardous Materials, 164*, 146–153.
Pereira, L., & Alves, M. (2011). Dyes-environmental impact and remediation. In E. Theodorou, & K. K. Grohmann (Eds.). *Environmental protection strategies for sustainable development* (pp. 111–162). Springer.
Qiu, H., LV, L., Pan, B., Zhang, Q., Zhang, W., & Zhang, Q. (2009). Critical review in adsorption kinetic models. *Journal of Zhejiang University Science A, 10*, 716–724.
Ramasamy, D. L., Puhakka, V., Iftekhar, S., Wojtuś, A., Repo, E., Hammouda, S. B., ... Sillanpää, M. (2018). N- and O- ligand doped mesoporous silica-chitosan hybrid beads for the efficient, sustainable and selective recovery of rare earth elements (REE) from acid mine drainage (AMD): Understanding the significance of physical modification and conditioning of th. *Journal of Hazardous Materials, 348*, 84–91.
Ramasamy, D. L., Wojtuś, A., Repo, E., Kalliola, S., Srivastava, V., & Sillanpää, M. (2017). Ligand immobilized novel hybrid adsorbents for rare earth elements (REE) removal from waste water: Assessing the feasibility of using APTES functionalized silica in the hybridization process with chitosan. *Chemical Engineering Journal, 330*, 1370–1379.
Rêgo, T. V., Cadaval, T. R. S., Jr., Dotto, G. L., & Pinto, L. A. A. (2013). Statistical optimization, interaction analysis and desorption studies for the azo dyes adsorption onto chitosan films. *Journal of Colloid and Interface Science, 411*, 27–33.
Ren, Y., Abbood, H. A., He, F., Peng, H., & Huang, K. (2013). Magnetic EDTA-modified chitosan/SiO2/Fe3O4 adsorbent: Preparation, characterization, and application in heavy metal adsorption. *Chemical Engineering Journal, 226*, 300–311.
Repo, E., Warchoł, J. K., Bhatnagar, A., Mudhoo, A., & Sillanpää, M. (2013). Aminopolycarboxylic acid functionalized adsorbents for heavy metals removal from water. *Water Research, 47*, 4812–4832.
Repo, E., Warchol, J. K., Kurniawan, T. A., & Sillanpää, M. E. T. (2010). Adsorption of Co (II) and Ni (II) by EDTA-and/or DTPA-modified chitosan: Kinetic and equilibrium modeling. *Chemical Engineering Journal, 161*, 73–82.
Robinson, T., McMullan, G., Marchant, R., & Nigam, P. (2001). Remediation of dyes in textile effluent: A critical review on current treatment technologies with a proposed alternative. *Bioresource Technology, 77*, 247–255.
Sarkar, K., Debnath, M., & Kundu, P. P. (2012). Recyclable crosslinked O-carboxymethyl chitosan for removal of cationic dye from aqueous solutions. *Hydrology: Current Research, 3*, 1–9.
Särkkä, H., Bhatnagar, A., & Sillanpää, M. (2015). Recent developments of electro-oxidation in water treatment-A review. *Journal of Electroanalytical Chemistry, 754*, 46–56.
Sing, K., Everett, D., Haul, R., Moscou, L., Pierotti, R., Rouquerol, J., ... Siemieniewska, T. (1985). Reporting physisorption data for gas/solid systems with special reference to the determination of surface Area and porosity. *Pure & Applied Chemistry, 57*, 603–619.
Srivastava, V., & Sillanpää, M. (2017). Synthesis of malachite@clay nanocomposite for rapid scavenging of cationic and anionic dyes from synthetic wastewater. *Journal of Environmental Sciences, 51*, 97–110.
Tanhaei, B., Ayati, A., Bamoharram, F. F., Lahtinen, M., & Sillanpää, M. (2016). A novel magnetic preyssler acid grafted chitosan nano adsorbent: Synthesis, characterization and adsorption activity. *Journal of Chemical Technology and Biotechnology, 91*, 1452–1460.
Tanhaei, B., Ayati, A., Lahtinen, M., & Sillanpää, M. (2015). Preparation and characterization of a novel Chitosan/Al2O3/Magnetite nanoparticles composite adsorbent for kinetic, thermodynamic and isotherm studies of methyl Orange adsorption. *Chemical Engineering Journal, 259*, 1–10.
Tu, H., Huang, M., Yi, Y., Li, Z., Zhan, Y., Chen, J., & Du, Y. (2017). Chitosan-rectorite nanospheres immobilized on polystyrene fibrous mats via alternate electrospinning/electrospraying techniques for copper ions adsorption. *Applied Surface Science, 426*, 545–553.
Tu, H., Yu, Y., Chen, J., Shi, X., Zhou, J., Deng, H., ... Du, Y. (2017). Highly cost-effective and high-strength hydrogels as dye adsorbents from natural polymers: Chitosan and cellulose. *Polymer Chemistry, 8*, 2913–2921.
Türker, O. C., & Baran, T. (2017). Evaluation and application of an innovative method based on various chitosan composites and Lemna gibba for boron removal from drinking water. *Carbohydrate Polymers, 166*, 209–218.
Vakili, M., Rafatullah, M., Salamatinia, B., Abdullah, A. Z., Ibrahim, M. H., Tan, K. B., ... Amouzgar, P. (2014). Application of chitosan and its derivatives as adsorbents for dye removal from water and wastewater: A review. *Carbohydrate Polymers, 113*, 115–130.
Wu, S., Dai, X., Kan, J., Shilong, F., & Zhu, M. (2017). Fabrication of carboxymethyl chitosan–hemicellulose resin for adsorptive removal of heavy metals from wastewater. *Chinese Chemical Letters, 28*, 625–632.
Xin, S., Zeng, Z., Zhou, X., Luo, W., Shi, X., Wang, Q., ... Du, Y. (2017). Recyclable Saccharomyces cerevisiae loaded nanofibrous mats with sandwich structure constructing via bio-electrospraying for heavy metal removal. *Journal of Hazardous Materials, 324*, 365–375.
Yi, J., & Zhang, L. (2008). Removal of methylene blue dye from aqueous solution by adsorption onto sodium humate/polyacrylamide/clay hybrid hydrogels. *Bioresource Technology, 99*, 2182–2186.
Zhao, F., Repo, E., Yin, D., Meng, Y., Jafari, S., & Sillanpää, M. (2015). EDTA-cross-linked β-cyclodextrin: An environmentally Friendly bifunctional adsorbent for simultaneous adsorption of metals and cationic dyes. *Environmental Science & Technology, 49*, 10570–10580.
Zhao, F., Tang, W. Z., Zhao, D., Meng, Y., Yin, D., & Sillanpää, M. (2014). Adsorption kinetics, isotherms and mechanisms of Cd(II), Pb(II), Co(II) and Ni(II) by a modified magnetic polyacrylamide microcomposite adsorbent. *Journal of Water Process Engineering, 4*, 47–57.
Zhou, Q., Gao, Q., Luo, W., Yan, C., Ji, Z., & Duan, P. (2015). One-step synthesis of amino-functionalized attapulgite clay nanoparticles adsorbent by hydrothermal carbonization of chitosan for removal of methylene blue from wastewater. *Colloids and Surfaces A: Physicochemical and Engineering Aspects, 470*, 248–257.

Publication IV

Doshi, B., Hietala, S., Sirviö, J. A., Repo, E., Sillanpää, M.

A powdered orange peel combined carboxymethyl chitosan and its acylated derivative for the emulsification of marine diesel and 2T-oil with different qualities of water.

Reprinted with permission from

Journal of Molecular Liquids

Vol 291, 111327, pp. 1-13, 2019

Journal of Molecular Liquids 291 (2019) 111327

Contents lists available at ScienceDirect

Journal of Molecular Liquids

journal homepage: www.elsevier.com/locate/molliq

A powdered orange peel combined carboxymethyl chitosan and its acylated derivative for the emulsification of marine diesel and 2T-oil with different qualities of water

Bhairavi Doshi [a,*], Sami Hietala [b], Juho Antti Sirviö [c], Eveliina Repo [d], Mika Sillanpää [a]

[a] Department of Green Chemistry, LUT University, Sammonkatu 12, FI-50130 Mikkeli, Finland
[b] Department of Chemistry, University of Helsinki, P.O. Box 55, FIN-00014, Finland
[c] Fibre and Particle Engineering Research Unit, University of Oulu, P.O. Box 4300, FI-90014, Finland
[d] Department of Separation and Purification, School of Engineering Science, LUT University, Yliopistonkatu 34, FI-53850, Finland

ARTICLE INFO

Article history:
Received 26 March 2019
Received in revised form 11 June 2019
Accepted 6 July 2019
Available online 07 July 2019

Keywords:
Orange peel powder
Modified chitosan
Hydrophobic modification
Emulsion stabilization
Water quality
Electrosteric stabilization

ABSTRACT

The traces of hazardous chemicals used in oil spill response have harmed marine creatures with long-term cytotoxic impacts, so, a greener alternative is to use biodegradable components in the dispersant formulation. This study demonstrates the efficiency of carboxymethylated and acylated chitosan combined with powdered orange peel (OP-D) in the emulsification of marine diesel and 2T-oil with different qualities of water. OP-D particles undergo Pickering emulsions, whereas the amphiphilic behaviour of the Blend and hydrophobically modified carboxymethyl chitosan-orange peels (CSOP-A) favours conventional emulsions through steric and electrostatic stabilization. The emulsion formation rate was maximum with OP-D in saline water and autonomous of the water quality with Blend. Additionally, different hydrophobic moieties on the surface of the Blend and CSOP-A affected the oil droplets' stabilization rate. Changing pH altered the surface properties of particles and hence the nature of the formed emulsion range from gel-like to creamy, suggesting particle-particle to particle-oil interactions. An increase in electrolyte concentration enhanced the coalescence rate of marine diesel with CSOP-A. The oil droplet size in the formed emulsion increases with a temperature decrease up to 2 °C, and the emulsion stabilization rate was <10% at −20 °C. The traces of these synthesized materials were <1000 mg L^{-1} in the water phase after the removal of oils. Since these materials are bio-based, their presence in the ecosystem is less hazardousness than commercial dispersants.

1. Introduction

After a number of oil spill incidents such as Deepwater Horizon in the Gulf of Mexico and Exxon Valdez in Alaska, various rules, regulations and strategies have been enacted to control such spills in the future. Currently, various techniques such as mechanical methods, bioremediation, in-situ burning and dispersants are applied to oil spill response, depending on the climatic conditions. In the Arctic region, chemical herders forming thick oil slicks are key to effective in-situ burning [1], but the fracturing of oil during the herding process in the presence of ice reduces burning efficiency [2]. Secondly, the type of oil and its behaviour with ice and saline water also play a significant role in dispersant efficiency [3]. Although chemical dispersants have enhanced the biodegradation of spilled oil by reducing oil droplet size, these dispersants in water resources were cytotoxic for marine creatures [4,5]. Recently, many alternative eco-friendly dispersants based on food-grade amphiphiles have been studied [6,7]. In addition, oil emulsifiers based on biopolymers such as cellulose [8,9], chitosan [10,11], and xanthan gum [12] have been studied extensively for oil spill response.

Chitin found in the shells of crustaceans and molluscs is the second most abundant natural polymer [13,14], a major source of surface pollution in coastal areas and a waste material in seafood production industries [15]. Therefore, the utilization of leftover chitin would reduce the amount of sea waste [16]. Chitosan is the deacetylated form of chitin and widely used as a biomaterial and a sorbent, because of its diverse surface properties. The surface-active functional groups of chitosan can be modified by various methods such carboxyalkylation, acylation, alkylation, cross-linking, grafting and ionic-gelation, which can be effectively used in oil spill treatment [17]. Despite chemical modification, the fundamental skeleton remains intact in modified chitosan, which retains its original physicochemical and biochemical properties, and incorporates improved properties. Amphiphilic chitosan can be used as a surfactant, either in the form of a dispersing or herding agent. Recently, chitosan-based bio-polymeric blends [18] and magnetic

* Corresponding author.
E-mail address: bhairavi.doshi@lut.fi (B. Doshi).

https://doi.org/10.1016/j.molliq.2019.111327

nanoparticles [19,20] have also been studied for the removal and/or separation of oil from water resources.

Emulsion droplet stabilization is often achieved through the addition of amphiphilic molecules such as surfactants or emulsifiers, which decrease interfacial tension between the phases and increase steric hindrances and/or electrostatic repulsion between the droplets [21]. Furthermore, the emulsion stabilization also depends on particle concentration and particle-particle interactions [22]. Chitosan and modified chitosan produce stabilized conventional emulsions, where dissolved materials provide a steric barrier against coalescence of the oil droplets due to weak surface activity [23,24]. So far, the Pickering emulsions have attracted more interest in the field of nanoparticles, as they form kinetically stable emulsions through a physical barrier and not by decreasing the tension between the phases. In other ways, particles undergo Pickering emulsions via irreversible adsorption at the liquid-liquid interface to stabilize emulsions [21,25,26]. On the other hand, French et al. showed the exchange of particles between the droplets in Pickering emulsion [27]. The particles must be small enough for effective Pickering emulsion and to regulate the size of the oil droplets, while larger particles will improve steric hindrance and prevent coalescence [22,28,29]. The adsorbed surface-active particle at the interface provides electrostatic or steric barriers against coalescence, and thus enhances the emulsion stability.

A large amount of food waste (lignocellulosic-rich) is generated by agricultural and various food industries, and nearly 15.6 million tonnes of waste comes from citrus fruit peel [30]. This peel is rich in nutrients [31,32] and could be effectively applied in wastewater remediation [33–35] and many other alternative sustainable technologies [36–38]. Orange peel (OP) is composed of flavonoids, phenolics, carotenoids, pectin, lignin, cellulose, hemicellulose, limonene, soluble sugars, oil and fat [39]. The esterification of sugars (such as sucrose) [40] and flavonoids [41] by acid chlorides acts as a surfactant. Abudullah et al. demonstrated the removal of oil from saline water using orange peel, but its removal efficiency decreased with decreasing salinity [42]. Previously, we demonstrated the destabilization of marine diesel up to seawater salinity using a sodium form of chitosan derivative [43] but, to the authors' knowledge, the combined derivative of chitosan and orange peel has not yet been studied for the stabilization of oil.

The objective of conducting this study was to demonstrate the valorization of orange peel (OP) together with modified chitosan as surface-active particles and/or an emulsifier. These materials undergo hydrophobic modification via acylation, and are used to stabilize marine diesel and 2T-oil present on the water surface. The synthesized materials were characterized using a Fourier transform infrared spectrophotometer (FTIR), Proton nuclear magnetic resonance spectroscopy (^{1}H NMR), X-ray diffraction spectroscopy (XRD), Brauner, Emmet and Teller analysis (BET), Elemental analysis (EA), Scanning electron microscopy (SEM), Energy dispersive X-ray spectroscopy (EDS) and surface charge. The droplets stabilization rate of oils was studied using these materials with deionized and saline water. The emulsion behaviour of marine diesel and 2T-oil was also investigated as a function of solution pH and salinity. As these oils have different densities and composition, their stabilization rate varied. We used visual observations and optical microscopy to study the oil droplets formed due to the stabilization of oils. We also investigated the nature of the oil droplets with varying temperature, and furthermore, we studied the total organic carbon (TOC) amount of these derivatives in water using the non-purge organic carbon (NPOC) method after the removal of oils/emulsified oils.

2. Material and methods

2.1. Materials

Chitosan (from shrimp shells), acetone, oleoyl chloride (C18), lauroyl chloride (C12), hydrochloric acid (HCl), sodium hydroxide (NaOH) and ethanol were obtained from Sigma Aldrich Oy and Altia Oyj. All chemicals were used without further purification. OP waste was collected from oranges purchased from the local market. Marine diesel and 2T-oil were purchased from Neste Oyj, Finland. Deionized water (DI) was used throughout the experiments and saline water was collected from the area near Matinkylä Espoo, Finland.

2.2. Synthesis of powdered orange peels, hydrophobically modified carboxymethyl chitosan-orange peels and the Blend

Chitosan-based materials, sodium form of carboxymethyl chitosan (Na-CMCS) and sodium form of carboxymethyl oleoyl chitosan (NaO-CMCS) were synthesized as per our previous studies [43]. The synthesis routes (SR) are shown in Fig. 1.

In SR1, orange peel was washed and dried at room temperature (RT) for 48 h. This dried orange peel was ground in a tubemill and dried again for 24 h at 60 °C making powdered orange peel (OP-D). In SR2, equal portions of OP-D and NaO-CMCS were mixed to get the Blend. In SR3, the mixture of Na-CMCS (1.2 g) and OP-D (1.1 g) was soaked in acetone (20 mL) for 1 h at 5 °C. To this mixture, lauroyl chloride in acetone (1:1, 2.6 mL each) and NaOH solution (4 M) were added simultaneously after 30 min, and stirred continuously for 4 h at the same temperature. Ethanol (70%) was then added to the reaction mixture. The obtained solid was washed three times with ethanol (70–90%), dried overnight at RT and ground in the tubemill. This obtained dried solid is hydrophobically modified carboxymethyl chitosan-orange peel (CSOP-A).

2.3. Characterization

The synthesized materials were characterized using FTIR, SEM/EDS, XRD, ^{1}H NMR, elemental analysis, BET, and surface zeta potential (ZP). The interfacial tension between the oil and aqueous phases was also determined using these materials. The details about the characterization methods are available in SM1.

2.4. Effect of dosage and solution pH on the emulsion formation rate

The emulsion formation rate was studied by mixing 10 mL (0–2.5 g L^{-1}) of synthesized materials solutions in DI and SW, respectively, with an oil-to-water ratio of 0.1, so the material-to-oil-ratio would range from 0 to ~0.03 depending on the type of oil (Refer SM2). The mixing was conducted in a centrifuge tube (15 mL) with a test tube shaker (Heidolph) at 2000 rpm for 1 min. After mixing, these solutions were rested for a day to evaluate the stabilization rate, i.e. the emulsion formation rate (see Eq. (1)). The oil droplet size in the emulsion formed was also measured with an optical microscope (Zeiss Axio using the 206-camera unit Axio CamERc5s with ZEN software). Similarly, the effect of pH ranging from 3.5 to 10.5 was investigated in the stabilization rate with the optimized dosage (from the above studies). The amount of separated oil was measured simultaneously to determine the coalescence rate (see Eq. (2)) of oil after mixing and resting. This optimized concentration and solution pH were used for further studies.

$$\text{Emulsion formation rate } (\%) = \frac{C_i - C_s}{C_i} * 100 \quad (1)$$

$$\text{Coalescence rate } (\%) = 100 - \left(\frac{C_i - C_s}{C_i} * 100\right) \quad (2)$$

where C_i and C_s (g) are the initial weight of oil taken and the weight of the separated amount of oil collected after mixing and resting, respectively.

2.5. Water salinity and the effect of temperature on the stabilization of oil droplets

Solutions with different salinities (0–4 g L^{-1}) were prepared for this study. Optimized concentration solutions were prepared using these

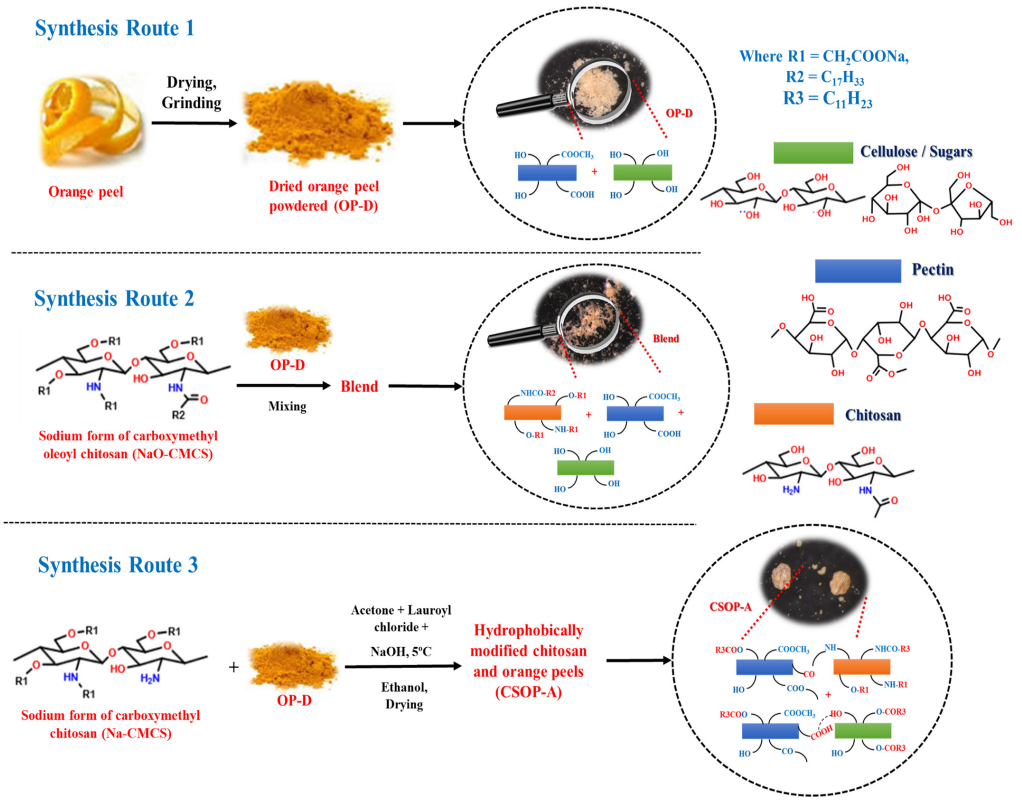

Fig. 1. Schematic of OP-D, Blend and CSOP-A synthesis along with the structural and functional change.

solutions, to which oil was added keeping the oil/water ratio at 0.1. The remaining procedure of mixing and resting was performed as per Section 2.4. The heights of the emulsified layer and coalescence layer were used to determine the oil droplets stabilization rate in the emulsion formed. Moreover, using optimized concentration and pH solution in DI and SW, the effect of temperature was studied at RT, 2 °C and −20 °C, respectively, with the same oil/water ratio. After mixing these solutions were rested at RT and 2 °C for one day. However, for −20 °C, the DI and SW with oil were stored in a deep freezer. After a day, these solutions were taken out and optimized concentration solution was added to them, mixed and stored back in the freezer. The oil droplet stabilization rate was studied periodically by measuring the oil droplet sizes with an optical microscope for 4 weeks. The oil droplets size was also measured with a laser diffraction spectrometer (Malvern Mastersizer 3000 with Hydro SV unit, UK).

2.6. Water quality after the emulsion stabilization and removal of oils

Traces of surface-active materials in water resources after the removal of oil are an important factor for the marine ecosystem after oil spill treatment. For this study, the top oil layer (either emulsified or separate oil) was removed and the aqueous layer was tested using the NPOC method (TOC Analyzer, Shimadzu) in order to determine the amount of surface-active particles traces in the water.

3. Results and discussions

Carboxymethylated chitosan and hydrophobically modified carboxymethylated chitosan possess surface-active moieties such as carboxyl, hydroxyl and amino groups, and undergo a nucleophilic reaction to enhance their physiochemical properties. Similarly, OP-D also consists of surface-active functional groups such as hydroxyl and carboxyl. In CSOP-A, nucleophilic acyl substitution takes places between the free amino groups of the carboxymethylated polymer (Na-CMCS) and lauroyl chloride through an addition/elimination type mechanism. Furthermore, the hydroxyl groups of OP-D are also acylated with lauroyl chloride via similar substitution mechanism. There might be a cross-linking between the free amino groups of Na-CMCS and carboxyl groups of OP-D. Since the Blend is a mixture of hydrophobically modified carboxymethylated chitosan and OP-D, no further surface modification between them takes place, so these molecules either underwent intermolecular interaction or modified their own surfaces (see Fig. 1) to enhance their existing physiochemical properties. The sizes of OP-D, CSOP-A and the Blend particles are shown in Fig. S1 (refer Supplementary Material SM3).

3.1. Characterization

3.1.1. Surface morphology

The surface morphology of the synthesized materials are shown in Fig. 2 and Fig. S1 (refer SM3). The surface of OP-D was clean and smooth (Fig. 2a) whereas, in CSOP-A the formation of slits and clumps (see the white circled part of Fig. 2b) suggests the mixed morphology of hydrophobic modification in chitosan derivative together with OP-D. However, in the Blend (Fig. 2c), the slit formation was not so remarkable, as hydrophobically modified chitosan does not undergo further modification, except for mixing with OP-D. The EDS elemental composition (see Fig. 2a–c) shows the presence of sodium, revealing that CSOP-A and Blend are in sodium form, which was absent in OP-D. Even though there was the addition of hydrocarbon chain, the presence of sodium in these materials reduced their %C content in comparison to OP-D. The CHNS-O elemental results are shown in Table S2 of SM4. The BET surface area of OP-D, CSOP-A and Blend was 0.09 m^2/g, 0.39 m^2/g and 0.34 m^2/g, respectively. This shows that combining OP-D with chitosan derivatives enhances the surface structure of CSOP-A and Blend, so they were rougher and more porous than OP-D, which is in good agreement with the SEM results.

3.1.2. Spectrometric analysis

The FTIR spectra of OP-D, CSOP-A and Blend are shown in Fig. 2d. In OP-D spectrum, the broad peak near 3400 cm^{-1} shows the –OH groups on pectin, cellulose, hemicellulose and lignin. 1733 cm^{-1} indicates C═O stretching, and 1615 cm^{-1} is attributed to C═C aromatic stretching, respectively. In addition, the peak at 1635 cm^{-1} is most likely the water

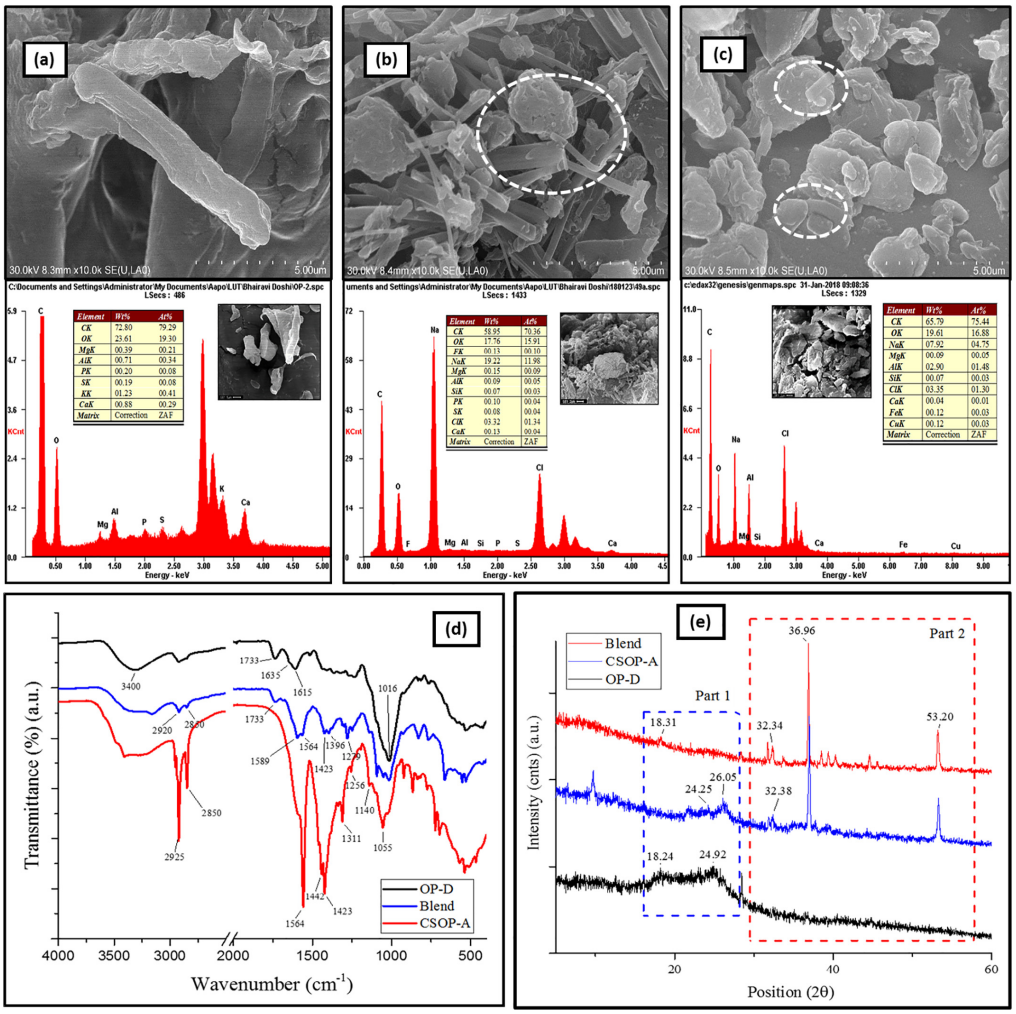

Fig. 2. SEM Images and EDS results of (a) OP-D, (b) CSOP-A and (c) Blend along with FTIR spectra (d) and XRD spectra (e).

peak. In CSOP-A, sharp peaks around 2925 cm^{-1} and 2850 cm^{-1} were attributed to the C—H stretching of lauroyl chains, 1564 cm^{-1} might be attributed to N—H (amide II) linkage revealing the incorporation of lauroyl moiety onto its surface after acylation [43]. Furthermore this peak might also be attributed to either imine (C=N) crosslinking between the sugar molecules of OP-D with the amino groups of chitosan through a Schiff base reaction [44] or amide bond (=C-NH) between the carboxyl group of OP-D and amino groups of Na-CMCS [45]. The peaks at 1591 cm^{-1} and 1423 cm^{-1} are attributed to the C═O symmetric stretching of –COONa, respectively, so the 1733 cm^{-1} peak was absent in CSOP-A, as the carboxyl groups are in sodium salt form due to the alkaline pH during the synthesis. In the Blend, peaks at 2920 cm^{-1} and 2850 cm^{-1} show the C—H stretching of oleoyl chains, 1733 cm^{-1} indicates C═O stretching due to the presence of OP-D, and 1589 cm^{-1} indicates the –NH– group, respectively. The peak at 1016 cm^{-1} in OP-D and the Blend were attributed to the C—O group [46]. Moreover, the peaks in the range of 850–1150 cm^{-1} were attributed to the C—O, C—C and C-O-C of the polysaccharide chain having a glycosidic bond and pyranoid ring [38] present in OP-D, CSOP-A and the Blend.

The XRD spectra are shown in Fig. 2e. The XRD spectra of OP-D shows two peaks at 18° and 25°, but there were no other well-defined peak regions, which indicates the absence of a discrete mineral phase in OP-D. Thus, OP-D has a completely amorphous structure as expected for organic materials, and similar behaviour has also been previously observed [47]. The spectra of chitosan, Na-CMCS and NaO-CMCS are available in the supplementary data (Fig. S2 in SM5). Compared to the XRD pattern of OP-D, the diffractogram of CSOP-A and the Blend showed sharper peaks indicating the formation of a new crystalline phase. The peak around 32° in CSOP-A and the Blend is attributed to the carboxymethylated part present in them, and similar results were previously observed for carboxymethylated chitosan [48]. In addition, the peaks around 37° and 53° (see part 2 of Fig. 2e) were observed in CSOP-A and the Blend, might also be attributable to the acylation of carboxymethylated chitosan, which was absent in OP-D.

The ^{1}H NMR spectra are shown in Fig. S3 of SM5. In the ^{1}H NMR spectrum of OP-D (Fig. S3a of SM5), the signals at ~0.8–1.7 ppm originate from the fatty components and the signals at ~1.9–2.2 ppm show the presence of O-linked acetate [49]. The spectral region of 3.0–6.0 ppm is associated with ring hydrogen and mainly the presence of sucrose, fructose and glucose, as witnessed by their respective intensities and previous literature results [50,51]. However, in the CSOP-A spectrum (Fig. S3b of SM5), the reduction of peak intensities in this region compared to OP-D reflects that the –OH groups of sugars moieties present in OP-D might have been substituted during acylation. Moreover, in the CSOP-A spectrum, the peaks in the range of 1.1–2.0 ppm are attributed to the alkyl (CH_2 and CH_3) group of the lauroyl chain. The signal obtained at 2.0 ppm corresponds to –NH-CH– linkage, obtained through linkage of the –C=O– group of carbohydrate or pectin in OP-D with the $–NH_2$ group of chitosan derivative [52], and also attributed to the CH_2 groups of the lauroyl chain. The new peak near 8.1 ppm is attributed to the imine bond for the linkage between $–NH_2$ group of chitosan derivative and the –C=O– group of OP-D. This is in agreement with the FTIR results. The peak resonance in the Blend (Fig. S3c of SM5) and CSOP-A near to 3.7 and 4.1–4.6 ppm is attributed to carboxymethyl protons such as N-CH_2-CO– and O-CH_2-CO-, respectively. Moreover, the signals at ~0.8–1.7 ppm in the Blend originate from the alkane proton of oleoyl chain as well as fatty components present in OP-D.

3.1.3. Surface charge of OP-D, CSOP-A and Blend with different water quality, interfacial tension (IFT) and wettability

The initial pHs of OP-D, CSOP-A and the Blend in DI were 5.5, 9.5 and 7.4, respectively. The magnitude of the surface charge depends on the acidic or basic strengths of the surface groups and on the pH of the solution. In OP-D, when pH is increased, deprotonation of the carboxyl group occurs, which then results in a decrease in zeta potential value (i.e. more negative zeta potential). On the other hand, when pH decreases, carboxyl groups are associated (i.e. protonated), which results in neutralization of charge and a consequent increase in zeta potential (see Fig. 3a). The ZP below pH 4 and above 10 were not considered due to the dissolution of OP-D components. In case of CSOP-A and the Blend, simultaneous protonation of carboxyl and amino groups occurred with a decrease in pH, which increased the ZP overall by neutralizing the charge (see Fig. 3b–c). Another reason might be the competing interactions between the oppositely charged amino groups and carboxyl groups to neutralize the surface charge, and similar behaviour has been previously observed [11]. So, when pH is decreased to 4, the surface charge in CSOP-A seems to be close to zero (i.e. no surface charge). In hypothesis, the hydrophobic segments in CSOP-A and the Blend affects the conformations of polymers, as they disturb the aggregation and formations of particles, and thus the ZP (see Fig. S4 of SM6 for the phase diagram). Furthermore, the carboxymethylated groups in the Blend and CSOP-A are attributable to a more negative surface than OP-D. As shown in Fig. 3a–c, the ZP were less negative in SW than in DI. One reason might be that the ions present in SW formed an electrical double layer with the surface charges of these materials. Furthermore, there might be ion exchange between the surface charge and electrolyte with decreasing pH (see SM6 for conductivity). In Fig. 3d, the hump near pH 6.5 shows the protonation of amino groups in the Blend and CSOP-A, which was absent in OP-D. The protonation rate in CSOP-A was less than the Blend, which suggests that some amino groups might have linked with OP-D, instead of linking with lauroyl moieties during acylation. This is in a good agreement with FTIR and NMR interpretations.

IFT is the prime parameter for the formation of emulsion and its stability. The surface-active agents, by orienting their hydrophilic groups towards the aqueous phase and hydrophobic groups towards the oil phase, reduce the IFT between these two phases. The initial IFT between marine diesel and the water phase (deionized water and saline water) without any OP-D, CSOP-A and the Blend was 15.55 ± 0.08 mN/m and 34.76 ± 0.68 mN/m, respectively. A small addition of OP-D, CSOP-A and the Blend in DI reduces the IFT by sequential, whereas with SW this reduction was drastic (refer Fig. 3e–f). This shows that the presence of hydrophobic moieties made CSOP-A and the Blend more amphiphilic, which drastically reduced the IFT. Generally, the lower the IFT, the higher the emulsion stability. The wettability of the particles was determined by contact angle using the sessile drop method. The contact angle of OP-D, Blend and CSOP-A were about 63°, 83° and 113°, respectively (see Fig. S6 of SM6). This shows that hydrophobic moieties in the Blend and CSOP-A enhanced the contact angle as compared to OP-D. Kaptay also suggested that the optimum contact angle for the stabilization of emulsions by a single or double layer of particles is <90° or <129°, for o/w emulsion [53]. Furthermore, the polar and non-polar parts of these materials show “like-dissolves-like” characteristics, i.e. the polar part will show the dissolution in the aqueous phase and non-polar in the oil phase.

3.2. Emulsion formation as a function of OP-D, CSOP-A and blend dosage

The behaviour of the surface-active particles mainly depends on water quality and type of oil, and IFT and wettability determine emulsion efficacy. Fig. 4a shows the emulsion formation rate of marine diesel versus surface-active particles dosage at native pH. The increase in OP-D concentration in DI increased the emulsion formation rate from 5% to 70%. This suggests the adsorption of OP-D at the interface, which resists droplet coalescence via electrosteric stabilization. On other hand, OP-D particles being smaller in size provides a barrier against droplets coalescence (Fig. 4b1), resulting in solid-stabilized (Pickering) emulsion. The presence of hydrophobic hydrocarbon segments in the Blend reduces the IFT as compared to OP-D (refer Fig. 3e), so the effectiveness of the Blend was >80% even with a low dosage (0.5 g L^{-1}). This reveals that the orientation of the hydrophobic hydrocarbon segments (oleoyl groups) of the Blend at the oil-water interface have generated a steric

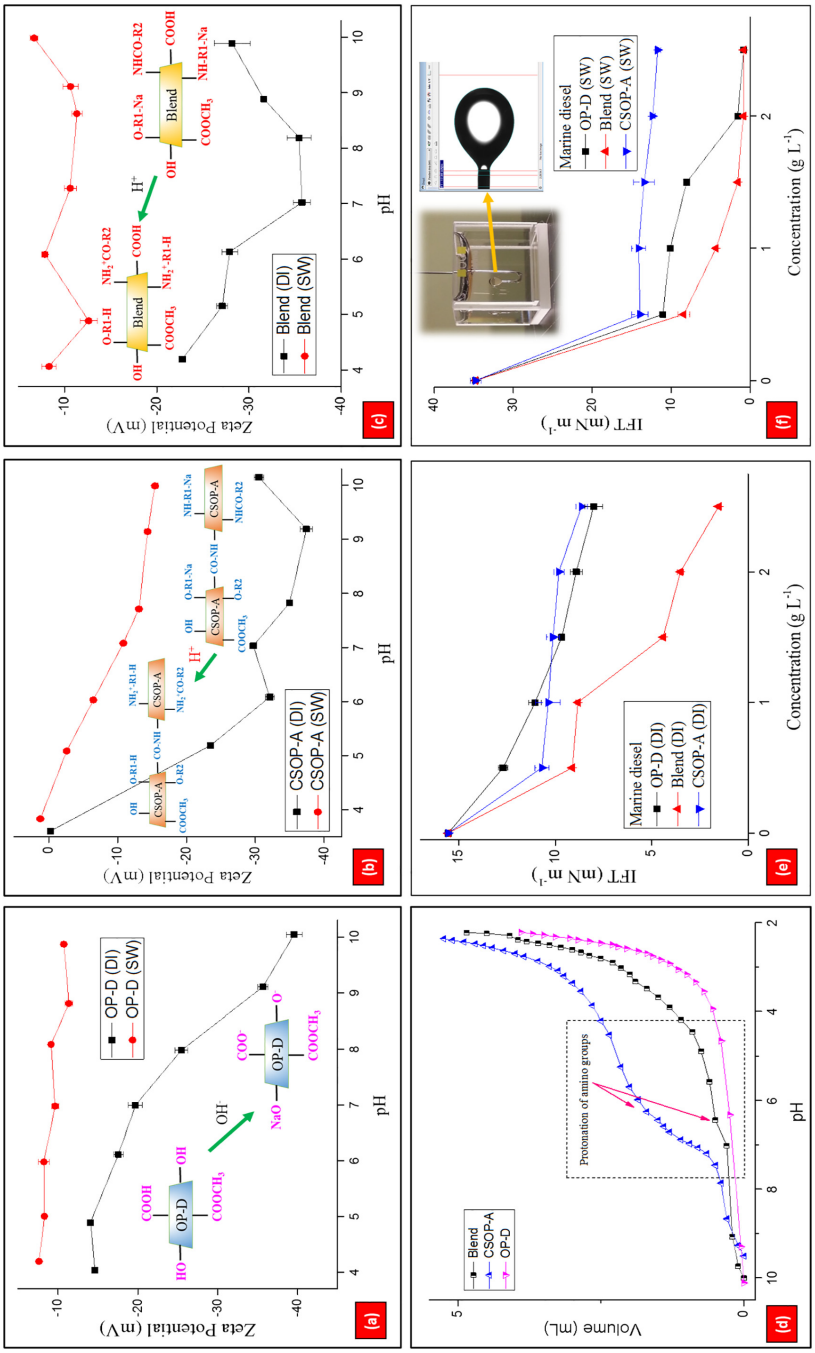

Fig. 3. Zeta potential of OP-D (a), CSOP-A (b) and the Blend (c) in deionized water (DI) and saline water (SW) at different pH levels. Potentiometric titration curve of OP-D, CSOP-A and the Blend (d). Interfacial tension (IFT) between marine diesel and the water phase (e) deionized water and (f) saline water in the presence of OP-D, CSOP-A and the Blend using the pendant drop method.

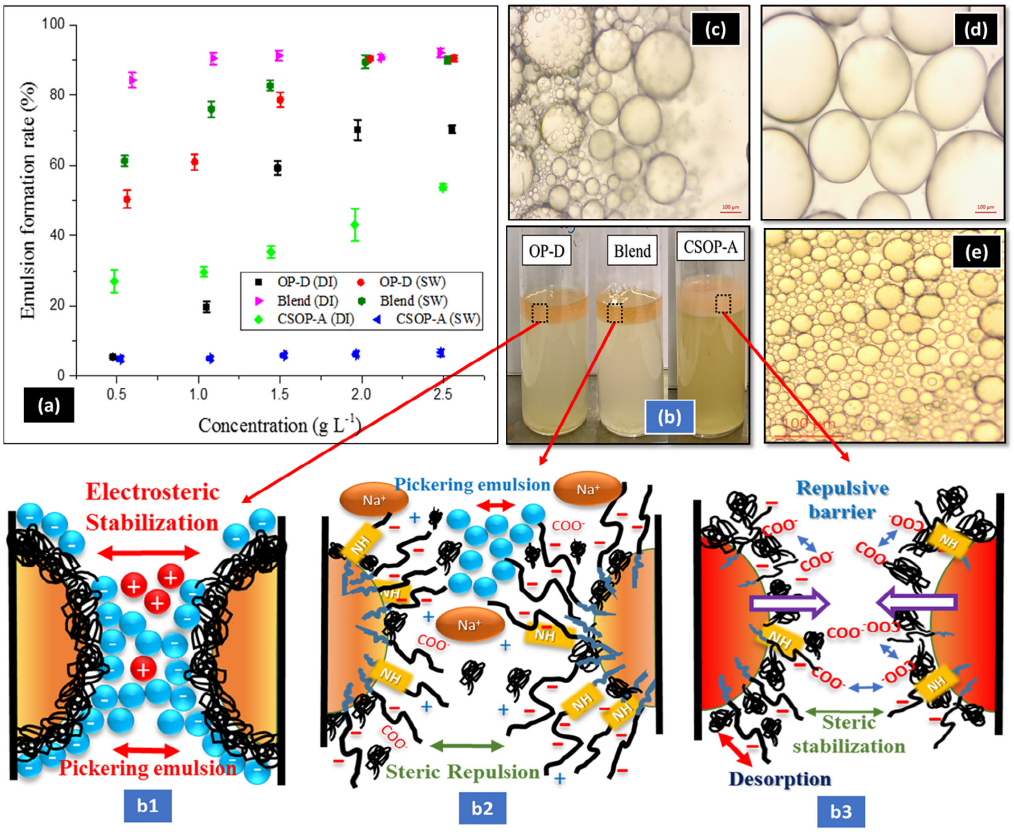

Fig. 4. (a) Effect of OP-D, CSOP-A and the Blend dosage in the emulsion formation of marine diesel, (b) emulsion formation with marine diesel having 2.0 g L^{-1} of dosage OP-D, CSOP-A and the Blend in DI along with the emulsion mechanism with OP-D (b1), the Blend (b2) and CSOP-A (b3). Microscopic images of o/w emulsion for (c) OP-D (d) the Blend and (e) CSOP-A with marine diesel in DI taken at a magnification of 100 µm.

barrier between the oil droplets. Furthermore, the magnitude of this steric barrier between the droplets was enhanced with the increasing concentration of the Blend, due to the dense packing and thick interface of the molecules around the oil droplets (Fig. 4b2). In addition, there is also formation of the Pickering emulsion in the Blend due to presence of OP-D. This resulted in an overall increase in the emulsion formation rate. Despite the hydrophobic moieties in CSOP-A, the maximum stabilization rate was about 50%, which might be because of the exposure of the non-polar region to the surrounding water, which has started generating hydrophobic attraction between the droplets [54] due to the rupturing of the steric interactions of CSOP-A from the oil droplets. This resulted in the aggregation of oil droplets and destabilization of the emulsion (Fig. 4b3). Although CSOP-A and the Blend have a negative surface ZP in DI (Refer Fig. 3b–c), the emulsion formation rate varied in them due to the presence of different hydrocarbon segments. Shiao et al. previously demonstrated the effect of the hydrocarbon chain on oil stabilization [55]. In addition, lengthening the hydrocarbon chain also enhanced ions exchange and hydrophobic interactions [56,57], so the interaction of CSOP-A with marine diesel differs from the Blend. Furthermore, the o/w emulsion behaviour was gel-like in the Blend due to the presence of OP-D whereas, with CSOP-A, creamy emulsions were observed (Fig. 4b). The oil droplet size in OP-D (Fig. 4c) and the Blend (Fig. 4d) was thus >100 µm, whereas it was <100 µm in CSOP-A (Fig. 4e). The coalescence rate dominated the droplets stabilization rate with CSOP-A in SW, whereas the presence of OP-D in the Blend showed >90% conversion of oil into emulsion, even at a very small dosage (refer Fig. S7 of SM7 for emulsion formation). Our previous results demonstrated that a dosage of about 2.0 g L^{-1} NaO-CMCS was required to form stable emulsion with SW [43]. On the other hand, this study shows that the addition of OP-D to NaO-CMCS reduces the dosage to half with the same SW. This shows that water salinity decreases the critical micelle concentration of the Blend. Similar results have been previously observed [58].

The emulsion formation 2T-oil (Refer Fig. 5a) differs from marine diesel in its composition. 2T-oil, being viscous, consists of solvent-dewaxed heavy paraffinic and polyaromatics, that can easily form a creamy layer with water even in the absence of oil emulsifier/surface-active particles. Furthermore, a small addition of either OP-D, the Blend or CSOP-A converts this creamy layer to an emulsified layer (Figs. 5b and S8). However, the droplet stabilization rate is more likely to be dependent on the type of water for CSOP-A as, with DI, this rate was about 22%, whereas with SW it was about 90%. This also shows

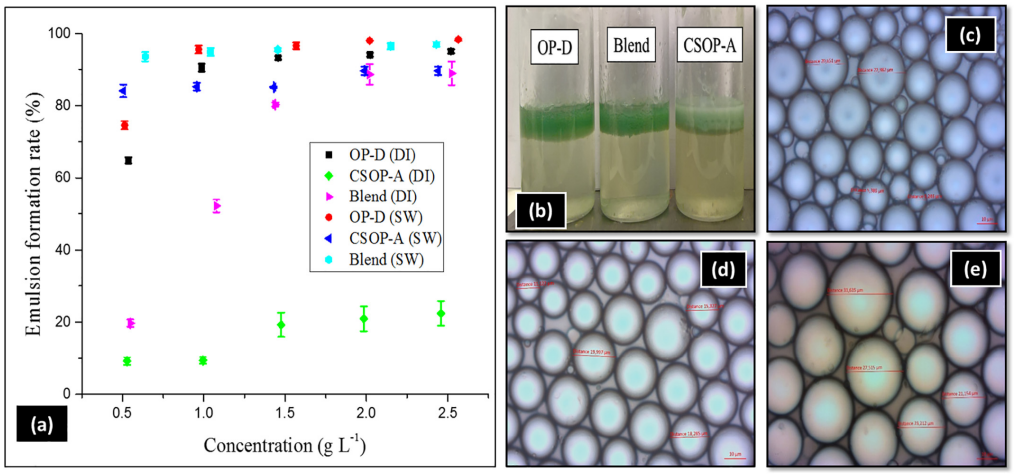

Fig. 5. (a) Effect of OP-D, CSOP-A and the Blend dosage in the emulsion formation of 2T-oil, (b) the o/w emulsion with 2T-oil with 1.5 g L^{-1} of dosage OP-D, CSOP-A and the Blend in SW, microscopic images of o/w emulsion for (c) OP-D (d) the Blend and (e) CSOP-A with 2T-oil in SW taken at a magnification of 10 μm.

that the presence of different hydrocarbon chains in CSOP-A might have affected the emulsion stability and behaviour as discussed earlier but, for the remaining materials, the droplet stabilization rate (emulsion formation) was >80% with DI and SW. Although the emulsion behaviours were not identical, the oil droplet sizes in the emulsions were <100 μm (Fig. 5c–e), so the optimal dosage of these materials was 2.0 g L^{-1} for all further studies.

3.3. Emulsification behaviour of oils with OP-D, CSOP-A and the blend at different pH levels

The pH of wastewater-containing oil or spilled oil plays a significant role in the applicability of the surface-active materials. When OP-D interacted with marine diesel at its initial pH (5.5), there was a formation of gel-like emulsion suggesting the bridging of particles between droplets and particle-particle interaction. So the obtained emulsion is either Pickering emulsion or can be attributed to the hydrogen bonding and to bonds between hydrophobic groups and oil droplets via steric barriers [59]. In addition to steric stabilization, the electrostatic contribution to this stabilization is quantified by electrophoretic mobility (EM) proportional to the surface charge. The EM value of OP-D at pH 4 is −1.14 μmcm/Vs, and decreases to −3.10 with increasing pH (Fig. 6a). This shows the dissociation of carboxyl groups present in OP-D at a lower pH, which forms a thicker adsorbed gel-like layer with oil via electrosteric barriers whereas, at higher pH, the lower value of EM tends to form o/w emulsion mainly due to steric stabilization or Pickering emulsion. The electrolyte in SW increases the EM (Fig. 6b) compared to OP-D in DI water, by shielding the negative charges and enhancing the emulsion rate [60] through the electrostatic barriers of electrical charges. The overall obtained emulsion was therefore due to steric and electrostatic stabilization. However, the OP-D solution contains some non-dispersible parts, which form sediments and do not take part in the formation of an emulsion (Fig. 6c).

The microscopic images of o/w emulsion at different pH levels in DI and SW are shown in Fig. 6d–i and Fig. S9 of SM8, respectively. Since CSOP-A possessed a glucosamine backbone along with OP-D, the EM values differ from OP-D at a different pH range, so the oil stabilization differs. In addition, the increment of EM values from the alkaline to acidic pH region implied the adsorption of surface-active particles via hydrophobic bonding, distributed on the external surfaces of aggregates. Although there were long hydrocarbon segments in CSOP-A, the simultaneous protonation of amino and carboxyl groups occurred in CSOP-A with decreasing pH and mitigated the oil droplets' resistance to coalescence by stepping down the emulsion rate (Refer Fig. 6f–g for the microscopic images). For the Blend, pH did not have a significant effect on the droplet stabilization rate, but rather changed the nature of the o/w emulsion, i.e. gel-like emulsion at acidic pH and creamy emulsion at alkaline pH (refer Fig. 6h–i for the microscopic images and Fig. 6j along with its mechanism). In addition, emulsion formation with the Blend was independent of water quality, as some of the hydrophobically modified chitosan in the Blend was effective in DI and some of OP-D present in the Blend was effective with SW.

The droplets stabilization rate of 2T-oil in DI was more dependent on pH, than that in SW (Fig. S10 in SM8), since the cation exchange from SW with H^+ of surface-active moieties (−COOH and –OH) of OP-D and the Blend formed bulky o/w emulsion. In addition, the IFT of 2T-oil is less in SW than DI, which resulted in the dissolution of some compounds of 2T-oil in SW, and a similar result was previously reported [61]. Furthermore, 2T-oil swells easily in SW, resulting in spontaneous oil-in-water emulsification, which diffuses the surfactants across the interface and forms bulky emulsion [62]. Nevertheless, for OP-D and the Blend, decreasing pH formed an interfacial monolayer that contributed to the prevention of dispersed 2T-oil droplets to coalescence, resulting in a creamy and gel-like emulsion. Even though the EM values of the Blend and CSOP-A do not differ much in SW with changing pH, the emulsion behaviour changes in them due to the presence of OP-D and crosslinked OP-D. Although the Blend and CSOP-A possess long hydrocarbon chains, the pH gradient at the interface affects the steric barriers and prevents the adsorption of long chains towards 2T-oil, which might have increased the coalescence rate. Moreover, the protonation of amino groups in the CSOP-A with decreasing pH provides repulsive barriers, which slightly resist the aggregation of droplets, so the coalescence rates of these hydrophobically modified materials varied in DI.

3.4. The role of water salinity in the stabilization rate of oil droplets

Different surface-active particles and their oil droplets stabilization capacity with respect to the salinity of water are equally as important

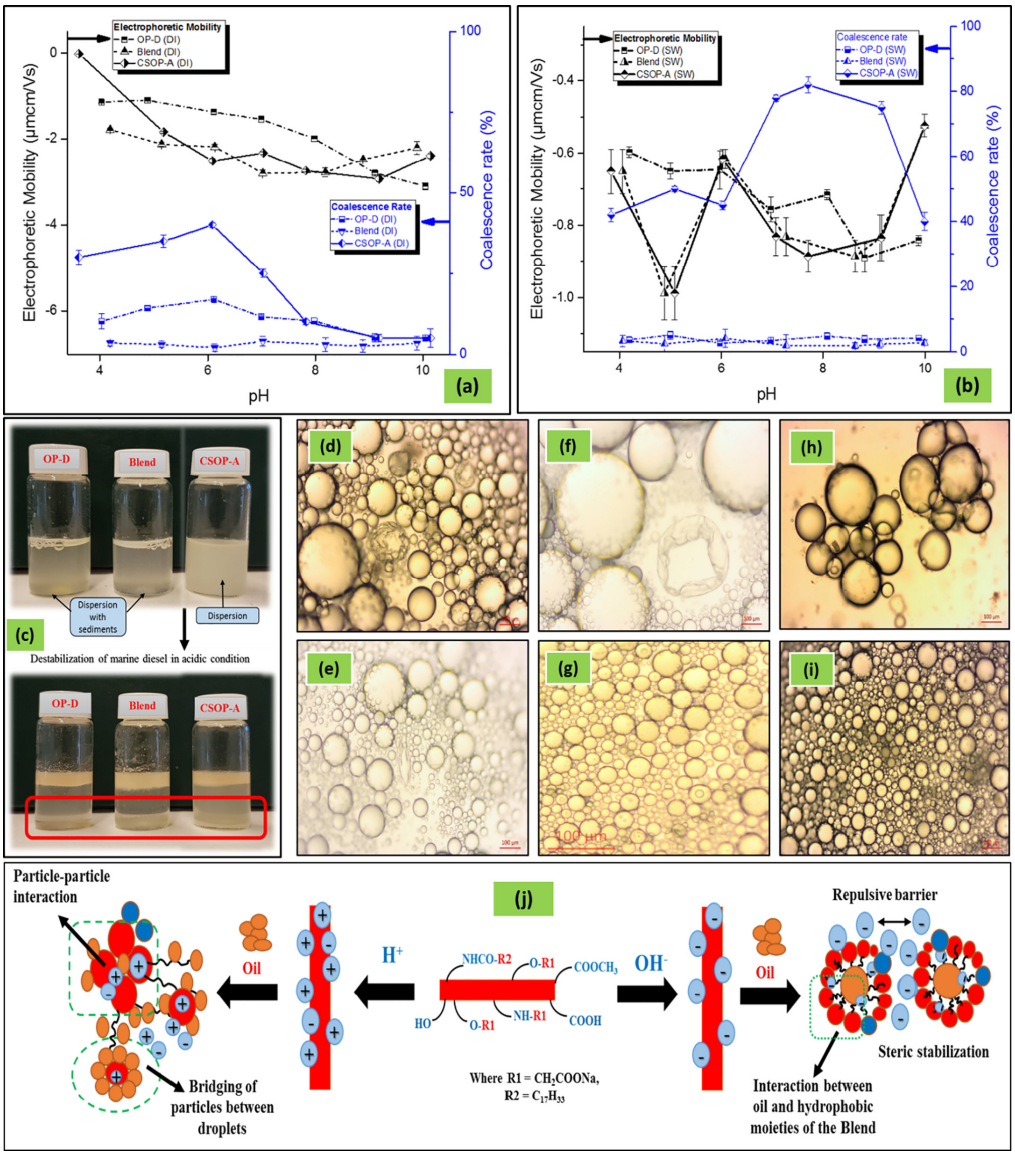

Fig. 6. Effect of solution pH of OP-D, CSOP-A and the Blend on the electrophoretic mobility and coalescence rate of marine diesel (a) with deionized water and (b) with saline water. Electrophoretic mobility is shown with black lines with symbols and coalescence rate is shown with blue lines with symbols. (c) The emulsion formation of marine diesel with OP-D, CSOP-A and the Blend in acidic condition. Microscopic images of the o/w emulsion of marine diesel in DI water with OP-D at (d) acidic pH 4.1 and (e) alkaline pH 9.9, with CSOP-A at (f) acidic and (g) alkaline pH, with the Blend at (h) acidic and (i) alkaline pH, at a magnification of 100 μm. (j) Emulsion mechanism of marine diesel with 2.0 g L^{-1} of Blend in DI at acidic and alkaline pH.

as pH. Fig. 7a shows the oil droplet stabilization of marine diesel in the formed emulsion as a function of salinity. With OP-D, the droplet stabilization rate of marine diesel increased with increasing electrolyte concentration, whereas the orange-chitosan derivatives indicated droplet stabilization in a different way. One of the reasons might be that the presence of electrolyte prevents hydration water around OP-D

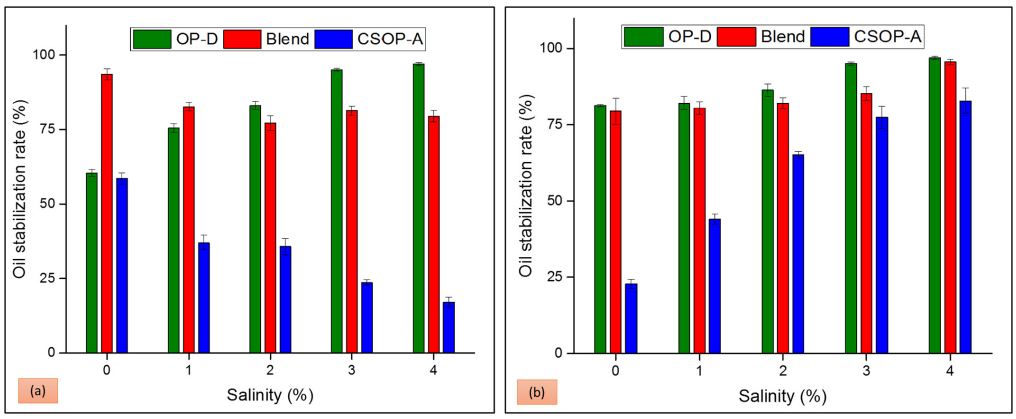

Fig. 7. Effect of salinity on the stabilization of oil droplets in the formed emulsion (a) Marine diesel and (b) Marine 2T oil using OP-D, CSOP-A and the Blend.

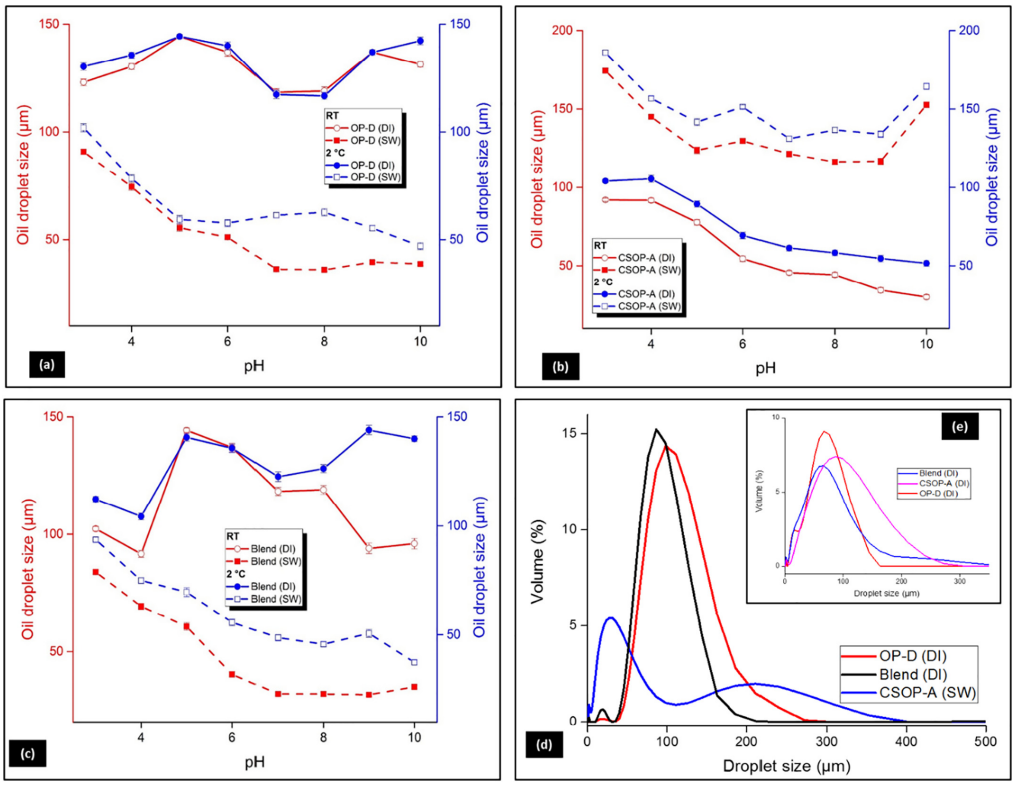

Fig. 8. Oil droplet size in the o/w emulsion at RT and 2 °C for marine diesel using (a) OP-D, (b) CSOP-A and (c) Blend using optical microscope. The droplet size measured with a laser diffraction spectrometer of (d) marine diesel with optimized dosage, i.e. 2.0 g $L^{-1}$of OP-D, CSOP-A and the Blend with a different quality of water at RT and (e) 2T-oil with the same dosage in DI.

molecules that reduces the electrostatic repulsion between the intermolecular hydrophilic groups, and enhances the hydrophobicity of OP-D. Similar behaviour of surfactant was previously observed [58]. Furthermore, the crosslinking of metal ions with carboxyl and hydroxyl groups present in OP-D might have reduced intermolecular electrostatic repulsion. Kasprzak et al. demonstrated the coordination of metal ions with flavonoids to form complexes [63]. In CSOP-A, the unavailability of carboxylic acid reduced crosslinking activity with ions, and thus reduced its effectiveness in the emulsion stability at SW salinity. Although CSOP-A possesses hydrocarbon chains, an increase in electrolyte concentration strengthened the electrostatic interaction of unreacted hydroxyl groups towards water, which enhanced the aggregation of oil droplets and destabilized the emulsion of marine diesel. In case of the Blend, the stabilization rate was not affected much with salinity variance in DI, due to the steric forces.

2T-oil consists of solvent-dewaxed heavy paraffinic and polyaromatics along with hydrocarbons, which immediately form clusters when mixed with SW. Even though the oil droplets stabilization rate is similar (Fig. 7b), the nature of emulsion with respect to these materials was different. OP-D formed stable emulsion that could be skimmed easily, whereas CSOP-A and the Blend formed bulky lumps due to the long hydrocarbon chain present in these derivatives. Secondly, the presence of electrolyte led to stronger interfacial activity with these surface-active species, by limiting the coalescence effect and then the stabilization [64].

3.5. Behaviour of oil droplets in the formed emulsion with changing temperature

The measured oil droplet sizes in the o/w emulsion in varying pH at RT and 2 °C for marine diesel using optical microscope are shown in Fig. 8(a–c). The emulsion rate of the oils at RT and 2 °C does not fluctuate much apart from the size of oil droplets in the emulsion. In addition, the water quality also affected the oil droplet size. The droplet size of marine diesel fluctuates with different surface-active particles used at RT (Fig. 8d). In the case of 2T-oil, the oil droplet size in the emulsion was <100 μm (Fig. 8e), but at −20 °C due to the ice formation, the water quality did not play a significant role in the formation of o/w emulsion due to the ice, but was rather more dependent on surface-active materials concentration. Therefore, the oil droplets stabilization rate (emulsion formation) on the surface of ice in the presence of these surface-active materials decreased to <10%. Despite hydrophobic moieties in CSOP-A and the Blend, the absence of the liquid-dispersed phase suppressed the hydrophilic properties of these surfactants, which in turn inhibited the formation of emulsion. Secondly, in such cold conditions, the viscosity of the oils increases, which might be one reason for the ineffectiveness of these materials in the formation of emulsion. These particle-formed surfactants were effective for spilled oil above 0 °C, due to their dispersion in water, but below 0 °C there was a decline in the dispersion rate and particle effectiveness in the stabilization of oil droplets or formation of the emulsion also declined.

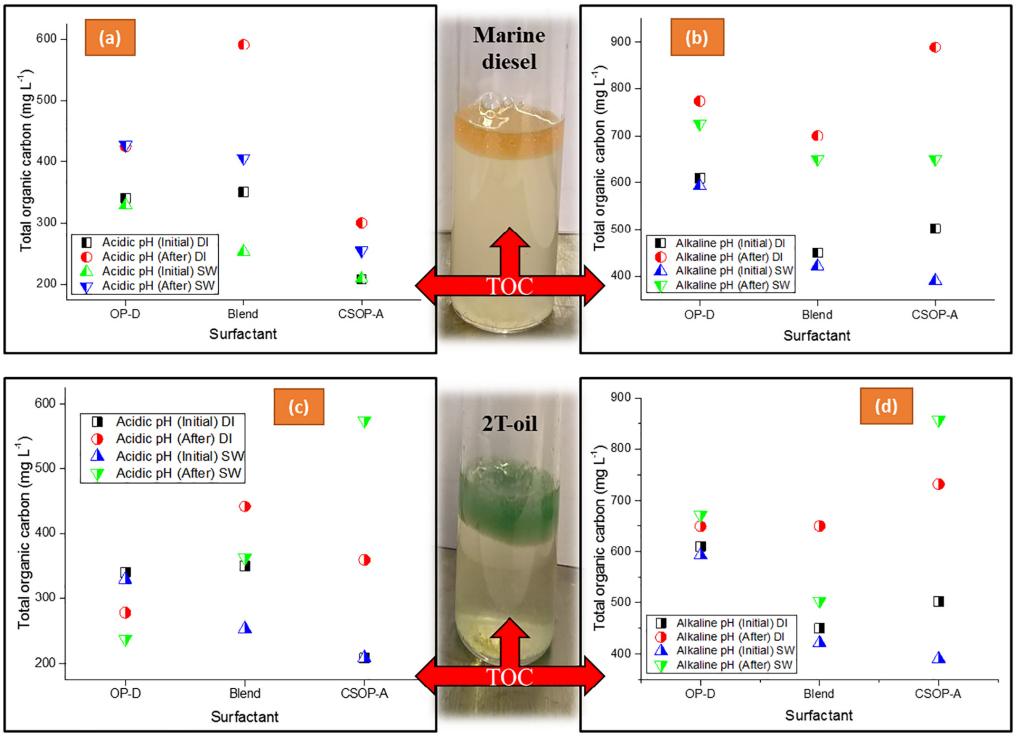

Fig. 9. Total organic carbon (TOC) content after the removal of marine diesel (a) at acidic pH and (b) at alkaline pH, and after the removal of 2T-oil (c) at acidic pH and (d) at alkaline pH from the water surface.

3.6. Water quality after the removal of oil

The remains of toxic chemical dispersants in water resources after the removal of spilled oil adversely affects marine creatures, due to their poor biodegradability, so to investigate the amount of dispersant traces in water is equally as important as the removal of spilled oil. Traces of organic matter after the removal of emulsified/separated oil were investigated using TOC through the NPOC method. The aqueous layer was not cleared (see Figs. 4b, 5b and 6c), indicating traces of unreacted surface-active particles. Fig. 9a and b shows the traces of OP-D, the Blend and CSOP-A after the removal of the oil/emulsified marine diesel and the 2T-oil layer. Despite the removal of the oil layer, the increase in the amount of organic carbon was attributed to either the adsorption of oil molecules on the surface-active moieties or the presence of degraded oil in the continuous aqueous phase along with these particles. Especially for 2T-oil, the spontaneous oil-in-water emulsification implies the leaching of surfactant from oil to the aqueous phase [62]. However, the amount of increased TOC after 2T-removal was less (Fig. 9c–d) than that obtained from marine diesel due to the formation of bulky emulsion, in which the surface-active particles might have become trapped. Various biosurfactants derived from varied microbial sources are present in the water, enhancing the biodegradation of the dispersed crude oil through bioremediation [65]. Moreover, earlier studies demonstrate orange peel as a substrate for *Bacillus Licheniformis* biosurfactant production and the biodegradation of hydrocarbons [66], so traces of OP-D in the water phase proved to be non-toxic. Chitosan being non-toxic and biodegradable, its derivatives, the Blend and CSOP-A, might not have many adverse effects, if found in water resources.

4. Conclusions

The use of bio-waste such as orange peel together with chitosan derivatives facilitate oil droplet breakup through faster adsorption of their surface-active moieties at the oil-water interface. The spectrometric measurements confirmed hydrophobic modification along with the presence of surface-active moieties on the surface of OP-D, CSOP-A and the Blend. The emulsion formation rate of marine diesel followed the order of the Blend > OP-D > CSOP-A, whereas for 2T-oil the order was OP-D > Blend > CSOP-A. The emulsion formation was solid-stabilized (Pickering) emulsion with OP-D, a combination of Pickering and conventional o/w emulsion with the Blend and only conventional emulsion with CSOP-A. The emulsion formation rate was >90% with OP-D in saline water, whereas, the Blend balanced the same rate independent of the water quality with optimized concentration. For CSOP-A, the droplets stabilization rate in the formed emulsion was more dependent on water quality and oil. This revealed that different hydrophobic moieties on the surface of the Blend and CSOP-A affected the oil droplets stabilization rate. The presence of glucosamine unit and carboxymethyl moieties in the Blend and CSOP-A altered the nature of emulsion with changing pH. There was a direct influence by temperature on the oil-droplet formation and its stability. The emulsion formed at RT was most stable, and at −20 °C this rate decreased to 10%, but the stabilization rate was not affected much at 2 °C except the increase in droplet size, so the studied surface-active particles could be used in dispersant formulation even at Arctic temperatures. Since the origin of these materials is bio-based, their hazardousness could be less than materials used in commercial dispersants. The future need is to identify different types of bio-waste and reutilize them as dispersants in oil spill response and accordingly minimize the use of hazardous chemicals.

Note.

The authors declare no competing financial interest.

Acknowledgement

The authors are grateful to the Academy of Finland (decision number 283200) for funding this project.

Appendix A. Supplementary data

Supplementary data to this article can be found online at https://doi.org/10.1016/j.molliq.2019.111327.

References

[1] R.T. Ranellone, P. Tukaew, X. Shi, A.S. Rangwala, Ignitability of crude oil and its oil-in-water products at arctic temperature, Mar. Pollut. Bull. 115 (2017) 261–265, https://doi.org/10.1016/j.marpolbul.2016.12.021.
[2] L. van Gelderen, J. Fritt-Rasmussen, G. Jomaas, Effectiveness of a chemical herder in association with in-situ burning of oil spills in ice-infested water, Mar. Pollut. Bull. 115 (2017) 345–351, https://doi.org/10.1016/j.marpolbul.2016.12.036.
[3] S.M. Beladi-Mousavi, B. Khezri, L. Krejčová, Z. Heger, Z. Sofer, A.C. Fisher, M. Pumera, Recoverable bismuth-based microrobots: capture, transport, and on-demand release of heavy metals and an anticancer drug in confined spaces, ACS Appl. Mater. Interfaces 11 (2019) 13359–13369, https://doi.org/10.1021/acsami.8b19408.
[4] C.F. Wise, J.T.F. Wise, S.S. Wise, W.D. Thompson, J.P. Wise, J.P. Wise, Chemical dispersants used in the Gulf of Mexico oil crisis are cytotoxic and genotoxic to sperm whale skin cells, Aquat. Toxicol. 152 (2014) 335–340, https://doi.org/10.1016/j.aquatox.2014.04.020.
[5] M. Zheng, M. Ahuja, D. Bhattacharya, T.P. Clement, J.S. Hayworth, M. Dhanasekaran, Evaluation of differential cytotoxic effects of the oil spill dispersant Corexit 9500, Life Sci. 95 (2014) 108–117, https://doi.org/10.1016/j.lfs.2013.12.010.
[6] J.C. Athas, K. Jun, C. McCafferty, O. Owoseni, V.T. John, S.R. Raghavan, An effective dispersant for oil spills based on food-grade amphiphiles, Langmuir 30 (2014) 9285–9294, https://doi.org/10.1021/la502312n.
[7] D.A. Riehm, J.E. Neilsen, G.D. Bothun, V.T. John, S.R. Raghavan, A.V. McCormick, Efficient dispersion of crude oil by blends of food-grade surfactants: toward greener oil-spill treatments, Mar. Pollut. Bull. 101 (2015) 92–97, https://doi.org/10.1016/j.marpolbul.2015.11.012.
[8] X. Wu, L. Zhang, X. Zhang, Y. Zhu, Y. Wu, Y. Li, B. Li, S. Liu, J. Zhao, Z. Ma, Ethyl cellulose nanodispersions as stabilizers for oil in water Pickering emulsions, Sci. Rep. 7 (2017), 12079. https://doi.org/10.1038/s41598-017-12386-4.
[9] J. Ojala, J.A. Sirviö, H. Liimatainen, Nanoparticle emulsifiers based on bifunctionalized cellulose nanocrystals as marine diesel oil–water emulsion stabilizers, Chem. Eng. J. 288 (2016) 312–320, https://doi.org/10.1016/j.cej.2015.10.113.
[10] B. Doshi, E. Repo, J.P. Heiskanen, J.A. Sirviö, M. Sillanpää, Effectiveness of N,O-carboxymethyl chitosan on destabilization of marine diesel, diesel and marine-2T oil for oil spill treatment, Carbohydr. Polym. 167 (2017) 326–336, https://doi.org/10.1016/j.carbpol.2017.03.064.
[11] S. Kalliola, E. Repo, V. Srivastava, F. Zhao, J.P. Heiskanen, J.A. Sirviö, H. Liimatainen, M. Sillanpää, Carboxymethyl chitosan and its hydrophobically modified derivative as pH-switchable emulsifiers, Langmuir 34 (2018) 2800–2806, https://doi.org/10.1021/acs.langmuir.7b03959.
[12] G. Pi, Y. Li, M. Bao, L. Mao, H. Gong, Z. Wang, Novel and environmentally friendly oil spill dispersant based on the synergy of biopolymer xanthan gum and silica nanoparticles, ACS Sustain. Chem. Eng. 4 (2016) 3095–3102, https://doi.org/10.1021/acssuschemeng.6b00063.
[13] K. Kurita, Chitin and chitosan: functional biopolymers from marine crustaceans, Mar. Biotechnol. 8 (2006) 203–226, https://doi.org/10.1007/s10126-005-0097-5.
[14] M. Rinaudo, Chitin and chitosan: properties and applications, Prog. Polym. Sci. 31 (2006) 603–632, https://doi.org/10.1016/j.progpolymsci.2006.06.001.
[15] FAO, The State of World Fisheries and Aquaculture 2106. Contributing to Food Security and Nutrition for all, 2016 (doi:92-5-105177-1).
[16] N. Yan, X. Chen, Sustainability: don't waste seafood waste, Nature 524 (2015) 155–157, https://doi.org/10.1038/524155a.
[17] B. Doshi, M. Sillanpää, S. Kalliola, A review of bio-based materials for oil spill treatment, Water Res. 135 (2018) 262–277, https://doi.org/10.1016/j.watres.2018.02.034.
[18] R.R. Fouad, H.A. Aljohani, K.R. Shoueir, Biocompatible poly(vinyl alcohol) nanoparticle-based binary blends for oil spill control, Mar. Pollut. Bull. 112 (2016) 46–52, https://doi.org/10.1016/j.marpolbul.2016.08.046.
[19] S.F. Soares, M.I. Rodrigues, T. Trindade, A.L. Daniel-da-Silva, Chitosan-silica hybrid nanosorbents for oil removal from water, Colloids Surfaces A Physicochem. Eng. Asp. 532 (2017) 305–313, https://doi.org/10.1016/j.colsurfa.2017.04.076.
[20] S. Zhang, T. Lü, D. Qi, Z. Cao, D. Zhang, H. Zhao, Synthesis of quaternized chitosan-coated magnetic nanoparticles for oil-water separation, Mater. Lett. 191 (2017) 128–131, https://doi.org/10.1016/j.matlet.2016.12.092.
[21] M. Rayner, D. Marku, M. Eriksson, M. Sjöö, P. Dejmek, M. Wahlgren, Biomass-based particles for the formulation of Pickering type emulsions in food and topical applications, Colloids Surfaces A Physicochem. Eng. Asp. 458 (2014) 48–62, https://doi.org/10.1016/j.colsurfa.2014.03.053.
[22] R. Aveyard, B.P. Binks, J.H. Clint, Emulsions stabilised solely by colloidal particles, Adv. Colloid Interf. Sci. 100–102 (2003) 503–546, https://doi.org/10.1016/S0001-8686(02)00069-6.
[23] L. Payet, E.M. Terentjev, Emulsification and stabilization mechanisms of O/W emulsions in the presence of chitosan, Langmuir 24 (2008) 12247–12252, https://doi.org/10.1021/la8019217.
[24] X.-Y. Wang, M.-C. Heuzey, Chitosan-based conventional and Pickering emulsions with long-term stability, Langmuir 32 (2016) 929–936, https://doi.org/10.1021/acs.langmuir.5b03556.
[25] Y. Yang, Z. Fang, X. Chen, W. Zhang, Y. Xie, Y. Chen, Z. Liu, W. Yuan, An overview of Pickering emulsions: solid-particle materials, classification, morphology, and applications, Front. Pharmacol. 8 (2017) 287, https://doi.org/10.3389/fphar.2017.00287.

[26] V. Calabrese, J.C. Courtenay, K.J. Edler, J.L. Scott, Pickering emulsions stabilized by naturally derived or biodegradable particles, Curr. Opin. Green Sustain. Chem. 12 (2018) 83–90, https://doi.org/10.1016/j.cogsc.2018.07.002.
[27] D.J. French, P. Taylor, J. Fowler, P.S. Clegg, Making and breaking bridges in a Pickering emulsion, J. Colloid Interface Sci. 441 (2015) 30–38, https://doi.org/10.1016/j.jcis.2014.11.032.
[28] I. Kalashnikova, H. Bizot, P. Bertoncini, B. Cathala, I. Capron, Cellulosic nanorods of various aspect ratios for oil in water Pickering emulsions, Soft Matter 9 (2013) 952–959, https://doi.org/10.1039/C2SM26472B.
[29] M. Matos, A. Marefati, R. Bordes, G. Gutiérrez, M. Rayner, Combined emulsifying capacity of polysaccharide particles of different size and shape, Carbohydr. Polym. 169 (2017) 127–138, https://doi.org/10.1016/j.carbpol.2017.04.006.
[30] C.S.K. Lin, L.A. Pfaltzgraff, L. Herrero-Davila, E.B. Mubofu, S. Abderrahim, J.H. Clark, A.A. Koutinas, N. Kopsahelis, K. Stamatelatou, F. Dickson, S. Thankappan, Z. Mohamed, R. Brocklesby, R. Luque, Food waste as a valuable resource for the production of chemicals, materials and fuels. Current situation and global perspective, Energy Environ. Sci. 6 (2013) 426, https://doi.org/10.1039/c2ee23440h.
[31] F.D. Romelle, A. Rani, R.S. Manohar, Chemical composition of some selected fruit peels, Eur. J. Food Sci. Technol. 4 (2016) 12–21.
[32] L.A. Pfaltzgraff, M. De bruyn, E.C. Cooper, V. Budarin, J.H. Clark, Food waste biomass: a resource for high-value chemicals, Green Chem. 15 (2013) 307–314, https://doi.org/10.1039/c2gc36978h.
[33] F. Meng, B. Yang, B. Wang, S. Duan, Z. Chen, W. Ma, Novel dendrimerlike magnetic biosorbent based on modified orange peel waste: adsorption–reduction behavior of arsenic, ACS Sustain. Chem. Eng. 5 (2017) 9692–9700, https://doi.org/10.1021/acssuschemeng.7b01273.
[34] B.H. Hameed, A.A. Ahmad, Batch adsorption of methylene blue from aqueous solution by garlic peel, an agricultural waste biomass, J. Hazard. Mater. 164 (2009) 870–875, https://doi.org/10.1016/j.jhazmat.2008.08.084.
[35] D. Sud, G. Mahajan, M. Kaur, Agricultural waste material as potential adsorbent for sequestering heavy metal ions from aqueous solutions – a review, Bioresour. Technol. 99 (2008) 6017–6027, https://doi.org/10.1016/j.biortech.2007.11.064.
[36] R. Diaz-Ruiz, M. Costa-Font, J.M. Gil, Moving ahead from food-related behaviours: an alternative approach to understand household food waste generation, J. Clean. Prod. 172 (2018) 1140–1151, https://doi.org/10.1016/j.jclepro.2017.10.148.
[37] S. Achinas, V. Achinas, G.J.W. Euverink, A technological overview of biogas production from biowaste, Engineering 3 (2017) 299–307, https://doi.org/10.1016/J.ENG.2017.03.002.
[38] J. González-Rivera, A. Spepi, C. Ferrari, C. Duce, I. Longo, D. Falconieri, A. Piras, M.R. Tinè, Novel configurations for a citrus waste based biorefinery: from solventless to simultaneous ultrasound and microwave assisted extraction, Green Chem. 18 (2016) 6482–6492, https://doi.org/10.1039/C6GC02200F.
[39] P. Putnik, D. Bursać Kovačević, A. Režek Jambrak, F. Barba, G. Cravotto, A. Binello, J. Lorenzo, A. Shpigelman, Innovative "green" and novel strategies for the extraction of bioactive added value compounds from Citrus wastes—a review, Molecules 22 (2017) 680, https://doi.org/10.3390/molecules22050680.
[40] S. Thévenet, A. Wernicke, S. Belniak, G. Descotes, A. Bouchu, Y. Queneau, Esterification of unprotected sucrose with acid chlorides in aqueous medium: kinetic reactivity versus acyl- or alkyloxycarbonyl-group migrations, Carbohydr. Res. 318 (1999) 52–66, https://doi.org/10.1016/S0008-6215(99)00079-8.
[41] J.H. Bridson, W.J. Grigsby, L. Main, Synthesis and characterization of flavonoid laurate esters by transesterification, J. Appl. Polym. Sci. 129 (2013) 181–186, https://doi.org/10.1002/app.38731.
[42] M. Abdullah, S.H.A. Muhamad, S.N. Sanusi, S.I.S. Jamaludin, N.F. Mohamad, M.A.H. Rusli, Preliminary study of oil removal using hybrid Peel waste: Musa Balbisiana and Citrus Sinensis, J. Appl. Environ. Biol. Sci. 6 (2016) 59–63.
[43] B. Doshi, E. Repo, J.P. Heiskanen, J.A. Sirviö, M. Sillanpää, Sodium salt of oleoyl carboxymethyl chitosan: a sustainable adsorbent in the oil spill treatment, J. Clean. Prod. 170 (2018) 339–350, https://doi.org/10.1016/j.jclepro.2017.09.163.
[44] J.W. Wang, M.H. Hon, Preparation and characterization of pH sensitive sugar mediated (polyethylene glycol/chitosan) membrane, J. Mater. Sci. Mater. Med. 14 (2003) 1079–1088, https://doi.org/10.1023/B:JMSM.0000004005.52762.ea.
[45] D. Zhang, W. Zhou, B. Wei, X. Wang, R. Tang, J. Nie, J. Wang, Carboxyl-modified poly (vinyl alcohol)-crosslinked chitosan hydrogel films for potential wound dressing, Carbohydr. Polym. 125 (2015) 189–199, https://doi.org/10.1016/j.carbpol.2015.02.034.
[46] M. Thirumavalavan, Y.-L. Lai, L.-C. Lin, J.-F. Lee, Cellulose-based native and surface modified fruit peels for the adsorption of heavy metal ions from aqueous solution: Langmuir adsorption isotherms, J. Chem. Eng. Data 55 (2010) 1186–1192, https://doi.org/10.1021/je900585t.
[47] M.R. Mafra, L. Igarashi-Mafra, D.R. Zuim, É.C. Vasques, M.A. Ferreira, Adsorption of remazol brilliant blue on an orange peel adsorbent, Brazilian J. Chem. Eng. 30 (2013) 657–665, https://doi.org/10.1590/S0104-66322013000300022.
[48] R.L. Patale, V.B. Patravale, O,N-carboxymethyl chitosan–zinc complex: a novel chitosan complex with enhanced antimicrobial activity, Carbohydr. Polym. 85 (2011) 105–110, https://doi.org/10.1016/j.carbpol.2011.02.001.
[49] L. Bédouet, B. Courtois, J. Courtois, Methods for obtaining neutral and acid oligosaccharides from flax pectins, Biotechnol. Lett. 27 (2005) 33–40, https://doi.org/10.1007/s10529-004-6314-x.
[50] L.M.A. Silva, E.G. Alves Filho, R. Choze, L.M. Lião, G.B. Alcantara, 1H HRMAS NMR spectroscopy and chemometrics for evaluation of metabolic changes in citrus sinensis caused by Xanthomonas axonopodis pv. citri, J. Braz. Chem. Soc. 23 (2012) 1054–1061, https://doi.org/10.1590/S0103-50532012000600009.
[51] C.R. de Oliveira, R.L. Carneiro, A.G. Ferreira, Tracking the degradation of fresh orange juice and discrimination of orange varieties: an example of NMR in coordination with chemometrics analyses, Food Chem. 164 (2014) 446–453, https://doi.org/10.1016/j.foodchem.2014.05.026.
[52] B. Gullón, M.I. Montenegro, A.I. Ruiz-Matute, A. Cardelle-Cobas, N. Corzo, M.E. Pintado, Synthesis, optimization and structural characterization of a chitosan–glucose derivative obtained by the Maillard reaction, Carbohydr. Polym. 137 (2016) 382–389, https://doi.org/10.1016/j.carbpol.2015.10.075.
[53] G. Kaptay, On the equation of the maximum capillary pressure induced by solid particles to stabilize emulsions and foams and on the emulsion stability diagrams, Colloids Surfaces A Physicochem. Eng. Asp. 282–283 (2006) 387–401, https://doi.org/10.1016/j.colsurfa.2005.12.021.
[54] D.J. McClements, C.E. Gumus, Natural emulsifiers — biosurfactants, phospholipids, biopolymers, and colloidal particles: molecular and physicochemical basis of functional performance, Adv. Colloid Interf. Sci. 234 (2016) 3–26, https://doi.org/10.1016/j.cis.2016.03.002.
[55] S. Shiao, V. Chhabra, A. Patist, M. Free, P.D. Huibers, A. Gregory, S. Patel, D. Shah, Chain length compatibility effects in mixed surfactant systems for technological applications, Adv. Colloid Interf. Sci. 74 (1998) 1–29, https://doi.org/10.1016/S0001-8686(97)00005-5.
[56] S.R. Valandro, P.C. Lombardo, A.L. Poli, C.E. Posakoda, C.C.S. Cavalheiro, Effect of hydrocarbon chain length surfactants on particle size of SWy-1 montmorillonite suspensions, Int. J. Basic Appl. Sci. 13 (2013) 1–6.
[57] S.W. Benner, V.T. John, C.K. Hall, Simulation study of hydrophobically modified chitosan as an oil dispersant additive, J. Phys. Chem. B 119 (2015) 6979–6990, https://doi.org/10.1021/acs.jpcb.5b01092.
[58] T. Jiao, X. Liu, J. Niu, Effects of sodium chloride on adsorption at different interfaces and aggregation behaviors of disulfonate gemini surfactants, RSC Adv. 6 (2016) 13881–13889, https://doi.org/10.1039/C5RA25727A.
[59] U.S. Schmidt, K. Schmidt, T. Kurz, H.-U. Endreß, H.P. Schuchmann, Pectins of different origin and their performance in forming and stabilizing oil-in-water-emulsions, Food Hydrocoll. 46 (2015) 59–66, https://doi.org/10.1016/j.foodhyd.2014.12.012.
[60] U.S. Schmidt, L. Schütz, H.P. Schuchmann, Interfacial and emulsifying properties of citrus pectin: interaction of pH, ionic strength and degree of esterification, Food Hydrocoll. 62 (2017) 288–298, https://doi.org/10.1016/j.foodhyd.2016.08.016.
[61] S. Ghorbanizadeh, B. Rostami, Surface and interfacial tension behavior of salt water containing dissolved amphiphilic compounds of crude oil: the role of single-salt ionic composition, Energy Fuel 31 (2017) 9117–9124, https://doi.org/10.1021/acs.energyfuels.7b01394.
[62] D.A. Riehm, D.J. Rokke, P.G. Paul, H.S. Lee, B.S. Vizanko, A.V. McCormick, Dispersion of oil into water using lecithin-tween 80 blends: the role of spontaneous emulsification, J. Colloid Interface Sci. 487 (2017) 52–59, https://doi.org/10.1016/j.jcis.2016.10.010.
[63] M.M. Kasprzak, A. Erxleben, J. Ochocki, Properties and applications of flavonoid metal complexes, RSC Adv. 5 (2015) 45853–45877, https://doi.org/10.1039/C5RA05069C.
[64] D.R. Alves, J.S.A. Carneiro, I.F. Oliveira, F. Façanha, A.F. Santos, C. Dariva, E. Franceschi, M. Fortuny, Influence of the salinity on the interfacial properties of a Brazilian crude oil–brine systems, Fuel 118 (2014) 21–26, https://doi.org/10.1016/j.fuel.2013.10.057.
[65] R. Mohanram, C. Jagtap, P. Kumar, Isolation, screening, and characterization of surface-active agent-producing, oil-degrading marine bacteria of Mumbai Harbor, Mar. Pollut. Bull. 105 (2016) 131–138, https://doi.org/10.1016/j.marpolbul.2016.02.040.
[66] A.P. Kumar, A. Janardhan, B. Viswanath, K. Monika, J.-Y. Jung, G. Narasimha, Evaluation of orange peel for biosurfactant production by Bacillus licheniformis and their ability to degrade naphthalene and crude oil, 3 Biotech 6 (2016), 43. https://doi.org/10.1007/s13205-015-0362-x.

ACTA UNIVERSITATIS LAPPEENRANTAENSIS

823. YLÄ-KUJALA, ANTTI. Inter-organizational mediums: current state and underlying potential. 2018. Diss.

824. ZAFARI, SAHAR. Segmentation of partially overlapping convex objects in silhouette images. 2018. Diss.

825. MÄLKKI, HELENA. Identifying needs and ways to integrate sustainability into energy degree programmes. 2018. Diss.

826. JUNTUNEN, RAIMO. LCL filter designs for paraller-connected grid inverters. 2018. Diss.

827. RANAEI, SAMIRA. Quantitative approaches for detecting emerging technologies. 2018. Diss.

828. METSO, LASSE. Information-based industrial maintenance - an ecosystem perspective. 2018. Diss.

829. SAREN, ANDREY. Twin boundary dynamics in magnetic shape memory alloy Ni-Mn-Ga five-layered modulated martensite. 2018. Diss.

830. BELONOGOVA, NADEZDA. Active residential customer in a flexible energy system - a methodology to determine the customer behaviour in a multi-objective environment. 2018. Diss.

831. KALLIOLA, SIMO. Modified chitosan nanoparticles at liquid-liquid interface for applications in oil-spill treatment. 2018. Diss.

832. GEYDT, PAVEL. Atomic Force Microscopy of electrical, mechanical and piezo properties of nanowires. 2018. Diss.

833. KARELL, VILLE. Essays on stock market anomalies. 2018. Diss.

834. KURONEN, TONI. Moving object analysis and trajectory processing with applications in human-computer interaction and chemical processes. 2018. Diss.

835. UNT, ANNA. Fiber laser and hybrid welding of T-joint in structural steels. 2018. Diss.

836. KHAKUREL, JAYDEN. Enhancing the adoption of quantified self-tracking wearable devices. 2018. Diss.

837. SOININEN, HANNE. Improving the environmental safety of ash from bioenergy production plants. 2018. Diss.

838. GOLMAEI, SEYEDMOHAMMAD. Novel treatment methods for green liquor dregs and enhancing circular economy in kraft pulp mills. 2018. Diss.

839. GERAMI TEHRANI, MOHAMMAD. Mechanical design guidelines of an electric vehicle powertrain. 2019. Diss.

840. MUSIIENKO, DENYS. Ni-Mn-Ga magnetic shape memory alloy for precise high-speed actuation in micro-magneto-mechanical systems. 2019. Diss.

841. BELIAEVA, TATIANA. Complementarity and contextualization of firm-level strategic orientations. 2019. Diss.

842. EFIMOV-SOINI, NIKOLAI. Ideation stage in computer-aided design. 2019. Diss.

843. BUZUKU, SHQIPE. Enhancement of decision-making in complex organizations: A systems engineering approach. 2019. Diss.

844. SHCHERBACHEVA, ANNA. Agent-based modelling for epidemiological applications. 2019. Diss.

845. YLIJOKI, OSSI. Big data - towards data-driven business. 2019. Diss.

846. KOISTINEN, KATARIINA. Actors in sustainability transitions. 2019. Diss.

847. GRADOV, DMITRY. Experimentally validated numerical modelling of reacting multiphase flows in stirred tank reactors. 2019. Diss.

848. ALMPANOPOULOU, ARGYRO. Knowledge ecosystem formation: an institutional and organisational perspective. 2019. Diss.

849. AMELI, ALIREZA. Supercritical CO2 numerical modelling and turbomachinery design. 2019. Diss.

850. RENEV, IVAN. Automation of the conceptual design process in construction industry using ideas generation techniques. 2019. Diss.

851. AVRAMENKO, ANNA. CFD-based optimization for wind turbine locations in a wind park. 2019. Diss.

852. RISSANEN, TOMMI. Perspectives on business model experimentation in internationalizing high-tech companies. 2019. Diss.

853. HASSANZADEH, AIDIN. Advanced techniques for unsupervised classification of remote sensing hyperspectral images. 2019. Diss.

854. POPOVIC, TAMARA. Quantitative indicators of social sustainability applicable in process systems engineering. 2019. Diss.

855. RAMASAMY, DEEPIKA. Selective recovery of rare earth elements from diluted aqueous streams using N- and O –coordination ligand grafted organic-inorganic hybrid composites. 2019. Diss.

856. IFTEKHAR, SIDRA. Synthesis of hybrid bio-nanocomposites and their application for the removal of rare earth elements from synthetic wastewater. 2019. Diss.

857. HUIKURI, MARKO. Modelling and disturbance compensation of a permanent magnet linear motor with a discontinuous track 2019. Diss.

858. AALTO, MIKA. Agent-based modeling as part of biomass supply system research. 2019. Diss.

859. IVANOVA, TATYANA. Atomic layer deposition of catalytic materials for environmental protection. 2019. Diss.

860. SOKOLOV, ALEXANDER. Pulsed corona discharge for wastewater treatment and modification of organic materials. 2019. Diss.

ISBN 978-952-335-392-3
ISBN 978-952-335-393-0 (PDF)
ISSN-L 1456-4491
ISSN 1456-4491
Lappeenranta 2019